2001

# Investigation of Amphoteric Materials for Treatment of Heavy Metals in Storm Water.

Dingfang Liu
*Louisiana State University and Agricultural & Mechanical College*

# INFORMATION TO USERS

This manuscript has been reproduced from the microfilm master. UMI films the text directly from the original or copy submitted. Thus, some thesis and dissertation copies are in typewriter face, while others may be from any type of computer printer.

**The quality of this reproduction is dependent upon the quality of the copy submitted.** Broken or indistinct print, colored or poor quality illustrations and photographs, print bleedthrough, substandard margins, and improper alignment can adversely affect reproduction.

In the unlikely event that the author did not send UMI a complete manuscript and there are missing pages, these will be noted. Also, if unauthorized copyright material had to be removed, a note will indicate the deletion.

Oversize materials (e.g., maps, drawings, charts) are reproduced by sectioning the original, beginning at the upper left-hand corner and continuing from left to right in equal sections with small overlaps.

Photographs included in the original manuscript have been reproduced xerographically in this copy. Higher quality 6" x 9" black and white photographic prints are available for any photographs or illustrations appearing in this copy for an additional charge. Contact UMI directly to order.

Bell & Howell Information and Learning
300 North Zeeb Road, Ann Arbor, MI 48106-1346 USA
800-521-0600

# INVESTIGATION OF AMPHOTERIC MATERIALS FOR TREATMENT OF HEAVY METALS IN STORM WATER

A Dissertation

Submitted to the Graduate Faculty of the
Louisiana State University and
Agricultural and Mechanical College
in partial fulfillment of the
requirements for the degree of
Doctor of Philosophy

in

The Department of Civil and Environmental Engineering

By
Dingfang Liu
B.S., Nanchang Institute of Aeronautical Technology, 1993
M. S., Chinese Academy of Sciences, 1999
December 2001

ProQuest Information and Learning Company
300 North Zeeb Road
P.O. Box 1346
Ann Arbor, MI 48106-1346

# ACKNOWLEDGMENTS

I would like to express my great appreciation to my advisor, Dr. John J. Sansalone, who given me the chance to work on my favorite area. While his encouragement, counsel and support have shaped my attitude toward my work, his character has shaped my concept of the true scholar.

I would also like to particularly thank Dr. Frank K. Cartledge for his generous advise both on my papers and work.

I am grateful to my committee members for their helpful advise: Dr. Paul N. Kirk, Dr. John H. Pardue, Dr. Amitava Roy and Dr. Vijay Singh.

I would like to thank Dr. Xiaogang Xie and Dr. Tingzong Guo for their assistance with SEM analysis, and Mr. Ping Zhou for ICP-MS analysis. I am also thank Zeng Teng and my former student workers, Mr. Jonathan Kolich and Mr. Christopher Dean. My thanks also go to those folks in our group, who shown interest in my work and shared me with their knowledge and helpful discussion.

My parents and brothers also have my deepest thanks for their support and love in spite of the great distance separating us.

Finally, I would like to express my gratitude to my wife, Ms Xiao Hu who supports me with love and patience.

TABLE OF CONTENTS

# LIST OF TABLES

# LIST OF FIGURES

# NOMENCLATURE

$[A]_0$: The boundary condition of reactants A at $t = 0$;
$[B]_0$: The boundary condition of reactants B at $t = 0$;
$\equiv MnOH$: Solid sorbent surface;
$(M_s^{2+})$: The activity of $M^{2+}$ (mol/L) on the sorbent surface the surface;
$(M^{2+})$: Metal concentration in the solution (mol/L);
$(\equiv MnOM_s)^+$: Monodentate surface complex metal species on the sorbent surface;
$(\equiv MnO)_2 M_s$: Bidentate surface complex metal species on the sorbent surface;
$a$: The sorbent dosage (g/L).
Å: $10^{-10}$ m;
$\alpha$: Elovich constants (mg/g-min);
atm: Atmosphere (standard), 1 atm = $1.0133\times10^2$ kPa (kN/m$^2$);
$\beta$: Elovich constants (mg/g);
BV: Bed volumes, water volumes divided by the volume of packed bed;
BCM: Birnessite coating method;
BMP: Best Management Practices;
BSPET: Bench scale partial exfiltration trench;
BSE: Backscattered electron;
BTC: Breakthrough curves;
$C$: Percentage of manganese oxide coverage on the media (%);
$C_1$: Inner layer capacitance (F/m$^2$);
$C_2$: Outer layer capacitance (F/m$^2$);
$C_0$: The initial metal concentration (mg/L);
$C_t$: The metal concentration in time $t$ (mg/L);
$C_e$: The metal concentration at equilibrium (mg/L);
C: Effluent heavy metal concentration (mg/L);
$C_0$: Influent heavy metal concentration (mg/L);
CC: Constant capacitance model;
CCM: Cyptomelane coating method;
CPP: Crashed pavement particles.
CST: Continuously-stirred tank;
$D$: Apparent diffusion coefficient (cm/s);
d: Pore diameter.
$\psi_0$: The average potential of the near-surface;
$\psi_\beta$: The electric surface potential of β-plane;
$\psi_d$: The electric surface potential of $d$-plane;
$d_{50}$: The 50% diameter value located on the media diameter distribution;
DF: Degree of freedom.
DI: Deionization;
DL: Diffuse layer model;
$E(x_i)$: Expected value (modeled data)

| | |
|---|---|
| EBCT: | Empty bed contact time (minute); |
| EGME: | Ethylene glycol monoethyl; |
| EDS: | Energy dispersive X-ray spectrometer; |
| EXAFS: | Extended X-ray absorption fine structure spectroscopy. |
| $F$: | Faraday constant (96480 C/mol); |
| GAC: | Granular activated carbon; |
| $H_s^+$: | Hydrogen ion at the media surface (0-plane); |
| $H^+$: | Hydrogen ion at the bulk solution; |
| $H_3O^+$: | Hydrogen ion complex representation with a water molecular; |
| ICP-MS: | Inductive coupled plasma mass spectrometer; |
| IOCB1: | Iron oxide coated polyethylene beads; |
| IOCB2: | Iron oxide coated polyethylene beads; |
| IOCM: | Ion oxide coating method; |
| IR: | Infrared; |
| $k$: | Reaction kinetic constant($M^{-1}s^{-1}$); |
| $K_{a1}^{int}$: | Intrinsic surface acidity constant; |
| $K_{a2}^{int}$: | Intrinsic surface acidity constant; |
| $K_{Cd}^{int}$: | Intrinsic surface reaction constant for Cd; |
| $K_{Pb}^{int}$: | Intrinsic surface reaction constant for Pb; |
| $K_{Cu}^{int}$: | Intrinsic surface reaction constant for Cu; |
| $K_{Zn}^{int}$: | Intrinsic surface reaction constant for Zn; |
| $K_{Na}^{int}$: | Intrinsic surface reaction constant for Na; |
| $k_B$: | Boltzmann's constant; |
| $M_s^{2+}$: | Metal species of $M^{2+}$ on the sorbent surface the surface |
| mA: | Milliampere ($10^{-3}$ ampere); |
| $Me(H_2O)_n^{2+}$: | Divalent metal complex with water molecules; |
| MOCB1: | Manganese oxide coated polyethylene beads; |
| MOCB2: | Manganese oxide coated polyethylene beads; |
| MOC: | Manganese oxide coating; |
| MOCM: | Manganese oxide coated cementitious media using MOC method; |
| $MOCM_{(ad)}$: | Manganese oxide coated cementitious media (admixture added) using MOC method; |
| MOCP: | The precipitation in MOC coating process; |
| MOCS: | Manganese oxide coated silica sand using MOC method; |
| $MnOPb^+$: | Surface specie of Pb; |
| $MnOZn^+$: | Surface specie of Zn; |
| $MnOCu^+$: | Surface specie of Cu; |
| $MnOCd^+$: | Surface specie of Cd; |
| MOPM: | Manganese oxide coated polymeric media; |
| MTZ: | Mass transfer zone; |

m/z: Mass to charge ratio;
$n$: the number of data points;
$N_{MOCM}$: Surface site of MOCM (sites/g);
$N_{MOCP}$: Surface site of MOCP (sites/nm$^2$);
$N_A$: Avogadro's number ($6.022\times10^{23}$ sites/mol of sites);
NGE: Natural green sand effect;
$O(x_i)$: Observation data;
PER: Partial exfiltration reactor;
$pH_{PZC}$: pH of point of zero charge;
ppm: Part per million;
PZC: Point of zero charge;
$\rho_s$: Specific gravity;
$\rho_w$: The density of water (0.998 g/cm$^3$);
$q_{sf}$: Urban pavement sheet flow ;
$Q_t$: The amount of sorbate per unit mass of sorbent at time $t$ (mg/g);
$Q_e$ or $Q_\infty$: The amount of sorbate per unit mass of sorbent at equilibrium (mg/g);
$Re_d$: The Reynolds number;
rpm: Revolutions per minute;
SBMC: Sorptive buoyant media clarifier;
SEM: Scanning electron microscopy;
$R$: Ideal gas constant (8.314 J/mol K);
r: Radius of the cylinder;
$R_0$: The solute radius;
$S_t$: The number of active sites occupied on MOCPM at time $t$;
$S_e$: The number of active sites occupied at equilibrium on the test media;
SOS: Sum of squares;
SSA: Specific surface area (m$^2$/g);
$SSA_{MOCM}$: SSA of MOCM (m$^2$/g);
$T$: Absolute temperature (K);
$t$: The reaction time (s);
TCB1: Two step coated polyethylene beads;
TCB2: Two step coated polyethylene beads;
TCM: Two step coating method;
TL: Triple layer model;
TLM: Triple layer model;
μ: The dynamic viscosity ($1.009\times10^{-2}$ g/(cm-sec));
μm: Micrometer ($10^{-6}$ m);
$V_b$: 10% breakthrough bed volumes;
V: Superficial velocity (cm/sec);
v/v: volume to volume ratio;
$\chi^2$: Result for computed goodness of fit value which follows a chi-square distribution.
$X/M_b$: Breakthrough capacity (mg/g);

| | |
|---|---|
| $X/M_{exh}$: | Exhaustion capacity (mg/g); |
| XRD: | X-ray diffraction. |

# ABSTRACT

Urban storm water runoff mobilizes and transports significant loads of heavy metals. Promulgation of NPDES Phase II regulations has spurred development of Best Management Practices (BMPs) for in-situ control of heavy metals. In this study, Amphoteric materials such as manganese oxides and iron oxides on the various substrates including silica sands, polymeric beads and cementitious particles were investigated. Surface characterization results indicated that oxide coatings ranged from 20 to 200-μm in depth, and surface areas were significantly increased by greater than a factor of one thousand compared to uncoated media. Point of zero charge (PZC) for manganese oxide coated media generally ranged from 4 to 6. For manganese oxide coated polymeric media (MOPM), Freundlich type adsorption isotherms were observed, and MOPM has a comparable adsorption capacity for the divalent heavy metals compared to other commercial and research media. For manganese oxide coated cementitious media (MOCM), removal mechanisms proved to be more complicated with a parabolic isotherm results indicating the combination of surface precipitation and surface complexation. A surface complexation model, triple layer model, was utilized to model adsorption of divalent heavy metals for MOPM used as adsorptive media in storm water BMPs. Intrinsic surface acidity constants for MOPM were determined using FITEQL-TLM as $\log K_{a1}^{int} = 3.196$ and $\log K_{a2}^{int} =$ -5.802 and the intrinsic surface reaction constants as $\log K_{Pb}^{int} = -1.91$, $\log K_{Cu}^{int} =$ -2.53 and $\log K_{Zn}^{int} =$ -4.45. For MOCM, the intrinsic surface complexation constants were $\log K_{Pb}^{int} = -1.84$, $\log K_{Cu}^{int} =$ -4.11, $\log K_{Zn}^{int} =$ -5.04, and $\log K_{Zn}^{int} =$ -7.84. Surface complexation on the solid-water interface and precipitation in bulk solution were distinguished from the speciation distribution as a function of pH and it was found that surface complexation was the dominant removal mechanism in the typical storm water pH range. An overall rate kinetic, potential driving model, was developed based on an elementary second order rate law. This model was successfully utilized for the kinetic data of both MOPM and MOCM. Based on column experiment performances of all the media and substrates examined in this study, amphoteric oxide coating significantly improved the adsorption capacity, with MOCM demonstrating the greatest adsorptive capacity.

# CHAPTER 1. INTRODUCTION

## 1.1 Pollutants in Urban Storm Water Runoff

Waterways and receiving waters near urban and suburban area are often adversely affected by urban storm water runoff. The degree and type of impact varies from location to location, but it is often significant relative to other sources of pollution and environmental degradation. According Nation Water Quality Inventory 1996 Report (USEPA 1996) to Congress, polluted storm water runoff is a leading cause of impairment to nearly 40 percent of U.S water bodies which do not meet water quality standards. Recently promulgated National Pollutant Discharge Elimination System (NPDES) Phase II Stormwater Regulations (1999a) are intended to regulate and control discharges to receiving waters. These discharges include overland flow, pavement sheet flow or discharges from municipal separate storm sewer system (MS4s). Storm water runoff from anthropogenic land uses or activities can harm surface water resources and, in turn, cause or contribute to an exceedance of water quality standards by changing natural hydrological patterns, accelerating stream flows, destroying aquatic habitat, and elevating pollutant concentrations and loadings. Such runoff may contain or mobilize high levels of contaminants, such as sediment, suspended solids, nutrients, heavy metals and other toxic pollutants (USEPA 1992).

Pollutants associated with urban storm water runoff potentially harmful to receiving waters fall into the categories listed below (Horner et al. 1994):

- Solids

- Oxygen-demanding substances
- Nitrogen and phosphorus
- Pathogens
- Petroleum hydrocarbons
- Metals
- Synthetic organics.

These pollutants degrade water quality in receiving waters near urban areas, often contribute to the impairment of use, and exceedences of criteria included in State water quality standards. The quantity of these pollutants per unit area delivered to receiving water tends to increase with the degree of development in an urban area.

Based on available information and data, the USEPA described characterization and impacts of urban storm water impacts (USEPA 1999a).

- Impacts to water quality in terms of water column chemistry, particularly in rivers.
- Impacts to habitat and aquatic life are generally more profound, and are easier to see and quantify than changes in water column chemistry.
- Impacts are typically complex because urban storm water is often one of several sources including municipal discharges and diffuse runoff from agricultural and rural areas that affect urban waterways.
- Impacts are often interrelated and cumulative. For example, both degraded water quality and increased water quantity join to impact habitat and biological resource.

### 1.1.1 Heavy Metal Concentrations in Urban Storm Water Runoff

Table 1.1 Median event mean concentrations for urban land uses.

| Pollutant | Units | Residential | | Mixed | | Commercial | | Open/Non-urban | |
|---|---|---|---|---|---|---|---|---|---|
| | | Median | COV | Median | COV | Median | COV | Median | COV |
| BOD | mg/l | 10 | 0.41 | 7.8 | 0.52 | 9.3 | 0.31 | -- | -- |
| COD | mg/l | 73 | 0.55 | 65 | 0.58 | 57 | 0.39 | 40 | 0.78 |
| TSS | mg/l | 101 | 0.96 | 67 | 1.14 | 69 | 0.85 | 70 | 2.92 |
| Total Lead | µg/l | 144 | 0.75 | 114 | 1.35 | 104 | 0.68 | 30 | 1.52 |
| Total Copper | µg/l | 33 | 0.99 | 27 | 1.32 | 29 | 0.81 | -- | -- |
| Total Zinc | µg/l | 135 | 0.84 | 154 | 0.78 | 226 | 1.07 1 | 95 | 0.66 |
| Total Kjeldahl Nitrogen | µg/l | 1900 | 0.73 | 1288 | 0.5 | 1179 | 0.43 9 | 65 | 1 |
| Nitrate +Nitrite | µg/l | 736 | 0.83 | 558 | 0.67 | 572 | 0.48 5 | 43 | 0.91 |
| Total Phosphorus | µg/l | 383 | 0.69 | 263 | 0.75 | 201 | 0.67 1 | 21 | 1.66 |
| Soluble Phosphorus | µg/l | 143 | 0.46 | 56 | 0.75 | 80 | 0.71 | 26 | 2.11 |

COV: Coefficient of variation
Source: Nationwide Urban Runoff Program (US EPA 1983)

Between 1978 and 1983, Nationwide Urban Runoff Program (NURP) by conducted by USEPA in order to examine the characteristics of urban runoff and similarities or differences between urban land uses. This program also examined the extent to which urban runoff is a significant contributor to water quality problems nationwide, and the performance characteristics and effectiveness of management practices to control pollution loads from urban runoff (US EPA 1983). Sampling was conducted for 28 NURP projects which included 81 specific sites and more than 2,300 separate storm events. As a major finding of the NURP study, heavy metals (especially copper, lead and zinc) are by far the most prevalent priority pollutant constituents found in urban runoff. End-of-pipe concentrations exceed EPA ambient water quality criteria and drinking water standards in many instances. Some of the metals are present often enough and in high enough concentrations to threaten to beneficial uses. The medians

values of total Pb, Cu and Zn concentrations as well as other selected pollutant concentrations are presented in Table 1.1 as an event mean concentrations (EMCs) for various urban land use categories. The results indicate that there is not a significant difference in pollutant concentrations in runoff from different urban land use categories. There is a significant difference, however, in pollutant concentrations in runoff from urban sources as compared to nonurban areas.

The results of typical pollutant loadings from different urban land uses indicated that the concentrations of pollutants found in urban runoff are directly related to degree of development within the watershed as shown in Table 1.2.

Table 1.2 Typical pollutant loadings from runoff by urban land use (lbs/acre-yr)

| Land Use | TSS | TP | TKN | $NH_3$-N | $NO_2$+$NO_3$-N | BOD | COD | Pb | Zn | Cu |
|---|---|---|---|---|---|---|---|---|---|---|
| Commercial | 1000 | 1.5 | 6.7 | 1.9 | 3.1 | 62 | 420 | 2.7 | 2.1 | 0.4 |
| Parking Lot | 400 | 0.7 | 5.1 | 2 | 2.9 | 47 | 270 | 0.8 | 0.8 | 0.04 |
| HDR | 420 | 1 | 4.2 | 0.8 | 2 | 27 | 170 | 0.8 | 0.7 | 0.03 |
| MDR | 190 | 0.5 | 2.5 | 0.5 | 1.4 | 13 | 72 | 0.2 | 0.2 | 0.14 |
| LDR | 10 | 0.04 | 0.03 | 0.02 | 0.1 | NA | NA | 0.01 | 0.04 | 0.01 |
| Freeway | 880 | 0.9 | 7.9 | 1.5 | 4.2 | NA | NA | 4.5 | 2.1 | 0.37 |
| Industrial | 860 | 1.3 | 3.8 | 0.2 | 1.3 | NA | NA | 2.4 | 7.3 | 0.5 |
| Park | 3 | 0.03 | 1.5 | NA | 0.3 | NA | 2 | 0 | NA | NA |
| Construction | 6000 | 80 | NA | NA | NA | NA | NA | NA | NA | NA |

HDR: High Density Residential, MDR: Medium Density Residential, LDR: Low Density Residential
NA: Not available; insufficient data to characterize loadings
Source: Horner et al, 1994

A comparison of the concentration of water quality parameters in urban runoff with the concentrations in domestic wastewater is shown in Table 1.3. The concentrations of select water quality parameters in urban runoff are comparable to that found in untreated domestic wastewater. When untreated urban runoff is discharged directly to receiving streams, the loadings of pollutants can be much higher than the

loadings attributable to treated domestic wastewater. The frequency with which metals were detected as priority pollutants in the NURP study is presented in Table 1.4.

Table 1.3. Comparison of water quality parameters in urban runoff with domestic wastewater (mg/l)

| Constituent | Urban Runoff | | Domestic Wastewater | | |
|---|---|---|---|---|---|
| | Separate Sewers | | Before Treatment | | After Secondary |
| | Range | Typical | Range | Typical | Typical |
| COD | 200-275 | 75 | 250-1,000 | 500 | 80 |
| TSS | 20-2,890 | 150 | 100-350 | 200 | 20 |
| Total P | 0.02-4.30 | 0.36 | 4-15 | 8 | 2 |
| Total N | 0.4-20.0 | 2.00 | 20-85 | 40 | 30 |
| Lead | 0.01-1.20 | 0.18 | 0.02-0.94 | 0.1 | 0.05 |
| Copper | 0.01-0.40 | 0.05 | 0.03-1.19 | 0.22 | 0.03 |
| Zinc | 0.01-2.90 | 0.02 | 0.02-7.68 | 0.28 | 0.08 |
| Fecal Coliform per 100 ml | 400-50,000 | | 106-108 | | 200 |

Source: Bastian, 1997

Table 1.4 Most frequently detected priority pollutants in nationwide urban runoff program samples (1978-83).

| **Inorganic** | **Organics** |
|---|---|
| **Detected in 75% or more** | |
| 94% Lead<br>94% Zinc<br>91% Copper | None |
| **Detected in 50-74%** | |
| 58% Chromium<br>52% Arsenic | None |
| **Detected in 20-49%** | |
| 48% Cadmium<br>43% Nickel<br>23% Cyanides | 22% Bis(2-ethylhexyl)phthalate<br>20% Hexachloro-cyclohexane |
| **Detected in 10-19%** | |
| 13% Antimony<br>12% Beryllium<br>11% Selenium | 19% Endosulfan<br>19% Pentachlorophenol*<br>17% Chlordane*<br>15% Lindane*<br>15% Pyrene** |

* Chlorinated hydrocarbon
** Polynuclear aromatic hydrocarbon
Source: US EPA 1983

A major study of the quality of Wisconsin storm water (Bannerman et al 1996) found that the probability of event mean concentrations for some metals (particularly copper and zinc) exceeding Wisconsin water quality criteria for cold water fish communities was high (Table 1.5).

Table 1.5. Probability of event mean concentration of constituents in Wisconsin storm water exceeding Wisconsin surface water and ground water quality standards: metals

| Constituent | Probability of exceeding acute toxicity criteria for cold water fish communities (percent) | |
|---|---|---|
| | Storm Sewers | Streams |
| Cadmium, total recoverable | 11 | 0 |
| Copper, total recoverable | 87 | 9 |
| Lead, total recoverable | 18 | 0 |
| Silver, total recoverable | 20 | - |
| Zinc, total recoverable | 91 | 7 |

Source: Bannerman et al, 1996.

Compared to typical domestic wastewater and USEPA metal discharge criteria, heavy metal concentration in urban runoff can exhibit significantly elevated levels on an event basis as showed in Table 1.6 (Sansalone and Buchberger1997; Drapper *et al* 2000; Barrett *et al* 1995, 1993; Driscoll *et al* 1990). Storm water from urban areas and roadways transports dissolved, colloidal and suspended solids in a heterogeneous mixture that includes inorganic and organic anthropogenic constituents. Parameters such as pH, alkalinity, traffic levels and residence time have been shown to influence the partitioning of heavy metals (Sansalone and Buchberger 1997). Results from partitioning analysis between the dissolved and particulate-bound fractions on a mass basis indicate that Zn, Cd, Cu and Pb are predominately dissolved in urban pavement sheet flow ($q_{sf}$) for residence times less than several hours at pH levels between 6 and

7.5 (Sansalone and Glenn 2001). Recent research on highway runoff in Cincinnati indicated that dissolved fractions for Cd, Cu and Zn typically exceed 70%, while Pb exceeds 50% based on partitioning data for lateral pavement sheet flow (Sansalone and Buchberger 1997). Urban storm water characterization in urban residential areas of London showed dissolved fractions for Cd of 69%, Cu of 87%, Pb of 47% and Zn of 82% (Revitt et al. 1990).

Table 1.6. Heavy metal concentration in urban highway runoff as compared to the level of domestic wastewater and discharge criteria

| Parameter | Units | Domestic wastewater | Urban highway runoff | | | | Discharge criteria[2] |
|---|---|---|---|---|---|---|---|
| | | Metcalf and Eddy, (1991) Mean (Range) | Sansalone (1997)[1] Median (Range) | Drapper (2000) (Range) | Barrett (1995; 1993) (Range) | Driscoll (1990) (Median) | |
| TSS | [mg/L] | 720 (350-1200) | 750 (150-22000) | 60-1350 | 19-798 | 142 | |
| Total Zn | [mg/L] | 75 (40-120) | 628 (336-15244) | 150-1850 | 22-929 | 330 | 120.0 |
| Dissolved Zn | [mg/L] | --- | 1322 (209-14786) | --- | --- | --- | 110.0 |
| Total Cu | [mg/L] | 35 (20-45) | 88 (43-325) | 30-340 | 22-7033 | 50 | 18.0 |
| Dissolved Cu | [mg/L] | --- | 44 (13-279) | --- | --- | --- | 17.0 |
| Total Pb | [mg/L] | 10 (2-15) | 88 (31-1457) | 80-620 | 7-1780 | 400 | 82.0 |
| Dissolved Pb | [mg/L] | --- | 16 (13-21) | --- | --- | --- | 65.0 |
| Total Cd | [mg/L] | 1 (N/D-3) | 8 (5-32) | --- | --- | --- | 5.6 |
| Dissolved Cd | [mg/L] | --- | 3 (2-9) | --- | --- | --- | 3.7 |

[1]: The concentration is event mean concentration (EMC)
[2]: the total metal discharge criteria are State EPA criteria for discharge to modified warmwater surface water, and the dissolve metal discharge criteria are USEPA criteria for discharge to modified warmwater surface water

### 1.1.2 Sources of Heavy Metals in Storm Water Runoff

The pollutants that are found in urban storm water runoff originate from a variety of sources. The major sources include contaminants from residential and commercial areas, industrial activities, construction, roadways and parking lots. Contaminants commonly found in storm water runoff and their likely sources are summarized in Table 1.7.

Table 1.7. Sources of contaminants in urban storm water runoff

| Contaminant | Contaminant Sources |
|---|---|
| Sediment and Floatables | Streets, lawns, driveways, roads, construction activities, atmospheric deposition, drainage channel erosion |
| Pesticides and Herbicides | Residential lawns and gardens, roadsides, utility right-of-ways, commercial and industrial landscaped areas, soil wash-off |
| Organic Materials | Residential lawns and gardens, commercial landscaping, animal wastes |
| Metals | Automobiles, bridges, atmospheric deposition, industrial areas, soil erosion, corroding metal surfaces, combustion processes |
| Oil and Grease/ Hydrocarbons | Roads, driveways, parking lots, vehicle maintenance areas, gas stations, illicit dumping to storm drains |
| Bacteria and Viruses | Lawns, roads, leaky sanitary sewer lines, sanitary sewer cross-connections, animal waste, septic systems |
| Nitrogen and Phosphorus | Lawn fertilizers, atmospheric deposition, automobile exhaust, soil erosion, animal waste, detergents |

Source: USEPA, 1999a.

The deposition and accumulation of these dissolved and particulate-bound constituents result from traffic activities, vehicular component wear, fluid leakage, pavement degradation, and roadway maintenance (Armstrong 1994; Ball *et al.* 1991; Lygren *et al.* 1984; Muschack 1990). Pavement, tire, and vehicular part abrasion are sources of solids, ranging from rapidly soluble, submicron particles to insoluble gravel-

size aggregates abraded from the roadway surface. Winter maintenance practices such as deicing salt application generate chlorides and associated cations, in particular sodium and calcium.

### 1.2 Storm Water Regulation

In 1972, Congress enacted the Clean Water Act (CWA) to prohibit the discharge of any pollutant to waters of the United States from a point or nonpoint source unless the discharge was authorized by an NPDES permit. Congress added Section 402(p) to the Clean Water Act in 1987 to require implementation of a comprehensive approach for addressing storm water discharges in two phases. Section 402(p)(4) required USEPA to develop permit application regulations under the National Pollutant Discharge Elimination System (NPDES), submission of NPDES permit applications, issuance of NPDES permits, and compliance with NPDES permit conditions. Section 402(p)(6) requires USEPA to designate storm water discharges to be regulated (within the statutory definitions provided in section 402(p)(2)) and establish a comprehensive regulatory program, which may include performance standards, guidelines, guidance, and management practices and treatment requirements.

#### 1.2.1 Phase I NPDES Storm Water Regulation

In response to the 1987 Amendments to the Clean Water Act (CWA), USEPA promulgated the first phase of NPDES storm water permit application regulations ("Phase I") on November 16, 1990 (US EPA 1990). The Phase I program addressed sources of storm water runoff that had the greatest potential to negatively impact water quality. Under Phase I, USEPA required NPDES permit coverage for storm water

discharges from: "medium" and "large" municipal separate storm sewer systems (MS4s) located in incorporated places or counties with populations of 100,000 or more; and 11 categories of industrial activity, one of which was construction activity that disturbs five or more acres of land. Operators of the facilities, systems, and construction sites regulated under the Phase I NPDES Storm Water Program could obtain permit coverage under an individually tailored NPDES permit (developed for MS4s and some industrial facilities) or a general NPDES permit (used by most operators of industrial facilities and construction sites).

### 1.2.2 Phase II NPDES Storm Water Regulation

USEPA promulgated the NPDES storm water regulations for the second phase of storm water discharge control in 1999. The regulation designates two classes of facilities for automatic coverage on a nationwide basis under the NPDES program, (1) small municipal separate storm sewer systems located in urbanized areas (about 3,500 municipalities would be included in the program); and (2) construction activities (pollutants include sediments and erosion from these sites) that disturb and equivalent of one to five acres of land (about 110,000 sites per year will be included in the program). Those facilities designated above would need to apply for NPDES storm water permits by 2002. USEPA is anticipating that most permittees would be covered under general permits. USEPA is also proposing to conditionally exclude from the NPDES storm water program Phase I facilities that have "no exposure" of industrial activities, such as industrial products, processes, or raw materials, to storm water, thereby reducing application of the program to many industrial activities currently

covered by the program that have no industrial storm water discharges. Some facilities that USEPA is proposing to cover under the Phase II rule are currently subject to state and/or local storm water management requirements.

### 1.3 Storm Water BMPs

A storm water best management practice (BMP) is a technique, measure or structural control that is used for a given set of conditions to manage the quantity and/or improve the quality of storm water runoff in the most cost-effective manner. BMPs fall into two categories BMPs can be either engineered and constructed systems ("structural BMPs") that improve the quality and/or control the quantity of runoff such as detention ponds and constructed wetlands. BMP can also be institutional, education or pollution prevention practices designed to limit the generation of storm water runoff or reduce the amounts of pollutants contained in the runoff ("non-structural BMPs"). No single BMP can address all storm water problems. Each type has certain limitations based on drainage area served, available land space, cost, pollutant removal efficiency, as well as a variety of site-specific factors such as soil types, slopes, depth of groundwater table, etc. Careful consideration of these factors is necessary in order to select the appropriate BMP or group of BMPs for a particular location.

#### 1.3.1 Structural BMPs

There are a wide variety of structural BMPs in use for storm water management. Structural BMPs include engineered and constructed systems that are designed to provide for water quantity and/or water quality control of storm water runoff. Structural

BMPs can be grouped into several general categories. An example of application of typical BMPs for the highway storm water runoff is shown in Figure 1.1.

- **Infiltration systems** capture a volume of runoff and infiltrates/exfiltrates into the subsurface.
- **Detention systems** capture a volume of runoff and temporarily retains that volume for subsequent release. Detention systems do not retain a significant permanent pool of water between runoff events.
- **Retention systems** capture a volume of runoff and retain that volume until it is displaced in part or in total by the next runoff event. Retention systems therefore maintain a significant permanent pool volume of water between runoff events.
- **Constructed wetland systems** are similar to retention and detention systems, except that a major portion of the BMP water surface area (in pond systems) or bottom (in meadow-type systems) contains wetland vegetation. This group also includes wetland channels.
- **Filtration systems** use some combination of a granular filtration media such as sand, soil, organic material, carbon or a membrane to remove constituents found in runoff.
- **Vegetated systems (biofilters)** such as swales and filter strips are designed to convey and filter either shallow flow (swales) or sheetflow (filter strips) runoff.
- **Minimizing directly connected impervious surfaces** describes a variety of practices that can be used to reduce the amount of surface area directly connected to the storm drainage system by minimizing or eliminating traditional curb and gutter. This is considered by some to be a non-structural practice, but is has been included under the

structural heading in this report due to the need to design and construct alternative conveyance and treatment options.

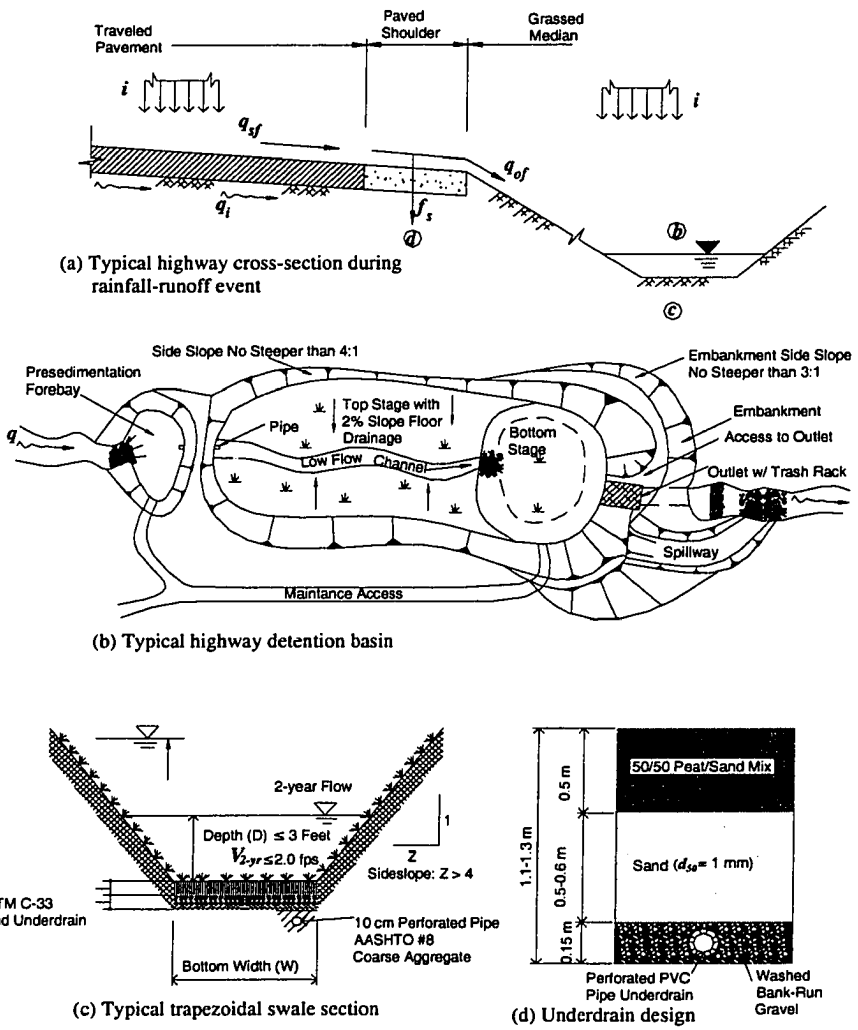


(a) Typical highway cross-section during rainfall-runoff event

(b) Typical highway detention basin

(c) Typical trapezoidal swale section

(d) Underdrain design

Figure 1.1. A typical highway shoulder section with several common in-situ treatment (as BMPs) alternatives.

- **Miscellaneous and vendor-supplied systems** include a variety of proprietary and miscellaneous systems that do not fit under any of the above categories. These include catch basin inserts, hydrodynamic devices, and filtration devices.

The BMPs are loaded by direct runoff from the edge of pavement shoulder, pavement sheet flow, $q_{sf}$. The implication of BMPs includes a detention basin (b), a roadside swale (c), and a media filter (d).

### 1.3.2 Filtration Systems

A filtration system is a device that uses a media such as sand, gravel, peat or compost to remove a fraction of the constituents found in storm water. There are a wide variety of filter types in use. There are also a variety of proprietary designs that use specialized filter media made from materials such as leaf compost. Filter is primarily a water quality control device designed to remove particulate pollutants. Media filters are commonly used to treat runoff from small sites such as parking lots and small developments, in areas with high pollution potential such as industrial areas, or in highly urbanized areas where land availability or costs preclude the use of other BMP types. Filters should be placed off-line (i.e., a portion of the runoff volume, called the water quality volume, is diverted to the BMP, while any flows in excess of this volume are bypassed) and are sometimes designed to intercept and treat only apportion of the runoff and bypass larger storm water flows. A benefit of using filters in highly urbanized areas is that the filter can be placed under parking lots or in building basements, limiting or eliminating costly land requirements.

Filter types in common use include surface sand filters such as the "Austin" sand filter and underground vault filters such as the "D.C." sand filter and the "Delaware" sand filter (USEPA 1999b). There are a number of variations of these basic designs in common use. In addition, there are a number of proprietary filtering systems in use. There are also a number of variations in the types of filtration media that are in use in media filters. Designs may incorporate features such as a layer of filter cloth or a plastic screen, a gravel layer, a peat layer, a compost layer, a layer of peat or a peat/sand mixture. Typical variations in filtration media BMPa are shown below.

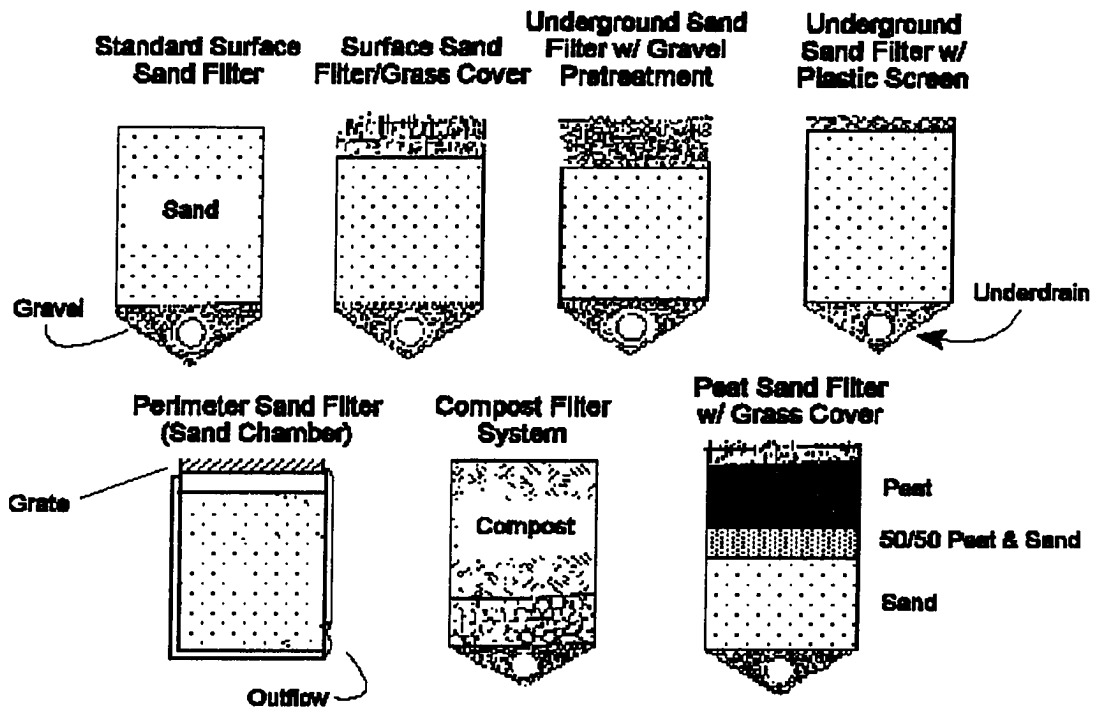


Figure 1.2. Common filter media BMP configurations (Claytor and Schueler 1996).

BMPs for heavy metals and solids are essentially garbage cans and as such they must be emptied and cleaned occasionally (Sansalone and Glenn 2001). The purpose of

design is to provide effective capture, reasonable time between clean outs and an optimal cost between treatment alternatives.

With respect to dissolved heavy metal removal, the adsorption capacity of filter media is a critical factor to determine the volumes of this "garbage can" (media filter). The higher the adsorption capacity of the filter media, the longer time between cleaning or regenerating interval. No adsorption capacity data has been available for heavy metal removal by storm water media filter BMPs. Since storm water filtration systems are traditionally designed for particle removal, silica sand and sand/peat mix are the most common media used, and adsorption was generally considered an auxiliary removal mechanism. However, recent research has demonstrated the high percentage of dissolved heavy metals in urban storm water (Sansalone and Buchberger 1997). As a result, control of heavy metals in storm water runoff should involve adsorption as well as filtration. Heavy metal adsorption capacity of media also should be considered because of longer regeneration time intervals and lower cost for regeneration. For dissolved heavy metal removal, silica sands were utilized unsuccessfully as filter media for storm water BMPs according to the current National Stormwater BMP Database (2001). Previous research has demonstrated the low capacity of silica snad for heavy metal (Sansalone 1999). In 1998 EPA conducted sampling activities at a peat/sand filter in Montgomery County, Maryland, and the results indicated a limit treatment capability for heavy metals (USEPA 1999b). Engineered media for us in BMPs, such as iron oxide or manganese oxide coated media can combine the unit operation of filtration and the

unit process of adsorption or surface complexation. Figure 1.3 is an example of field filtration for the treatment of urban storm water runoff.

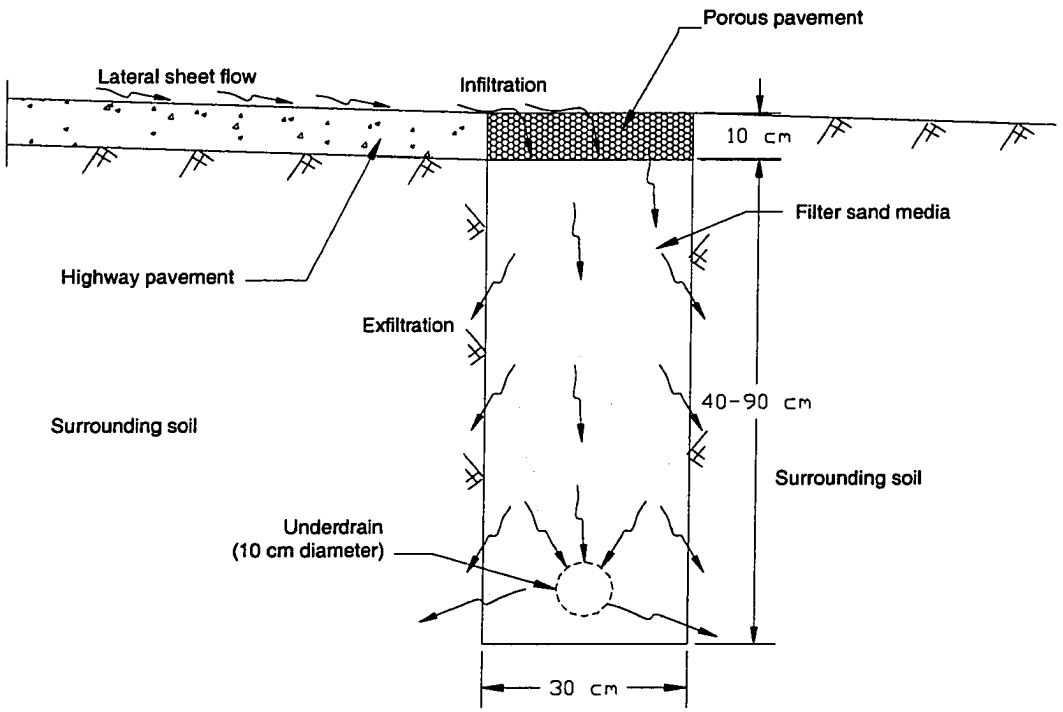


Figure 1.3. Schematic of a partial exfiltration reactor (PER) utilized for adsorptive filtration of urban lateral pavement sheet flow.

## 1.4 Amphoteric Materials

Amphoteric materials are the substances that have the characteristics of an acid and a base and are capable of reacting chemically either as an acid or a base (Stumm and Morgan 1996). Oxide surfaces such as iron oxides, aluminum oxides and manganese oxides are amphoteric. Common hydrous oxides, such as those of iron, aluminum, manganese, and silicon, can sorb a host of chemical species. They are

dominant sorbents in nature because of their tendency to be finely dispersed and to coat other particles (Dzombak and Morel 1990). In this section, the discussions focuses on iron oxides and manganese oxides from which, specific mineral characteristics are studied in later chapter. In general, the surface ionization reactions responsible for the amphoteric behavior of oxide surfaces can be represented by the following equations.

$$\equiv XOH_2^+ \;=\; \equiv XOH^\circ + H^+ \qquad K_{\alpha 1}^{int} = \frac{(\equiv XOH^\circ)\{H_s^+\}}{(\equiv XOH_2^+)} = \frac{(\equiv XOH^\circ)(H^+)}{(\equiv XOH_2^+)}\exp(\frac{-F\psi}{RT})$$

$$\equiv XOH^o \;=\; \equiv XO^- + H^+ \qquad K_{\alpha 2}^{int} = \frac{(\equiv XO^-)\{H_s^+\}}{(\equiv XOH^o)} = \frac{(\equiv XO^-)(H^+)}{(\equiv XOH^o)}\exp(\frac{-F\psi}{RT})$$

where $\equiv XOH_2^+$, $\equiv XOH^\circ$ and $XO^-$ represent positively charged, neutral and negatively charged surface hydroxyl groups, $K_{\alpha 1}^{int}$ and $K_{\alpha 2}^{int}$ are intrinsic acidity constants, ( ) represent concentrations, { } represent activities, $H_s^+$ denotes a proton released at the surface but not yet transported to the bulk solution, $H^+$ is the proton in the bulk solution, $\psi$ is the surface potential, F is the Faraday constant (96,485 C/mol), T is absolute temperature (K), and R is the gas constant.

Modeling metal ion adsorption has been a subject of interest in recent year and surface complexation model such as triple layer model (TLM) has became more and more widely implicated model especially in the environmental engineering and science area. The general scope of surface complexation model has been developed and summarized by a number of scientists such as Stumm and Morgan (1996), Dzombak and Morel (1990), etc. Application of TLM assumes that the surfaces on which adsorption of metal ions takes place are composed of a number of discrete sites

undergoing ionization in the aqueous environment as described above. Adsorption occurs as a result of the formation of complexes between the metal ions and the ionized sites as well as between the hydrolysis products of the ions and ionized sites. The reactions between metal ions and with surface hydroxyl groups is analogous to the formation of soluble complexes (albeit immobile complexes in this case) and can be described by mass law equations. However, the corresponding equilibrium constants are not, in fact, constant. Ionization of the surface sites and the formation of complexes between these sites and different ionic species implies the oxide surfaces, in general are charged. These charges are influenced by the presence of an electrostatic field which, in turn, affects the equilibrium between the oxide surface and the aqueous environment. These surface reactions are distinguished from reactions among solutes is the variable electrostatic energy of interaction caused by the variable charge on the surface (Dzombak and Morel 1990). These electrostatic effects are taken into account by applying a coulombic correction factor, derived from electric double-layer (EDL) theory proposed by Gouy and Chapman and later extended by Stern and Graham (Stumm and Morgan 1996). In addition, ionized sites may also form complexes with electrolyte ions present in the aqueous environment outside the oxide surface.

### 1.4.1 Specific Surface Area

The ability of a mineral to sorb chemical species from either liquids or gases is strongly dependent on the surface area that a unit mass or volume of the solid presents to the liquid or gas phase, that is, on the specific surface area (SSA). This exposed solid surface at the solid/liquid or solid gas interface contains the functional groups and/or

lattice ions and atoms that interact with liquid or gas phase species to effect sorption reactions. A number of experimental techniques were developed to measure the surface areas associated with finely divided solid materials. Most of these techniques involve measurement of sorption, under specified conditions, of gas or solute molecules having known dimensions, and interpretation of the resulting data utilizing a particular mechanistic model. The widely utilized specific surface area measurement method is the BET method, a gas sorption and data analysis method proposed by Brunauer, Emmett, and Teller (1938). This model is widely utilized because of the consistency of the BET data analysis technique combined with the simplicity of the experimental procedures leads to reproducible results as well as the speed with which the experimental test can be performed, particularly since the development of specialized BET equipment. For BET method, a gas adsorption isotherm is obtained by measuring the nitrogen gas sorption on the dried solid at constant temperature and variable gas pressure. Then the resulting isotherms are analyzed to determine the surface area of the solids. However, BET method has serious limitations in some cases, such as measuring SSA of solid oxides typically suspended in water or hydrated. For example, amorphous or poorly crystalline metal oxides can change significantly in the drying step required in the BET methods.

Important alternatives for specific surface area measurement to avoid the limitations of BET method employs adsorption of dyes or other relatively large organic molecules with well-characterized dimension. The sorbed molecules are usually considered to exist as monolayer on the exposed solid surface. The measurement can

conduct in situ, which is within the solid-liquid system and measure the decrease of aqueous solutes such as dyes or other large organic molecules to the solid surface. Surface are also can be carried out ex-situ in a solid-gas system by measuring the amount of volatile substances sorbed under the constant vapor pressure while maintaining a monolayer adsorbed on the solid surface. The example of ex-situ method is ethylene glycol monoethylether (EGME) method (Carter *et al*, 1986; Sansalone *et al.*, 1998). Because of the differences between the BET method and theEGME method for metal oxides, surface area measurements made with the various methods may differ by a factor of 2 to 4.

Table 1.8. Specific surface area of synthesized iron oxides.

| Iron oxides | Formula | SSA ($m^2/g$) | $logK_{so}$ |
|---|---|---|---|
| Goethite (from Fe(III) system) | α-FeOOH | 20 | 0.491 |
| Goethite (from Fe(II) system) | α-FeOOH | 80 | 0.491 |
| Al-substituted Goethite | $(Fe_{1-x}Al_x)OOH$ | 20-30 | -- |
| Lepidocrocite | γ-FeOOH | 70-80 | 1.371 |
| Feroxyhyte | δ'-FeOOH | 200 | --- |
| Ferrihydrite | $5Fe_2O_3 \cdot 9H_2O$ | 180-300 | 3.191 |
| Akaganeite | β-FeOOH | 30-100 | -- |
| Hematite | $\alpha$-$Fe_2O_3$ | 30-90 | -1.418 |
| Al-substituted Hematite | $\alpha$-$Fe_{2-x}Al_xO_3$ | 40-50 | -- |
| Magnetite | $Fe_3O_4$ | 4 | 3.403 |
| Al-substituted Magnetite | $Fe^{2+}_{0.88}Fe^{3+}_{1.88}Al_{0.2}O_4$ | 20 | -- |
| Maghemite | γ-$Fe_2O_3$ | 130 | 6.386 |

The bulk structure of hydrous ferric oxide (HFO) is uncertain and its chemical composition is represented by the general stoichiometic formula $Fe_2O_3 \cdot nH_2O$ (Cotton and Wilkinson 1980). Dzombak and Morel (1990) summarized the SSA of HFO ranged from 159 to 720 $m^2/g$ measured using different methods. A theoretic surface area of 840

$m^2/g$ for HFO was calculated (Davis 1977) assuming 2-nm-diameter spheres and using the density of 3.57 $g/cm^3$ determined by Murphy et al. (1976). Schwertmann and Cornell (1991) developed laboratory methods for various iron oxides and characterized resulting iron oxides. A summary of SSA the pure minerals of iron oxide from their work is shown in Table 1.8.

In comparison to iron, the mineralogy of Mn is complicated by the large number of oxides and hydroxides formed, in which substitution of $Mn^{2+}$ and $Mn^{3+}$ for $Mn^{4+}$ occurs extensively. These substitutions result in changes in average Mn—O bond lengths, with consequent changes in the unit cell size, and are accompanied by the substitution of some $O^{2-}$ by $OH^-$ to maintain electrical neutrality. In fact, only pyrolusite and ramsdellite are true modifications of $MnO_2$, and all others are nonstoichiometric, and may cover a relatively large range of compositions (McKenzie 1989). Most of oxides may conveniently be discussed under the headings of tunnel structures, and layer structures. The tunnel structures are formed from single, double, or wider chains of $MnO_6$ octahedra that are linked, by sharing corners, into a framework of enclosed tunnels throughout their structure (McKenzie, 1989). Large foreign cations and water molecules occupy these tunnels. Ramsdellite and cryptomelane belong to the tunnel structure manganese oxide family. The second major structural classification of manganese oxides is layer structures. Birnessite is a layered manganese oxide consisting of octahedral $MnO_6$ units, with exchangeable hydrated ions between layers (such as K- and Na-birnessite). Layer structures can undergo ion-exchange reactions, replacing the cations between the layers with other alkali or alkaline earth metal ions as well as protons

(Stephanie, *et al*, 1998).Because of the complicity of manganese oxide structure, the preparation of manganese oxide with reproducible surface properties is very difficult (Stroes-Gascoyne *et al.* 1986). Catts (1982) has measured SSA for fresh, aged and natural birnessite of 290, 143, and 180 $m^2/g$ respectively. McKenzie (1971) has synthesized different manganese oxides and measured their SSA as summarized in Table 1.9.

Table 1.9. Properties of nature manganese oxides and hydroxides.

| Manganese oxides or hydroxides | Formula | SSA ($m^2/g$) | $logK_{so}$ |
|---|---|---|---|
| Hausmannite | $Mn_3O_4$ | 41 | 61.03 |
| Partridgeite | | 13 | -- |
| Birnessite | $(Na_{0.7}Ca_{0.3})Mn_7O_{14}\cdot 2\cdot 8H_2O$ | 32-75 | 18.09 |
| Cryptomelane | $K_2Mn_8O_{16}$ | 58-222 | -- |
| Pyrolusite | $MnO_2$ | 3-178 | 41.38 |

### 1.4.2 Surface Charge and Surface Site Density

Solid particle surface can develop electric charge in the following five principal ways (Stumm and Morgan 1996; Langmuir 1997).

1. The charge may arise from chemical reactions at the surface. Ionization of many solid surface containing ionizable function groups, such as –OH and –SH, can create negative charge on the surfaces. For metal oxides, the electric charge of a hydrous oxide can be explained by the acid base behavior of the surface hydroxyl group $\equiv XOH$ .
2. Isomorphous substitution in the crystal lattice. This can cause permanent surface charge. For example, if in any array of solid $SiO_2$ tetrahedral an Si

atom is replaced by an Al atom, a negatively charged framework is established.

3. Lattice imperfections or defects, such as a deficit in oxtahedral $Mn^{4+}$ or interlayer $K^{+}$.
4. Broken or unsatisfied bonds at crystal plate corners and edges lead to the ionization of surface groups, usually resulting in a net negative surface charge due to exposed $O^{2-}$ and $OH^{-}$.
5. Adsorption of hydrophobic species or a surfactant ion may also establish a surface charge on the oxide surfaces.

Although aquatic particles bear electric charge, this charge is balanced by the charges in the diffuse swarm which move about freely in solution while remaining near enough to colloid surface to create the effective (counter) charge that balances the net surface charge. Points of zero charge (pzc) are pH values where the net surface charge is zero.

Summarized by Dzombak and Morel (1990), surface densities for sorption sites on HFO are divided into two types. One type sites correspond to a smaller set of high-affinity cation binding sites, and the density of these sites is determined from sorption isotherms as the sorption density at which sorption becomes less than proportional to dissolved concentration. The range of this type surface charge was 0.001-0.01 mol/mol Fe (for conversions from g/L HFO to mol/L Fe, we assumed the stoichiometry $Fe_2O_3 \cdot H_2O$ (89 g HFO/mol Fe)). Another type of sites ranged from 0.1 – 0.91 mol/mol Fe as the total reactive sites available for sorption of proton, cations and anions as determined from observed sorption maxima. Surface site density also can be expressed

by the unit of sites/nm$^2$ using the following equations for conversion from μmol/mol Fe to sites/nm$^2$.

$$N_S(sites/nm^2) = \Gamma_{\equiv XOH}(\mu mol/m^2) \times N_A(site/mol\ \ of\ site) \times 10^{-24}\left(\frac{m^2}{nm^2} \times \frac{mol}{\mu mol}\right)$$

$$= \Gamma_{\equiv XOH}(\mu mol/m^2) \times 0.6022\left(\frac{site}{nm^2} \times \frac{m^2}{\mu mol}\right)$$

where $N_S$ is site density in the unit of sites/nm2, $\Gamma_{\equiv XOH}$ is the site density in the unite of μmol/mol, and $N_A$ is Avogadro's number ($6.022 \times 10^{23}$). The surface site densities for iron oxides and manganese oxides are summarized in Table 1.10.

Table 1.10. Maximum surface-site densities for iron oxides and manganese oxides.

| Oxides | Surface-site densities (sites/nm$^2$) | Source |
|---|---|---|
| α-FeOOH (goethite) | 2.6 to 16.8<br>18 | Davis and Kent 1990<br>Hsi 1981 |
| α-$Fe_2O_3$ (hematite) | 5 to 22 | Davis and Kent 1990 |
| $Fe(OH)_3 \cdot nH_2O$ (ferrihydrite) | 20<br>18 | Davis and Kent 1990<br>Catts 1982 |
| $MnO_2$ (birnessite) | 2<br>5-7 | Davis and Kent 1990<br>McKenzie 1971 |
| $MnO_2$ (cryptomelane) | 13-15 | McKenzie 1971 |

The manganese oxides posses a pH-dependent surface charge. The point of zero charge of the types of oxides occurring in soil range from 1.5 for birnessite to 4.6 for the hollandite group (Healy et al. 1966). Because of the low PZC, the manganese oxides have a very high negative surface charge in the range of pH values of 6 to 8 found in most of storm water runoff. The total charge on the oxide surface will be determined by the PZC, the pH, and any residual permanent charge associated with the substitution of

$Mn^{2+}$ and $Mn^{3+}$ for $Mn^{4+}$. The PZC of manganese oxides and iron oxides are summarized in Table 1.11.

Table 1.11. The pH of point zero charge of some manganese and iron minerals.

| Oxide | $pH_{PZC}$ | Oxide | $pH_{PZC}$ |
|---|---|---|---|
| $\alpha$-$Fe_2O_3$ ( natural hematite) | 4.2-6.9 | Synthesized birnessite | 1.5-3.0 |
| $Fe(OH)_3$ (amorphous) | 8.5-8.8 | $\alpha$-$MnO_2$ (cryptomelane) | 4.5 |
| $\alpha$-FeOOH (goethite) | 5.9-6.7 | Synthesized cryptomelane | 1.5-2.0 |
| Mn(II) manganite | 1.8 | $\beta$-$MnO_2$ (pyrolusite) | 4.6-7.8 |
| $\sigma$-$MnO_2$ (birnessite) | 1.5-2.8 | $MnO_x$ (general) | 1.5-7.3 |

Sources: Values are from Parks 1965, McKenzie 1981, Sverjensky 1994, and Stumm and Morgan 1996.

### 1.4.3 Cation Adsorption

In the presence of water the surfaces of metal oxides are generally covered with surface hydroxyl group (Stumm and Morgan 1996). While the various surface hydroxyls formed may not be fully structurally and chemically equivalent, but to facilitate the schematic representation of reactions and of equilibria, surface complexation models consider the chemical reaction of one representative surface hydroxyl group, $\equiv XOH$. Surface complexation model are generally used to describe the adsorption behavior in the solid-water interface. According to Dzombak and Morel (1990), the following criteria are characteristic of all surface complexation models:

1. Sorption takes place at specific surface coordination sites;
2. Sorption reactions can be described by mass law equation;
3. Surface charge results from the sorption (surface complexation formation) reaction itself.

4. The effect of surface charge on sorption (extent of complex formation) can be taken into account by applying a correction factor derived from the electric double layer theory applied to the mass law constants for surface reactions.

Iron oxides are one of the most extensively studied oxides for cation adsorption. Adsorption of heavy metal cations can be specific and nonspecific. The nonspecific adsorption of heavy metal cations by iron oxide is an electrostatic (coulombic) binding. The counter ions are treated as point charges to balance the surface charges or the respective charged regions of polarizable molecules held in the outer diffuse electric double layer. Specific adsorption can occur on a neutral surface, or even on a surface with a charge of the same sign as the ion, and can thus reverse the net surface charge, whereas nonspecifically absorbed species cannot. The pH of the PZC for iron oxides generally ranges between 7 and 9 without any marked difference between the various mineral forms (Borggaard 1983), Adsorption of heavy metal cations by iron oxides are mostly due to the specific adsorption of such cation in storm water runoff, which typically has a pH range of 6 to 8. Heavy metals are adsorbed by goethite and hematite in the order of Cu > Pb > Zn > Cd > Co > Ni > Mn except for an interchange in position of Cu and Pb for hematite (Schwertmann and Taylor 1989). Adsorption of heavy metal cations by iron oxide are highly sensitive to pH. As pH increases, a steep rise in adsorption occurs within a narrow pH range. The pH range of maximum increase in adsorption is found to be linearly related the first hydrolysis constant of the metal (Schwertmann and Taylor 1989).

Specific adsorption occurs strongly in all of the cryptocrystalline manganese oxides, regardless of mineral type. Some of the manganese oxide minerals contain foreign ions, which are exchangeable to varying degrees, and differentiation between ions adsorbed on the surface and those in the structural sites is often difficult (McKenzie 1989). In the natural environment, trace metals (Ni, Mo, Cu, Zn, Pb, Cr) can be strongly associated with manganese oxides (Burns, 1976; Crowther *et al*, 1983). Even in the presence of a large excess of indifferent electrolytes, anions of weak acids and weakly hydrolyzed cations are strongly adsorbed on manganese oxides surface. Because of the low PZC, high negative charge, and large surface area of manganese oxides, adsorption can occur in excess of the surface charge. For example, cations may be adsorbed on a positively charged surface and anions on a negatively charged surface (specific adsorption), and the primary adsorption can reverse the net surface charge (McKenzie 1989). The specific adsorption by manganese oxide can be so strong that it is very difficult to differentiate between ions adsorbed on the oxide surface and those ions incorporated into structural sites. Indeed, in some circumstances, it may be that ions initially adsorbed will later become incorporated into these structural sites. For instance, Tsuji and Komarneni (1993) have found that several divalent transition metal ions (Pb, Mn, Co, Cu, Hg, Cd, Zn, Ni) are sorbed within the tunnels of $H^+$-cryptomelane (via charge balancing ion exchange with $H^+$). Studies found $H^+$ forms and $K^+$ forms of cryptomelane have a strong capability of ion exchange within the tunnel, not only with alkaline and alkaline earth cations (Feng *et al.*, 1995; Tsuji and Komarneni, 1993a; Tsuji and Abe, 1985), but also with other divalent transition metal ions (include Pb, Mn, Co, Cu, Hg, Cd, Zn, Ni)

(Tsuji and Komarneni, 1993b; Elabsy *et al.*, 1993; Elnaggar *et al.*, 1993). Even at a pH as low as 2.0, Randall (1998) found that cryptomelane was able to sorb up to two thirds of the available $Cd^{2+}$ in solution. Uptake of such a large amount of $Cd^{2+}$ at such low pH was unexpected, given the fact that the PZC of the material is reported to be 4.5±0.5 (Healy *et al.*, 1966). Using extended X-ray absorption fine structure (EXAFS) spectroscopy analysis, Healy *et al.* found that $Cd^{2+}$ sorption by ion exchange at tunnel sites, rather than adsorption on the amphoteric external surface of cryptomelane, could account for the unexpected adsorption. Heavy metal adsorption on manganese oxide has been studied by many researchers (Appelo, and Postma, 1999; Randall et al., 1998; Mckenzie, 1980a, b, 1981, 1983.), and in general, McKenzie (1980a) had summarized the heavy metal ion adsorption order: Pb > Cu > Mn > Zn > Ni.

# CHAPTER 2. SURFACE CHARACTERISTICS OF SORPTIVE-FILTRATION STORM WATER MEDIA – LOW DENSITY ($\rho_S < 1.0$) OXIDE COATED BUOYANT MEDIA

## 2.1 Introduction

Urban storm water often contains elevated levels of dissolved and particulate-bound metal elements. These metal elements, principally Pb, Cd, Cu, Ni, Zn and Cr can pose acute and chronic threats to receiving water bodies and soils. Unlike organic compounds, metal elements are not degraded in the environment and constitute an important class of contaminants generated by urban activities. For example, for urban highway runoff in Cincinnati, total Zn levels ranged from 15,244 μg/L to 459 μg/L, Cu from 325 μg/L to 43 μg/L, Pb from 88 μg/L to 33 μg/L, Cr from 35 μg/L to 13 μg/L, Cd from 11 μg/L to 5 μg/L as event mean concentrations over a two-year period (Sansalone et al 1997; Sansalone *et al* 1998). Metal elements transported in urban storm water partition into dissolved and particulate-bound fractions as a function of pH, transport residence time and solids concentration. Partitioning data for lateral pavement sheet flow from an urban highway in Cincinnati indicate that dissolved fractions for Cd, Cu and Zn typically exceed 70%, while Pb exceeds 40% (Sansalone et al 1997). Urban storm water in urban residential areas of London was characterized by dissolved fractions for Cd of 69%, Cu of 87%, Pb of 47% and Zn of 82% (Revitt et al. 1990). These partitioning findings for urban areas and the high dissolved fractions for metals have significant implications for the development and selection of effective environmental media as well as in-situ treatment methods.

The deposition and accumulation of dissolved and particulate-bound constituents, metal elements and other constituents result from traffic activities, vehicular component wear, fluid leakage, pavement degradation, and roadway maintenance (Armstrong 1994; Ball *et al.* 1991; Lygren *et al.* 1984; Muschack 1990). Pavement, tire, and vehicular part abrasion are sources of solids, ranging from sub-micron particles to gravel-size aggregates abraded from the roadway surface.

**2.2 Objectives**

In the present research, methods for coating iron oxide and manganese oxide onto polymeric buoyant media (polyethylene spherical beads) were developed. Fundamental analytical techniques were employed to characterize the surface of iron oxide coated polyethylene beads (IOCB) and manganese oxide coated polyethylene beads (MOCB). Comparing media surface characteristics; the goal of this study was to develop a potentially viable buoyant media for heavy metal and particulate removal from storm water using treatment devices such as sorptive buoyant-media clarifiers (SBMC). These objectives were based on previous research indicating the need for such media development and characterization of surface properties based on physical and chemical characteristics of storm water and initial testing of iron coated storm water media at lab and prototype scales (Sansalone et al 1997, Sansalone et al 1998, Sansalone 1999).

**2.3 Previous Work**

Many conventional technologies for removing metals from solution involve precipitation of the metals (typically as oxides, hydroxides, carbonate or sulfides), and

the separation of entrained particulate metals by settling, usually aided by coagulant addition. In neutral to slightly alkaline solutions, iron forms iron oxides that function as adsorbents for many metals. Since adsorptive treatments are most effective with large quantities of adsorbents, increasing the coagulant dose leads to improved treatment efficiency. However, this will add to the cost of sludge disposal and energy requirement. Thus, this method has a practical limitation for treatment of storm water as a waste stream that contains relatively low metal concentrations (typically less than 1-mg/L for many metals except Zn and Cu on an event basis). In natural aquatic systems, iron oxide, manganese oxide and aluminum oxide play controlling roles for heavy metal adsorption (Dong et al 2000; Jenne 1968; Krauskopf 1956). Research has confirmed that iron oxide can remove dissolved heavy metals to a much lower level than that achieved by precipitation (Schindler 1981; Schultz *et al.* 1986; Dzomback *et al.* 1990). Many researchers have studied the adsorptive characteristics of anions, cations and organics onto the metal oxide surface in recent years (Meng and Letterman 1996;Theis *et al* 1992; Mihelcic and Luthy 1986). However, despite the high affinity of iron oxide for metal ions, it has not been widely used as a surface complexation media for storm water, because its physical properties are not conducive to this process. For example, it is bulky, hydrated, amorphous, flocculent material with extremely low hydraulic conductivity. However, iron oxide coated media was developed to overcome this physical limitation.

Coated substrates occur frequently in natural aquatic systems. In soils, metals are released from primary minerals by weathering or originate from the deposition of

translocated substances and lead to particle coatings which consist of clays, iron sesquioxide, calcite, silica and manganese oxides (Fitzpatrick 1980; Robert and Terce 1989). To understand heavy metal chemistry behavior in soil, research has focused on the effect of environmental factors. pH, ionic strength and redox potential have effects on heavy metal adsorption to the oxide surface of many soil types (typically iron oxide, manganese oxide and aluminum oxide) (Ran and Gschwend 1994; Randal and Bruce 1991a, b; Tsadilas et al. 1998; Coston 1995). To facilitate both adsorption and filtration, practical methods of coating iron oxide onto silica sand and other media were developed for storm water treatment (Sansalone 1999). A number of practical pathways to synthesize oxide- coated media can generate a number of different iron oxide minerals. Iron oxide crystal structure, physical and chemical characteristics depend on the preparation temperature, aging time, Fe-to-OH ratio and other parameters (Schwertmann et al 1989). Researchers in other fields found that iron oxide media is an effective heavy metal sorbent (Khaodhiar *et al* 2000; Edwards 1996; Joshi and Chaudhuri 1996; Lai et al 1996; Satpathy and Chaudhuri 1995).

To facilitate surface complexation of heavy metals in storm water by engineered amphoteric oxide-coated media the pH of the storm water must be considered in respect to the point of zero charge (PZC) of the media's surface coating. Controlling pH, synthesizing mineral coatings of the appropriate PZC, or both will enhance removal capability and efficiency of the storm water treatment device. For example, an oxide-coated media surface with a net negative charge is preferred to remove the dissolved heavy metals that exist as cations in the storm water. Negatively charged filtration

media with a PZC sufficiently below the pH of storm water could simplify the design for in-situ storm water treatment by eliminating the need for pH control. Compared to the iron oxide, manganese oxides have a very high negative surface charge in the range of typical storm water pH values (usually pH 6-8). For example, at a pH of 7, a synthetic goethite ($\alpha$-FeOOH) has a positive charge of approximately 0.2 $\mu mol/m^2$, while pure cryptomelane ($\alpha - MnO_2$) has negative charge of 4.0 $\mu mol/m^2$, and birnessite ($\delta - MnO_2$) has a negative charge of 18 $\mu mol/m^2$ (McKenzie 1981; 1989). Therefore, coating manganese oxide onto storm water treatment media surfaces offers potential for heavy metal removal. Although manganese coated media may offer potential for heavy metal removal, no storm water related research has been carried out; in contrast to efforts devoted to development of oxide coating in other environmental fields. Knocke *et al* (1999; 1997a; 1997b; 1996; 1993; 1991; 1988) have studied $Mn^{2+}$ removal from drinking water using manganese coated filter media, carried out characterization of such media (Merkle and Knocke *et al* 1996) while also modeling $Mn^{2+}$ removal (Coffey *et al* 1991).

To examine natural metal sorption processes by soils containing natural iron or manganese oxides, surrogate manganese oxide coating processes were developed for silica sand. Such coatings generated a larger surface area and increased adsorption capability with increasing pH as compared to uncoated silica sand (Stahl and James 1991b). Based on autocatalysis theory of $Mn^{2+}$ oxidization on manganese oxide surfaces, in the presence of a regenerative oxidant such as hypochlorite, oxide-coated media removed soluble $Mn^{2+}$ through an abiotic adsorption and oxidation processes

known as the "natural green sand effect" (NGE). The mineral deposits were developed in situ within weeks to months on new, uncoated filter media during normal filter operation. Merkle and Knocke *et al* (1997a; 1997b; 1996) developed a manganese oxide coating method on anthracite to improve the removal of $Mn^{2+}$ from drinking water and hazardous waste effluent. They generated a filter media with an increased surface area after coating with manganese oxides (from ~0.18 $m^2/g$ to 0.53-0.9 $m^2/g$) and found manganese oxide coated media have the ability to adsorb and coprecipitate a variety of inorganic species. Manganese dioxide coated sand was effective for removal of arsenic from ground water in column experiments (Bajpai and Chaudhuri 1999). However, these manganese oxides have a lower specific surface area than that reported for iron oxides.

Manganese oxide minerals exist in many different forms in nature, ranging from the sheet structures of birnessite and buserite to the tunnel structure of hollandite and todorokite (Golden *et al*, 1987). Birnessite is a layered manganese oxide consisting of octahedral $MnO_6$ units, with exchangeable hydrated ions between layers (such as K- and Na-birnessite). Those mineral structures can undergo ion-exchange reactions, replacing the cations between the layers with other alkali or alkaline earth metal ions as well as protons (Stephanie *et al* 1998). Cryptomelane is a tunnel structure manganese oxide. Studies found $H^+$ forms and $K^+$ forms of cryptomelane have a strong capability of ion exchange within the tunnel, not only with alkaline and alkaline earth cations (Feng *et al.* 1995; Tsuji and Komarneni 1993a; Tsuji and Abe 1985), but also with other divalent transition metal ions (include Pb, Mn, Co, Cu, Hg, Cd, Zn, Ni) (Tsuji and

Komarneni 1993b; Elabsy *et al.* 1993; Elnaggar *et al.* 1993). Even at a pH as low as 2.0, Randall (1998) found that cryptomelane was able to sorb up to two thirds of the available $Cd^{2+}$ in solution. Uptake of such a large amount of $Cd^{2+}$ at such low pH was unexpected, given the fact that the PZC of the material is reported to be 4.5±0.5 (Healy *et al.* 1966). Using extended X-ray absorption fine structure (EXAFS) spectroscopy analysis, Healy *et al.* found that $Cd^{2+}$ sorption by ion exchange at tunnel sites, rather than adsorption on the amphoteric external surface of cryptomelane, could account for the unexpected adsorption. Pure manganese oxide as a filter media is not favorable for both economic reasons and unfavorable physical and chemical characteristics. However, as with iron oxides, coating manganese oxide to a media surface may provide an effective surface and may be a promising media for heavy metal removal from storm water runoff.

In natural soils, manganese oxides are often associated with large amounts of iron oxide. Manganese oxides occur widely as poorly crystalline dark brown to black segregations on the solid particles, in cracks or veins or in the form of nodules (Geenland and Hayes 1983). Burns and Burns suggested that the nucleation and growth of many Mn nodules is initiated by a deposit of ferrihydrite on a nucleating agent, followed by epitaxial growth of manganese oxide (vernadite) and iron oxide (ferrihydrite) on one another. Observations in soils using electronic microprobe analyses (McKenzie 1975) showed that microscopic accumulations of Mn were always accompanied by relatively high concentrations of Fe, and these phenomena suggest that Mn tends to deposit at sites where both Mn and Fe oxides already exit. Iron oxide may

promote accumulation of manganese oxide on the media surface. This suggests that a scratch iron oxide coating on the media may facilitate manganese oxide coating on the media surface.

## 2.3 Methods and Materials

### 2.3.1 Media Coating Methods

A number of manganese and iron synthesis methods were utilized to generate various mineral oxide coatings. For manganese, the specific target minerals were birnessite and cryptomelane because of the combination of surface area and negative surface charge density each provide. For iron oxide, the specific target mineral was ferrihydrite. The polymeric media were round polyethylene beads with a diameter of 2-5 mm ($d_{50}$=3.44 mm) and a mean specific gravity of 0.913.

#### 2.3.1.1 Birnessite Coating Methods (BCM)

The birnessite coating method utilized was a reductive procedure (McKenzie 1971) modified to precipitate colloids of birnessite on the media surface. Two moles of concentrated hydrochloric acid (37.5%) were added dropwise over 20 minutes period to a boiling solution of 0.5-mole potassium permanganate in 1-liter of DI water, where 500-mL filtration media (acid washed polyethylene beads) had already been added and vigorously stirred before adding HCl. After boiling for an additional 10-minutes, the beads were filtered, washed to pH 7.0 using DI water, dried at 25° C, and stored in polypropylene bottles for future use.

### 2.3.1.2 Cryptomelane Coating Method (CCM)

The cryptomelane coating method utilized a wet redox procedure (McKenzie 1971) modified to precipitate colloids of cryptomelane on the media surface. A solution of 0.35 moles of $KMnO_4$ in 800-mL of DI water was heated to 60° C. This solution was added drop-wise over a 20-minute period into a solution containing 0.5 moles of $MnSO_4$ in 1-L of 2-M acetic acid that was heated with 500-mL of filtration media (acid-washed polyethylene beads) to 80°C. After stirring for 15 minutes, the beads were filtered, washed to pH 7.0 using DI water, dried in room temperature, and stored in polypropylene bottles for future use.

### 2.3.1.3 Iron oxide Coating Method (IOCM)

To produce an iron oxide coating, 500-g $FeCl_3$ (or $Fe(NO_3)_3$) were dissolved in 1-L of DI water. The iron solution was mixed with 3-L of acid-washed polyethylene beads and then dried at 90°C for 48-hours. Coated beads were neutralized in 5-L of 5-M NaOH solution for 24-hours and then dried at 90°C for 24-hours. After drying, the coated beads were rinsed with deionized water to pH 7, re-dried at room temperature, and sealed in polypropylene bottles for later use.

### 2.3.1.4 Two Step Coating Method (TCM)

To generate a greater specific surface area, media was first coated with iron oxide as a scratch coating using the iron oxide coating method described above and then coated with manganese oxide either using the birnessite coating method or the cryptomelane coating method. The various coating procedures that were applied to polymeric spherical media are summarized in Table 2.1.

Table 2.1 Media descriptions and coatings

| Media | Description |
|---|---|
| Plain polyethylene beads | Uncoated polyethylene beads |
| IOCB1 (FN) | Iron oxide coated beads using $Fe(NO_3)_3$ as iron source |
| IOCB2 (FC) | Iron oxide coated beads using $FeCl_3$ as iron source |
| MOCB1 (BCM) | Manganese oxide coated bead using birnessite coating method |
| MOCB2 (CCM) | Manganese oxide coated bead using cryptomelane coating method |
| TCB1 (FC+BCM) | Two step coated beads, IOCM then BCM |
| TCB2 (FC+CCM) | Two step coated beads, IOCM then BCM |
| Modified polypropylene beads (MB) | Uncoated modified polypropylene beads |
| MOCMB (BCM) | Manganese oxide coated MB using birnessite coating method |

### 2.3.2. Surface Characterization

#### 2.3.2.1 Specific Surface Area (SSA) and Specific Gravity ($\rho_s$)

SSA measurements were conducted using a modified ethylene glycol monoethyl ether (EGME) method described elsewhere (Carter *et al* 1986; Sansalone *et al.* 1998). Specific gravity analyses utilized helium gas pycnometry and the ASTM standard test method (ASTM 5550-94, 1994) for specific gravity of solids.

#### 2.3.2.2 Surface Charge

Surface charge was measured using a potentiometric titration methodology of Van Raij and Peech (1972). 5-g of oxide coated media were suspended in 20-mL of 0.01-M KCl and the pH increased across a range between 2 to 11 using measured amounts of 0.01-M HCl or KOH. The suspensions were purged with nitrogen gas and sealed. The samples were kept at 25 °C in sealed airtight 50-mL glass beakers and kept mixed on a reciprocating table shaker for 48 hours after which the pH values of the supernatant were recorded. The amounts of $H^+$ and $OH^-$ adsorbed by the oxide coated

media were estimated from the amount of acid or base necessary to bring the samples to the final equilibrium pH, minus the amount necessary to bring 20-mL of a blank solution to the same pH. In each sample series, triplicate samples were prepared for measurement.

**2.3.2.3 Scanning Electronic Microscope (SEM)**

SEM was carried out to obtain media surface topography and morphology information, as well as qualitative chemical composition. Backscattered electron (BSE) imaging can provide direct (but not specific) information on compositional heterogeneity through the mechanism of atomic number contrast, while X-ray area scanning (dot mapping) can provide qualitative abundance information for a specific element (Goldstein et al 1992). SEM samples were dried at 60 °C in an oven for 24 hours, glue-mounted and gold-coated by a vacuum electric arc. Sample cross-sections were embedded in epoxy, ground to a thickness less than 5-μm, polished to 0.05-μm and carbon coated. Standard qualitative elemental analysis of the coatings was carried out using a HNU energy dispersive X-ray spectrometer system (EDS) and associated JSM-840A Scanning Microscope. The chemical compositions and bonding of the coatings in the edge of the thin sections were determined by X-ray area compositional scanning.

**2.3.2.4 Powder X-ray Diffraction (XRD)**

XRD was carried out to identify the structure of the oxide coating. XRD analysis was conducted on coating precipitates. Samples were rinsed with DI water and dried at 60°C for 24 hours. XRD analyses were carried out on a Siemens D5000 diffractometer.

Cu $K_\alpha$ was employed, with a tube current of 40 mA and a tube voltage of 45 kV. The detector was Kevex solid psi. All results were analyzed with a Siemens Diffrac AT V3.1.

#### 2.3.2.5 Infrared Spectrometry (IR)

Diffuse reflection IR spectra of the samples were taken on a Perkins Elmer IR system 1760X FT-IR spectrometer. Samples of the oxide surface coatings were obtained, washed with DI water and dried at 40°C for 24-hours. To investigate the actual morphology on the media surface, coating materials were removed from the coated media surface for FTIR analysis. Dried samples were prepared by encapsulation in a KBr pellet in the ratio of 0.5-mg of oxide mineral to 300-mg of KBr. The metal oxide and KBr were carefully ground and mixed to a uniformly colored powder. The powder was placed in a die with a 13-mm diameter and held under a 10000-kg pressure and under vacuum for 10 to 15 minutes. The transparent pellets were analyzed within 1-hour of the pellet preparation.

## 2.4 Results and Discussion

### 2.4.1 Specific Surface Area and Specific Gravity

Surface roughness is a key factor for determining media filtration efficiency, and in some circumstances it may play a major role for media filtration and adsorption when the charge interaction between the media and particle or ion is unfavorable (Merkle *et al* 1996). Results of specific surface area (SSA) and specific gravity ($\rho_s$) are summarized in Table 2.2. Compared with uncoated polyethylene beads, the SSA values of all oxide-coated media are significantly larger, varying from 2.53 $m^2/g$ for MOCB1 to 27.34 $m^2/g$

for TCB1, while SSA of the uncoated beads were all less than 0.05 $m^2/g$. For single layer coatings, iron oxide coated beads have much larger SSA than those of manganese oxide coated media. For the two layer coatings, the first layer of iron oxide generated a significantly larger SSA for the second layer of manganese (about 7-10 fold SSA increase). Although the reported SSA of synthetic birnessite (32 $m^2/g$) using the same synthesis methods as this study is much smaller than synthetic cryptomelane (222 $m^2/g$), SSA of both MOCB1 and MOCB2 showed no statistically significant difference (T-test, n=3, $p<0.05$ significance level). For a typical mono-media filter beds, if we assume the porosity of the bead bed is 40%, the corresponding surface area concentration would be roughly $1.4\times10^6$ $-1.5\times10^7$ $m^2/m^3$ for a bed of synthetic manganese oxide coated beads (specific gravity = 0.92).

Table 2.2 Specific surface area and specific gravity of media

| Media | SSA ($m^2/g$) | Standard deviation[†] | Specific Gravity ($\rho_s$) | Standard deviation[‡] |
|---|---|---|---|---|
| Plain polyethylene beads | <0.05 | --- | 0.913 | 0.007 |
| IOCB1 (FN) | 16.33 | 0.75 | 0.920 | 0.002 |
| IOCB2 (FC) | 13.92 | 1.30 | 0.921 | 0.004 |
| MOCB1 (BCM) | 2.53 | 0.68 | 0.923 | 0.006 |
| MOCB2 (CCM) | 3.54 | 0.27 | 0.920 | 0.004 |
| TCB1 (FC+BCM) | 27.34 | 1.13 | 0.928 | 0.001 |
| TCB2 (FC+CCM) | 21.17 | 1.23 | 0.926 | 0.002 |
| (MB) | <0.05 | --- | 0.886 | 0.001 |
| MOCMB(BCM) | 2.85 | 0.57 | 0.862 | 0.005 |

[†] The standard deviation base on 3 samples;
[‡] The standard deviation base on 3 samples.

The specific gravity of the uncoated polymeric media ranged from 0.89 to 0.91 while a coating of oxide on the bead surface increased the aggregate bead/coating

density only slightly considering the much higher density of iron oxide or manganese oxide coating. However in both cases the aggregate density of the substrate/coating was less than 1.0. While thicker oxide coating resulted in greater aggregate specific gravity, in all cases the coated media remained as a buoyant media bed in the experimental SBMCs.

### 2.4.2 Surface Charge

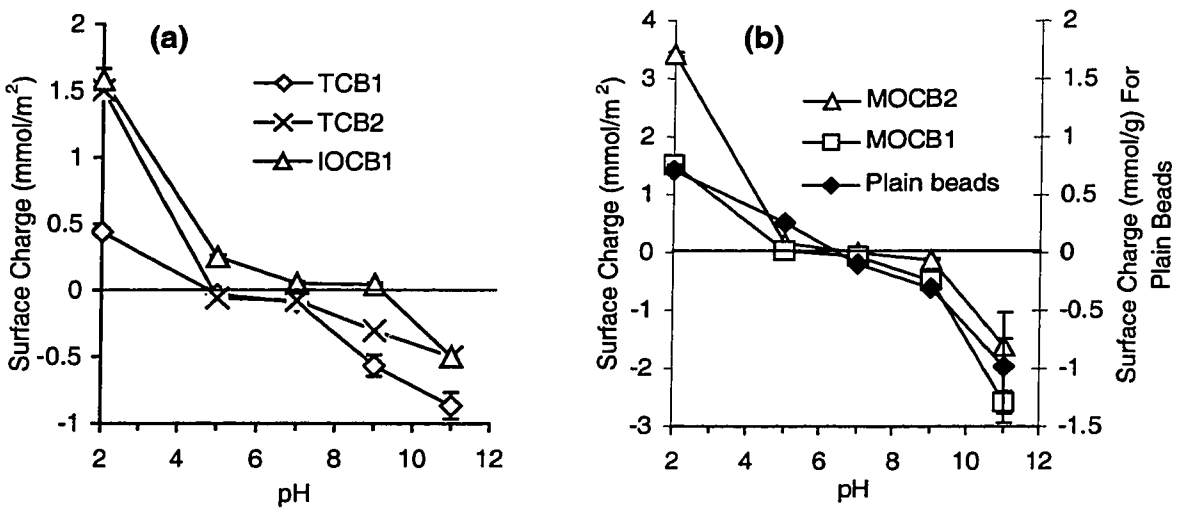


Figure 2.1 Surface charge of oxide coated polyethylene beads, (a) two-step coated beads and iron oxide coated beads; (b) manganese oxide coated beads and plain beads. The surface charge of plain beads is in the unit of μmol/g.

In combination with surface area, surface charge is a critical parameter for heavy metal adsorption or filtration. Even simple electrostatic interaction are sufficient to generally account for differences in observed filtration efficiencies over a range of pH and ionic strength condition for the individual media. The net surface charge of

manganese oxide coated media at different pH values is shown in Figure 2.1. The manganese oxide coated media begin to show a net negative surface charge at a pH level of 6 or greater. Storm water pH values are typically in the range of 6 to 8, generally above most manganese oxide coated minerals PZC values. This would facilitate heavy metal adsorption on the negatively charged media since the target heavy metals in storm water are cations. The design of an adsorptive filter would also take advantage of the net negative surface charge of manganese media with a minimal to negligible need for a pH adjustment unit before the filter. The net negative charge increases sharply with a pH over 9 as well as does the net positive charge in pH less than 5. For iron oxide coated media (polymeric beads), measured PZC were in the range of pH 9.2, and therefore the surface had a net positive charge in the pH range of 6 to 8.

Although the reported cryptomelane and birnessite minerals have a high net negative charge density, for example, at a pH of 7, the net surface charge is 4.0-$\mu mol/m^2$, and 18-$\mu mol/m^2$ respectively (McKenzie 1981; McKenzie 1989); the coated media produced have a lower surface charge density. The heterogeneous coating process may produce some inert surface sites or possibly change the chemical structure of manganese oxide on the polymeric media surface. For instance, powder XRD results indicated that the precipitate in the birnessite coating process has strong peaks of cryptomelane, and this structural and mineral change may reduce the surface charge density. Also, incomplete oxidation of $Mn^{2+}$ may be another reason for the lower surface charge density, because manganese cations can be adsorbed onto the manganese oxide surface very strongly and reduce the available surface sites. The uncoated

polyethylene beads have very little surface charge across the range of pH we tested, since polyethylene has no active functional group and is a non-polar organic polymer molecule.

Table 2.3 Surface charge of oxide coated media (μmol/g)*.

| pH | TCB1 | TCB2 | MOCB1 | MOCB2 | IOCB1 | Plain beads |
|---|---|---|---|---|---|---|
| 2 | 12.015±0.802 | 31.867±1.072 | 3.870±0.305 | 12.094±0.115 | 25.834±1.418 | 0.712±0.042 |
| 5 | -0.910±0.143 | -1.268±0.032 | 0.060±0.001 | 0.534±0.011 | 4.080±0.231 | 0.250±0.014 |
| 7 | -2.502±0.3317 | -1.654±0.014 | -0.194±0.020 | -0.055±0.002 | 0.842±0.191 | -0.093±0.006 |
| 9 | -15.478±2.182 | -6.437±0.760 | -1.207±0.076 | -0.407±0.011 | 0.687±0.227 | -0.301±0.001 |
| 11 | -23.692±2.745 | -10.552±0.569 | -6.542±0.498 | -5.672±0.419 | -8.149±0.653 | -0.988±0.475 |

*All surface charge data here are Mean ± Standard deviation (n=3).

Except for MOCB2, no significant difference ($P<0.05$, n=3) in surface charge density occurred between manganese oxides coated beads at pH 7 when surface charge is expressed as μmol/$m^2$. All beads are of the same spherical shape of nearly the same diameter (3-5 mm), and similar specific gravity, thus, using units of μmol/g or μmol/mL can be better understood as density of media surface site as shown in Table 2.3. In pH 7, two step-coated beads have much higher (8-50 times) surface charge than those of single step coated beads. Higher roughness and more manganese oxide coating of TCB may be the main reasons for this difference. SEM and BSE images that follow verify that, after an iron oxide scratch coating, there is more manganese oxide coated to the beads (a thicker manganese oxide layer can be observed). To investigate whether the coating step or the coating chemical combination makes a better surface coating, ferric chloride was also mixed with potassium permanganate at different ratio in both BCM

and CCM, but the mixture did not adhere to the beads. Therefore, the increase in surface area appears to be a result of the process of coating a layer of manganese oxide onto an iron oxide layer.

### 2.4.3 Powder X-ray Diffraction (XRD)

XRD analyses were also carried out to identify the mineral composition of the coatings. Figure 2.2 illustrates the measured response spectra in comparison to a library simulation pattern shown just above the measured spectra in each figure. In all cases the major peak coincidence and general pattern coincidence can be recognized. Compared with the sample pattern and simulations, the precipitate of cryptomelane coating method matches well with the cryptomelane simulation demonstrating strong peaks at d = 2.4, 3.1, 2.1, 1.8, 4.9, 6.9, 2.4 Å. As shown in Figure 2.2b, the precipitate in the birnessite coating method is mostly cryptomelane but it also has a relatively strong peak at 7.1Å,

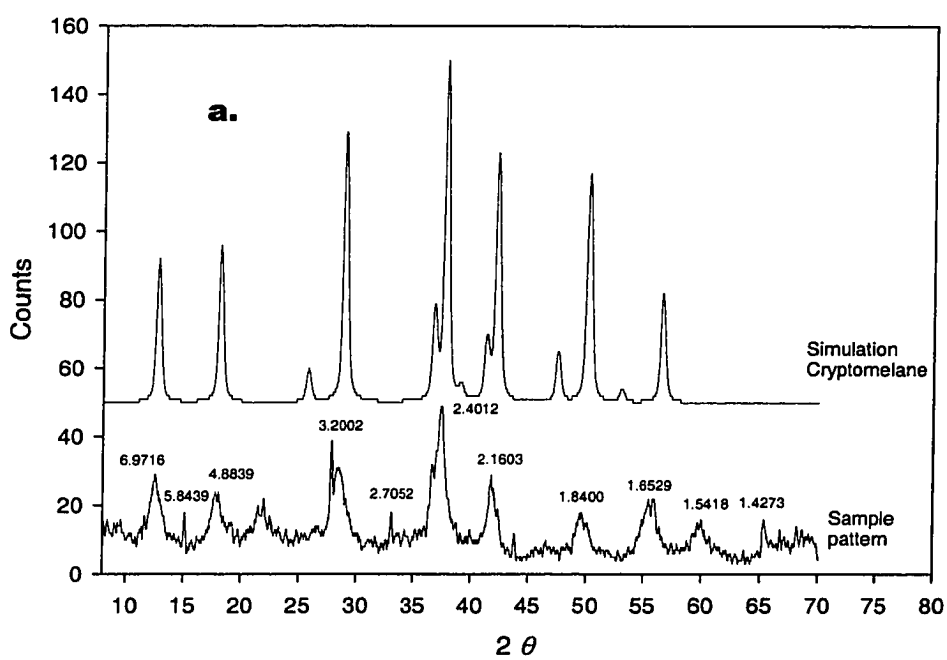

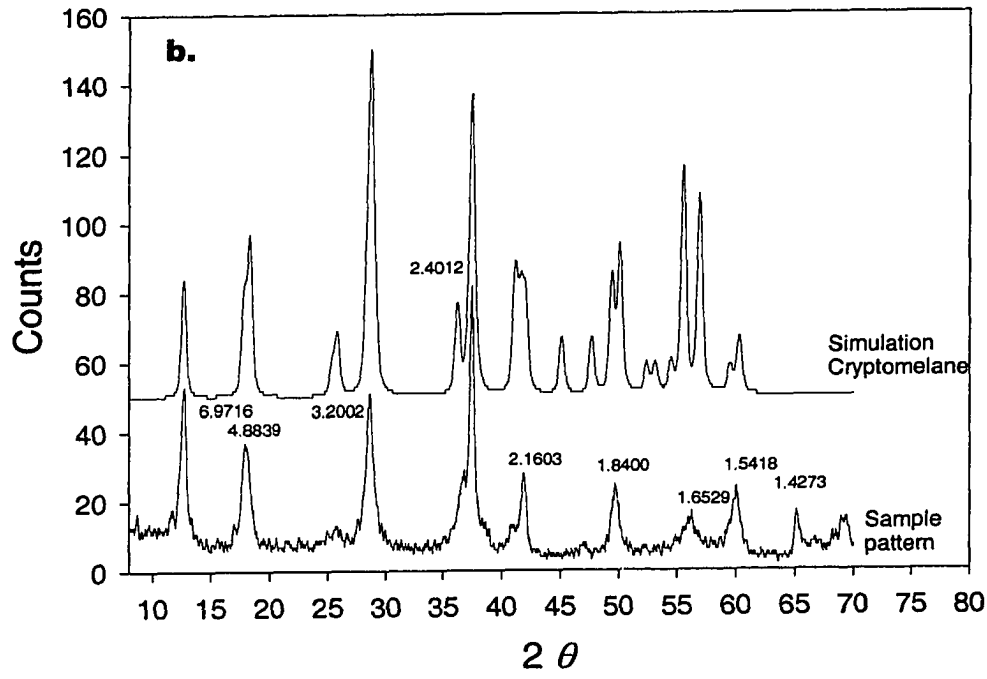


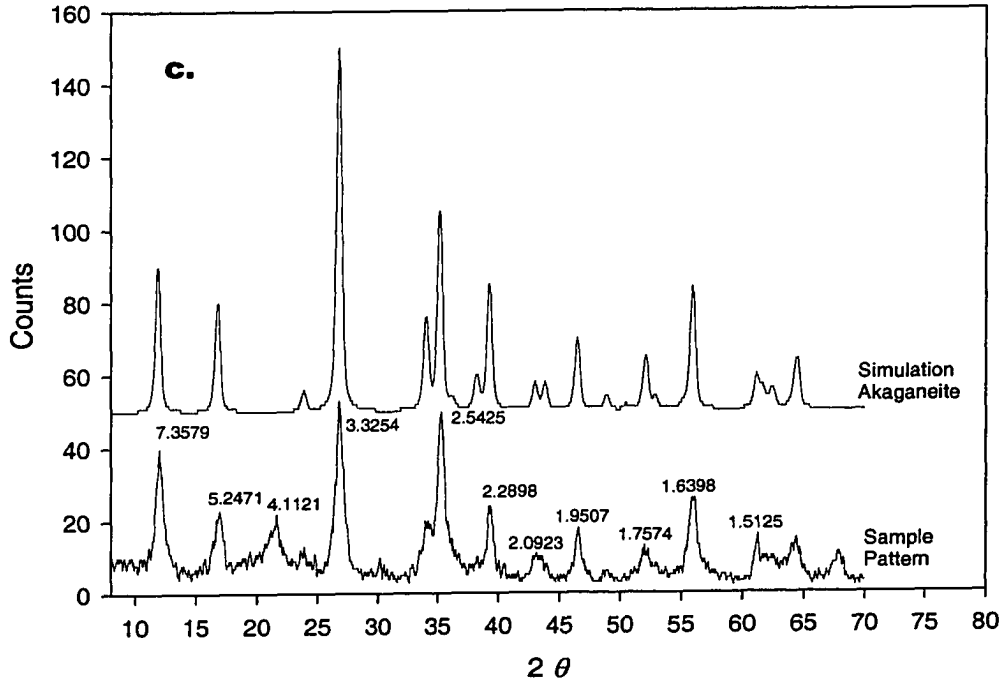

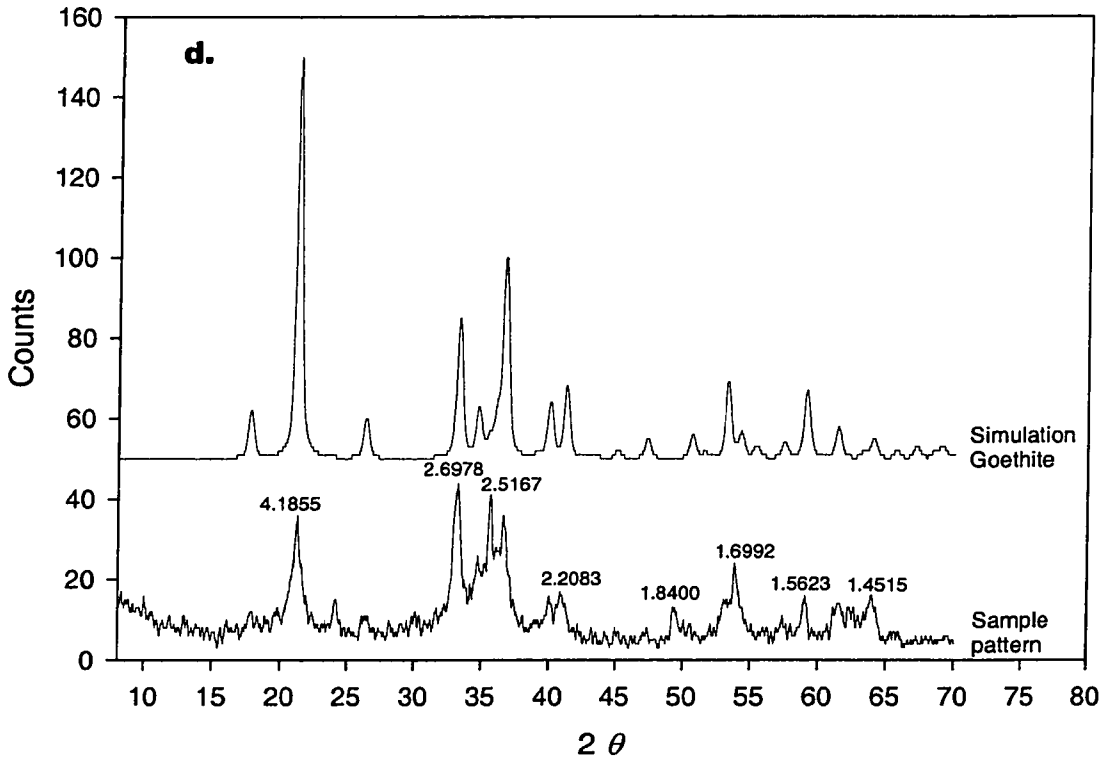


Figure 2.2 a. Simulation of synthetic cryptomelane (JCPDS-ICDD, 1992, PDF-2 Sets 1-42 database) and sample pattern of precipitate using cryptomelane coating method; b. Simulation of synthetic cryptomelane and sample pattern of precipitate using birnessite coating method; c. Simulation of synthetic akaganeite and sample pattern of residuals in iron oxide coating process (using $FeCl_3$); d. Simulation of synthetic goethite and sample pattern of residuals in iron oxide coating process (using $Fe(NO_3)_3$ ).

which is the strongest line of birnessite. It is hypothesized that the manganese oxide structure might have changed from birnessite to cryptomelane due to the solution being heated an additional 20-minutes (compared with the reported birnessite synthesis method). SEM images also reveal the presence of spherical particles, the same as precipitates observed in the cryptomelane coating process. Most of the crystallized

manganese oxides on the bead surface are spheres or needles as indicated in SEM images, a typical morphology of birnessite.

The iron oxide coating produced using $FeCl_3$, as an iron source initially, was akaganeite, an unexpected result. To inhibit such a transformation required control of a number of pathways in the process of going from dissolved $Fe(OH)_x^{3-x}$ to precipitated iron oxide. These included pathways of hydrolysis, nucleation and crystallization (dehydration and crystalline bond rearrangement) to avoid producing akaganeite in favor of ferrihydrite. Therefore a revised coating process for iron was required. Control was facilitated by pH manipulation either by adjusting the pH value > 1 to produce α-FeOOH (goethite) or adjusting pH > 2 to produce ferrihydrite ($Fe_5HO_8 \cdot 4H_2O$) (Schwertmann and Cornell, 1991). The iron oxide coatings using $Fe(NO_3)_3$ produced mainly goethite although the coating process and conditions are the same as that using $FeCl_3$ as an iron source.

**2.4.4 FTIR Spectroscopy Analysis**

Infrared spectroscopic analysis is a complementary tool for mineral determination when combined with XRD. IR spectroscopy is also sensitive to amorphous components and those with short-range order, as well as to more crystalline minerals, and therefore can provide information about materials that are not amenable to XRD analysis (White and Roth, 1986). The major IR spectra bands of IOCB1 coating (Figure 3a) are matched well with those of the synthetic goethite (Schwertmann and Cornell, 1991). The sharp peaks indicate a well-crystallized coating. The sharp and high intensity peaks in the range of 3390-2500 $cm^{-1}$ indicate a strong bonded O-H stretch. As

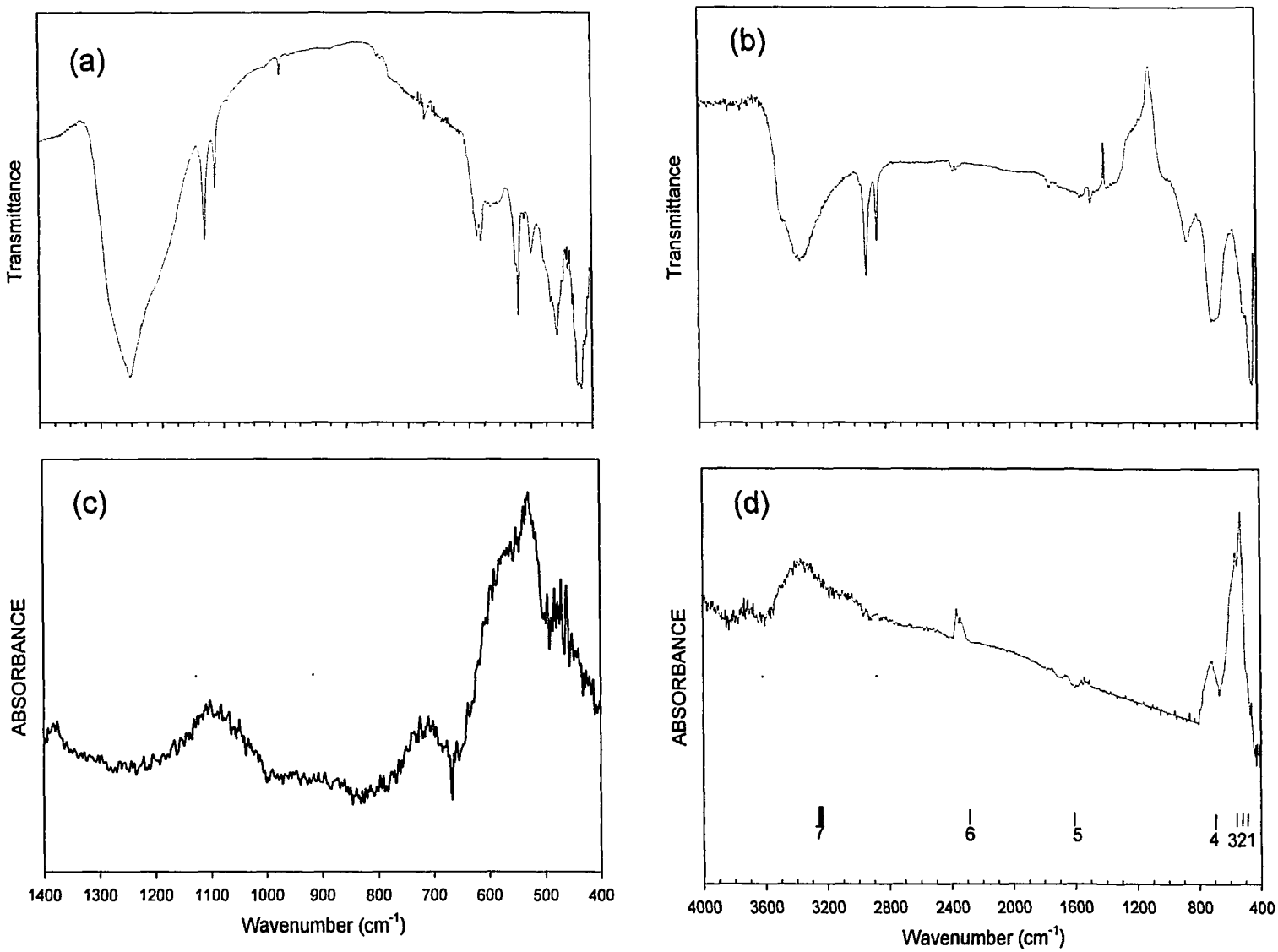


Figure 2.3 IR spectra of (a). IOCB1(FN) coating, (b). IOCB2(FC) coating, (c). BCM coating, and (d). CCM coating.

identified by XRD spectroscopy, IR spectra also demonstrate that the IOCB2 coating (Figure 3b) is akaganeite (compared to the spectra of synthetic akaganeite identified by Schwertmann and Cornell 1991). Strong O-H stretch also was found in the IR spectra of the IOCB2 coating. The IR pattern of MOCB2 (Figure 3c) coating is similar to that of the cryptomelane patterns of Potter and Rossman (1979). The IR spectrum of MOCB2 (Figure 3d) is identical to that of MOCB1 coating, and the two are very similar in the XRD analysis. Bands 1, 2, 3 are analogous to birnessite bands reported by Potter and Rossman (1979), but band 4, located at ~720 $cm^{-1}$, is a band that appears in cryptomelane (Potter and Rossman 1979). This appearance verifies the XRD analysis that indicates that MOCB2 coating probably is a mixture of birnessite and cryptomelane. The intensity of the peaks may demonstrate that the percentage of birnessite may be much more than that of cryptomelane. Band 5 is a weak peak of a $H_2O$ bending vibration. Bands 6 and 7 are indicative of hydroxide in a specific crystallographic site (Potter and Rossman 1979).

### 2.4.5 Scanning Electronic Microscopy Analysis (SEM)

SEM imagines of plain beads and oxide-coated beads are shown in Figure 2.4. Uncoated polyethylene beads have a very uniform surface and almost no roughness over a scale from 2-20 μm. Therefore, using a nominal spherical geometry we can estimate SSA of approximately 0.00022-$m^2/g$, using a mean diameter of 3.44-mm (based on 21 randomized observations, standard deviation is 0.47-mm) and specific gravity of 0.913.

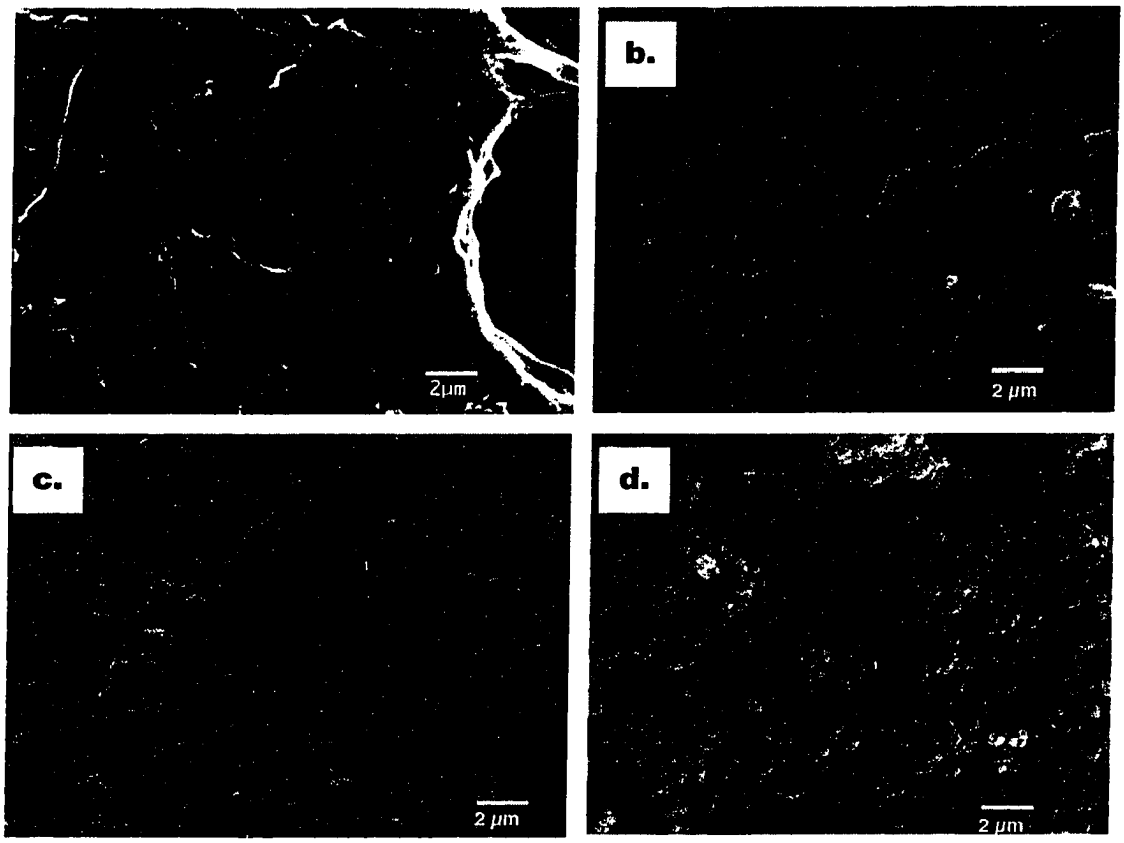


Figure 2.4 a. Uncoated polyethylene illustrating a smooth surface of very low specific surface area; b. & c. Manganese oxide coated polyethylene (MOCB1), with a rough surface, different morphology of manganese oxide; d. manganese oxide coated polyethylene beads (MOCB2), spheroidal particles.

The elements indicated as being associated with specific oxide coatings were detected by the energy dispersive X-ray spectrometer system (EDS) using a standardless qualitative EDS analytical technique. Compared to the very smooth surface of uncoated polyethylene beads, the manganese oxide coated bead surface is very rough with a thickness of 2-30 μm. This explains the much larger SSA of manganese oxide coated beads (2-30 $m^2/g$) than uncoated beads (~0.000224 $m^2/g$). The EDS spectra of MOCB1 indicated that manganese and oxygen were the primary constituents of the

coatings. Varying morphology of the manganese oxide on the bead surface implies a heterogeneous chemical composition. The spherical manganese surface morphology is the same morphology as the SEM images of pure surface precipitate using the cryptomelane coating method. The surface minerals were identified as cryptomelane by XRD and FTIR spectral analysis, and their morphology is that of cryptomelane patches on the top of or mixed with nondescriptive birnessite coatings. The strong birnessite and cryptomelane peaks that occurred simultaneously in the BCM precipitate also verify this. The SEM image of BCM precipitate (Figure 2.5) has the same varied morphology as those of MOCB1.

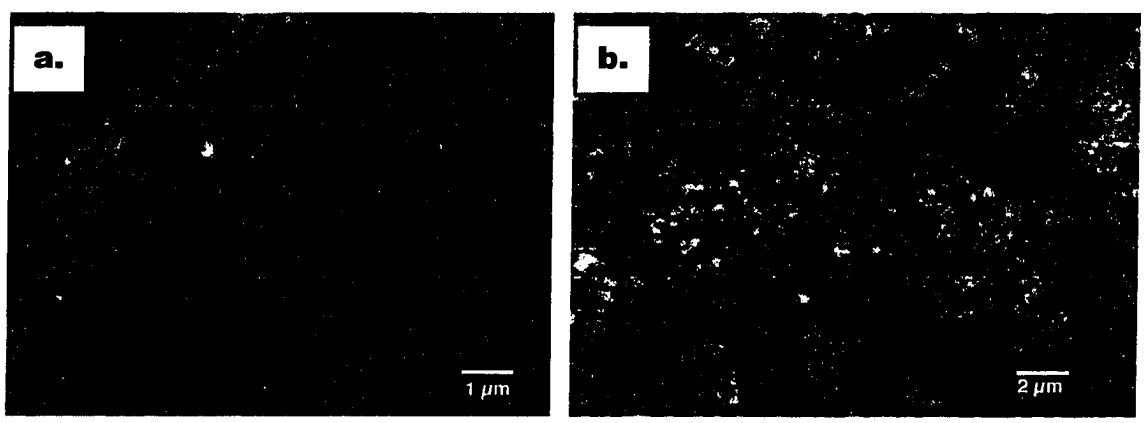


Figure 2.5 (a) Synthetic birnessite, a needle-shape material; and (b) Synthetic cryptomelane, spherical manganese oxide particles on the media surface with a diameter of about 0.25-μm.

On the TCB surface, EDS spectra indicated that the major elements are Mn and O, and Fe was not detected. Those results indicated that manganese oxide completely encapsulated the iron oxide coated surface. The SEM images (Figure 2.6) also provide evidence of the significantly larger SSA of TCB. Even in relatively large scales of 100-

500 μm, a significantly rougher surface can be observed and many more cracks than those of MOCB illustrating a large interior surface area. Beside the surface roughness, more manganese oxide coating on the iron oxide scratch coating may also be an important factor accounting for the larger surface area. Figure 2.7 is the BSE image and X-ray dot map of the polished thin section of TCB2. The BSE image (Figure 2.7a) illustrates two well-defined coating layers: a looser iron oxide layer near the polyethylene surface and a manganese oxide layer with a relatively high density. The coating is not homogeneous, with a thickness from roughly 20 μm to as high as 200 μm (Figure 2.7b). In the outer layer there is a high density dot of Mn (Figure 2.7c) but an expected Fe layer in the dot map of Fe did not occur (Figure 2.7d), although EDS spectra indicated the inner layer is of high Fe content. The likely reason for missing Fe layer is that, because of the rougher surface of the inner layer as a result of the thin section preparation, X-rays were trapped in the inner layer.

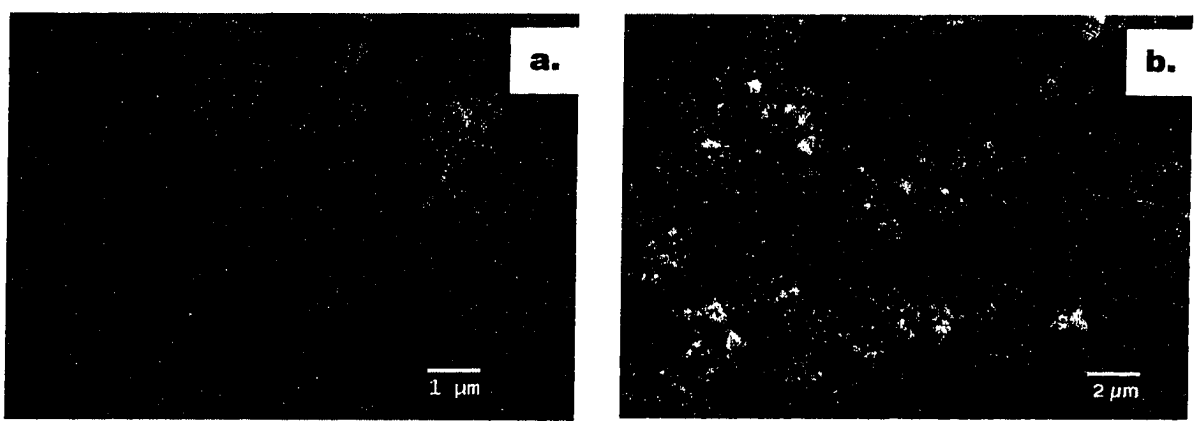


Figure 2.6 (a) Manganese oxide coated polyethylene (TCB1), b. Manganese oxide coated polyethylene beads (TCB2), with spheroidal particles mangenese oxide particles on the surface.

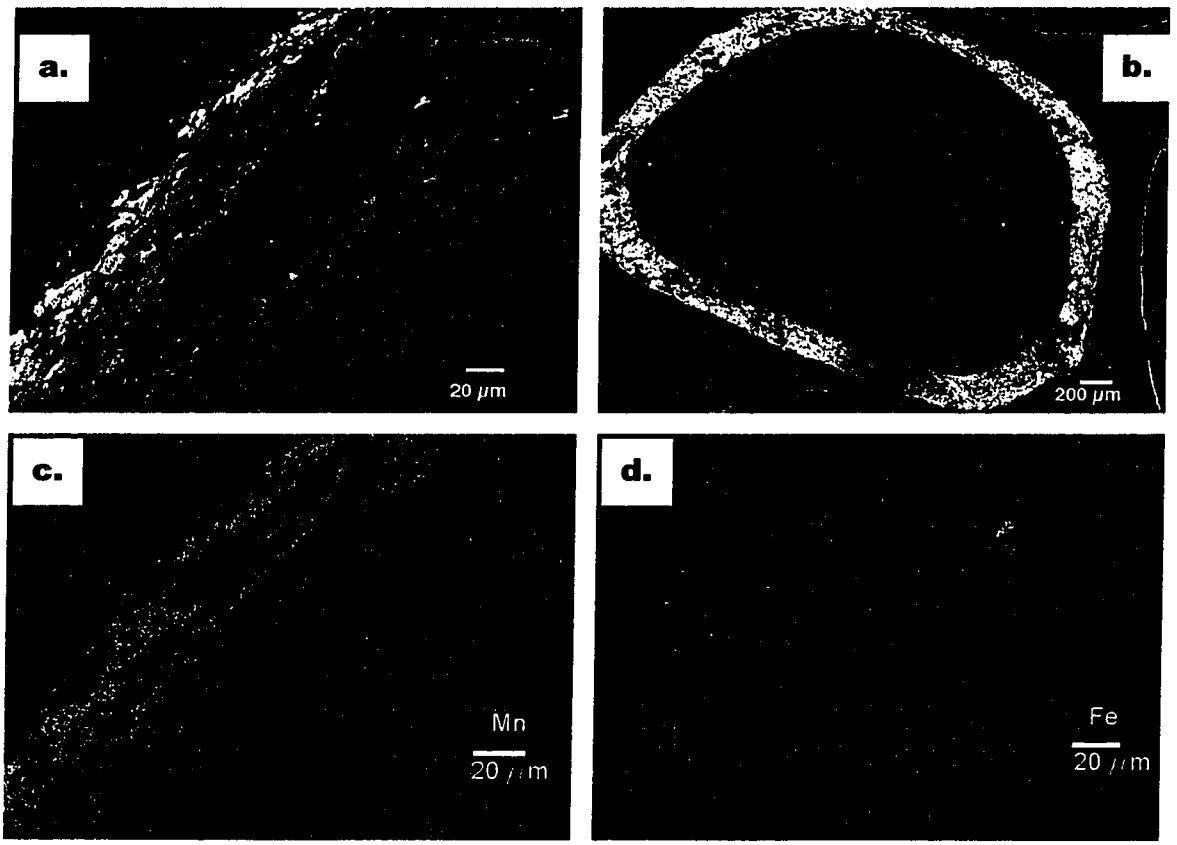


Figure 2.7 (The X-ray mapping area is the same as that of BSE imagine (a)). The density of the white dot illustrating the abundance of the background element.

In the presence of iron oxide, manganese oxide colloids can more readily attach to the higher surface area scratch coating surface. We can hypothesize a two-step coating mode of manganese oxide coating to the iron oxide surface. The first step is that manganese oxide colloids are entrapped by iron oxide until complete encapsulation of the iron oxide surface (both physical and chemical adsorption mechanisms can affect the coating process). We propose the second step to include two mechanisms of sorption. The colloidal manganese oxide is continuously embedded on to the manganese

oxide coating surface, and at the same time a surface oxidation reaction occurs on a fraction of the surface sites as indicated by the following self catalysis model (Coffey *et al*, 1993).

$$Mn^{2+} + MnO(OH)_2 \text{ (or Site-Solid)}_{(s)} \Longleftrightarrow MnO_2MnO \text{ (or } Mn^{2+}\text{-Solid)}_{(s)} + 2H^+ \quad (2.1)$$

$$MnO_2MnO \text{ (or } Mn^{2+}\text{-solid)}_{(s)} + H_2O + MnO_4^- \Longleftrightarrow 4\ MnO_2 \text{ (or Site-Solid)}_{(s)} + 2H^+ \quad (2.2)$$

In the first step, the manganese oxide coating on the beads surface is the controlling step (the rate is much lower than the oxidation step as compared to the manganese oxide adsorbed by an initially oxide coated surface). Therefore an iron oxide scratch coated bead provides a much more effective surface. More manganese oxide creates more surface area on the media surface. Merkle et al (1996) had found that media surface area has a linear relationship with extractable manganese content (SSA = 1.25(extractable Mn, mg/g media)-4.07, $R^2$=0.97). This also supports the result of larger SSA on the TCB media.

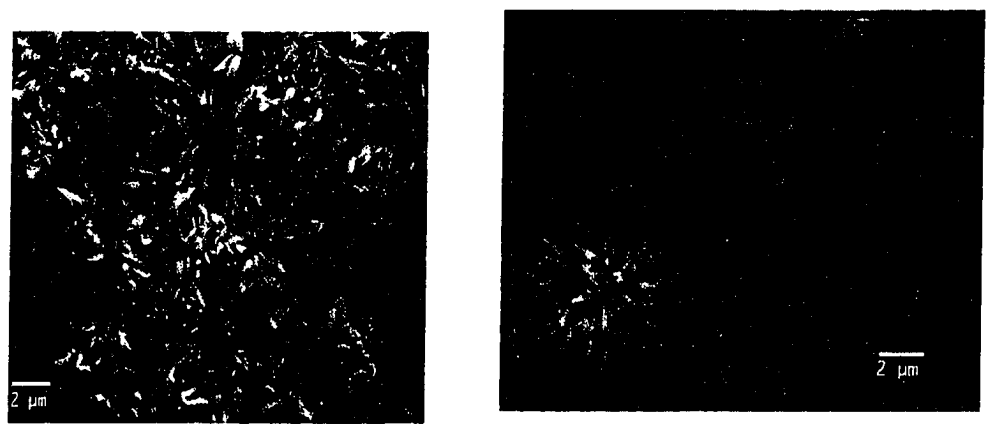


Figure 2.8 Iron oxide coated polyethylene beads with a rough surface of needle-shaped goethite crystal covering the surface; The large and highly ordered akaganite crystaline surface underneath the needle shape crystal and create significant internal surface area. An area of amorphous ferrihydrite can be observed in the very top of the SEM on the right.

Figure 2.8 illustrates the surface morphology of iron oxide coated beads. The coating can be described as large and highly ordered crystalline (Fe, Cl and O are the major elements by EDS analysis) sparsely covered with needle shaped iron oxide crystals (Fe, Si and O are primary element by EDS analysis.). SEM imaging also provides evidences of larger SSA of IOCB than MOCB. Compared to the manganese oxide coating, it is a thicker and rougher coating with many cracks on the surface with a thickness of 20-100 μm. The thicker and rougher coating provides morphology conducive to filtration.

**2.5 Conclusions**

The SSA of all oxide-coated media varied from 2.53-$m^2/g$ for MOCB1 to 27.34-$m^2/g$ for TCB1, while SSA of uncoated beads is always less than 0.05-$m^2/g$. An iron oxide scratch coating significantly increases SSA for the two-step coated beads, increasing the SSA by a factor of 7 to 10. The manganese oxide coated media (TCB1, TCB2 and IOCB1) generated a net negative surface charge in the range of pH 5 to 7, which is a lower pH value than the typical storm water pH values in the range of 6 to 8. The design of adsorptive filtration systems such as an upflow SBMC or designs such as a downflow PER could also take advantage of negatively charged media with no need for a pH adjustment unit before the filter.

Using powder XRD and FTIR spectroscopy, the surface coatings produced by each method were analyzed. The manganese oxides of MOCB2 and TCB2 (using CCM) are poorly crystallized cryptomelane, and the manganese oxide of MOCB1 and TCB2 (using BCM) poorly crystallized mixtures of birnessite and cryptomelane. For

iron oxide coated beads, IOCB2 ($FeCl_3$ as iron source) is an akaganeite coating, and IOCB1 ($Fe(NO_3)_3$) is a goethite coating. Although akaganeite is an unexpected oxide coating, it is an effective scratch coating for manganese based on the results of SSA and surface charge of the final coating. Coating of iron oxide using $FeCl_3$ is a practical choice, since $FeCl_3$ is more economical than $Fe(NO_3)_3$ and available as a waste-byproduct.

Using SEM images, SSA differences for different coating methods can be observed, and EDS provides both qualitative element identification and structure information of the coating. SSA and part of the surface charge result can be interpreted from the SEM analysis. Thin section BSE and dot mapping demonstrate 20-100-μm-manganese oxide coating thickness for MOCB1 and 20-200 μm oxide coatings for TCB2.

# CHAPTER 3. SURFACE CHARACTERISTICS OF SORPTIVE-FILTRATION STORM WATER MEDIA –HIGHER SPECIFIC GRAVITY ($\rho_S > 1.0$) OXIDE COATED FIXED MEDIA

## 3.1 Introduction

In-situ treatment design for pavement storm water runoff continues to pose unique challenges due to the unsteady nature of processes including rainfall runoff, mobilization, partitioning and delivery of heavy metals. Storm water from urban areas and roadways transports dissolved, colloidal and suspended solids in a heterogeneous mixture, and with additional parameters of pH, alkalinity, traffic levels and residence time, influences the partitioning of heavy metals. Results from partitioning analysis between the dissolved and particulate-bound fractions indicate that Zn, Cd, Cu and Pb mass are predominately dissolved in urban pavement sheet flow ($q_{sf}$) for residence times less than several hours at pH levels between 6 and 7.5 (Sansalone and Glenn 2000). These high dissolved fractions can be attributed to low urban rainfall pH levels (between 3.5 to 5.5), pavement residence times for $q_{sf}$ of less than 2-hours and low pavement runoff alkalinity, less than 50-mg/L as $CaCO_3$ (Sansalone *et al* 1997).

There are no simple solutions for the removal of a heavy metal or particle once released in the urban storm water environment, and there are best management practices (BMPs) that can be misapplied for the intended purpose, unfortunately at a significant cost. BMPs for heavy metals and solids are essentially garbage cans and as such they must be emptied and cleaned occasionally. The purpose of design is to provide effective capture, reasonable time between media backwashing or replacement and an optimal cost between treatment alternatives.

Unit processes for in-situ storm water heavy metal removal or partitioning must be based on an understanding of the unsteady hydrology and flow-regime hydraulics, water chemistry (particularly pH, alkalinity and redox potential), particulate matter, competing solute species such as chlorides, urban residence time parameters, and constraints of the urban environment. Unit processes such as adsorption and precipitation onto high surface area materials or unit operations such as filtration can represent a viable storm water treatment for dissolved heavy metals and particulate-bound heavy metals, respectively. In natural waters and storm water runoff, the transport and eventual fate of heavy metals is controlled by reactions with solid surfaces. Surfaces of natural mineral oxides and oxide-coated media can serve as reservoirs for heavy metals and are characterized by large surface area to solid volume ratios. In the presence of water, oxide surfaces such as Mn and Fe are covered with surface hydroxyl groups, protons and coordinated water molecules. Surface complexation of metal ions (cations) by hydrated oxides involves coordination of metal ions with surface hydroxyl atoms and also proton release from the surface (Stumm 1992).

These mineral surfaces are amphoteric with protons and hydroxyl ions co-existing at the surface in relative populations determined by solution pH. For example, the sorption of a metal ion to the hydrous oxide surface (manganese and iron) is strongly pH dependent. This amphoteric behavior leads to the point of zero charge (PZC) definition. The PZC in its most simple definition is the pH at which the net surface charge is zero. For example, since many iron oxides have a PZC typically

above 7 (in contrast most manganese oxides have a PZC between 3 and 6), a storm water solution pH greater than 7.0 can result in a predominance of negatively charged surface sites while a solution pH less than 7.0 would result in an increasing amount of positively charged surface sites at least for Fe-oxides. This leads to the idea that engineered amphoteric oxide coated surfaces on storm water filter media can have large surface areas for adsorption and precipitation processes in a chosen pH range.

Therefore engineered media such as the oxide coated filter sand or cementitious media with high surface area and amphoteric surface charge can be utilized to carry out the combined unit operations of filtration and processes of surface complexation for a range of treatment configurations for either decentralized treatment or centralized treatment. Such treatment can be designed as a passive and integral part of existing urban infrastructure, for example urban and transportation infrastructure, or can be designed as a centralized storm water treatment component.

**3.2 Objectives**

There were four objective of this research. The first objective was the development of coating methods for manganese oxides onto silica sand and cementitious media (generated from concrete). The second objective was to provide a fundamental characterization of the resulting surface produced from those methods. The third objective was to provide a comparison between coatings properties for various manganese coatings on silica sand and various manganese coatings or admixtures for cementitious media. Based on these characterizations, examinations and comparisons, the final goal of this study was the selection of a preferred coating method and a preferred media with a specific

gravity greater than 1.0 for utilization in combined unit operations and processes for adsorption and filtration of heavy metals in urban storm water. This final goal provides a critical foundation for ongoing research in the development of media for in-situ sorptive-filtration for storm water such as a downflow partial exfiltration reactor (PER), or a fluidized or upflow sorptive buoyant media clarifier (SBMC).

### 3.3 Background and Previous Study

Previous research with respect to performance of iron oxide-coated media for sorptive-filtration of storm water has demonstrated proof-of-concept for such media and systems such as a PER applied as a full-scale passive treatment system in the urban environment (Sansalone 1999). Based on initial studies of surface characterization and controlled treatment performance of oxide-coated (iron and manganese) on sand (Sansalone 1996) or other substrates, it was determined that a more rigorous synthesis of oxide-coated media and more fundamental characterization of these media should be carried out as a foundation for assessing mechanisms of heavy metal and particulate removal from storm water. Results from this previous work (Sansalone 1996; Sansalone 1999) demonstrated two important conclusions; namely that uncoated silica sand media (Ottawa 2030) has insignificant surface area ($< 0.1$ $m^2/g$) and is ineffective for removal of storm water heavy metals, and secondly that cementitious media such as graded concrete media can be an effective media for heavy metal removal both uncoated and especially with an oxide coating.

The utilization of oxide-coated media for heavy metal removal has parallels in nature that include both iron and manganese coatings on soils (Sansalone 1996). The

focus of this study is manganese oxide coatings. Generally, most manganese oxides can conveniently be classified in two major structures, tunnel structures or layer structures, which account for their different physical and chemical characteristics. The tunnel structures are formed from single, double, or wider chains of $MnO_6$ octahedra that are linked, by sharing corners, into a framework of enclosed tunnels throughout their structure (McKenzie 1989). Large foreign cations and water molecules occupy these tunnels. Ramsdellite and cryptomelane belong to the tunnel structure manganese oxide family.

The second major structural classification of manganese oxides is layer structures. Birnessite is a layered manganese oxide consisting of octahedral $MnO_6$ units, with exchangeable hydrated ions between layers (such as K- and Na-birnessite). Layer structures can undergo ion-exchange reactions, replacing the cations between the layers with other alkali or alkaline earth metal ions as well as protons (Stephanie *et al* 1998).

In the natural environment, trace metals (Ni, Mo, Cu, Zn, Pb, Cr) can be strongly associated with manganese oxides (Burns 1976; Crowther *et al* 1983). Even in the presence of a large excess of indifferent electrolytes, anions of weak acids and weakly hydrolyzed cations are strongly adsorbed on manganese oxides surface. Because of the low PZC, high negative charge, and large surface area of manganese oxides, adsorption can occur in excess of the surface charge—i. e., cations may be adsorbed on a positively charged surface and anions on a negatively charged surface (specific adsorption), and the primary adsorption can reverse the net surface charge (McKenzie 1989). The specific adsorption by manganese oxide can be so strong that it is very difficult to differentiate between ions adsorbed on the oxide surface and those ions incorporated into structural

sites. Indeed, in some circumstances, it may be that ions initially adsorbed will later become incorporated into these structural sites. For instance, Tsuji and Komarneni (1993) have found that several divalent transition metal ions (Pb, Mn, Co, Cu, Hg, Cd, Zn, Ni) are sorbed within the tunnels of $H^+$-cryptomelane (via charge balancing ion exchange with $H^+$). Heavy metal adsorption on manganese oxide has been studied by many researchers (Appelo and Postma 1999; Randall et al. 1998; Mckenzie 1980a; 1981b; 1981; 1983), and in general, McKenzie (1980a) had summarized the heavy metal ion adsorption order: Pb > Cu > Mn > Zn > Ni.

Using a wet oxidation procedure, manganese oxide colloids can be precipitated onto the soil surface (Stahl and James 1991; Golden *et al* 1986). Stahl and James made manganese oxide coated soil (birnessite-hausmannite-coated soil) with a surface area of 5.4-$m^2$/g, extractable Mn of 2-mg/g sand and PZC of 3.6. The surface area was not significantly different from uncoated soil. The manganese oxide coating was found to promote Zn retention. Bajpai and Chaudhuri (1999) used a similar method to coat manganese dioxide onto silica sand by oxidation of manganous ion with permanganate to yield coated sand with extractable Mn of 0.1-mg/g. However, none of these media were used to study heavy metal removal through column experiments. To obtain a practicable and effective filtration media for heavy metal removal, many of these coating methods require improvement (larger SSA and more manganese oxide coating).

Greensand is a glauconite mineral treated with $KMnO_4$, and typically used in a fixed-bed contactor as a primary unit process to remove dissolved $Mn^{2+}$ in drinking water treatment. In the presence of oxidants, such as free chlorine, $Mn^{2+}$ can be removed

autocatalytically by the manganese oxide coated media through an abiotic sorption and oxidation process known as the natural greensand effect (NGE) (Knocke et al 1990). Based on Nakanishi's (1967) model, the overall reaction of NGE was described by Coffey *et al* (1993) as follows:

$$Mn^{2+} + MnO(OH)_{2(s)} + HOCl + H_2O \Leftrightarrow MnO_{2(s)} + MnO(OH)_{2(s)} + 3H + Cl^- \ Mn^{2+} \quad (1)$$

Using those naturally oxide coated media, soluble manganese removal was extensively studied (Knocke *et al* 1991; 1990; 1988; Merkle *et al* 1997a; 1996; Coffey *et al* 1993). By simulating this "naturally" occurring process, Merkle et al (1997b) developed a method to coat anthracite and sand with synthetic manganese oxides. Four qualitative aspects were noted as the critical conditions for a successful coating. 1). Potential adsorption sites are needed for raw media to initiate the process; 2). Initial manganese oxide coating would promote and establish autocatalysis on the media surface; 3). Homogeneous $Mn^{2+}$ oxidation must be minimized; 4). pH needs to be controlled to produce a pH of ~7.0 to avoid both homogeneous $Mn^{2+}$ oxidation above a pH of 9 and low pH generated by oxidation. The manganese oxide coated media have manganese oxide encapsulation thickness up to 30-μm with 4-mg/g extractable Mn. The media were evaluated with a laboratory-scale column test for Mn removal capability, and results indicated that the coating method might help improve the removal of $Mn^{2+}$ from drinking water.

Scanning electron microscopy (SEM), powder X-ray diffraction (XRD) and infrared spectroscopy (FTIR) are fundamental analytical techniques for analyses of oxide coatings. These analytical techniques provide extensive details of surface chemical and

physical characteristics of the oxide coating that are critical parameters influencing adsorption and filtration capability of the media. Using these techniques, Merkle *et al* (1996) analyzed the naturally oxide-coated anthracite and sand from different treatment facilities and found $MnO_{x(s)}$-bearing coatings and other mineral deposits can be of importance for a variety of filtration phenomena. They also found that these analytical techniques provide a foundation for model development and evaluation of fundamental filtration theory and filter surface chemistry for storm water.

Silica sand is a common conventional filter media and research media because of its economy, inertness and availability. Because of poor performance of plain silica sand for heavy metal adsorption and filtration, modifications are needed for storm water treatment (Sansalone 1996; Sansalone 1999). While there is a significant database for aqueous heavy metal treatment by iron oxide-coated sand for waste streams other than storm water, there is no database on the oxide (manganese or iron) coating of cementitious media or its performance for treatment of urban storm water. Cementitious media can be generated from concrete rubble or recycled concrete. The idea of using cementitious infrastructure material or recycled cementitious material is based on three advantages. First, cementitious media usually can create an alkaline aqueous environment since calcite ($CaCO_3$), portlandite ($Ca(OH)_2$) and calcium silicate hydrate are major components of the concrete, and all contribute alkalinity. This alkaline environment will not only improve the heavy metal removal efficiency by precipitation of dissolved metals, but also benefit from the electrostatic interaction between the manganese oxide and dissolved cationic heavy metal, because manganese oxides have larger negative surface charge in higher pH

solutions. Another advantage is the rough surface, and the use of dilute aqueous admixtures (such as manganese solution) to the initial water-cement-sand mixture offer promise for cementitious materials produced as such sorptive-filtration media. In addition, a highly alkaline layer of cementitious media provides strong oxidation reactions near cementitious surfaces because the oxidation reaction is favored when the pH is above 9 and thus homogenous oxidation would be minimized.

### 3.4 Methods and Materials

#### 3.4.1 Media Preparation

Silica sand was obtained from Industrial Sand Co. Inc., Baton Rouge, LA. The chemical composition of the silica sand was 99.48% $SiO_2$, 0.21% $Al_2O_3$, and 0.06% $Fe_2O_3$. The sand ($d_{50}$ = 1.19-mm) had a 12 mesh (1.68-mm) to 20 mesh (0.85-mm) gradation with a measured specific gravity of 2.65. The sand was soaked in 8% trace metal nitric acid solution for 24 hours, rinsed with deionized water (18.2 MΩ) to pH ~7, and dried at 105°C in preparation for surface coating.

There were two basic methods for applying manganese to the cementitious matrix. Manganese oxide was either applied as a surface coating or integrated into the cementitious matrix as an admixture in place of water. The cementitious media was made by mixing Type I cement, water (or manganese admixture) and sand aggregate. The mass ratio of water-cement-sand was 1.5-1-2. After mixing with DI water, the slurry was cured 24 hours at 25 °C, and crushed to between No. 8 mesh (2.38-mm) and No. 20 mesh (0.85-mm) sizes with a resulting $d_{50}$ of 1.41-mm. Control cementitious media was rinsed with DI water, dried at 60 °C and used as control media without a

manganese coating or a manganese admixture. As an admixture, manganese oxide was integrated into the cementitious matrix as part of the mixing and curing process. This method of adding manganese oxide produced a cementitious media using the same mass ratios of water-cement-sand with the water replaced by a manganese oxide (cryptomelane) emulsion (containing about 0.5-M manganese). This cementitious slurry with the manganese admixture was cured and sized using the same procedure for the control cementitious media. All cementitious media and coating descriptions are summarized in Table 3.1.

### 3.4.2 Media Coating Methods

#### 3.4.2.1 Manganese Oxide Coating Methods (MOC)

Surface coating methods were modified based on the surface characterization results of Merkle et al (1997). Schematic coating system was show in Figure 3.1. 1-kg of dry media (silica sand or cementitious media) were coated in a reaction column (5.08-cm ID and 60-cm length). A 6-L solution containing $10^{-3}$ M $HCO_3^-$ and 0.035 mol/L $Mn^{2+}$ was recirculated in the column using a saltwater pump at a flow rate that fluidized the media bed. $Mn^{2+}$ was oxidized by adding 250-mL 0.185-M NaOCl at a flow rate of 5-mL/minute for 50 minutes. The solution was recirculated again for 2-hours through the fluidized media, drained from the column and replaced with DI water in sufficient volume to cover the media. 250-mL 0.185-M NaOCl was again added in one step, and the solution was re-circulated for 15-minutes. The column was drained and the media was rinsed with DI water to pH 7 and dried at 25°C overnight before final use.

Table 3.1 Media and media coating descriptions

| Media Designation | Coating | Admixture | Water-cement-sand ratio (mass basis) | Size gradation | $d_{50}$ (mm) | Notes |
|---|---|---|---|---|---|---|
| Plain Sand | No coating | No admixture | - - - - | 12-20 mesh | 1.19 | Control |
| MOCS sand | Manganese oxide | No admixture | - - - - | 12-20 mesh | 1.19 | Experimental |
| BCS sand | Manganese oxide | No admixture | - - - - | 12-20 mesh | 1.19 | Experimental |
| Cementitious | No coating | No admixture | 1.5-1-2 | 8-20 mesh | 1.41 | Control |
| $Concrete_{(ad)}$ | No coating | Manganese oxide | 1.5-1-2 | 8-20 mesh | 1.41 | Experimental |
| $MOCM_{(ad)}$ | No coating | Manganese oxide | 1.5-1-2 | 8-20 mesh | 1.41 | Experimental |
| MOCM | Manganese oxide | No admixture | 1.5-1-2 | 8-20 mesh | 1.41 | Experimental |

Plain sand: Silica sand
MOCS: Manganese oxide coated sand
BCM: Birnessite coated media
Cementitious: Portland cement concrete crushed and sieved to designated size gradation
$Concrete_{(ad)}$: Manganese oxide emulsion admixture used in place of water (no coating)
$MOCM_{(ad)}$: Manganese oxide coated concrete with manganese oxide admixture used in place of water (no coating)
MOCM: Manganese oxide concrete (no admixture)

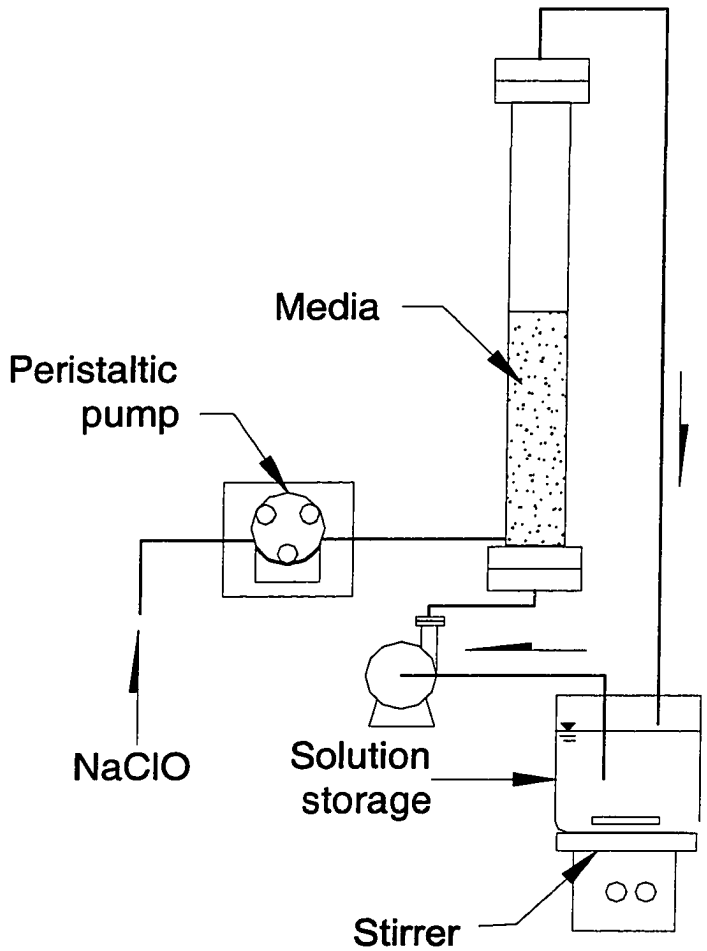


Figure 3.1 Schematic manganese oxide coating system

### 3.4.2.2 Birnessite Coating Methods (BCM)

The birnessite coating method utilized was a reductive procedure (McKenzie 1971) modified to precipitate colloids of birnessite on the media surface as described in Part I.

### 3.4.3 Characterization

Characterization methods utilized for SSA, specific gravity ($\rho_s$), powder x-ray diffraction (XRD), infrared spectroscopy (FTIR) and scanning electron microscopy (SEM) were described in chapter 2 with the following exceptions. For XRD analysis,

surficial material was taken from the surface coating precipitate. Cementitious media was ground to a very fine powder (< 1-μm) for analyses.

### 3.5 Results and Discussion

#### 3.5.1 Scanning Electron Microscopy Analysis

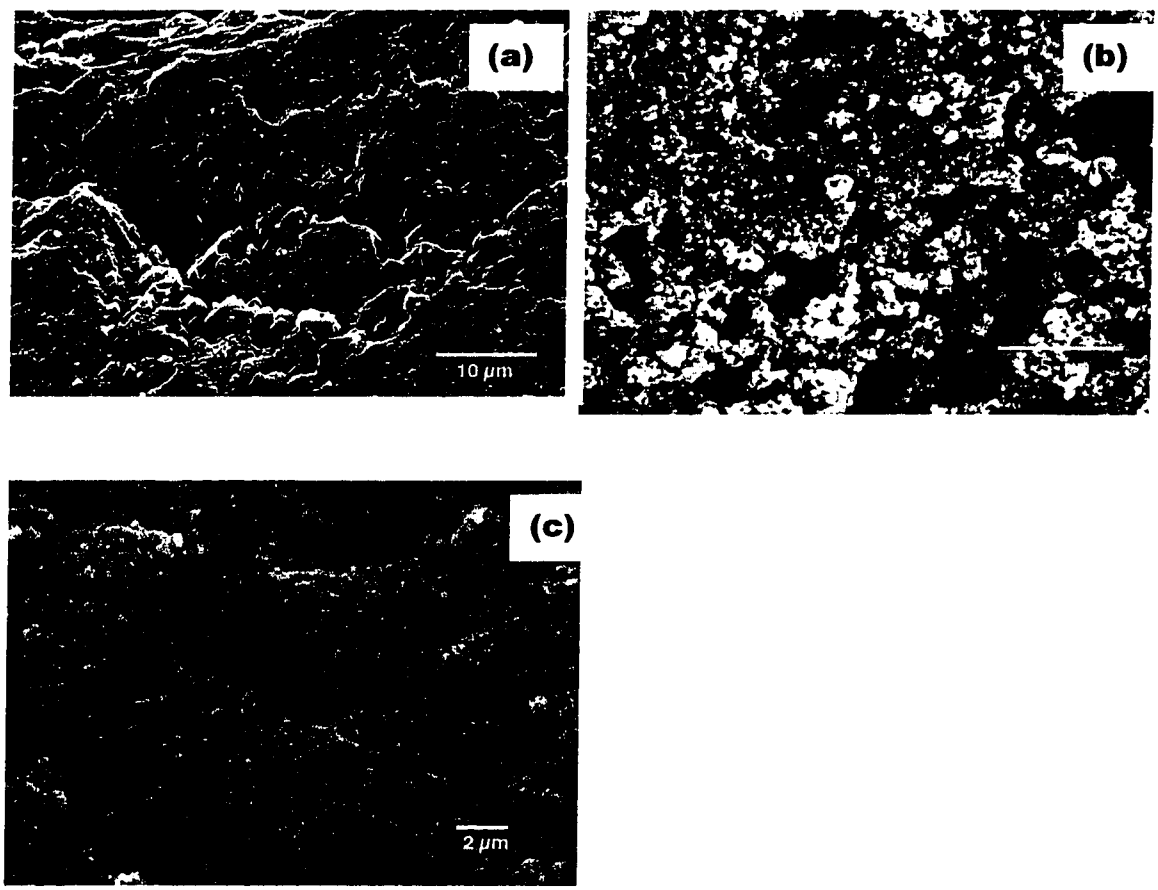


Figure 3.2 SEM imaging of plain silica sand and manganese oxide-coated sand. (a) plain sand with silica crystal on surface; (b) manganese oxide coated sand (using NGE method), porous manganese oxide surface reveals a nondescriptive morphology; (c) manganese oxide coated sand (using birnessite coating method), spheroidal particles (about 0.25-micron diameter) on sand surface.

SEM images of acid-washed uncoated silica sand shown in Figure 2a show very ordered silica crystals at the surface. Qualitative energy dispersive X-ray spectrometer (EDS) analysis reveals that the primary elements are Si and O. On the MOCS sand surface, a layer of porous oxide particles was deposited in the coating process. The qualitative EDS spectra for these particles indicate that Mn, O, Na and Si are the main constituents. Although the silica sand surface may lack the adsorption and catalysis sites to initiate the MOC process, internal bonding of minerals that intersect the sand grain surface may serve as nucleation sites for initiation of manganese oxide coating growth. Inner-sphere and outer-sphere complexation models (Stumm 1992) can be utilized as explanations for the initiation of coating growth. A porous manganese oxide coating would facilitate the adsorption of heavy metals and trapping of the particles.

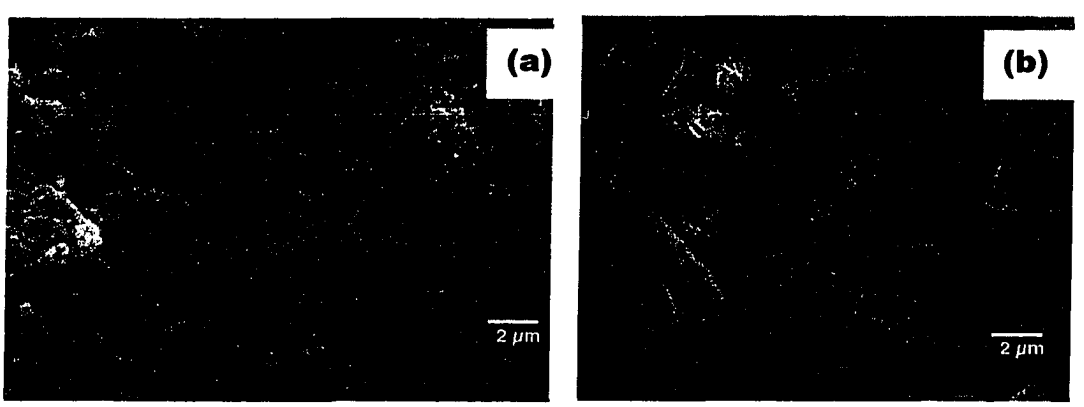


Figure 3.3 (a) Uncoated concrete illustrating a rough surface with $Ca_xAl_ySi_zO_l$ crystal; (b) Manganese oxide coated concrete using MOC method, illustrating a very uniform surface covered with mixture of Calcite and manganese oxide which appears as ball between the platelets.

Compared to the nearly complete manganese oxide coverage of the MOCS sand, the manganese oxide coated sand using the birnessite coating method (BCM sand) resulted in a less complete coverage by spherical manganese oxide particles of about 0.25-μm diameter at the scale of 1-20 μm as shown in Figure 3.2c. Both MOC sand and BCM sand have a significantly rougher surface than plain sand, and this is evidenced by the much larger specific surface area of the manganese oxide coated sand.

Figure 3.3 illustrates an SEM image of cementitious media without manganese oxide admixture (Figure 3.3a) and manganese oxide coated cementitious media using the MOC method (Figure 3.3b) (MOCM). The uncoated cementitious media (Figure 3.3a) had a non-uniform surface, and the different crystal morphologies, determined by qualitative EDS analyses, indicate chemical heterogeneity of the cementitious surface containing the primary constituents Ca, Al, Si, O. This chemical heterogeneity of uncoated concrete implies the fact that there may exist a larger number of surface sites for the initiation of the MOC procedure. The MOCM surface appears smooth and uniform at low magnification, while at higher magnification, it appears as numerous smaller particles (needle or platelet aggregated together to form spherical-shaped particles) in-filled among the larger crystals of calcite. Weathered cement materials contain calcite, particularly on the surface, due to the reaction of basic calcium compounds with atmospheric $CO_2$. The presence of calcite as part of the coating implies the reaction with $CO_{2(g)}$ is continuous during and after the coating process. Qualitative EDS determined the chemical compositions, and XRD spectra of the coated surface showed strong calcite peaks as discussed latter. The EDS spectra of those particles

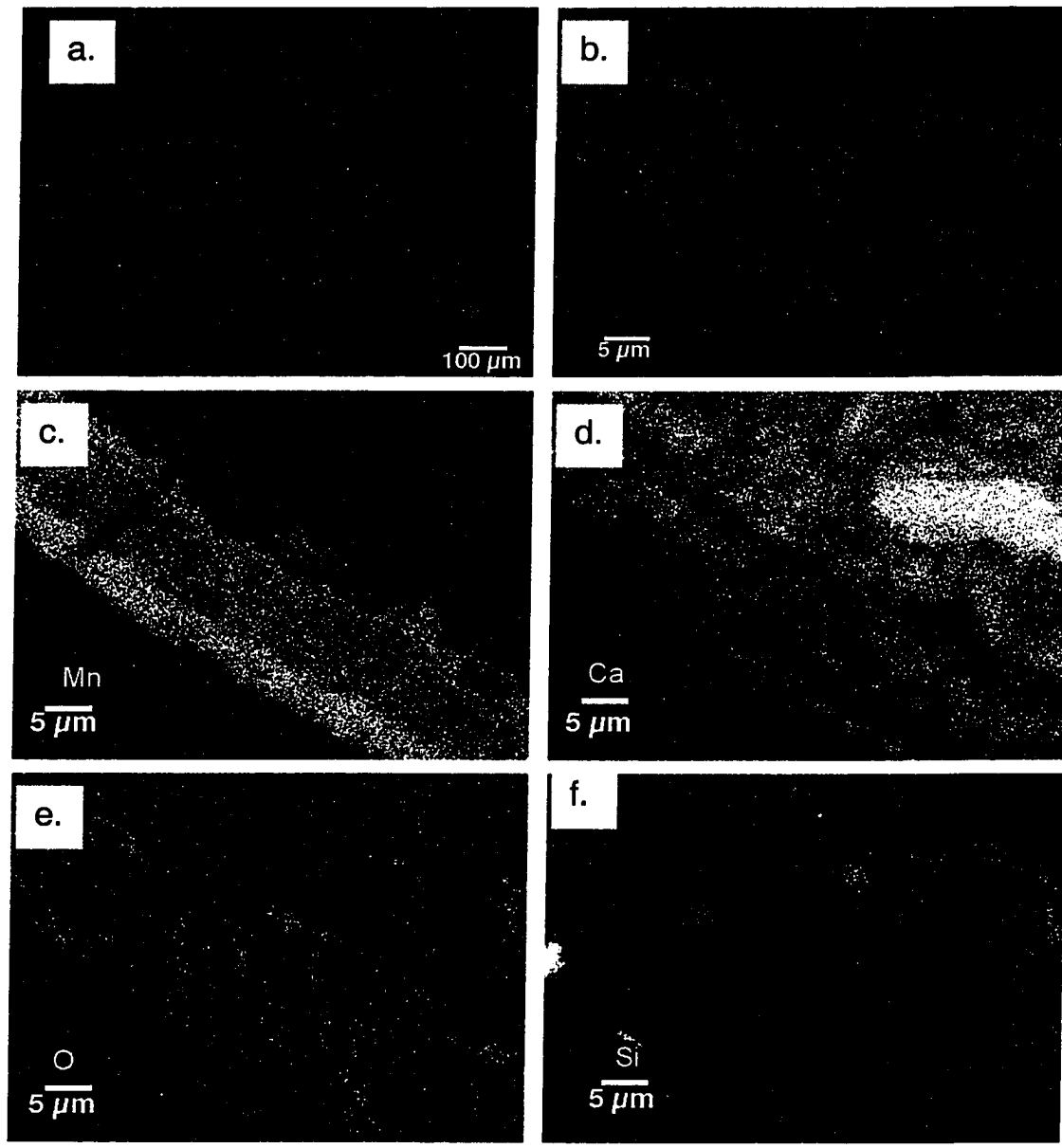


Figure 3.4 a.& b. BSE of the polished cross section of MOCM. The manganese oxide appears as bright areas. 4 c, d, e & f. X-ray mapping of the MOCM (the same area as the BSE illustrated in (b)). The densities of the white dot illustrate the abundances of the mapping element.

primary elements. Backscattered electron (BSE) images of polished cross sections in Figure 3.4a and Figure 3.4b reveal a manganese oxide-coating layer with a thickness of 10-30 μm.

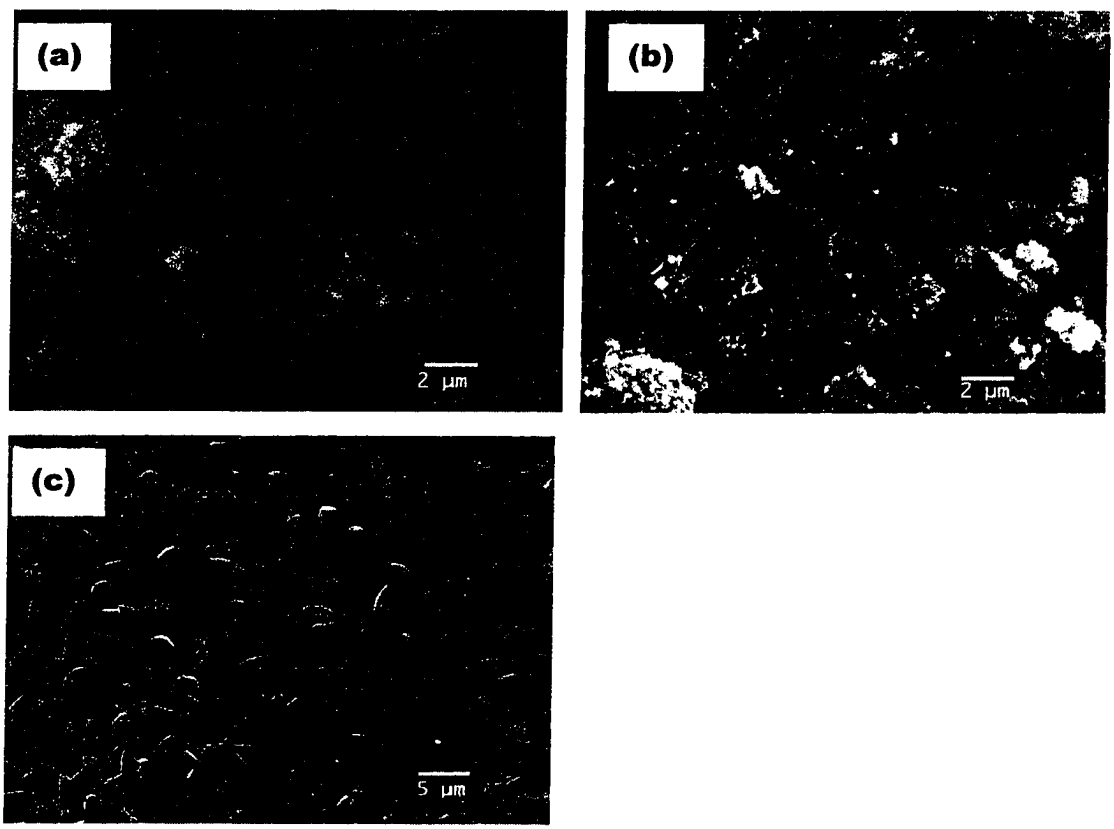


Figure 3.5 (a) & (b) uncoated concrete with synthetic cryptomelane admixture illustrating two different surface morphologies. (c) Manganese oxide coated concrete using MOC coating method, illustrating a relatively uniform surface which is a mixture of calcite and manganese oxide, as balls or needle.

Dot mapping (or X-ray area scanning) can provide an indication of the qualitative abundance of mapping elements. A layer of manganese oxide coating is clearly shown in the dot map for Mn in Figure 3.4c, and a high density of white dots

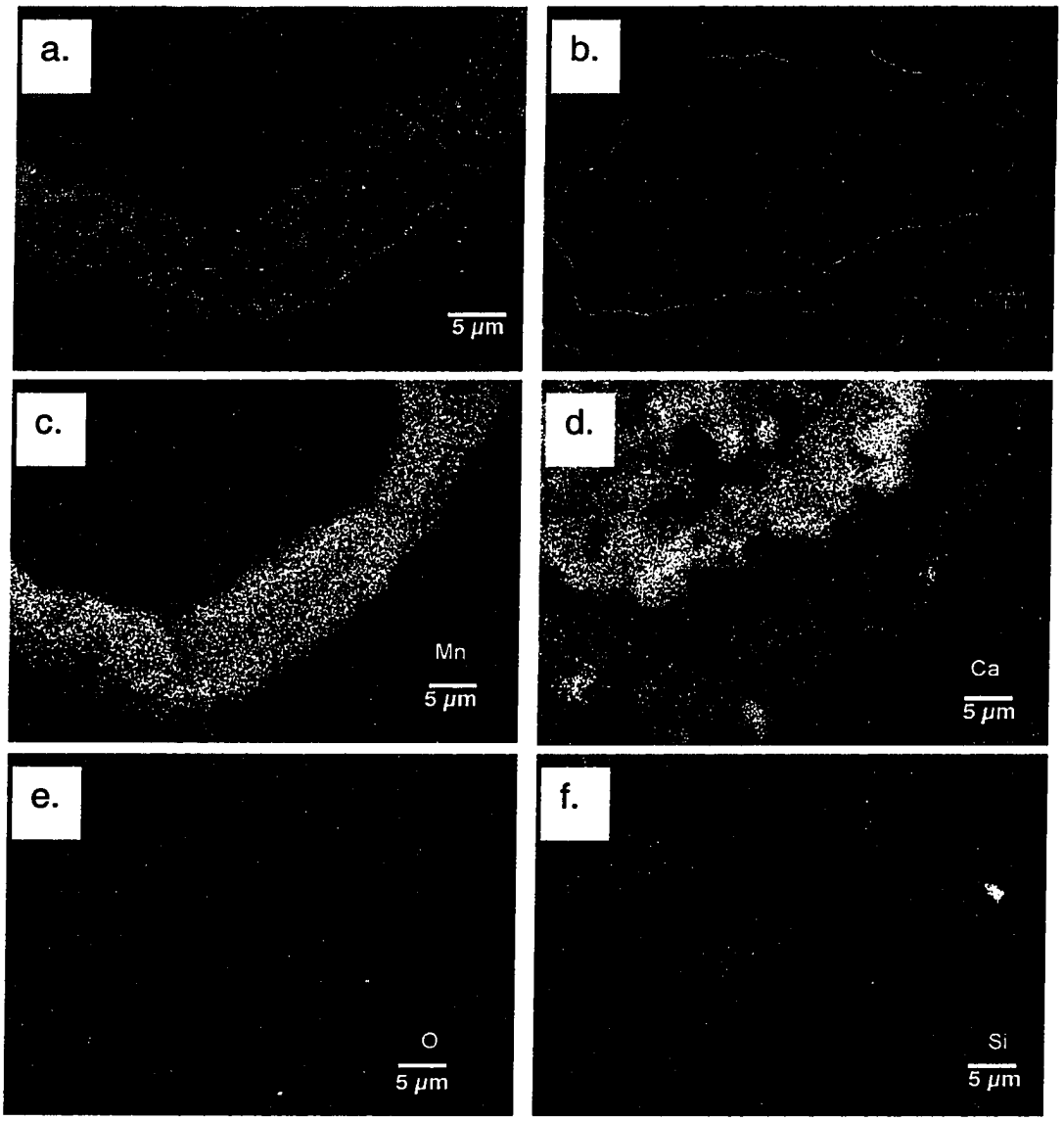


Figure 3.6 a.&b. BSE of the polished cross section of MOCM(ad). The manganese oxide appears as bright areas. 6 c, d, e & f. X-ray mapping of the MOCM(ad) (the same area as the BSE in (a)). The densities of the white dot stand for the abundances of the mapping element.

indicates manganese is the most abundant element. This indicated that the manganese oxide coating layer has completely encapsulated the cementitious media surface. As shown in the dot map for Ca in Figure 3.4d, another important element in the coating

layer is Ca, which is present as calcite. Based on information from the dot map, the MOC coating layer contains the primary element Mn, Ca, and O. Associated crystal morphology analyses indicate that the bright outer layer is mainly a mixture of manganese oxide and calcite.

To add initial manganese oxide adsorption sites to the cementitious media surface, synthetic manganese oxides (the oxide is cryptomelane as identified by powder XRD spectra) were added as a water-based admixture when cement was mixed with fine sand. The SEM images of this uncoated cementitious media (Figure 3.5a and 3.5b) with a Mn admixture (MOCM $_{(ad)}$) illustrates different surface morphologies, and the main constituents are Ca, Al, Si, O and Mn. The morphology of MOCM $_{(ad)}$ illustrating balls and needles in Figure 3.5c is similar to that of MOCM, which is a mixture of calcite and manganese oxide. Comparing the BSE images and dot maps of MOCM and MOCM $_{(ad)}$ in Figure 3.6, the manganese oxide coating layer, including the additional coating thickness, reveals no significant difference. This demonstrates that the manganese oxide admixture does not change the chemical composition of the concrete media, and it also does not cause more manganese oxide deposition onto the concrete surface. The surface chemical heterogeneity between manganese oxide and calcite would facilitate heavy metal adsorption because $CaCO_3$ will create a relatively high pH solution layer around the media thus creating a high pH environment in a packed or fluidized filtration bed. Heavy metals such as Pb and Cu could be easily precipitated and other heavy metals captured on the sorptive filter media through surface complexation mechanisms. Another important benefit is the higher negative surface

charge on manganese oxide obtained with the increase of the pH on the media surface layer. The hypothesized adsorption mechanism is depicted schematically in Figure3. 7.

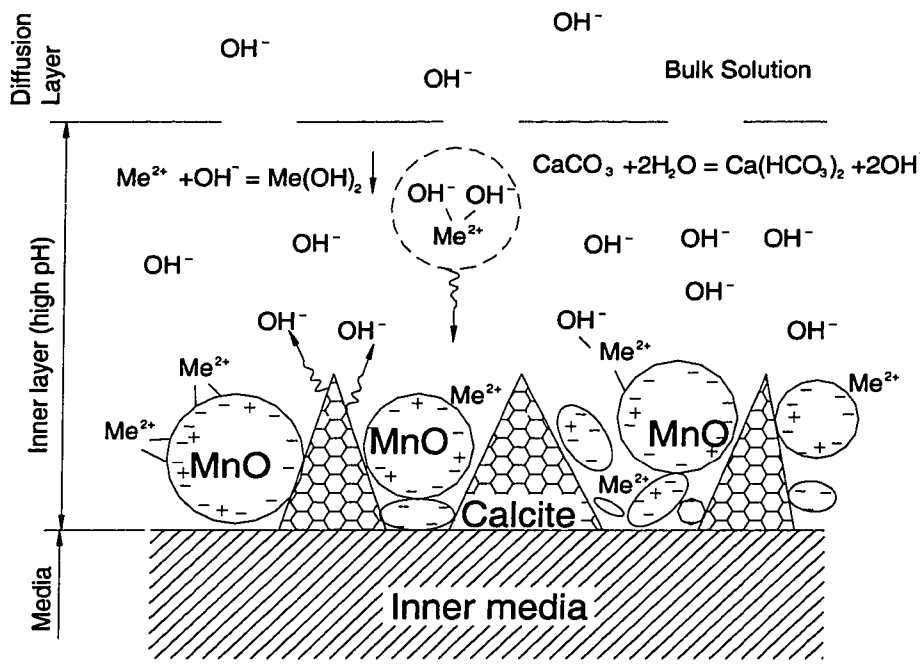


Figure 3.7 Schematic of surface complexation metal removal mechanisms by manganese oxide coated concrete.

### 3.5.2 Powder X-ray Diffraction Analysis

The precipitate in the "birnessite" coating method is basically cryptomelane as shown in Figure 3.8a, but it also has a relatively strong peak at 7.1Å, which is the strongest line of birnessite. This indicates that the manganese oxide in the birnessite coating process is probably a mixture of a birnessite type (layer structure) and a cryptomelane type (tunnel structure). This change may be caused by an additional heating time of 20-minutes (compared with the reported birnessite synthesis method). SEM images also reveal the presence of spherical particles, the same as the precipitates

observed in the cryptomelane coating process. The XRD spectra of MOC precipitate is difficult to identify because of line broadening, which can be caused by a number of factors, such as disorder, small crystallite size and cation substitution. However, all strong lines of the spectra match those in ramsdellite (7-222, JCPDS-ICDD, 1992, PDF-2 Sets 1-42 database) as shown in Figure 3.8b. Ramsdellite is the stoichiometric manganese dioxide with a chain of $MnO_6$ octahedra, and it is considered to have a tunnel structure (McKenzie, 1989). To investigate the actual manganese oxide coating on the cementitious surface, fine cementitious media < No. 100 mesh (150-μm), were coated using the NGE method and analyzed using XRD. Very strong lines of quartz and calcite were present, and also lines of ramsdellite and hausmannite were found in the spectra. Hausmannite is a lower oxide, $Mn_3O_4$. It contains divalent and trivalent Mn and is formulated as $Mn^{2+}(Mn^{3+})_2O_4$. The presence of hausmannite indicated that there is incomplete oxidation in the NGE process. As discussed above, the high pH environment would promote the oxidation reaction, and $OH^-$ would neutralize $H_3O^+$ produced in the oxidation reaction, forcing the equilibrium in equation (1) to the right. Based on this assumption, the presence of the lower oxide $Mn_3O_4$ seems unreasonable. However, in the initiation of the coating, $Mn(OH)_2$ and other lower valence manganese ion possibly are the major manganese species adsorbed or precipitated on the concrete surface because such a strong alkaline layer is created near the concrete surface. The adsorption of $Mn^{2+}$ is so strong that the competition of $Mn^{2+}$ between adsorption and oxidation may cause an incomplete oxidation of manganese oxide species if we consider adsorption as a surface complexation reaction (Stumm and Morgan, 1995).

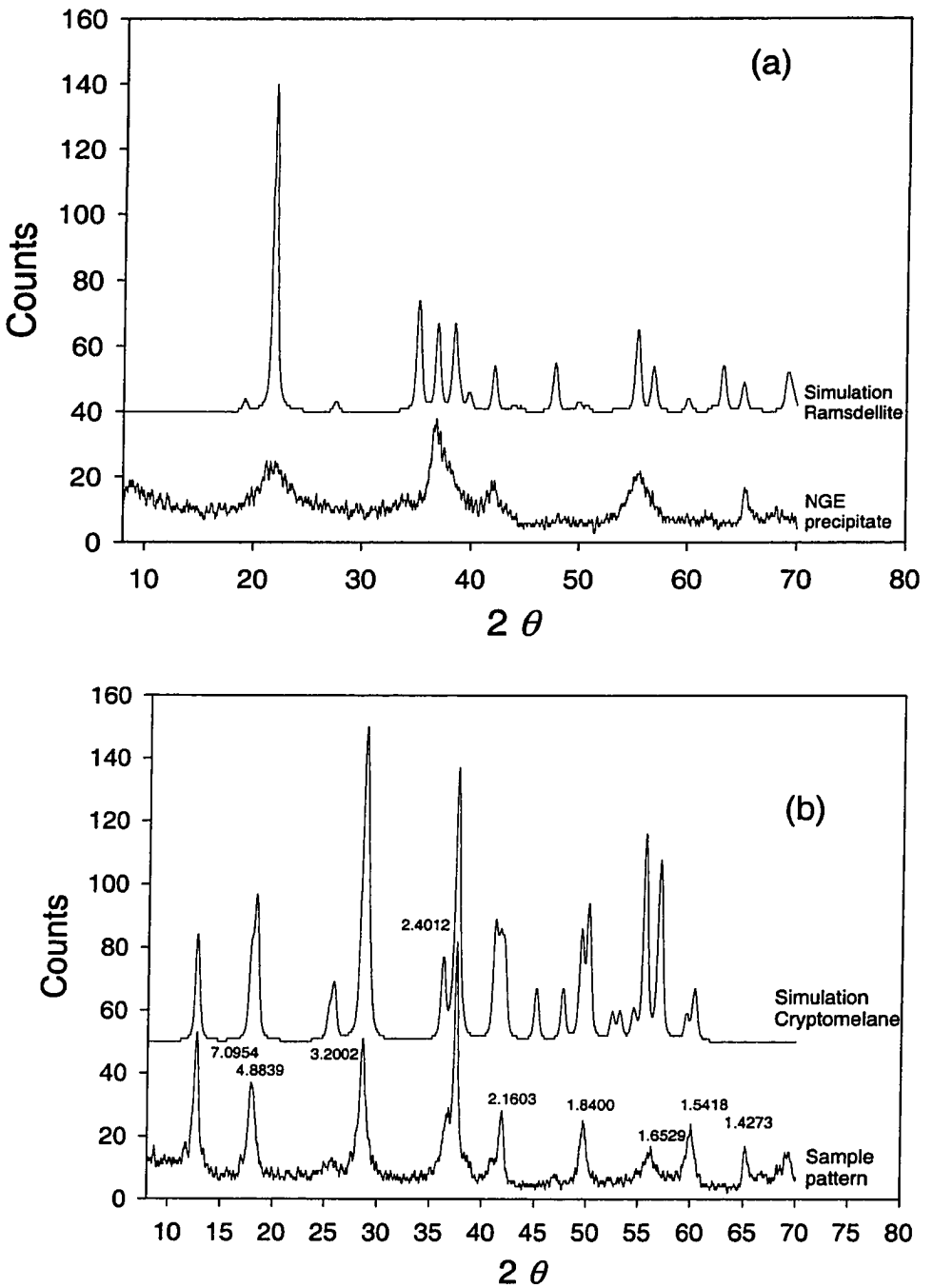


Figure 3.8 (a) Simulation of synthetic ramsdellite (7-222, JCPDS-ICDD, 1992) and sample pattern of precipitate using MOC method; (b) Simulation of synthetic cryptomelane and sample pattern of precipitate using birnessite coating method.

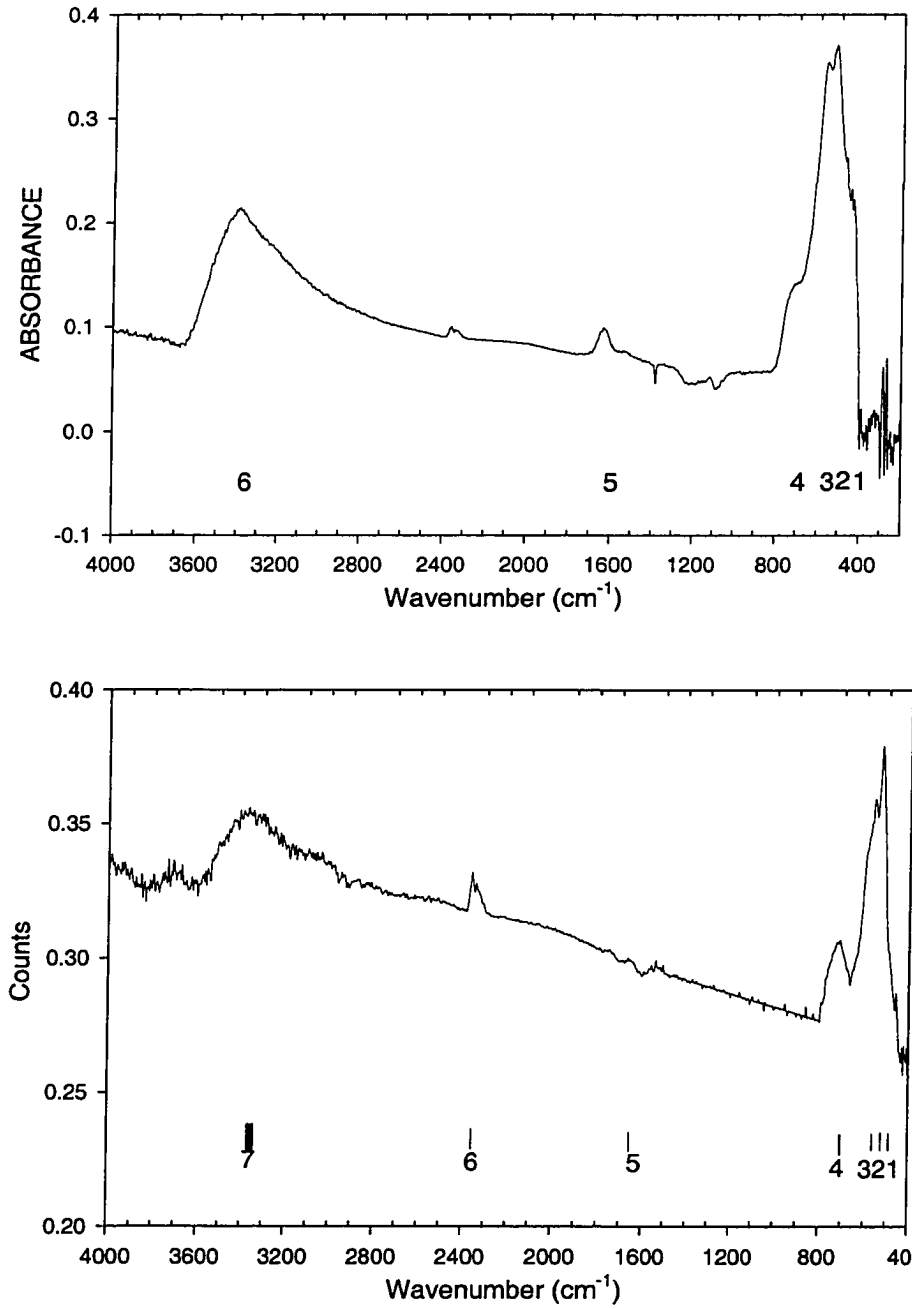


Figure 3.9 (a). IR spectra of the precipitate using MOC method; (b). IR spectra of the precipitate using birnessite coating method.

### 3.5.3 Infrared Spectroscopy (FTIR) Analysis

Infrared spectroscopy can provide a very useful supplement when the identification of manganese oxide is difficult because of amorphous structures, lack of stoichiometry and other factors which would result in line broadening in XRD spectra, as happened for the precipitate of the MOC process. The IR spectra of precipitates in the MOC and BCM methods are shown in Figure 9. All 6 bands of the MOC precipitate in Figure 9a can be matched with the spectra of ramsdellite (Potter and Rossman, 1979) except for the sharpness of the bands, which reflects the crystalline order. Band 5 (at 1640 $cm^{-1}$) is due to an $H_2O$ vibration, and the intensity of the band indicates that the major species is $H_2O$. Potter and Rossman considered that band 5 and band 6 reveal that water is in a well-defined crystallographic site. The presence of a broad band near 3400 $cm^{-1}$ together with a relatively strong band at about 1640 $cm^{-1}$ ($H_2O$ deformation or bending) in the spectrum of an amorphous material may be attributed to this (White and Roth, 1986). Therefore, the FTIR spectra provide additional evidence that the manganese oxide coating produced on the media surface using MOC methods is in the an amorphou phase as indicated by low intensity and broad line spectra in the XRD. The broad band at ~3600 to ~3000 $cm^{-1}$ (absorbance peak at 3390 $cm^{-1}$) in the IR spectrum indicated that the hydroxyl group may exist in the manganese oxide structure because OH stretching frequencies often lie in the region of ~3600 to ~2600 $cm^{-1}$ for amphoteric compounds (Ryskin, 1974) such as goethite (OH stretch at 3095 $cm^{-1}$) and manganite (MnOOH). Hydroxyls are active surface sites for adsorption or ion exchange.

The FTIR spectrum of the BCM precipitate shown in Figure 9b is identical to that of MOC precipitate in the long wavelength region. The sharper bands illustrate the higher crystalline order of manganese oxide, as is also indicated in the XRD analysis. Bands 1, 2 and 3 are analogous to these birnessite bands reported by Potter and Rossman (1979), but band 4, located at ~720 $cm^{-1}$, is the band for cryptomelane (Potter and Rossman, 1979). This appearance verifies the XRD analysis indicating that the BCM precipitate probably is a mixture of birnessite and cryptomelane. Band 5 is a very weak peak for the $H_2O$ vibration. The pattern from bands 6 and 7 may be interpreted as a hydroxide ion in a specific crystallographic site (Potter and Rossman, 1979).

### 3.5.4 Specific Surface Area (SSA) and Specific Gravity ($\rho_s$)

Table 3.2 Specific surface area and specific gravity of media

| Media | SSA ($m^2/g$) | standard deviation† | Specific Gravity ($\rho_s$) | standard deviation‡ | PZC |
|---|---|---|---|---|---|
| Cementitious | 4.08 | 0.05 | 2.579 | 0.012 | --- |
| MOCM | 17.30 | 1.54 | 2.580 | 0.009 | 5.2* |
| $Concrete_{(ad)}$ | 10.74 | 1.08 | 2.493 | 0.014 | --- |
| $MOCM_{(ad)}$ | 19.49 | 0.23 | 2.487 | 0.013 | 5.2* |
| Plain Sand | 0.07 | --- | 2.657 | 0.032 | --- |
| MOCS | 2.48 | 0.3 | 2.597 | 0.041 | 6.4 |
| BCS | 1.51 | 0.49 | 2.603 | 0.091 | 6.6 |
| BCM precipitate | 52.59 | 8.08 | 4.663 | 0.182 | 2.8 |
| MOC precipitate | 34.62 | 1.65 | 1.247 | 0.076 | 5.2 |

† The standard deviation based on 3 samples;
‡ The standard deviation based on 3 samples.
* Calculated value.

The specific surface areas of the media are summarized in Table 2. Concrete is a porous cementitious media and has a very rough surface as shown in the SEM images.

Plain uncoated concrete (No. 8-20 mesh size) has a SSA of 4.08-$m^2/g$. A surface coating of manganese oxide significantly increases the SSA of the cementitious media to 17.30 $m^2/g$. For instance, SSA of MOCM is 4 times that of plain cementitious media, and the SSA of $MOCM_{(ad)}$ (concrete with manganese oxide admixture) is about 2 times that of the plain cementitious media with the manganese admixture ($Concrete_{(ad)}$). Simply adding the manganese oxide admixture increases the surface area from 4.08-$m^2/g$ to 10.74-$m^2/g$. This may be caused by the increase in both inner and surface porosity after adding the manganese oxide admixture because specific gravity decreases at the same time as shown in Table 3.2. SSA of plain silica sand (No. 12-20 mesh) is 0.07-$m^2/g$. Manganese oxide coating using the MOC method increases the SSA of the sand media to 2.48-$m^2/g$. Compared to uncoated sand there is a statistically significant increase in SSA ($P < 0.05$, $n = 3$). SEM images indicate a much rougher surface after the MOC coating.

For a typical dual media filter bed, the porosity is 40-45% for sand bed and 50-55% for concrete media (concrete media is more angular than sand and similar to anthracite) (AWWA and ASCE, 1998). The corresponding surface area concentration would be roughly $1.14\times10^6$ $m^2/m^3$ for uncoated silica sand (specific gravity = 2.65), $4.19\times10^6$-$m^2/m^3$ for uncoated concrete (specific gravity = 2.58), $3.55\times10^6$ to $3.87\times10^6$-$m^2/m^3$ for the synthetic manganese oxide coated bed of MOCS (specific gravity = 2.6), and $2.0\times10^7$ to $2.2\times10^7$-$m^2/m^3$ for a MOCM bed (specific gravity = 2.58).

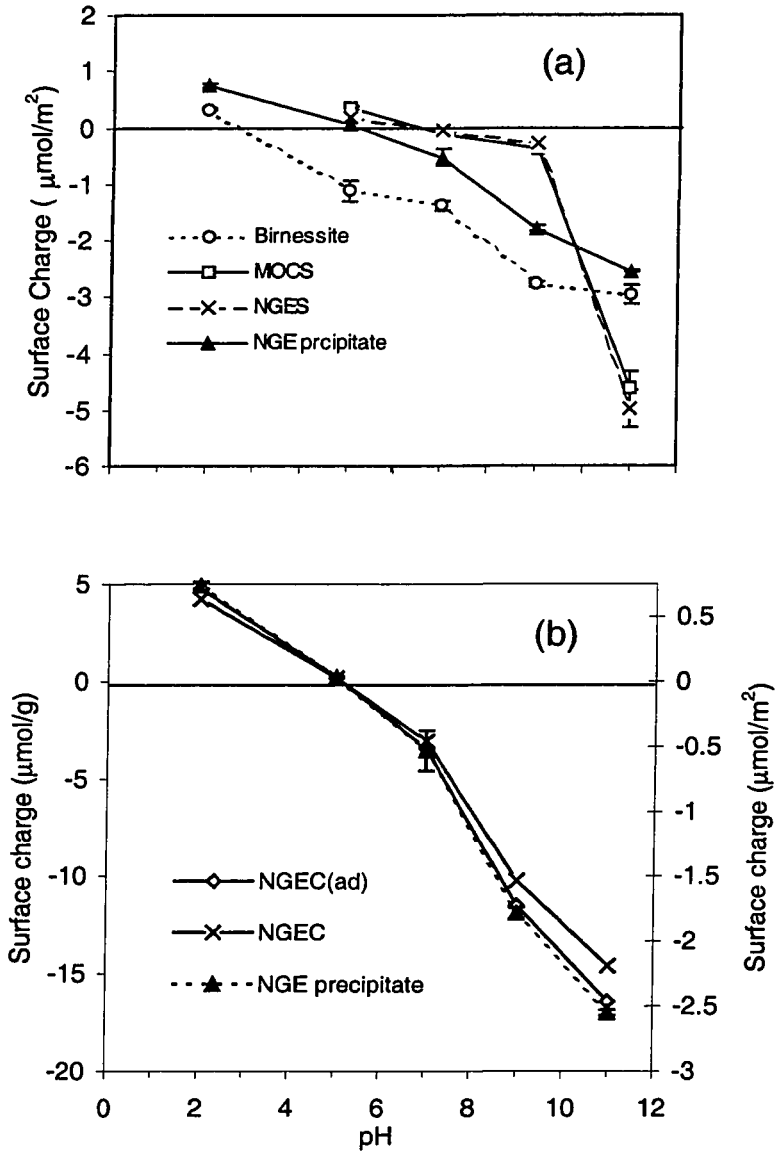


Figure 3.10 (a) Surface charge of manganese oxide coated sand and precipitate at different pH. (b) Surface charge of MOC precipitates (right side axis) and calculated surface charge of manganese oxide coated concrete at different pH.

### 3.5.5 Surface Charge

The importance of the surface properties (including sorptive and filtration properties) of a given mass of material exposed to solution, increases in proportion to

the surface area of that material as well as to the surface charge density or number of charged sites per unit area or weight (Langmuir 1997). As shown in Figure 3.10, the surface charge of manganese oxide is strongly pH dependent as is that of the manganese oxide coated media. The BCM precipitate has a point of zero charge (PZC) of about 2.6, which is in the typical PZC range of birnessite, 1.5 to 2.8 (Sverjensky 1994). The PZC of BCM precipitate also confirm the results of chemical analyses, indicating the presence of both birnessite and cryptomelane manganese oxide. Recall that the PZC of cryptomelane is roughly 4.5, and the reported surface charge of birnessite (McKenzie 1981) in the higher pH range is much larger than for BCM precipitate. Manganese oxide coated sands have relatively lower surface charge sites and higher PZC (roughly 6.4 for MOCS and BCS) compared to pure manganese oxide. Incomplete oxide coverage is an important reason for a low density of surface sites as shown in SEM images typified by Figure 2. Although surface charges are very similar for MOCS and BCS in terms of μmol per surface area, MOCS has a much higher number of surface charge sites than BCS in terms of μmol per weight. Cementitious media contain a large percent of calcium minerals such as calcite ($CaCO_3$), portlandite ($Ca(OH)_2$) and calcium silicate hydrate that are relatively soluble and create a highly alkaline solution. It is very difficult to measure the actual surface charge site with the methods involving water and pH measurement, such as potentiometric titration or ion adsorption method. To avoid this, we measured the surface charge of pure MOC precipitate at different pH levels. Although the surface charge of MOCM and MOC precipitate may be somewhat different, theoretically, we can estimate the surface charge sites on the MOCM surface

by calculating the percentage of manganese oxide coverage with the unit surface site per surface area (or surface site density) of the MOC precipitate.

$$N_{MOCM}(sites/g) = SSA_{MOCM} \times C(\%) \times N_{MOCP}(sites/nm^2) \quad (2)$$

Where $N_{MOCM}$, $SSA_{MOCM}$, $C$, and $N_{MOCP}$ are, respectively, surface site density of MOCM, SSA of MOCM, percentage of manganese oxide coverage, and surface site density of MOC precipitate.

$$N_{NGEP}(sites/nm^2) = N_{NGEP}(\frac{\mu mol}{m^2}) \times N_A(site/mol \quad of\ site) \times 10^{-24}\left(\frac{m^2}{nm^2} \times \frac{mol}{\mu mol}\right) \quad (3)$$

$$= N_{NGEP}(\mu mol/m^2) \times 0.6022\left(\frac{site}{nm^2} \times \frac{m^2}{\mu mol}\right) \quad (4)$$

In equation (3) $N_A$ is Avogadro's number ($6.022 \times 10^{23}$). The calculated surface charges of manganese oxide coated cementitious media at different pH are shown in Figure 9b (assuming $C$=55%). Since the equilibrium pH is around 11 after chemical equilibrium is achieved between the manganese oxide coated concrete and the 0.1-N KCl electrolyte solution, and effluent pH is greater than 9.0 even for a storm water surface loading rate of 50 L-min$^{-1}$-m$^{-2}$ (Sansalone 1999), the manganese oxide coated concrete has very high surface charge in such a high pH solution.

### 3.6 Conclusion

A number of oxide coating methods were developed to coat manganese oxide onto sand and cementitious media surfaces. XRD and FTIR spectroscopy analysis indicated the manganese oxide of BCM coating is a mixture of birnessite and cryptomelane, and the manganese oxide of the MOC coating is mainly ramsdellite.

For sand media, compared to BCM sand, MOC sands have a higher specific surface area (2.48 $m^2/g$) and more complete manganese oxide coverage, which is mainly ramsdellite as identified by XRD and FTIR. The surface charge of both sand media coatings is almost the same with a PZC of 6.4, although the BCM precipitate has a higher negative charge (PZC = 2.6) than the MOC precipitate (PZC = 5.2). This is attributed to more coverage by the manganese oxide coating on the MOC sand surface.

Cementitious media have a much larger SSA than sand because of its inherent surface roughness and porosity. SEM analyses indicated that the surface of oxide-coated cementitious media was fully encapsulated by the manganese oxide coating layer with a thickness that varied from 10 to 30 μm. Manganese oxide admixture (cryptomelane) incorporated into the cementitious matrix increased the SSA of the plain concrete from 4.08 to 10.47-$m^2/g$, but results in only a slight increase in SSA when both media batches also received a surface coating of manganese oxide (from 17.30-$m^2/g$ to 19.49-$m^2/g$). SEM imaging, BSE imaging and dot mapping also showed no significant differences in either chemical composition or coating thickness for MOCM and $MOCM_{(ad)}$.

All coated media evaluations were based on surface and media characterization. Such characterization can provide very useful information for the interpretation of heavy metal removal mechanisms by the media. Batch and column studies are ongoing to fully assess the performance of the media and coatings for storm water treatment.

# CHAPTER 4. ADSORPTION CHARACTERISTICS OF OXIDE COATED POLYMERIC MEDIA ($\rho_S$ <1.0)—BATCH EQUILIBRIA AND KINETICS

## 4.1 Introduction

Unit processes such as adsorption and precipitation onto high surface area materials or unit operations such as filtration can represent viable storm water treatment for dissolved heavy metals and particulate-bound heavy metals, respectively. Therefore engineered media such as the oxide coated filter media with high surface area and amphoteric surface charge can be utilized to carry out the combined unit operations of filtration and processes of surface complexation for a range of treatment configurations for either decentralized treatment or centralized storm water treatment. Such treatment can be designed as a passive and integral part of existing urban infrastructure, for example urban and transportation infrastructure, or can be designed as a centralized storm water treatment component. For process design, control and optimization, it is important to know the quantitative heavy metal adsorption properties of the engineered media. Experimental studies and modeling of media heavy metal adsorption properties is required for a quantitative evaluation of storm water media. One particular combined unit operation/process for in-situ storm water treatment as a best management practice for heavy metal removal in storm water is an upflow sorptive buoyant media clarifier (SBMC). SBMCs are particularly well-suited for storm water discharges from elevated urban infrastructure such as elevated roadway over water.

## 4.2 Objectives

In the present research study, manganese oxide coated polymeric buoyant media (MOPM) were evaluated through batch scale adsorption equilibrium and kinetic studies. There were three objectives of this present study. Although the physical and chemical characteristics of manganese oxide coated media have been examined, heavy metal adsorption equilibria have not been studied (Liu *et al* 2001). Therefore the first objective was to evaluate the adsorption capacity for heavy metals typically found in urban storm water, Pb, Cu, Cd and Zn. The second objective was to develop adsorption isotherms, examine an adsorption isotherm model for the media and evaluate the parameters required for model selection. The third objective was to evaluate the adsorption kinetics for the heavy metal and media studied. The goal of this study was to evaluate the adsorptive capacity and simulate adsorptive behavior for heavy metal removal from storm water using MOPM utilized in treatment devices such as a SBMC.

## 4.3 Background

Amphoteric materials are used for heavy metal adsorption because of their relatively high surface area and their surface charge characteristics. Heavy metal adsorption behavior for specific media, such as silica sand, soils, granular activated carbon, and iron oxide, have been studied extensively in the past (Langmuir 1997; Stumm and Morgan 1996; Stumm 1992). Applications of such adsorption behavior for selected engineering process treatment have proved successful for use in engineering design with specific engineered media. Manganese oxides have shown an affinity for heavy metals, including Pb, Cu, Cd, and Zn (Tamura 1997; Fu *et al.* 1991; Catts and

Langmuir 1986). The point of zero charge (PZC) of manganese oxide in soils range from 1.5 for birnessites to 4.6 for the hollandite group (Healy *et al.* 1966). PZC of synthetic birnessite was reported from 1.5 to 3.0 for different manganese oxide synthesis methods and surface charge measurement methods (Fu et al. 1991; McKenzie 1989; McKenzie 1981; Zasoski and Burau 1988; Morgan and Stumm 1964). Manganese oxides have very high negative charge at pH levels higher than their PZC and their cation adsorption capabilities generally increase with increasing pH. The adsorption of specific heavy metals near the PZC illustrates that specific adsorption chemical forces, in addition to electrostatic forces, are involved in the adsorption process (Murray 1974). Using extended X-ray absorption fine structure (EXAFS) spectroscopy analysis and other techniques, researches have explained this excessive uptake of heavy metals as ion exchange to the inner structure of manganese oxides, such as tunnel sites of cryptomelane (Randall *et al.*, 1998; Tsuji and Komarneni 1993). This mechanism contrasts with heavy metal adsorption onto the amphoteric external surface of manganese oxides, as most surface complexation models describe.

Natural oxide coated particles are common in soils, for example metal oxides are released from primary minerals by weathering or originate from the deposition of translocated substances and lead to particle coatings which consist of clays, iron sesquioxide, calcite, silica and manganese oxides (Fitzpatrick 1980; Robert and Terce 1989). To enhance the treatment efficiency and capabilities for engineered heavy metal and particle removal, organic and/or inorganic coatings such as manganese oxides have been widely studied for a variety of metal-bearing wastewaters. For example, practical

methods of coating iron oxide onto silica sand and other media were developed for storm water treatment (Sansalone 1999a; 1999b). Merkle and Knocke *et al* (1997a; 1997b; 1996) developed a manganese oxide coating method on anthracite to improve the removal of $Mn^{2+}$ from drinking water and hazardous waste effluent. They generated a drink water filter medium with an increased surface area after coating with manganese oxides (from ~0.18 $m^2/g$ to 0.53-0.9 $m^2/g$) and found manganese oxide coated media have the ability to adsorb and coprecipitate a variety of inorganic species. Stahl and James (1991) found their manganese oxide coated sands generated a larger surface area and increased adsorption capability with increasing pH as compared to uncoated silica sand.

## 4.4 Materials and Methods

### 4.4.1 Materials for Batch Studies

Manganese oxide coated polymeric media (MOPM) were prepared using a two step coating method (details were described in chapter 2). The MOPM were spherical in shape with a diameter range of from 2 to 5 mm ($d_{50}$ = 3.44-mm) and a mean specific gravity, $\rho_s$ = 0.928. Specific surface area, SSA of the media was 27-$m^2/g$ determined by a modified ethylene glycol monoethyl ether (EGME) measurement method (Sansalone *et al* 1998). Surface charge was measured the using the potentiometric titration methodology of Van Raij and Peech (1972). All the surface characteristics of the coated media utilized in this study have been detailed chapter 2.

Batch solutions of Pb, Cu, Cd and Zn were prepared from 1000-ppm reference standard solutions of $Cd(NO_3)_2$, $Cu(NO_3)_2$, $Pb(NO_3)_2$, and $Zn(NO_3)_2$. The ionic

strength for all the solutions was fixed as 0.01-M $NaNO_3$. Adjustments for pH were carried out with trace-metal 1-N $HNO_3$ or 1-N NaOH. The pH of the metal solutions were adjusted to the initial experimental values, the containers sealed and allowed to stand overnight. The following day the pH was readjusted to the initial experimental value before initiating batch experiments. Heavy metal analysis was carried out by inductively coupled plasma-mass spectroscopy (ICP-MS) (Perkin-Elmer Elan 6000).

### 4.4.2 Adsorption Equilibrium Studies

The sorption equilibrium, which is usually characterized by the adsorption isotherm, is commonly measured by adding a known amount of sorbate to a known amount of sorbent in an aqueous solution and analyzing the resulting concentration of solute in solution. United States Environmental Protection Agency (US EPA) and National Bureau of Standards (NBS) recommend 2-liter bottles in a rotary tumbler for completely mixed batch reactor for batch-type procedures for estimating soil adsorption of chemicals (Roy *et al.* 1992a). In spite of the apparent ease of such experiments, many source of errors are possible (Roy 1992b). With respect to the use of a rotary tumbler in this study, one problem encountered was the abrasion of the oxide coating from MOPM in the tumbling process. Such abrasion and separation led to significant experimental difficulty and representative analyses were difficult.

An important alternative technique for the classic batch experiment is the use of a re-circulating flow-through reactor for the determination of sorption parameters (Carski 1985; Miller 1989; Celorie 1989; Qualls 1992). In this form of a batch experiment, heavy metal solution is recirculated through a short column containing

sorbents as a flow-through reactor. In this study, to avoid experimental difficulties associated with abrasion of the oxide surface from media, a short column (25.4-mm ID, 50.8-mm length, Teflon PFA column) packed with test media served as the flow-through reactor. The pH was not adjusted during the reaction period, and any pH drift was measured and recorded throughout the experiment. A series of metal solutions, in which sorbent to solute ratio ranged from 0.1-g/L to 10-g/L, were recirculated through the batch reactor by a peristaltic pump at a surface loading rate of 500 ml/cm$^2$-min. Metal aqueous solutions were studied at initial contaminated heavy metal concentration (1 to 5-ppm), ionic strength of 0.01-M as $NaNO_3$ and pH of 5 to 7, and all reactions were kept under a nitrogen atmosphere. After a reaction period that ranged from 48 to 72-hours in the flow-through reactor, the equilibrium pH values were measured and samples taken from each reactor were fractionated, acidified and analyzed. The filtered samples (using a 0.45-μm membrane filter) were acidified with trace metal $HNO_3$ on a 5% v/v basis and analyzed for equilibrium aqueous phase heavy metals using ICP-MS analysis. A reactor containing no sorbent was included as control at each pH. The solid phase heavy metal concentrations were calculated at the difference between initial and final concentrations. The relationship between aqueous and solid phase heavy metal equilibrium concentration was developed for each given set of solution conditions. pH drift from the initial pH in each reactor was expected because of the surface complexation reactions at the interface between the solid phase (manganese oxide) and aqueous phase (heavy metal cation). Exhausted media was utilized for spectroscopic and microscopic analyses.

The goals for another set of isotherm experiments were to enable extensive evaluation of the effects of pH on heavy metal adsorption. These experiments were conducted in an identical process as described above except for the following two changes. First, all samples had the same dry mass of sorbents (5-g/L), and secondly, the initially adjusted pH of individual samples was varied between 3 and 10. At the end of the reaction period, equilibrium pH values were measured as well as the aqueous heavy metal concentrations. The amount of heavy metal adsorbed by the solid phase was calculated based on the difference between the initial contaminated heavy metal concentrations and the final equilibrium aqueous heavy metal concentrations.

### 4.4.3 Adsorption Kinetic Study

Adsorption kinetics were investigated in the recirculating flow-through reactor described above. Each experiment used 2-L of solution (supplied from Teflon PFA reservoirs) containing 5-mg/L heavy metal concentrations at 0.01-M ionic strength as $NaNO_3$. The pH was not adjusted during the reaction period, and any pH drift was measured and recorded every 10 minutes by a computer controlled data acquisition system. Prior to recirculating, two filtered and two unfiltered aqueous samples were taken from the reactor to verify the initial target heavy metal concentration. 5-mL samples were extracted from the solution and filtered though a 0.45-μm membrane filter using a syringe sampler and polypropylene syringe filter at predetermined time intervals. The drift was measured every 10 minutes. The duration of experimental runs ranged from 48 to 72 hours. The samples were acidified in trace metal $HNO_3$ to a 5% v/v basis and analyzed for the target heavy metal concentrations by ICP-MS analysis.

The solid phase heavy metal concentrations were calculated based on the difference between initial and final concentrations. The relationship between liquid and solid phase heavy metal equilibrium concentration was developed for each given set of solution conditions.

### 4.4.4 Metal Analysis

Metal analysis was conducted with an inductively coupled plasma mass spectrometer (ICP-MS) (Elan 6000, Perkin-Elmer) employing four-point standard calibration prior to analysis of samples. The measuring conditions were 100-ms, 50 sweeps/reading with 3 replications of each sample analysis. The internal standards were Scandium (Sc 45), Germanium (Ge 74), Rhodium (Rh 103) and Lutetium (Lu 175) which were added to the samples at a concentration of 10-ppb respectively. The elements were measured at m/z values of 63 for copper, 64 for zinc, 114 for cadmium and 208 for lead. Analytical controls were maintained throughout including use of control and blank samples, mass balance checks, and standard solution quantity checks of every 7 samples.

## 4.5 Results and Discussion

### 4.5.1 Adsorption Equilibrium and Freundlich Isotherm

Figure 4.1 depicts the adsorption isotherms obtained for the solution at initial pH values of 5, 6 and 7 and initial Pb(II) concentration of 5-mg/L ($2.41\times10^{-5}$ M). An increase in media capacity was observed as the initial solution pH was increased. There is a slight increase in media capacity from pH 5 to 6, while at pH 7 the capacity was several times greater than at a pH of 6. The Freundlich isotherm applies very well for

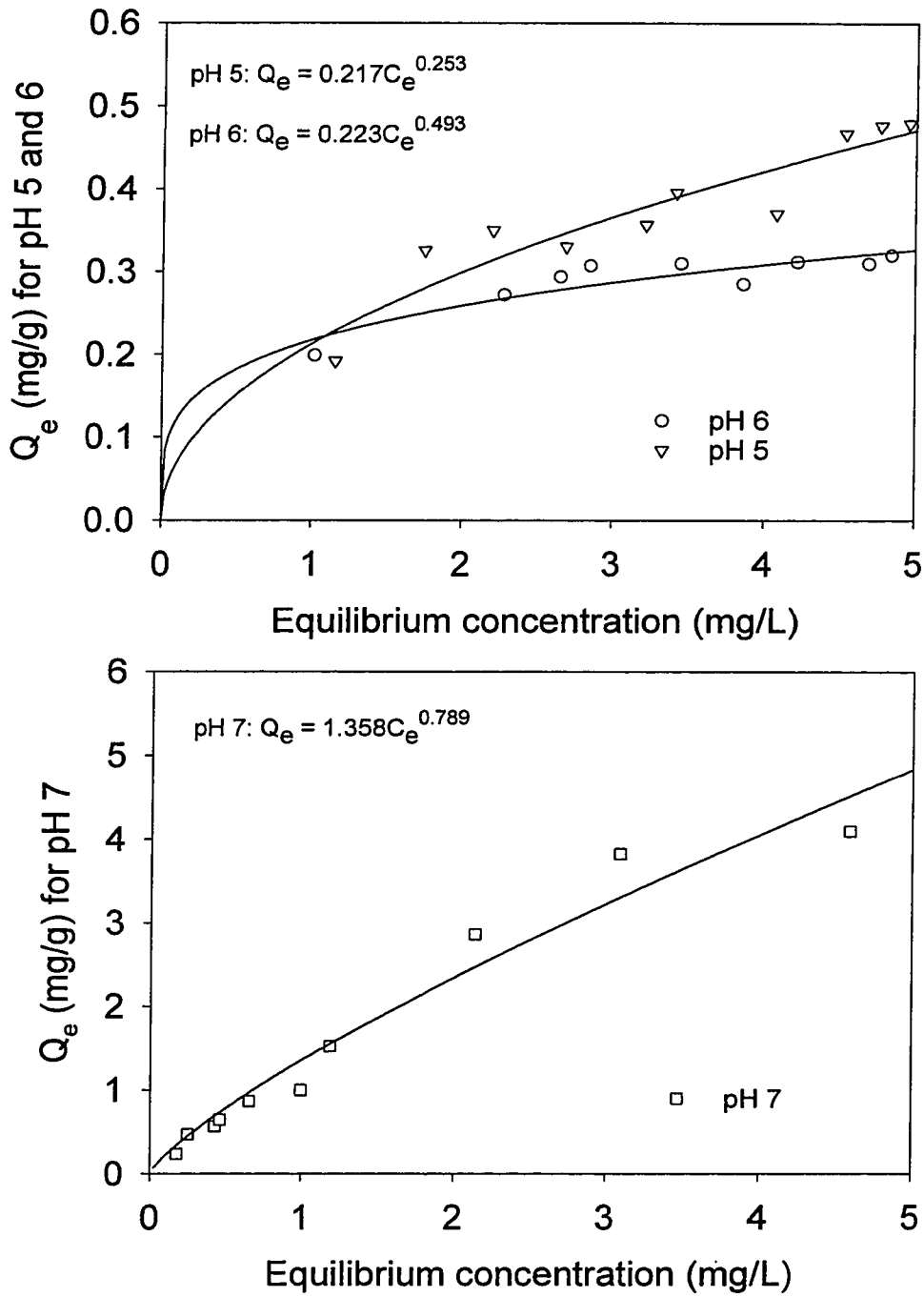


Figure4.1. Adsorption isotherm for Pb(II) on manganese oxide coated polymeric media at three pH values. Lines are Freundlich model curve. Sorbent dosages range from 0.1-g/L to 20-g/L. Initial concentration is 5-mg/L ($2.41\times10^{-5}$ M).

the solids with heterogeneous surface properties (Stumm 1992). Therefore, the Freundlich equation was able to model adsorption of MOPM well, given the heterogeneous surface properties of the media of which the surface characterization were described in Chapter 2. In the Freundlich isotherm equation, the coefficient $K_F$ is an indication of adsorption capacity while $n$ reflects the steepness of the curve whether plotted on an arithmetic or logarithmic scale. In this study, the Freundlich model fit quite well as shown in Figure 4.1, and the Freundlich isotherm constants and their standard error for the representative equilibrium studies are summarized in Table 4.1. The Freundlich curve patterns are very different for each of the three solute pH levels examined. The adsorption capacity of Pb(II) at pH 7 is 6 times larger than that at pH 6, and the higher the solute pH, the steeper the curve.

Table 4.1 Freundlich model coefficients for manganese oxide coated polymeric media sorbent isotherms.

| $pH_i$ | $pH_e$[a] | Experimental metrix | Metal | $C_o$ (mg/L) | $K_F$[d] | StdErr[e] | N[d] | StdErr | $r^2$ |
|---|---|---|---|---|---|---|---|---|---|
| 7 | 6.63-5.71 | [b]Single $Me^{2+}$ | Pb | 5 | 1.358 | 0.126 | 0.789 | 0.076 | 0.959 |
| 6 | 5.81-5.36 | Single $Me^{2+}$ | Pb | 5 | 0.223 | 0.022 | 0.493 | 0.077 | 0.878 |
| 5 | 5.07-4.96 | Single $Me^{2+}$ | Pb | 5 | 0.217 | 0.013 | 0.253 | 0.049 | 0.835 |
| 7 | 6.87-6.15 | Single $Me^{2+}$ | Zn | 5 | 0.276 | 0.013 | 0.351 | 0.036 | 0.956 |
| 7 | 6.74-6.03 | Single $Me^{2+}$ | Cu | 5 | 0.419 | 0.023 | 0.444 | 0.045 | 0.892 |
| 7 | 6.60-6.14 | [c]Mixed $Me^{2+}$ | Pb | 1 | 1.266 | 0.228 | 0.964 | 0.176 | 0.860 |
| 7 | 6.60-6.14 | Mixed $Me^{2+}$ | Cu | 1 | 0.748 | 0.056 | 1.022 | 0.094 | 0.965 |
| 7 | 6.60-6.14 | Mixed $Me^{2+}$ | Cd | 1 | 0.157 | 0.008 | 0.488 | 0.067 | 0.926 |
| 7 | 6.60-6.14 | Mixed $Me^{2+}$ | Zn | 1 | 0.077 | 0.005 | 0.978 | 0.022 | 0.819 |
| 6 | 6.13-5.46 | Mixed $Me^{2+}$ | Pb | 1 | 0.273 | 0.020 | 0.766 | 0.131 | 0.875 |
| 6 | 6.13-5.46 | Mixed $Me^{2+}$ | Cu | 1 | 0.119 | 0.024 | 4.254 | 1.414 | 0.689 |

[a] pH range of samples at equilibrium (0.1-20g/L dose range)
[b] only one testing metal in experimental solution
[c] the solution containing 1-mg/L $Pb^{2+}$, $Cu^{2+}$, $Cd^{2+}$ and $Zn^{2+}$.
[d] Based on the Freundlich model $Q_e = K_F C_e^n$ where $Q_e$ is in mg/g and $C_e$ is mg/L.
[e] Standard error for estimated parameter.

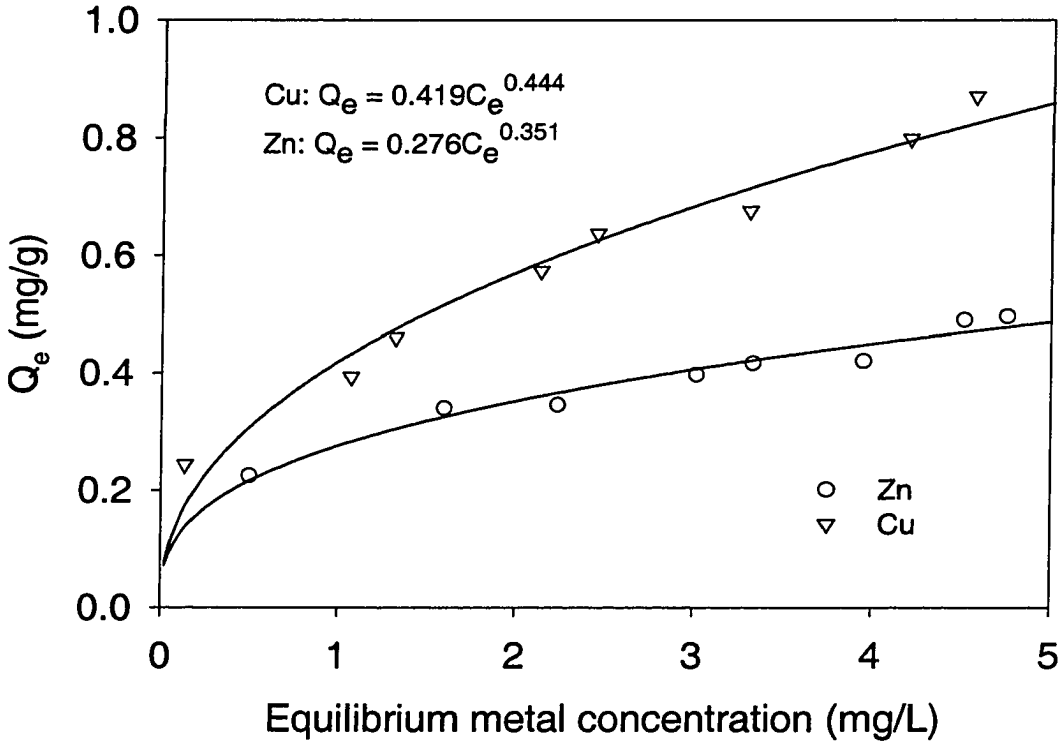


Figure 4.2. Adsorption isotherms for Cu(II) and Zn(II) on the manganese oxide coated polymeric media (MOCPM) at initial pH of 7.0, 5-mg/L ($7.81\times10^{-5}$ M) initial concentration as Cu and Zn respectively, I = 0.01 M as $NaNO_3$. Lines are Freundlich model curves.

Adsorption isotherms for Cu(II) and Zn(II) at initial pH 7 are shown in Figure 4.2. When results from Figure 2 are examined, the MOPM capacity for Pb(II), Cu(II) and Zn(II) at a pH of 7 reflects the adsorption affinity for manganese oxide where Pb(II) > Cu(II) > Zn(II) for the Freundlich isotherm model. This order of adsorption affinity is similar to the adsorption order reported elsewhere (Langmuir 1997; McKenzie 1980a). Although the adsorption capacities for MOPM are generally less than those for pure manganese oxide on the basis of gross media weight, the capacities are essentially the same when calculated using only the mass of the manganese oxide coating layer. For

example, Zasoski and Burau (1988) reported a Zn(II) adsorption capacity of 0.999 mmol/g (~64 mg/g) for pure manganese oxide at pH 8 and initial Zn(II) concentration of 0.1 mmol/L (~6.4 mg/L); while for the tested MOPM, the capacity is about 0.51 mg/g on the gross media weight basis, and 47.91-mg/g on the basis of the manganese oxide coating layer (6.5-mg-manganese/g-media). The average diameter of the MOPM tested is 3.44-mm; however, if the diameter was reduced to 1-mm, all other media characteristics remaining constant (the same coating thickness), the adsorption capacity per gross media weight would increase by a factor of 30. Although more studies are required for this media engineering process, and there are other engineering constraints such as head loss and hydraulic conductivity, adsorption capacity of MOPM for Pb, Zn and Cu can be comparable to those reported for granular activated carbon (GAC) (Reed et al. 1996; Reed et al. 1995), iron oxide coated sand and iron sorbent (Smith and Amini 2000; Sansalone 1997; Smith 1996; Sansalone 1999). Given the discussion above, the MOPM can be a viable alternative adsorption medium for heavy metal removal and take advantage of buoyant characteristics for designing upflow heavy metal removal devices such as sorptive buoyant media clarifiers (SBMC).

To investigate adsorption behavior under competitive conditions for MOPM, simulated storm water solutions were prepared with metal mixtures containing Pb(II), Cu(II), Cd(II) and Zn(II) at concentrations of 1-mg/L each. The adsorption isotherms and fitted Freundlich model curve are shown in Figure 4.3, and the Freundlich isotherm constants and their standard error for the representative equilibrium studies are summarized in Table 4.1. Competitive adsorption behavior of Zn, Cd, Cu and Pb onto

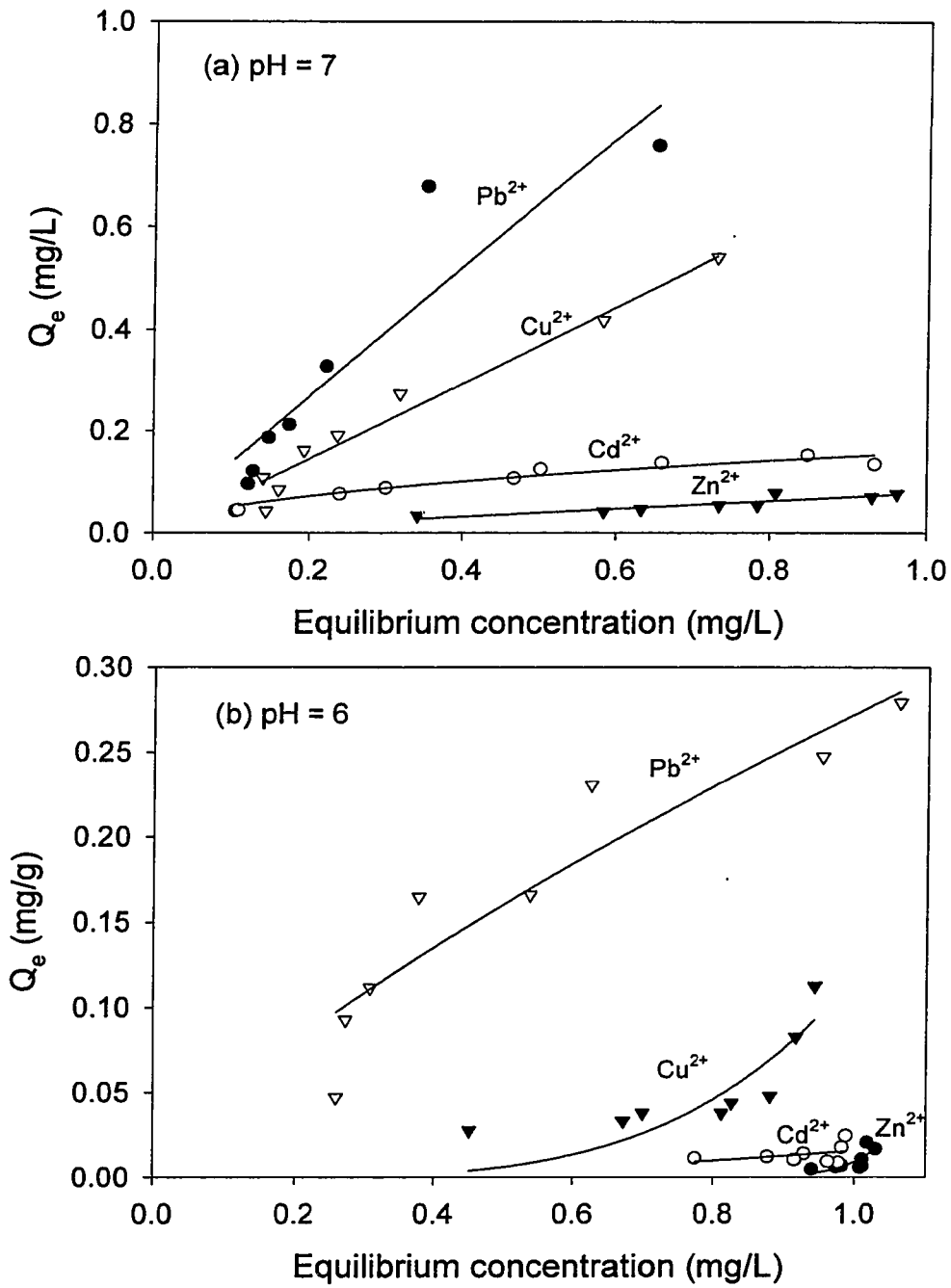


Figure 4.3. Freundlich isotherm for a mixture of metal solutes (1-mg/L of $Pb^{2+}$, $Cu^{2+}$, $Cd^{2+}$ and $Zn^{2+}$ each) at pH 7 (a) and pH 6 (b). The lines are the Freundlich model curves.

MOPM is clearly shown in the results. Adsorption affinity of the tested metals is Pb(II) > Cu(II) > Cd(II) > Zn(II) which is the same affinity as indicated from the results under noncompetitive conditions. These adsorption affinities of manganese oxides (generally $\delta$-$MnO_2$, the most common manganese mineral in soil) are similar to those reported by other studies (Langmuir 1997; McKenzie 1980a). Comparing the isotherm results of competitive and noncompetitive conditions, although the initial metal concentrations are different, the Freundlich isotherm constants are almost the same at both pH 6 and 7 for Pb which shows the highest affinity for MOPM. For Cd(II) and Zn(II) only a very small fraction of these metals was adsorbed, especially Zn(II), where almost no adsorption was observed at pH 6 under competitive conditions. We can hypothesize that the total number of adsorption sites were limited compared to the total metal concentrations, but still significant enough to preferentially accommodate those cations such as Pb(II) and Cu(II) with strong affinities. Therefore the behavior of Pb and Cu are similar under competitive and noncompetitive conditions. However, the presence of other cations diminishes the number of adsorption sites on the manganese oxide for other divalent heavy metals, for example Ca(II) can reduce the sorption sites of manganese oxide for Cd(II) and Zn(II) (Zasoski and Buran 1988).

The Pb, Cu and Zn adsorption data are shown in Figure 4.4 as a function of pH at a sorbent/solute ratio of 5-g/L and the initial metal concentration of 5-mg/L. As indicated in the isotherm results, adsorption of heavy metals is strongly pH dependent for MOPM. The surface charge of the media is strongly pH dependent and the PZC of MOPM was 4.8 (Liu *et al* 2001). For these amphoteric oxides, such as manganese oxide

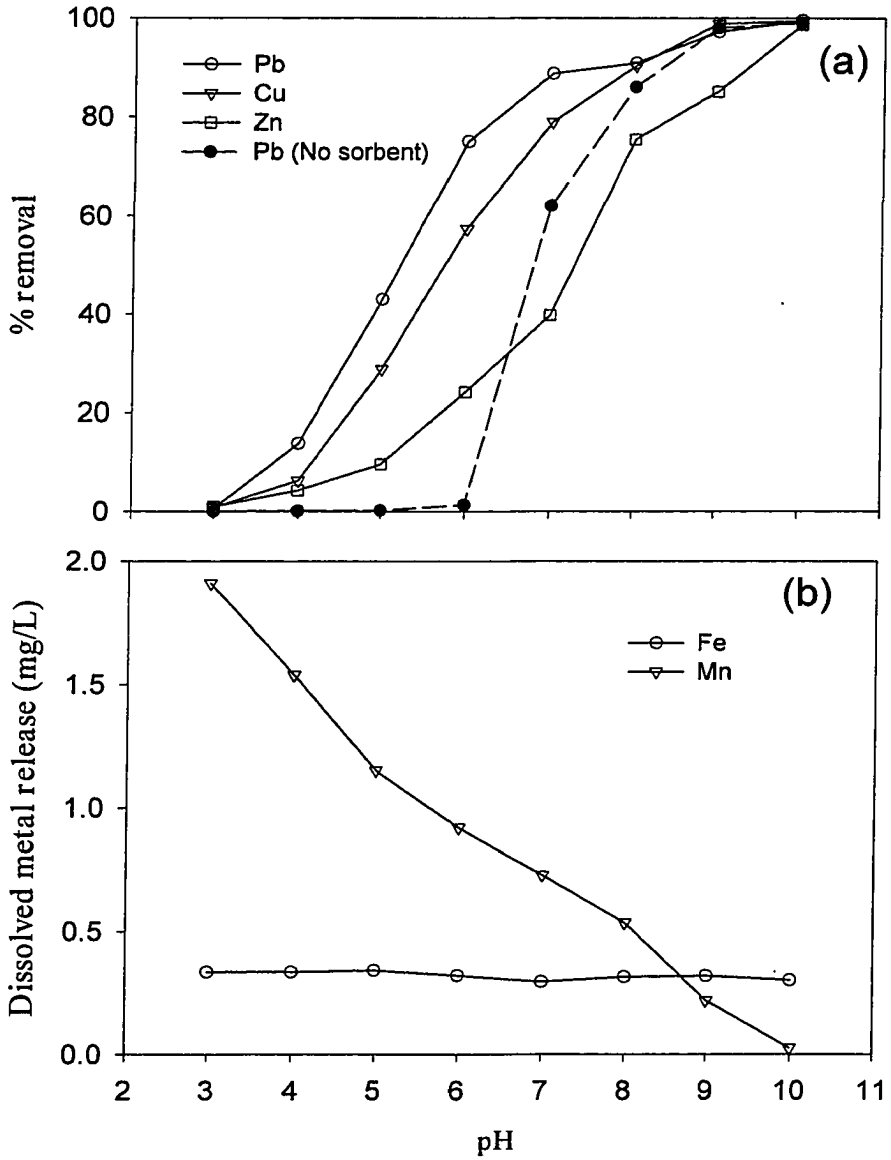


Figure 4.4. (a) Heavy metal removal for initial metal concentration of 5 mg/L, sorbent/solute ration of 5-g/L (32.5-mg-Mn/L), and ionic strength of 0.01-M $NaNO_3$. Pb (no sorbent) is only Pb solution and no MOPM runing in the reactor. (b) Fe and Mn release from MOPM at equilibrium for a sorbent/solute ratio of 5-g/L.

and iron oxides, the net surface charge becomes more negative as pH increases. This increase in negative charge results in an increase in cation adsorption and the typical "S" shaped adsorption edge is observed (Christophi and Axe 2000; Languir 1997;

Stumm and Morgan 1996). The rapid adsorption increase with increasing pH often takes place over a narrow pH range, and in some cases this range can start below the pH of the PZC, as is the case of Pb and Cu in this study. Murray (1974) summarized the adsorption properties of $\delta$-$MnO_2$ and indicated that there was significant adsorption of heavy metals at the PZC, illustrating that specific chemical forces, in addition to electrostatic forces, are involved in the adsorption process. Comparing the adsorption edge of the three metals, the adsorption follows the order of Pb > Cu > Zn as indicated in this isotherm study. The degree of affinity is a function of site capacity and the equilibrium constant, which often coincide with the electronegativity of the element (Christophi and Axe 2000; Nebergall *et al* 1980). Heavy metal adsorption on manganese oxide has been studied by many researchers (Appelo and Postma 1999; Randall *et al* 1998; McKenzie 1980a, 1980b, 1981, 1983). McKenzie (1980a) summarized the heavy metal ion adsorption order as Pb > Cu > Mn > Zn > Ni, in agreement with results of this study.

The Pb(II) removal as a function of pH shown in Figure 4.4 suggests that the removal mechanisms may involve adsorption and surface precipitation at higher pH. For example, at pH 7, 62% of the Pb was precipitated in the solution without sorbent, while 88.74% was removed in the solution with a sorbent/solute ratio of 5-g/L (32.5-mg manganese coating/L). To investigate the coating stability, we also measured the aqueous concentration of Mn and Fe released from the experimental media which had two layer coatings, including a iron oxide scratch inner layer coating and manganese oxide outer layer coating. Equilibrium aqueous Mn concentration increased with decreasing pH while Fe concentration remained very low (almost at background level).

The observation of an aqueous Mn concentration less than 2-mg/L at pH 3 suggests that the manganese oxide coatings are stable. In this study, MOPM have a favorable solute pH range of $> 6$ for heavy metal removal.

### 4.4.2 Kinetic Study

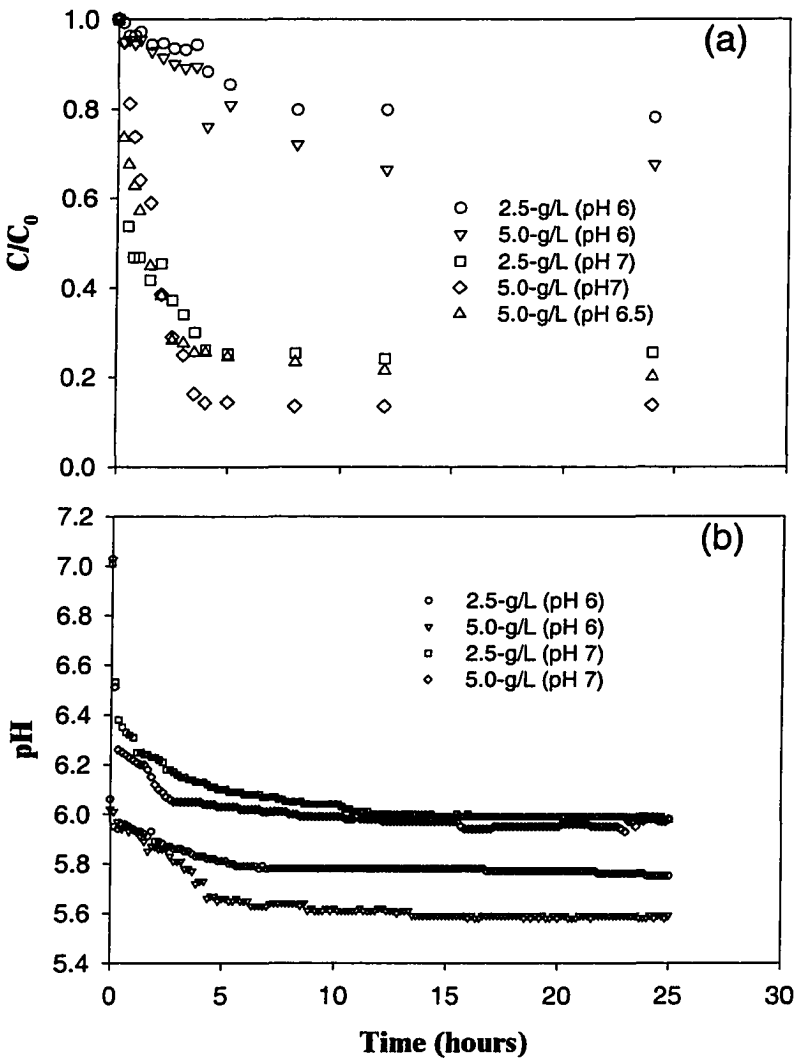


Figure 4.5. (a). Batch kinetic data for Pb at various sorbent dosage and initial pH; (b) pH drift for varying pH and sorbent dosage. The initial lead concentration is 5-mg/L; 0.01-M ionic strength.

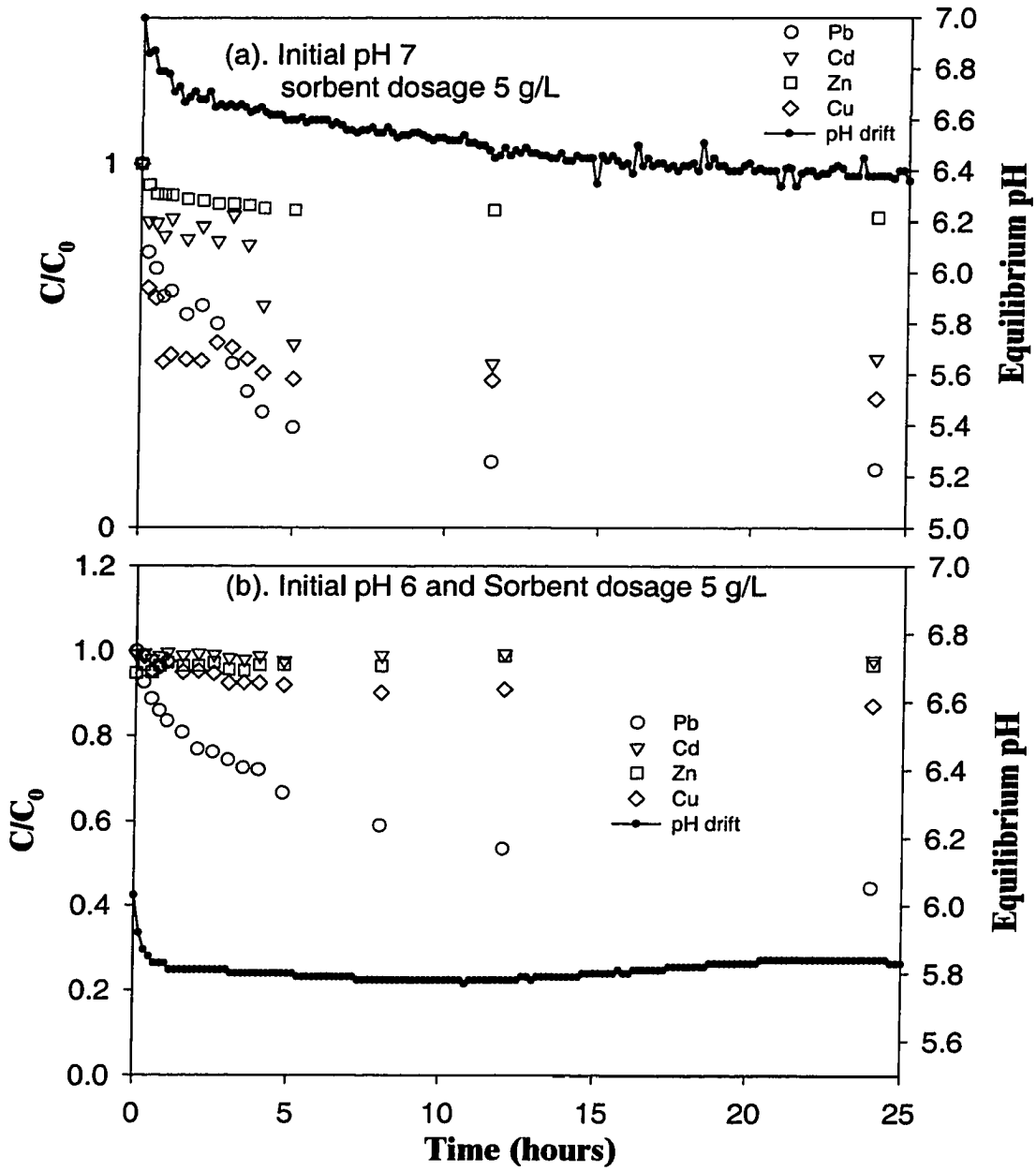


Figure 4.6. Kinetic data and pH drift for different initial pH for the metal mixture adsorption for the initial pH 7 (a) and pH 6 (b). The initial metal mixture concentration is 1-mg/L $Pb^{2+}$, $Cu^{2+}$, $Cd^{2+}$ and $Zn^{2+}$ respectively; 0.01 M ionic strength.

The batch kinetic experimental data and pH drift at selected sorbent dosages and initial pH values for lead alone as solute and for mixture solutes are shown in Figure 4.5 and Figure 4.6. An equilibrium time of 5-hours were achieved for different initial pH and sorbent dosages. Solution pH, aqueous metal concentration, adsorbent concentration and ionic strength can be the factors affected the adsorption profiles (Yiacoumi and Tien 1995), and the adsorption rate can last from as short as millisecond scale to month scale (Sparks 1999). The reported equilibrium time for divalent heavy metal adsorption onto manganese oxides varies from hour scale (Morgan and Stumm 1964; Murray *et al* 1968) to day scale (Laitinen and Zhou 1988; Trivedi and Axe 2000). In this study, a biphasic adsorption profile was observed. Over 50% total aqueous divalent heavy metal were removed within 30-minutes. Following the initial fast stage, a slower reaction stage continued, varying from 5 to 15-hours, as a function of different initial pH, sorbent dosages, and nature of the solutions. As adsorption involves heterogeneous reactions occurring among species at interface, the process may be considered to consist of three different steps, including transport of the sorbates to adsorbent surface by diffusion, chemical transformation of sorbates, and transport of some of the products away from the surface (Yiacoumi and Tien 1995). The secondary slow reactions have been observed on many different oxides and generally three possible explanations are applied: (1) diffusion to internal sites, (2) surface precipitation or, (3) adsorption to sites that have a slower rate due to low affinity (Strawn *et al* 1998; Axe and Anderson 1997; Towle *et al* 1997; Scheidegger *et al* 1996; Loehr and Webster 1996).

Adsorption of metal ions generally involves concurrent desorption of protons or other metals as indicated in the surface complexation reaction equation below.

$$\equiv MnOH + M_s^{2+} = (\equiv MnOM_s)^+ + H^+ \quad (1)$$

The concentration curves and the pH drift curves have very high coincidence with the equilibrium time patterns. This demonstrates that surface complexation reactions had taken place with release of protons. The profiles of pH drift can be considered as the pattern of transport of adsorption or surface complexation products away from adsorbent surface, since protons are the products for the surface complexation. The ratios of calculated proton released and sorbed metal were generally less than 0.5 over the entire reaction time. The pH change at equilibrium for different sorbent dosage and solution conditions are shown in Figure 4.7. The pH drop increases with increasing sorbent dosage, and the pH drift curves are all presented as biphasic curves. As the sorbent dosages were relatively low, < 5-g/L (32.5-mg Mn/L), the pH dropped sharply, and when sorbent dosages were high, the pH gradient significantly flattens. The low ratio of proton release to the divalent metal adsorbed and the biphasic pH drop indicates that the manganese oxide may act as a buffer in the solution because of its amphoteric characteristics. For manganese oxides, the ratios of proton release to the divalent heavy metal adsorbed were reported from 2 to less than 1(Laitinen and Zhou 1988; Murray 1975; Morgan and Stumm 1964), and some experiments did not observe the significant pH change accounting for the buffer capability of the metal oxides (Trivedi and Axe 2000).

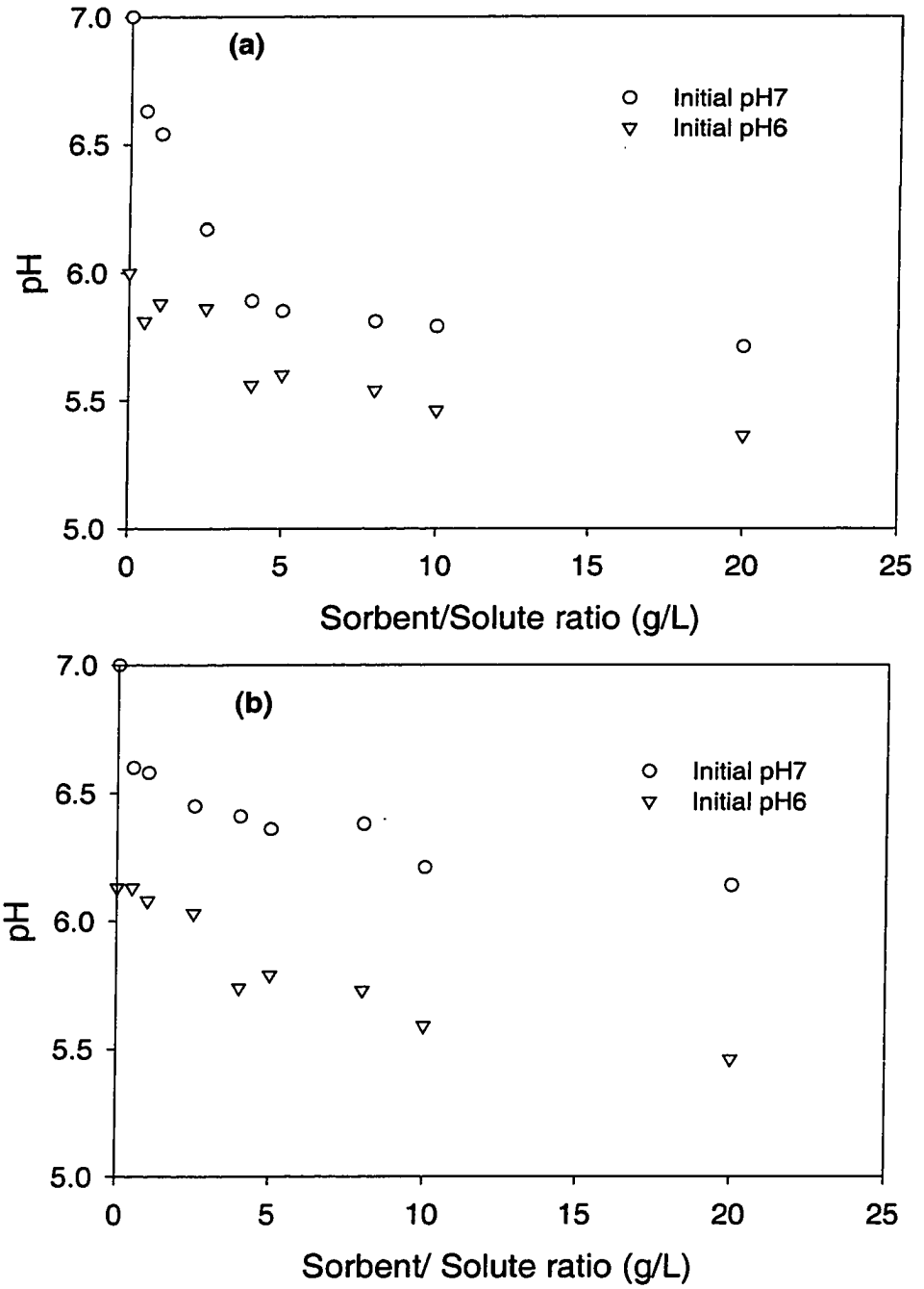


Figure 4.7. The pH drift at equilibrium for different sorbent dosages. (a). 5-mg/L Pb initial concentration; 0.01-M ionic strength; (b) The initial metal mixture concentration is 1-mg/L $Pb^{2+}$, $Cu^{2+}$, $Cd^{2+}$ and $Zn^{2+}$ respectively; 0.01-M ionic strength.

### 4.6 Summary and Conclusion

This study was undertaken to investigate divalent heavy metal adsorption onto a manganese oxide coated polymeric medium (MOPM) through batch adsorption experiments using flowthrough batch reactors. Freundlich adsorption isotherms, a surface complexation model and a potential driving second order kinetic model were fit to the experiment data.

Compared to the adsorption capacity of commercial adsorbents and studies on other sorbents (for example granular activated carbon and iron oxide coated sands), MOPM has similar adsorption capacity for divalent heavy metal removal. MOPM can serve as an alternative adsorption medium for heavy metal removal, and with an aggregate specific gravity of less than 1.0, such media can be utilized in upflow BMPs such as sorptive buoyant media clarifiers (SBMC).

Freundlich adsorption isotherms were fit to the experimental data for both single divalent metal solutions and for mixed solutions of $Pb^{2+}$, $Cu^{2+}$, $Cd^{2+}$ and $Zn^{2+}$. The order of adsorption affinity on this MOPM for the four divalent heavy metals studied is Pb(II) > Cu(II) > Cd(II) > Zn(II). Results indicate the adsorption onto the MOPM is very sensitive to pH. A "S" shape adsorption curve was observed as a function of pH, and adsorption increased over a very narrow pH range, which is located at or over the pH of the point of zero charge of the media coating. Results suggest a favorable solute pH range of 6 or greater for heavy metal removal by manganese oxide coated media. A pH of 6 is the lower end of the pH range that is observed for storm water runoff.

Adsorption rates were fairly fast for MOPM with over 50% removal in the first 30-minutes and over 90% removal with 5-hours. The pH drift patterns over all the reaction time coincided with the heavy metal removal rate curve. This indicated that the adsorption of the divalent heavy metals gives concurrent desorption of protons. The low ratio of proton release to the divalent metal adsorbed (0.5) and the biphasic pH drop at equilibrium indicated that the manganese oxide may act as a buffer in the solution because of its amphoteric characteristics.

# CHAPTER 5. ADSORPTION CHARACTERISTICS OF OXIDE COATED BUOYANT MEDIA ($\rho_S < 1.0$) - EQUILIBRIA MODELS

## 5.1 Introduction

Adsorption isotherm and ion-exchange models have selected applicability when modeling complex and variable natural systems, particularly when the sorbates of interest are minor or trace ionic species (< $10^{-4}$ to $10^{-5}$ mol/kg), and the sorbents exhibit pH-dependent surface charge (Langmuir 1997). For such conditions, the adsorption of trace ionic species often takes place as a function of the net surface charge of the sorbent. This is the behavior of most trace metal cations, including those of the heavy metals and radionuclides adsorbed by positively charged metal oxyhydroxides. The soluble heavy metal concentrations in complex anthropogenic aqueous systems such as storm water are generally in the range of $10^{-4}$ to $10^{-5}$ mol/kg or lower. Previous studies indicate that manganese oxide and manganese oxide coated filter media exhibit a very strong pH-dependent surface charge (Liu *et al* 2001a; 2001b; McKenzie 1981; McKenzie 1989). Therefore, a surface complexation or electrostatic adsorption model, based on double-layer theory, may provide a preferred simulation of adsorption-desorption behavior between these divalent heavy metals and manganese oxide coated media, such as MOPM.

Various possible mechanisms are involved in the transfer of an adsorbate into the adsorption layer. These include transport to the surface by convection or molecular diffusion, attachment to the surface, surface diffusion, dehydration, and formation of a bond with the surface constituents (Stumm 1992). Different kinetic models had been

applied to the heavy metal adsorption for various adsorbents, such as metal oxides (Morel Dzombak and Morel 1985; Hayes and Leckie 1986), granular activated carbon (Cheung *et al* 2001) and soils (Sparks 1999; Sposito 1994). While many empirical models have been fit to experimental data successfully, there is no general law of overall reaction kinetics in combination with the general laws of thermodynamics. To date a genetic relationship with which to connect kinetic species to thermodynamic species does not exist for these adsorbents (Sposito 1994). In this study, a potential driving second-order reaction kinetic model was applied to simulate divalent heavy metal adsorbed onto the surface of MOPM.

**5.2 Objectives**

Manganese oxide coated polymeric media (MOPM) were evaluated through batch adsorption equilibrium and kinetic experiments for the heavy metals, including Pb, Cu, and Zn that are typical of urban storm water runoff. Since the batch experiment results were presented and discussed in chapter 4, this chapter focuses on predicting and explaining results using a triple layer surface complexation model. Thus the objective of this chapter is to obtain the surface acidity constant for MOPM and the surface complexation reaction constants for divalent heavy metals typical of storm water runoff.

**5.3 Background**

A number of surface complexation models have been developed (Davis and Kent 1990; Dzombak and Morel 1990; Stumm 1992; Stumm and Morgan 1996), and research has shown that such models show promise in simulation of adsorption behavior between various sorbents and sorbates at trace level (Westall and Hohl 1980; Dzombak

and Morel 1987). In general such models consider hydrogen and hydroxyl ions to be specifically adsorbed to surfaces and are available for surface complexation reactions. Surface protonation and deprotonation reactions are fundamental to these surface complexation models. For manganese oxide coated media such as MOPM, these reactions can be written in the mass action form as follow.

$$\equiv MnOH + H_s^+ = \equiv MnOH_2^+ \quad (1)$$

$$\equiv MnOH = \equiv MnO^- + H^+ \quad (2)$$

In these equations, $\equiv MnOH_2^+$, $\equiv MnOH$ and $\equiv MnO^-$ represent three different types of solid sorbent surface species, $H_s^+$ represents a hydrogen ion at the surface, and the activity of $H_s^+$ can be assumed to be related to the bulk $H^+$ or $(H_3O)^+$ activity through a Boltzmann factor.

$$\left(H_s^+\right) = (H^+)e^{\left(\frac{-\psi_0 F}{RT}\right)} \quad (3)$$

In these equations, $\psi_0$ is the average potential of the near-surface (Stern layer) as postulated by the Stern-Grahae modification of the Gouy-Chapman description of the electrical double layer, $F$ is the Faraday constant (96480 C/mol), $R$ is the ideal gas constant (8.314 J/mol-K), and $T$ is the absolute temperature. From substitution of equation (3) into the mass action equations, the intrinsic constants are:

$$\frac{1}{K_{a1}^{\text{int}}} = \frac{\left(\equiv MnOH_2^+\right)}{\left(\equiv MnOH\right)(H^+)e^{\left(\frac{-\psi_0 F}{RT}\right)}} \quad (4)$$

$$\frac{1}{K_{a2}^{int}} = \frac{(\equiv MnO^-)(H^+)e^{\left(\frac{-\psi_0 F}{RT}\right)}}{(\equiv MnOH)} \qquad (5)$$

where $K_{a1}^{int}$ and $K_{a2}^{int}$ are intrinsic constants for equation (1) and (2), respectively.

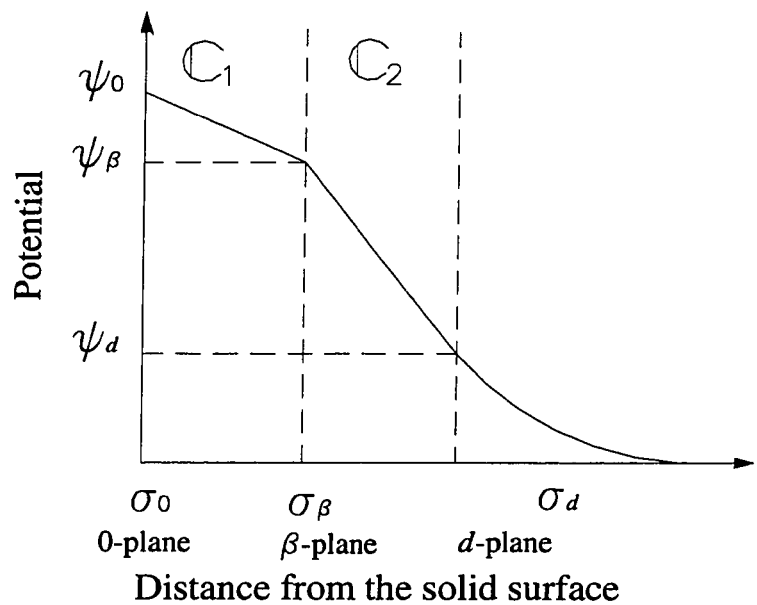


Figure 5.1. Schematic plot of surface charge ($\sigma$), and potential ($\psi$) relationships versus distance from the surface, used in the triple layer model.

Application of diffuse-layer (DL) model theory assumes that electrical potentials measured at the zero plane (0-plane) and diffuse-layer plane (d-plane) are equal ($\psi_0 = \psi_d$). In comparison to the DL model, the constant capacitance (CC) model can be viewed as a special case of the DL model that applies to conditions of low surface potential combined with high and constant ionic strength. In the triple-layer model, only protonation and deprotonation of surface sites are assigned to the 0-plane. Other

specifically adsorbed ions are assigned to the β-plane, a visualized plane where specifically adsorbed ions, except for protonation and deprotonation of surface sites, are assigned. These specifically adsorbed ions determine the surface charge $\sigma_\beta$ and electric surface potential $\psi_\beta$ in the β-plane. Non-specifically adsorbed ions are envisioned as residing in the diffuse layer and are influenced by the potential $\psi_d$. The schematic representation of surface charge and potential relationships versus distance from the solid surface is illustrated in Figure 5.1.

The triple-layer model is more versatile compared to the diffuse layer (DL) and constant capacitance (CC) models. The triple-layer model allows for the observation that adsorption of some species involves strong chemical bonding (chemical adsorption), while also incorporating other species having relatively weak electrostatic attraction (physical adsorption) to the surface (Langmuir 1997). Strongly adsorbed species, such as divalent transition-metal ions (including most heavy metals), are adsorbed at the 0-plane of the sorbent surface (Davis and Kent 1990). The bonding of these strongly adsorbed species is assumed comparable to the bonding experienced by aqueous cations and ligands of inner-sphere solution complexes (Ligands displace one or more cation-bonded water molecule ligands and form bonds usually with partial covalent characteristics.). β-plane species, separated from the surface by water of hydration and also by adsorbed species in the 0-plane, are surface bonded via long-range, weak coulombic forces. Such bonding is equivalent to that experienced by ions that form aqueous ion pairs or outer-sphere complexes, which involve the association of hydrated cations and anions held by long-range electrostatic forces (Smith and Jenne

1991). Monodentate and bidentate surface complex bonding have been considered under the hypothesis of different models for surface complexation of aqueous metals to manganese oxide. For a divalent heavy metal cation, the following surface complexation reaction and mass action expressions illustrate the determination of stoichiometric coefficients for these components. For a monodentate surface complex, the reaction is written as follows.

$$\equiv MnOH + M_s^{2+} = (\equiv MnOM_s)^+ + H^+ \tag{6}$$

The substitution of equation (1) together with

$$(M_s^{2+}) = (M^{2+})e^{\left(\frac{-\psi_\beta F}{RT}\right)^2} \tag{7}$$

provides the mass action expression, written as follows.

$$K_{M^{2+}}^{\text{int}} = \frac{(\equiv MnOM^+)(H^+)e^{\left(\frac{-\psi_0 F}{RT}\right)}}{(\equiv MnOH)(M^{2+})e^{\left(\frac{-\psi_\beta F}{RT}\right)^2}} \tag{8}$$

Here $(M_s^{2+})$ is the activity of $M^{2+}$ (mol/L) on the sorbent surface, $(M^{2+})$ is the metal concentration in the solution (mol/L), and $\psi_\beta$ is the electric potential at the β-plane.

For a bidentate complex, the reaction is written as follows.

$$2 \equiv MnOH + M_s^{2+} = (\equiv MnO)_2 M_s + 2H^+ \tag{9}$$

The resulting mass action expression can be written as follows.

$$K_{M^{2+}}^{\text{int}} = \frac{((\equiv MnO)_2 M_s)(H^+)^2 e^{2\left(\frac{-\psi_0 F}{RT}\right)}}{(\equiv MnOH)^2 (M^{2+})e^{\left(\frac{-\psi_\beta F}{RT}\right)^2}} \tag{10}$$

Considering the structural oxygen and the sorption sites on the manganese oxide (primarily birnessite) surface, which consists of three oxygens around a vacancy in the octahedral layer, carrying a charge of –2 (Drits *et al* 1997), a diprotic complexation model for birnessite was developed by Appelo and Postma (1999). The reactions were formulated as follows.

$$\equiv MnO_3H_2 + H^+ = \equiv MnO_3H_3^+ \quad (11)$$

$$\equiv MnO_3H_2 = \equiv MnO_3H^- + H^+ \quad (12)$$

$$\equiv MnO_3H^- = \equiv MnO_3^{2-} + H^+ \quad (13)$$

$$\equiv MnO_3^{2-} + M^{2+} = \equiv MnOM \quad (14)$$

$$\equiv MnO_3H^- + M^{2+} = \equiv MnOHM^+ \quad (15)$$

In principle, if the stoichiometry of the $H^+$ release is known, it is possible to distinguish between the formation of monodentate and bidentate surface complexes using a Kurbatov plot (Stumm 1992). Although the diprotic model for manganese oxide is applicable for all cation adsorption, it has been limited to sorption modeling of alkaline and alkaline earth ions only (Appelo and Postama 1999). In this study, a monodentate surface complexation model was applied to model the adsorption of divalent heavy metal ions onto our media because the ratios of the $H^+$ released to heavy metal adsorbed are generally less than 1.0.

Although the empirical adsorption models, such as the Freundlich model, can predict the adsorption capacity at a specific pH, the ability of such models to explain the mechanisms of adsorption behavior based on modern physico-chemical theories is

limited. Also, such models may have selected applicability when trying to explain behavior of complex and variable systems, particularly when the sorbates of interest are minor or trace ionic species (< $10^{-4}$ to $10^{-5}$ mol/kg), and the sorbents exhibit pH-dependent surface charge (Langmuir 1997). In this study, a surface complexation model was applied to simulate and predict the adsorption behavior of the MOPM. A nonlinear least square optimization algorithm, FITEQL, was used to solve the multi-component chemical equilibrium consisting of aqueous and solid-aqueous phase equilibria (Herbelin and Westall 1999). The first step in the FITEQL optimization procedure required development of the equilibrium model for the sorbent/solute system. The chemical equilibrium for the triple layer model is equations (1), (2) and (6). The next step required solution of the equilibrium surface complexation model at each of the experimental conditions. Finally, the last step required parameters in the model to be adjusted to minimize the difference between values calculated from the model and values observed experimentally. Since the problem is nonlinear, initial estimates for the values of the adjustable parameters are also needed. The first step of the calculation involves the estimation of the surface protolysis constants from potentiometric titration results at a background electrolyte concentration of 0.1-M $NaNO_3$.

Surface complexation models differ in how they conceptualize the structure of the double layer and describe changes in surface potential and surface charge from the surface of the sorbent phase to the bulk solution. For example, in the constant capacitance (CC) and diffuse-layer (DL) models, all adsorbed species are considered specifically adsorbed at the 0-plane and the adsorption of individual electrolyte ions is

ignored. In contrast, the triple layer (TL) model can assign adsorbed species to either a 0-plane or the more distant β-plane and considers the adsorption of electrolyte ions. As a guide to the position of the adsorbed species in the double layer it has been suggested that when adsoption is found to be independent of ionic strength, sorbate species occupy the 0-plane (Langmuir 1997). The triple layer model requires inner and outer layer capacitance $C_1$ and $C_2$, corresponding to zones between the 0- and the β-plane and the β-plane and d-plane, respectively. Generally, $C_2$ is set to be 0.2 F/m$^2$ (Davis *et al* 1978; Hayes *et al* 1986; Langmuir 1997), while $C_1$ is adjusted to optimize the fit of the TL model to empirical adsorption data. Published values of $C_1$ for δ-$MnO_2$ are 2.4 F/m$^2$ (Fu *et al* 1991; Catts and Langmuir 1986). For this study, initial estimates of modeling parameters and their reference sources are listed in Table 5.1.

Table 5.1. Surface complexation model parameters.

| Parameter | Values | Sources |
|---|---|---|
| Specific Surface Area (m$^2$/g) | 28.7 | This study, (Liu et al 2001a) |
| Initial estimate of site density (sites/nm$^2$) | 2 | Davis and Kent, 1990 |
| Solid concentration (g/L) | 5 | This study |
| Inner layer capacitance $C_1$ (F/m$^2$) | 2.4 | Langmuir, 1997 |
| Outer layer capacitance $C_2$ (F/m$^2$) | 0.2 | Langmuir, 1997 |
| $\log K_{Na}^{int}$ | 3.5 | Smith and Jenne, 1991 |
| Initial estimate of $\log K_{a1}^{int}$ | -6.2 | Smith and Jenne, 1991 |
| Initial estimate of $\log K_{a2}^{int}$ | 1.6 | Smith and Jenne, 1991 |

## 5.4 Material and Methods

The experimental materials, batch adsorption equilibrium, kinetic experiments, and metal analyses are described in chapter 4. In this chapter, adsorption equilibria were modeled using a triple layer surface complexation model in FITEQL (Herbelin and

Westall 1999), a computer program for determination of chemical equilibrium constants from experimental data. The adsorption kinetics were modeled using a potential driving second order model developed for this study.

**5.5 Results and Discussion**

Table 5.2. Equilibrium constants for triple-layer modeling of adsorption edge

| Reaction | Log K | Sources |
|---|---|---|
| Surface acidity reaction | | |
| $>MnOH + H^+ \Leftrightarrow >MnOH_2^+$ | 3.196 | This Study |
| $>MnOH \Leftrightarrow >MnOH_2^+ + H^+$ | -5.802 | This Study |
| Zinc | | |
| Surface reaction | | |
| $Zn^{2+} + >MnOH \Leftrightarrow >MnOZn^+ + H^+$ | -4.45 | This Study |
| Hydrolysis reaction | | |
| $Zn^{2+} + H_2O \Leftrightarrow >ZnOH^+ + H^+$ | -9.00 | Smith and Martell (1976) |
| $Zn^{2+} + 2H_2O \Leftrightarrow >Zn(OH)_2 + 2H^+$ | -17.90 | Smith and Martell (1976) |
| $Zn^{2+} + 3H_2O \Leftrightarrow >Zn(OH)_3^- + 3H^+$ | -28.40 | Smith and Martell (1976) |
| Lead | | |
| Surface reaction | | |
| $Pb^{2+} + >MnOH \Leftrightarrow >MnOPb^+ + H^+$ | -1.91 | This Study |
| Hydrolysis reaction | | |
| $Pb^{2+} + H_2O \Leftrightarrow >PbOH^+ + H^+$ | -7.71 | Smith and Martell (1976) |
| $Pb^{2+} + 2H_2O \Leftrightarrow >Pb(OH)_2 + 2H^+$ | -17.12 | Smith and Martell (1976) |
| $Pb^{2+} + 3H_2O \Leftrightarrow >Pb(OH)_3^- + 3H^+$ | -28.06 | Smith and Martell (1976) |
| Surface reaction | | |
| $Cu^{2+} + >MnOH \Leftrightarrow >MnOCu^+ + H^+$ | -2.53 | This Study |
| Hydrolysis reaction | | |
| $Cu^{2+} + H_2O \Leftrightarrow >CuOH^+ + H^+$ | -6.30 | Smith and Martell (1976) |
| $Cu^{2+} + 2H_2O \Leftrightarrow >Cu(OH)_2 + 2H^+$ | -12.80 | Smith and Martell (1976) |
| $Cu^{2+} + 3H_2O \Leftrightarrow >Cu(OH)_3^- + 3H^+$ | -14.50 | Smith and Martell (1976) |
| $Cu^{2+} + 4H_2O \Leftrightarrow >Cu(OH)_3^{2-} + 4H^+$ | -16.40 | Smith and Martell (1976) |
| $2Cu^{2+} + 2H_2O \Leftrightarrow >Cu_2(OH)_2^{2+} + 2H^+$ | -17.70 | Smith and Martell (1976) |

The surface reaction equations, optimized equilibrium constants and other hydrolysis reaction constants used in the FITEQL-TLM calculation are summarized in Table 5.2. All the model optimization solutions converged, and the fitting parameter,

SOS/DF, which represents the sum of the squares of the errors (SOS) between experimental and model values divided by the degrees of freedom (DF), was generally located in or close to the general range of 0.01-20 (Herbelin and Westall 1999). The surface acidity reaction constant for the MOPM of $\log K_{a2}^{int}$ = -5.802 is close to those reported for pure manganese oxide. For example, the $\log K_{a2}^{int}$ values reported by Catts and Langmuir (1986) and Fu *et al* (1991) are -4.2 and –5.34, respectively. The uncertainty associated with the $\log K^{int}$ value can arise from many sources including both experimental and numerical. In addition, because of the complexity of the manganese oxide structures, manganese oxides with heterogeneous surface properties (such as MOPM with a combination of birnessite and cryptomelane minerals) can contribute to such uncertainty. For this study, the difference may also come from the physical differences between manganese oxide coating on polymeric media and pure manganese oxides. Another important variation of surface reaction constants arises from uncertainties in site density and can be a significant source of uncertainty in the values of $\log K^{int}$ reported in the literature (Smith and Jenne 1991). Uncertainties in the numerical values of $\log K^{int}$ also can arise from differences in the surface loading of the adsorbate on the oxide surface. Although numerical values of the triple-layer intrinsic constants for adsorption of heavy metals by MOPM are somewhat different from the reported values because of the uncertainty discussed above, the order of the intrinsic constants, which imply the adsorption affinity, are the same. For example, Langmuir (1997) summarized triple-layer model intrinsic constants for adsorption by birnessite (δ-

$MnO_2$) with an order of intrinsic constants of $\log K_{Pb}^{int}$ (1.8) > $\log K_{Cu}^{int}$ (-0.1) > $\log K_{Zn}^{int}$ (-1.5).

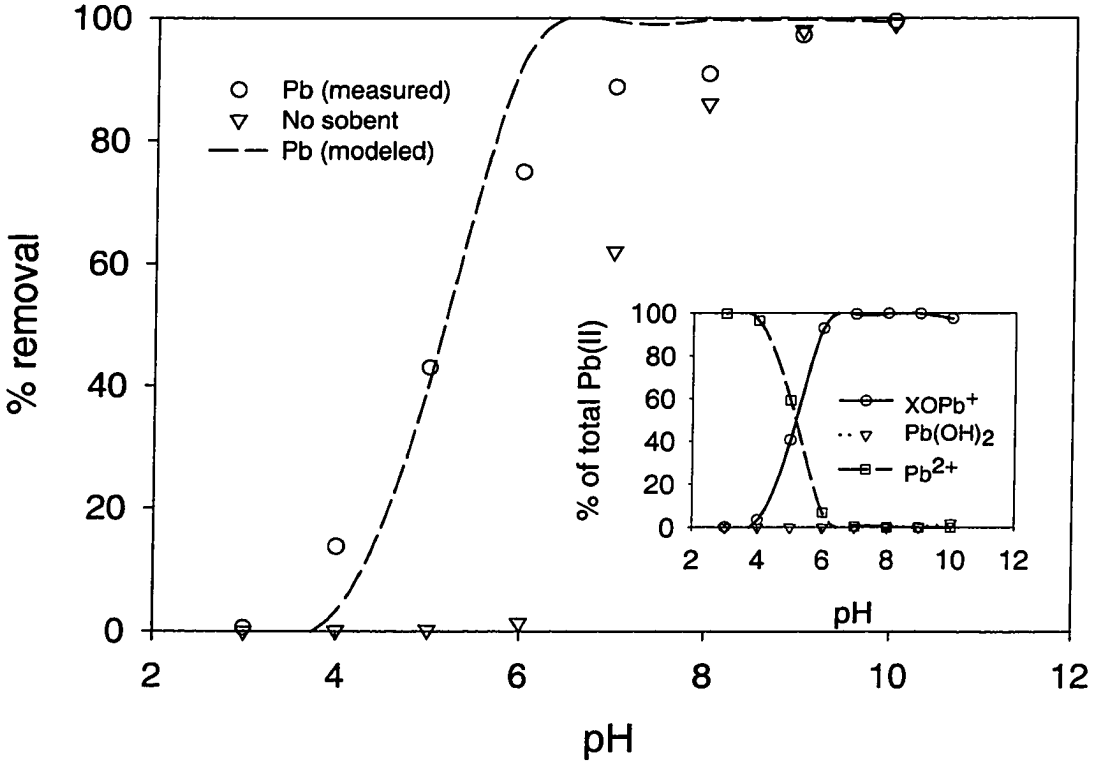


Figure 5.2. Pb(II) removal as a function of pH. Initial Pb(II) concentration is 5 mg/L and sorbent/solute ratio is 5-g/L (32.5-mg manganese/L). The adsorption edge is calculated with FITEQL-TLM using $\log K_{Pb^{2+}}^{int}$ of -1.91.

The adsorption edges of the triple layer model, experimental data and major species distribution of Pb(II), Cu(II) and Zn(II) are shown in Figures 5.2, 5.3 and 5.4 respectively. To investigate the importance of metal hydroxide precipitation, a series of batch experiments with no sorbent were conducted under the same conditions as the batch experiments with MOPM. The results of no sorbent experiments for Pb(II) shown

in Figure 5.2 indicate that precipitation was significant at pH levels greater than 6. However, the results of speciation calculated using FITEQL-TLM showed that the dominant species is still the surface complex of Pb (>MnOPb$^+$) at a pH as high as 10, a pH that resulted in almost 100% precipitation in the no sorbent experiments. This indicates that for Pb, the removal mechanism is predominantly adsorption or surface complexation for MOPM as sorbent media for the pH range of 6 to 8. Considering the species distribution and the conventional mechanisms of coordination chemistry, there are two ligands available, hydroxyl and surface sites of manganese oxides. According to the speciation results, manganese oxide surface sites are relatively stronger ligands for Pb than hydroxyl ligands.

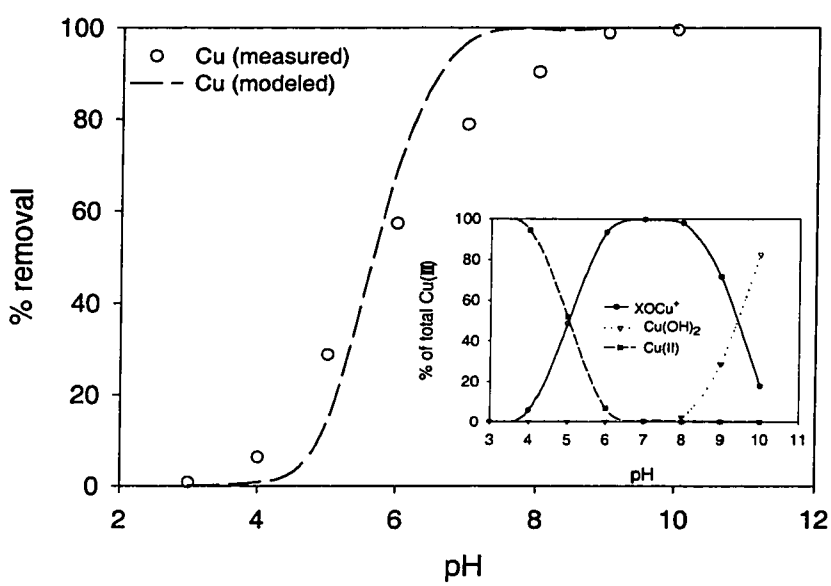


Figure 5.3. Cu(II) removal as a function of pH. Initial Cu(II) concentration is 5-mg/L and sorbent/solute ratio is 5-g/L. The adsorption edge is calculated with FITEQL-TLM using $\log K^{int}_{Cu^{2+}}$ of -2.53.

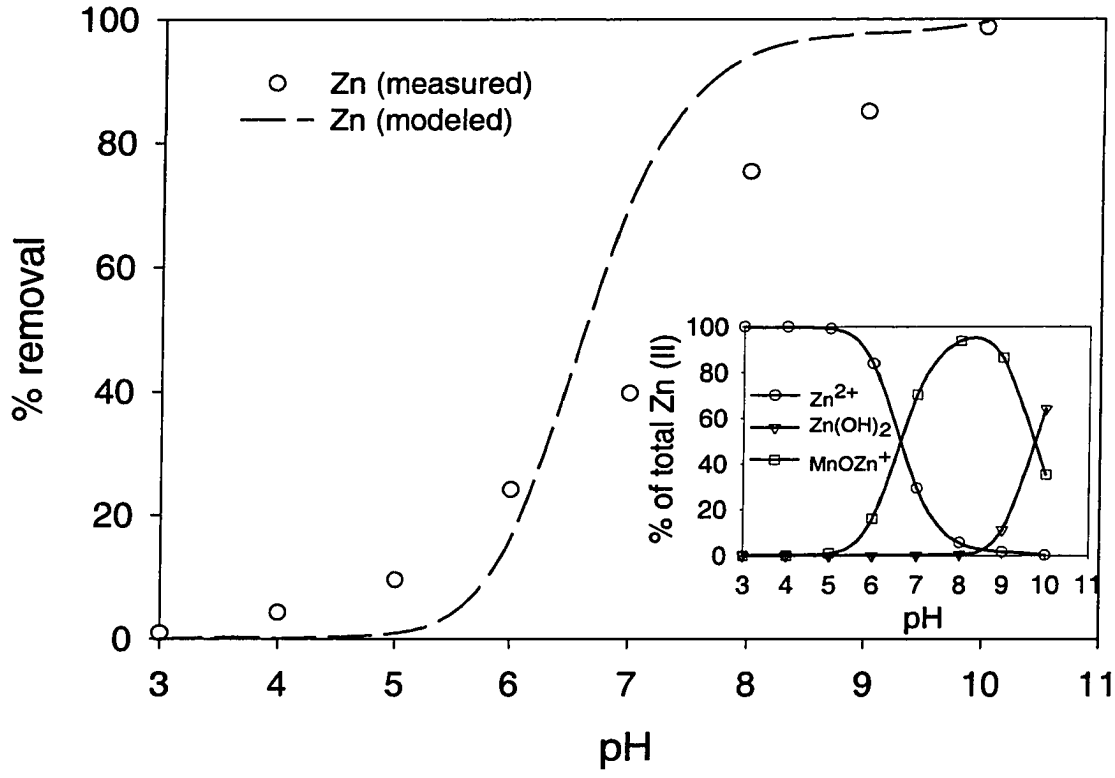


Figure 5.4. Zn(II) adsorption as a function of pH. Initial Pb(II) concentration is 5-mg/L and sorbent/solute ratio is 5-g/L. The adsorption edge is calculated with FITEQL-TLM using $\log K^{int}_{Zn^{2+}}$ of –4.45.

The speciation for Cu(II) and Zn(II) indicated that metal hydroxide precipitation is important at pH greater than 8. Since typically the pH of storm water is in the range of 6-8 and the batch experiments were conducted in a closed nitrogen atmosphere system (no effect of $CO_2$), we only consider metal hydroxide precipitation and surface complexation as the primary removal mechanisms. Adsorption and surface complexation would be the dominant removal mechanism using MOPM for the heavy metal removal using Best Management Practices such as sorptive buoyant media

clarifiers (SBMC) containing MOPM. The complexity of real storm water will require additional study, but these results suggest the treatment using SBMC with MOPM will be through adsorption and surface complexation.

**5.6 Summary and Conclusion**

The intrinsic surface acidity constants for MOPM were determined using FITEQL-TLM and are $\log K_{a1}^{int}$=3.196 and $\log K_{a2}^{int}$ = -5.802. The intrinsic surface reaction constants were determined through the adsorption data as a function of pH using FITEQL-TLM, and are $\log K_{Pb}^{int}$ = –1.91, $\log K_{Cu}^{int}$ = -2.53 and $\log K_{Zn}^{int}$ = -4.45. A potential driving second-order kinetic model has been developed and fitted successfully for the sorption of the divalent metal ion onto the MOPM. The general adsorption kinetics for MOPM can be described as a fast adsorption reaction occurring within 30-minutes followed by a slower reaction continuing from 5 to 15-hours, as a function of different initial pH and sorbent dosages. These secondary slower reactions may be explained by differences in MOPM surface coating morphology (Liu et al 2001a). These secondary slower reactions have been observed for other oxides and have typically been explained as either (1) diffusion to internal sites, (2) surface precipitation, or (3) adsorption to lower affinity sites (Strawn *et al* 1998; Axe and Anderson 1997; Towle *et al* 1997; Scheidegger *et al* 1996; Loehr and Webster 1996). The reaction kinetic mechanism can be interpreted using the assumptions of the potential driving second-order model that the dominant control forces are the chemical potential of the MOPM activated surface sites surface and chemical potential of sorbate in the solution.

# CHAPTER 6. OVERALL RATE KINETICS FOR HEAVY METAL ADSORPTION ONTO COMPOSITE OXIDE COATED POLYMERIC MEDIA

## 6.1 Introduction

Heavy metal adsorption onto specific media, such as silica sand, soils, granular activated carbon (GAC) and iron oxide coated media, have been studied extensively in the past (Langmuir, 1997; Stumm and Morgan 1996; Stumm 1992). Implementation of these results to engineered processes for these media has proved successful in engineering design. Manganese and iron oxides are used as adsorbents because they are prevalent in soils and sediments; they high affinity for metal ions and are often microporous. Manganese oxides have shown a very strong affinity for several heavy metals (Tamura et al 1997; Catts and Langmuir 1986). The point of zero charge (PZC) of manganese oxide ranges from 1.5 for birnessite to 4.6 for the hollandite group (Healey 1966). While the performance of engineered media such as GAC and iron oxide coated sand have been studied with respect to heavy metal adsorption there is very little documentation of manganese oxide coated media. Examples of such engineered media include manganese oxide coated polymeric media (MOPM) (Liu et al 2001a). The PZC of synthetic birnessite have been reported from 1.5 to 3.0 due to different manganese oxide synthesis methods and surface charge measurement methods (McKenzie 1989; Zasoski and Burau 1988; Morgan and Stumm 1964). Manganese oxides have a high negative charge at higher pH level and their cation adsorption capabilities increase with increasing pH. The significant adsorption of heavy metal at the PZC illustrates that other adsorption forces, in addition to electrostatic forces, are

involved in the adsorption process (McKenzie 1989; Murray 1974). Spectroscopic analyses of metal coordination by manganese oxide minerals utilizing extended X-ray absorption fine structure (EXAFS) indicated that uptake of cationic heavy metals at the pH lower than PZC is through the mechanism of ion exchange (Randall 1998; Manceau 1992), of which instead of being adsorbed on the amphoteric external surface of manganese oxides as most surface complexation models described, heavy metals are predominately occurred in manganese oxide's inner structure, such as tunnel sites of cryptomelane.

A number of different kinetic models had been applied to the heavy metal adsorption by various adsorbents, such as iron oxides (Dzombak and Morel 1985; Hayes and Leckie 1986), granular activated carbon (Cheung 2001) and soils (Sparks 1999; Sposito 1994). The kinetic of adsorption processes can be separated into chemical kinetics and multiple transport processes. Multiple transport processes include interparticle diffusion and intraparticle diffusion (Sparks 1999). However, in most cases, both chemical kinetics and multiple transport processes are occurring simultaneously (Sparks 1999; Sposito 1994). Thus, determination of chemical kinetics in heterogeneous systems including the rates of chemical reactions and of molecular processes by which reactions occur, where transport is not limiting, has been extremely challenging (Sparks 1999). In some cases, an overall rate covering all the multiple processes was assumed to simplify the representation of the adsorption kinetics on the solids (Sposito 1994). For example, average adsorption kinetics very similar to that of the complexation reactions for humic substances were applied to heterogeneous

surfaces by including the hypothesis that effective or average rate constants provide a useful representation of a system that in reality exhibits a broad spectrum of surface reactivity (Sposito 1994). In this study, a potential driving kinetic model, a model that considers the overall rate of all the multiple processes, was developed.

**6.2 Objectives**

Previous studies have reported on the development of MOPM for use as a buoyant adsorptive-filtration media for use in storm water BMPs (Liu et al 2001a). MOPM was synthesized as a high surface area media engineered as alternative sorptive medium for heavy metal removal in storm water treatment systems such as an upflow sorptive buoyant media clarifier (SBMC). To date, no laboratory or field studies with respect to the adsorption kinetic of this medium have been conducted. There were three objectives of this study. The first objective is to characterize the surface morphology of MOPM through scanning microscope (SEM) technique. The second objective of this study was to develop a potential-driving kinetic model based on an elementary second order rate law and evaluate this model with respect to the experimental data. The third objective was to examine the predictive ability of series kinetic models including a first order model, second order model, psuedo-second order model, power function model, parabolic diffusion model and simple Elovich model, with respect to the experimental data. The predictive abilities of each of these models were compared with the potential driving model by means of coefficients of determination and goodness of fit.

## 6.3 Modeling Approach

### 6.3.1 The Elovich Model

The Elovich model, an empirical chemisorption model, was originally developed to describe the kinetics of heterogeneous chemisorption of gases on a solid surface. The Elovich model has been used to describe the kinetics of sorption and desorption of various inorganic materials on many sorbents (Sparks 1999). The Elovich model can be expressed in the following form:

$$Q_t = \frac{1}{\beta}\ln(\alpha\beta) + \frac{1}{\beta}\ln(t) \tag{1}$$

$Q_t$ is the amount of sorbate per unit mass of sorbent at time $t$, and $\alpha$ and $\beta$ are constants during any one experiment. $\alpha$ and $\beta$ can be determined by plotting of $Q_t$ vs. $\ln(t)$.

### 6.3.2 Potential Driving Kinetic Model

The elementary second-order reaction with different reactants can generalized as the following reaction:

$$A + B \xrightarrow{k} P \tag{2}$$

The differential equation description and the analytical solution with initial condition of $[A] = [A]_0$ and $[B] = [B]_0$ at $t = 0$ are as follows.

$$\frac{d[A]}{dt} = -k[A][B] \tag{3}$$

$$[A] = \frac{[A]_0([A]_0 - [B]_0)}{[A]_0 - [B]_0 e^{-k([A]_0 - [B]_0)t}} \tag{4}$$

where $k$ is the reaction rate constant ($M^{-1}s^{-1}$), $t$ is the reaction time (s), $[A]_0$ and $[B]_0$ are the initial concentrations of reactants A and B at t = 0, respectively.

For a heterogeneous solution (the metal concentration at the near-surface differs from the bulk solution), the monodentate surface reaction mechanism between hydrous oxides and divalent heavy metal cations may be depicted as the following surface complexation reaction (Langmuir 1997; Stumm and Morgan 1996).

$$\equiv X-OH + Me^{2+} \Leftrightarrow \equiv X-OMe^{+} + H^{+} \quad (5)$$

where $\equiv X-OH$ is the hydrous oxide surface sites, $Me^{2+}$ is the divalent heavy metal cations, $\equiv X-OMe^{+}$ is the surface complex of divalent heavy metals, and $H^{+}$ is the proton released.

In developing any mathematical description of the sorption process, certain assumptions should be made. There can be various rate limiting steps, such as chemical reaction, film diffusion and intraparticle diffusion (Langmuir 1997; Sparks 1999; Sposito 1994). For the kinetic model of this study, an overall rate covering all the processes was utilized to simplify the presentation of adsorption kinetics from aqueous solution to MOPM. This overall rate was considered to be related to the adsorption potentials (chemical or electrical or other energy forces of the diffusion processes) of surface sites and sorbates. Since only differences in potential are ever physically meaningful (Israelachvili 1991), and the differences of potential can be from the variation of space or time, the potential in equilibrium ($t = \infty$) can be set to zero or as a standard potential. Thus the potential for any time, t is $\rho_t$ - $\rho_\infty$ ($\rho_t$ is the absolute potential at time t, and $\rho_\infty$ is the absolute potential at $t = \infty$). Concentration differences between the bulk solution and MOPM surface sites were utilized at time, t and at

equilibrium for model computations. Potential differences were assumed to be correlated to the difference in bulk solution concentration of heavy metals and number of surface sites. Moreover, it should be assumed that the sorption follows the Freundlich equation and this has been confirmed in chapter 4. Therefore, for the potential driving kinetic model of this study, following assumptions are made.

1. There is a monolayer of metal ion on the surface of hydrous oxide (Langmuir 1997; Sparks 1999);
2. The energy of sorption for each ion is different and dependent of surface coverage (Sparks 1999; Sposito 1994);
3. Energy potentials of all the driving forces are correlated to the available surface sites and metal ions concentrations;
4. The adsorption potential is the overall energy potential of all the driving forces in any of the limiting step, and it is a difference of time;

The overall assumption is that the rate of the second order type reaction (equation (5)) is dependent on two factors: (1) the divalent heavy metal concentrations and available surface site number; (2) the divalent heavy metal concentrations and surface site number at equilibrium. Using similar hypothesis, kinetics of divalent heavy metals adsorption onto peat were modeled successfully (Ho and McKay 1999).

A potential driving rate differential equation expression for the sorption described by the equation (5) can be represented as follows.

$$\frac{dC_t}{dt} = -k(S_e - S_t)(C_t - C_e) \qquad (6)$$

Here $S_t$ is the number of active sites occupied on MOPM at time $t$, $S_e$ is the number of active sites occupied at equilibrium (MOPM).

$S_t$ and $S_e$ can be represented as follows.

$$S_t = \frac{C_0 - C_t}{a} \tag{7}$$

$$S_e = \frac{C_0 - C_e}{a} \tag{8}$$

Here $C_0$ is the initial metal concentration, $C_t$ is the metal concentration at time $t$, $C_e$ is the metal concentration at equilibrium, and $a$ is the sorbent/solute ratio. Substituting into equation (6) and rearranging yields the following equation.

$$-\frac{dC_t}{(C_e - C_t)^2} = \frac{k}{a}dt \tag{9}$$

Integrating equation (9) for the initial and boundary conditions $t = 0$ to $t = t$ and $C_0$ to $C_t$,

$$-\int_{C_0}^{C_t} \frac{dC_t}{(C_e - C_t)^2} = \int_0^t \frac{k}{a}dt \tag{10}$$

yields:

$$\frac{1}{(C_0 - C_e) - (C_0 - C_t)} = \frac{1}{C_0 - C_e} + \frac{k}{a}t \tag{11}$$

Equation (11) is the integrated rate equation for the potential driving model.

Equation (11) can be rearranged to a linear form as the following equation.

$$\frac{t}{C_0 - C_t} = \frac{t}{C_0 - C_e} + \frac{a}{k(C_0 - C_e)^2} \tag{12}$$

The rate constant $k$ and equilibrium concentration $C_e$ can be determined experimentally by plotting $\frac{t}{C_0 - C_t}$ against $t$.

## 6.4 Materials and Methods

### 6.4.1 Materials

Manganese oxide coated polymeric media (MOPM) was prepared using a two-step coating method, an iron oxide scratch coating first, then a layer of birnessite coating. The details of preparation methods and characteristics of the media utilized in this study have been examined previously in chapter 4. The MOPM were approximately spherical in shape with a mean diameter of 3.44 mm and a mean specific gravity, $\rho_s$ = 0.928. The measured mean of specific surface area (SSA), of the media was 27.34-$m^2$/g with a standard deviation of 1.13 (n = 3) determined by a modified ethylene glycol monoethyl ether (EGME) method (Sansalone et al 1998). Surface charge distribution was measured using a potentiometric titration (Van Raij and Peech 1972) and discussed elsewhere (4). The PZC of MOPM was measured at 4.8.

Aqueous solutions of cadmium, copper, lead and zinc were prepared from 1000-ppm reference standard solutions of metal nitrates. The ionic background was fixed in 0.01-M as $NaNO_3$. pH adjustment was made with either 1-N $HNO_3$ or 1-N NaOH. The pH of the metal solution was adjusted to the designated values for each batch experiment run, sealed and set overnight. During the following day the pH was readjusted if required to the designated initial value before batch experiments were initiated.

### 6.4.2 Methods

**Scanning electronic microscope (SEM)**

SEM was carried out to obtain MOPM surface topography and morphology information, as well as qualitative chemical composition. Backscattered electron (BSE) imaging provided direct (but not specific) information on compositional heterogeneity through the mechanism of atomic number contrast, while X-ray area scanning (dot mapping) provided qualitative abundance information for a specific element (Goldstein et al 1992). SEM samples were dried at 60 °C in an oven for 24 hours, glue-mounted and gold-coated by a vacuum electric arc. Sample cross-sections were embedded in epoxy, ground to a thickness less than 5-μm, polished to 0.05-μm and carbon coated. Standard qualitative elemental analysis of the coatings was carried out using a HNU energy dispersive X-ray spectrometer system (EDX) and an associated JSM-840A Scanning Microscope. The chemical compositions and bonding of the coatings in the edge of the thin sections were determined by X-ray area compositional scanning.

**Kinetic study**

Adsorption experiment is commonly conducted by adding a known amount of sorbate to the sorbent in an aqueous solution and analyzing the resulting concentration of solute in solution. United States Environmental Protection Agency (USEPA) and National Bureau of Standards (NBS) recommend 2-liter bottles in a rotary tumbler in a completely mixed batch reactor for batch-type procedures for estimating soil adsorption of chemicals (Roy et al 1992a). In spite of the apparent ease of such experiments, many source of errors are possible (Roy et al 1992a; 1992b). For example, in a rotary tumbler,

oxide coating can be abraded and separated from the MOPM leading to large experimental error and thus making representative analysis difficult.

An important alternative technique for the classic batch experiment using a rotary tumbler is the use of a re-circulating flowthrough reactor for the determination of sorption parameters (Sparks 1999). In this form of a batch experiment, a fixed volume of heavy metal solution is constantly recirculated through a short column containing sorbents as a flowthrough reactor. In this study, to avoid abrasion of the oxide surface, a short column (25.4-mm ID, 50.8-mm length, Teflon PFA column) packed with test media served as the recirculating flowthrough reactor. Aqueous metal solutions were recirculated through the reactor by a peristaltic pump at a surface loading rate of 500 $ml/cm^2/min$ for reactor containing different sorbent/solute ratios. This surface loading rate is equal to that of the rotary tumbler operating at 29 rpm. Aqueous metal solutions were studied at initial contaminated heavy metal concentration of 1 to 5-ppm, ionic strength of 0.01-M as $NaNO_3$ and pH values from 5 to 7, a pH range typical of urban storm water (Sansalone et al 2001). All reactions were kept under a nitrogen atmosphere. The pH was not adjusted during the reaction period, and any pH drift were measured and recorded every 10-minutes by a computer controlled pH meter. Prior to recirculating, two filtered and two unfiltered aqueous samples were taken from the reactor to verify the initial target heavy metal concentration and identify any filter losses of solute. A 5-mL sample was extracted from the solution and filtered though 0.45-μm membrane using a syringe sampler with a polypropylene syringe filter at predetermined time intervals. The samples were acidified in trace metal $HNO_3$ to a 5%

v/v basis and analyzed for the target heavy metal concentrations by ICP-MS analysis. The solid phase heavy metal concentrations were calculated as the difference between initial and final concentrations. The relationship between liquid and solid phase heavy metal equilibrium concentration were developed for each set of solution conditions. pH drift from the initial pH in each reactor was also expected because of the surface complexation reactions at the interface between the solid phase (manganese oxide) and aqueous phase (heavy metal cation) through the release of hydrogen ions.

**Goodness of fit**

A goodness of fit test for distribution fitting was adopted for comparing models to experimental data and identifying the best-fit model (Buckland et al 1993). The goodness of fit equation utilized was:

$$\chi^2 = \sum_{i=1}^{n} \frac{[O(x_i) - E(x_i)]^2}{E(x_i)} \tag{15}$$

Here $O(x_i)$ is the observation data, $E(x_i)$ is the expected value (modeled data), $n$ is the number of data points, $\chi^2$ is the result for computed goodness of fit value and it follows a chi-square distribution (The degree of freedom is $n$ minus the number of estimated parameters). The model that provided the least $\chi^2$ value was considered the best-fit model.

## 6.5 Result and Discussion

### 6.5.1 Morphology of MOPM Coating

Althrough SEM were considered an ex-situ technique, it was still widely used as a morphology investigation method for oxide coated material (Merkle et al 1996; 1997).

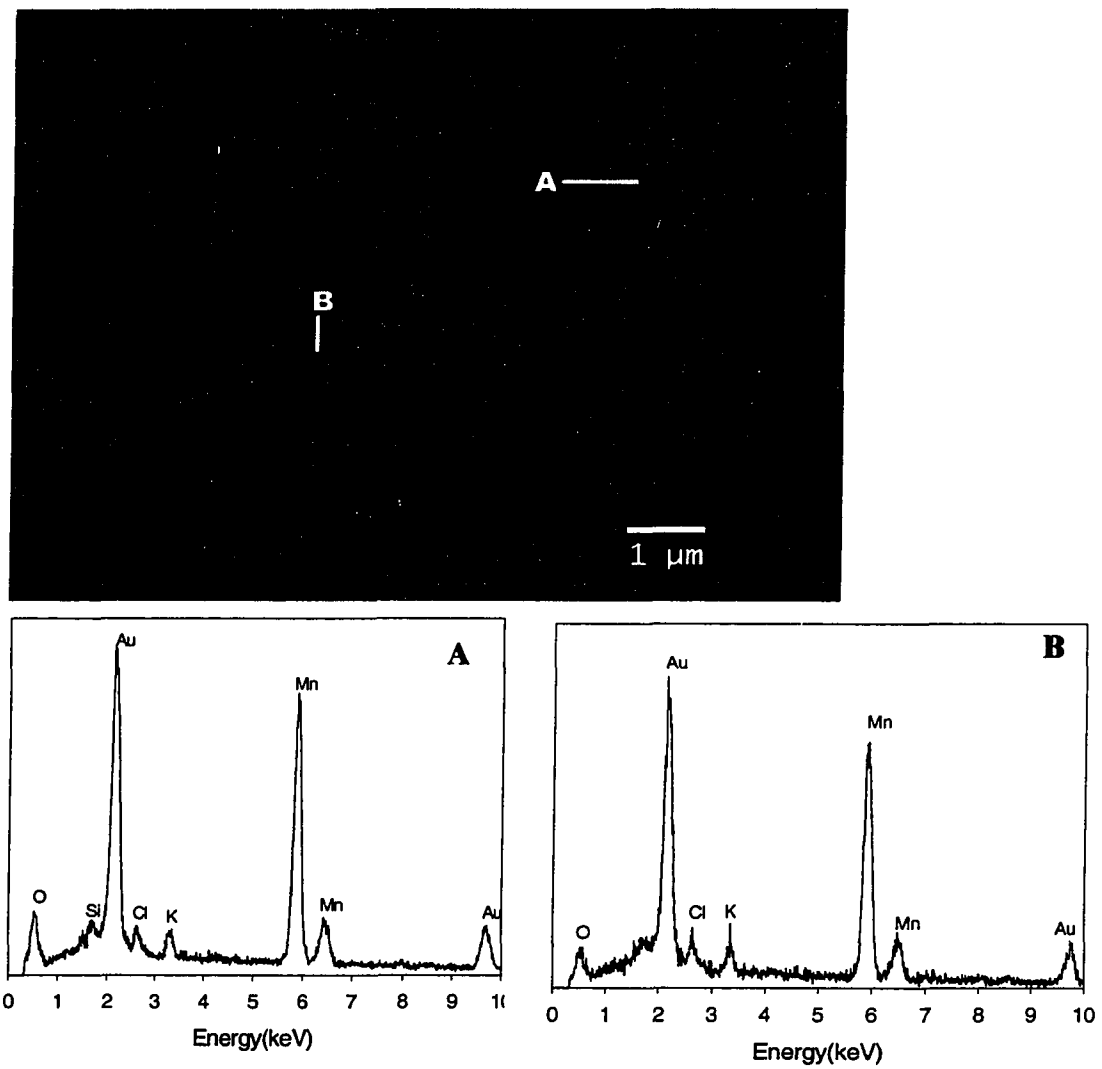


Figure 6.1 A needle shape manganese oxide coated polymeric media surface. The letters in the photo denote area where EDX spectra (A and B) were obtained.

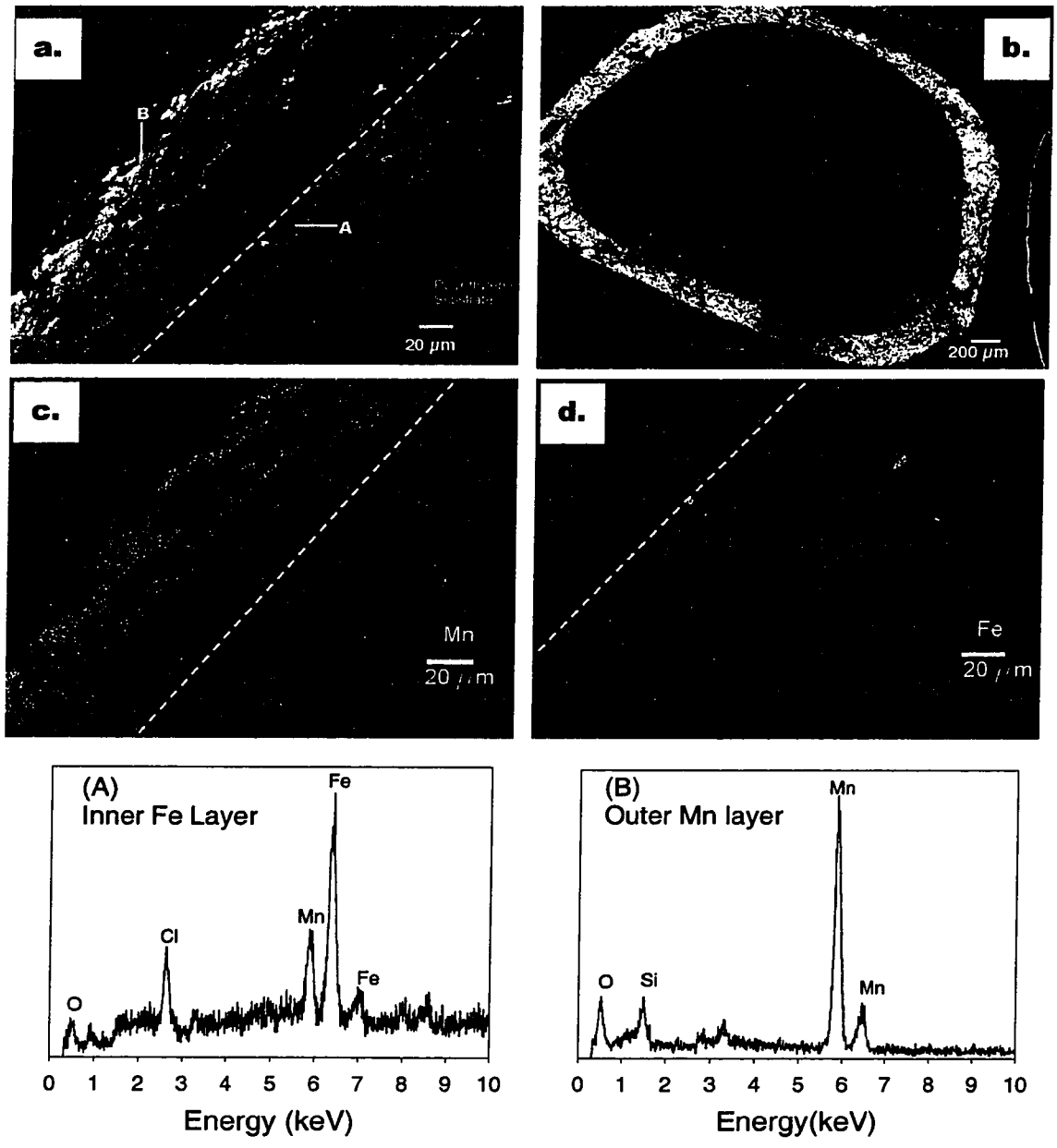


Figure 6.2 BSE images illustrating the Mn and Fe layers of a MOPM oxide surface in part (a) and a cross-section of the media in part (b). X-ray dot mapping areas in part (c) illustrate the predominance of Mn in surface layer while part (d) illustrates the predominance of Fe in the interface layer between the Mn surface and surface of the media substrate. The density of the white dot illustrate the abundance of the background element, either Mn or Fe.

The morphology of manganese oxide coating surface is that of needle shaped crystals shown in the SEM image illustrated in Figure 6.1. The roughness of manganese oxide coated surface indicates a significantly larger specific surface area compared to a smooth surface of the uncoated polymeric substrate.The SEM image also identified some irregular pores in the manganese oxide surface with dimensions varying from less than 0.1-μm to several μm. Media with micropores may have a relatively long equilibrium time or a two-stage adsorption kinetics, where the first step is fast and an adsorption reaction takes place on the outer layer of the coating with readily available sites, while the second step is a slower one in which ions must diffuse into the micropores and react with inner particle sites that are not readily available to the surface. The BSE image of Figure 6.2a illustrates two well-defined coating layers, an iron oxide layer near the polymeric surface and a manganese oxide layer. The coating is hetergeneous, with a thickness from roughly 20-μm to as high as 200-μm as shown in Figure 6.2b. The BSE image of the cross section of the coating layer also indicates a porous surface for MOPM. These macropores and micropores produce an intra-aggregate transport (intra-paticle diffusion) influence the kinetics of metal ion adsorption. In the outer layer there is a high density of Mn as shown in the dot map Figure 6.2c, but an expected Fe-rich layer in the dot map for Fe is not obvious in Figure 6.2d, despite the fact that the EDX spectra indicated the inner layer was of high Fe content. A likely reason for poor Fe layer detection is that because of the rougher surface of the inner layer, X-rays were trapped there and gave less backscattering.

Table 6.1 Coefficients of determination ($r^2$) and goodness of fit ($\chi^2$) for the fit of the time dependent of divalent heavy metal adsorption on MOPM to several kinetic models in single metal systems.

| Modeling metal element | pH | Sorbent dosage (g/L) | Coefficients of Determination for the Linearized Forms of Kinetic Equations ($r^2$) and Goodness of Fit ($\chi^2$) | | | | | | | | | | | | | |
|---|---|---|---|---|---|---|---|---|---|---|---|---|---|---|---|---|
| | | | [a]First Order | | [a]Power Function | | [a]Parabolic Diffusion | | [a]Simple Elovich | | [b]Second Order | | [b]Psuedo-second Order | | Potential driving | |
| | | | $r^2$ | $\chi^2$ | $r^2$ | $\chi^2$ | $r^2$ | $\chi^2$ | $r^2$ | $\chi^2$ | $r^2$ | $\chi^2$ | $r^2$ | $\chi^2$ | $r^2$ | $\chi^2$ |
| Pb | 6.0 | 2.5 | 0.741 | 0.04 | 0.414 | 0.11 | 0.851 | 0.02 | 0.827 | 0.01 | 0.742 | 0.02 | 0.895 | 0.01 | 0.768 | 0.00 |
| Pb | 6.0 | 5.0 | 0.722 | 0.11 | 0.381 | 0.14 | 0.822 | 0.08 | 0.793 | 0.03 | 0.723 | 0.05 | 0.852 | 0.16 | 0.828 | 0.02 |
| Pb | 6.5 | 5.0 | 0.434 | 3.31 | 0.797 | 0.20 | 0.991 | 0.22 | 0.859 | 0.47 | 0.436 | 1.01 | 0.909 | 0.50 | 0.998 | 0.08 |
| Pb | 7.0 | 2.5 | 0.431 | 4.72 | 0.202 | 1.60 | 0.978 | 1.09 | 0.852 | 0.49 | 0.368 | 1.33 | 0.938 | 0.93 | 0.993 | 0.13 |
| Pb | 7.0 | 5.0 | 0.363 | 2.94 | 0.231 | 1.30 | 0.685 | 0.42 | 0.870 | 5.21 | 0.431 | 2.24 | 0.856 | 0.85 | 0.998 | 0.99 |
| Cu | 7.0 | 2.5 | 0.655 | 0.15 | 0.179 | 0.21 | 0.965 | 0.37 | 0.791 | 0.01 | 0.647 | 0.02 | 0.874 | 0.02 | 0.988 | 0.01 |
| Cu | 7.0 | 5.0 | 0.693 | 1.67 | 0.693 | 0.29 | 0.983 | 0.41 | 0.927 | 0.05 | 0.696 | 0.35 | 0.922 | 0.25 | 0.992 | 0.10 |
| Zn | 7.0 | 5.0 | 0.623 | 0.33 | 0.876 | 0.43 | 0.914 | 0.03 | 0.898 | 0.04 | 0.633 | 0.10 | 0.928 | 0.01 | 0.973 | 0.03 |
| Cd | 7.0 | 5.0 | 0.685 | 0.46 | 0.579 | 0.15 | 0.965 | 0.08 | 0.883 | 0.03 | 0.687 | 0.13 | 0.907 | 0.09 | 0.969 | 0.02 |

[c]The linear kinetic equation and their linear plot:

First order: $\ln C_t = \ln C_0 - kt$, plot $\ln C_t$ vs $t$

Power function: $\ln Q_t = \ln k + \nu \ln t$, plot $\ln C_t$ vs $\ln t$

Parabolic diffusion: $(Q_t/Q_\infty)/t = (4/\pi^{0.5})(D/r^2)^{0.5}(t^{-0.5}) - D/r^2$, plot $(Q_t/Q_\infty)/t$ vs $t^{-0.5}$

Simple Elovich: $Q_t = (1/\beta)\ln(\alpha\beta) + (1/\beta)\ln(t)$, plot $Q_t$ vs $\ln t$

Second order: $\ln((C_t + aS_0 - C_0)/C_t) = \ln(aS_0/C_0) + kt(aS_0 - C_0)/a$, plot $\ln((C_t+aS_0-C_0)/C_t)$ vs $t$

Psuedo-second order: $\ln((C_t - C_e)/C_t) = \ln(C_0 - C_e/C_0) - ktC_e/a$, plot $\ln((C_t - C_e)/C_t)$ vs $t$

$C_0$ for all cases are 5 mg/L, $C_\infty$ was estimated with the $C_e$, $S_0$ is $9.53\times10^{-5}$ mol/g.

$\chi^2$: Chi-square values, the result of goodness of fit.

[a]: Adapted from Sparks (1999);

[b]: The derivations of the equations are listed in Appendix I and II;

[c]: All the symbols and notations in the equations can be found in the Nomenclature.

### 6.5.2 Kinetic Models

The divalent heavy metal adsorption kinetics in current study were described by the potential driving model. This model was capable of predicting the experimental data, as evaluated from coefficients of determination and goodness of fit tests as shown in Table 6.1. The parabolic diffusion equation is often used to indicate that diffusion-controlled phenomena are rate limiting (Sparks 1997). The good fit of parabolic diffusion model may also suggest that this type of kinetics is diffusion limited. This result is supported by observation of the morphology for the MOPM surface coatings. This coating is a porous surface with micropores and macropores capable of supporting intraparticle diffusion as an adsorption phenomenon. Since the potential driving model utilizes an overall rate and considers all the energy potentials including the diffusion energy in a macroscale and semi-empirical way through the simplification of the difference of time, the model represents the overall kinetics more generally and thus may overcome the limits of a specific mechanistic model, which is usually only focused on a single mechanism and often has some idealized assumptions for a more complex reality. For example, the parabolic diffusion model was originally derived based on radial diffusion in a cylinder. In parabolic model the ion concentration at the cylindrical surface is constant and initially the ion concentration throughout the cylinder is uniform (Sparks). However, neither the micropores or macropores on the real media surface are ideal cylinders nor are the ion concentrations constant and uniform throughout the pores, initially. Therefore, a semi-empirical model, which considers the overall rate and most important mechanisms (such as intra-particle diffusion, chemical reaction, and surface

precipitation), may provide a better representation of the experimental data and wider applicability, although the detailed mechanisms cannot be specified from the model fitting. In order to consider whether the potential driving model has wider applicability beyond the present study, the potential driving model was applied to several recently published kinetic data sets of heavy metal adsorption on different sorbents including ferrihydrite (Raven et al 1998), aluminum oxides (Strawn 1998), peat (Chen 2001), and granular activated carbon (Chen and Lin 2001) as shown in Table 2. In each case the result of the potential driving model indicate an excellent fit of the experiment data with coefficients of determination of greater than 0.99 for all cases and small goodness of fit values.

Table 6.2 Application of potential driving kinetic model to adsorption kinetic data of other researchers.

| Sorbate | Sorbent | $r^2$ | $\chi^2$ | Data Sources |
|---|---|---|---|---|
| Asenite @ pH 4.5 | Ferrihydrite | 0.999 | 0.004 | [1]Raven et al. 1998 |
| Asenite @ pH 9.2 | Ferrihydrite | 0.999 | 0.006 | Raven et al. 1998 |
| Asenate @ pH 4.6 | Ferrihydrite | 0.997 | 0.005 | Raven et al. 1998 |
| Asenate @ pH 9.2 | Ferrihydrite | 0.999 | 0.001 | Raven et al. 1998 |
| Pb | Aluminum Oxide | 0.999 | 0.029 | [2]Strawn et al. 1998 |
| Ni | Peat | 0.999 | 0.002 | [3]Chen et al. 2001 |
| Pb | Peat | 0.999 | 0.061 | Chen et al. 2001 |
| Cu | Peat | 0.999 | 0.001 | Chen et al. 2001 |
| Cu @ pH 4.5 | GAC | 0.999 | 0.015 | [4]Chen and Lin 2001 |
| Cu @ pH 6.0 | GAC | 0.998 | 0.088 | Chen and Lin 2001 |
| Co | GAC | 0.997 | 0.016 | Chen and Lin 2001 |
| Zn | GAC | 0.995 | 0.020 | Chen and Lin 2001 |

1: Sorbent dosage = 2-g/L, initial As addition of 13.3-$mol_{As}/kg_{ferrihydrite}$;
2: Sorbent dosage = 13.3-g/L, initial Pb concentration = 2-mM, pH =6.5;
3: Sorbent dosage = 0.5-g/L, initial concentrations are 200, 410 and 80 mg/L for Ni, Pb and Cu respectively, pH = 4.5;
4: Sorbent dosage = 10-g/L, initial concentration = $1\times10^{-4}$ M, pH = 4.5 or 6.0.

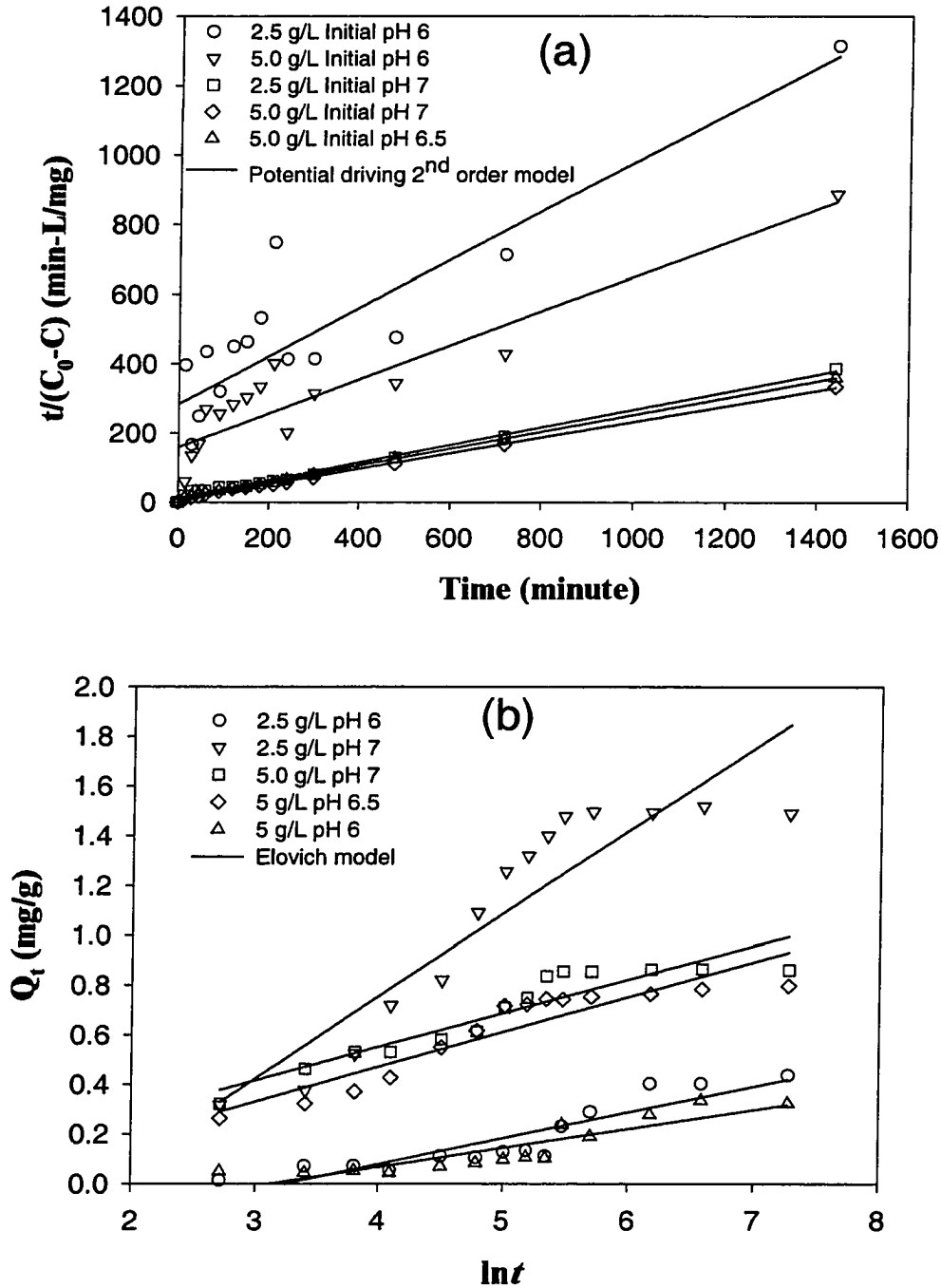


Figure 6.3 Linearized plots for the potential driving model (a) and Elovich model (b). Initial Pb(II) concentration is 5 mg/L and ionic strength is 0.01 M $NaNO_3$.

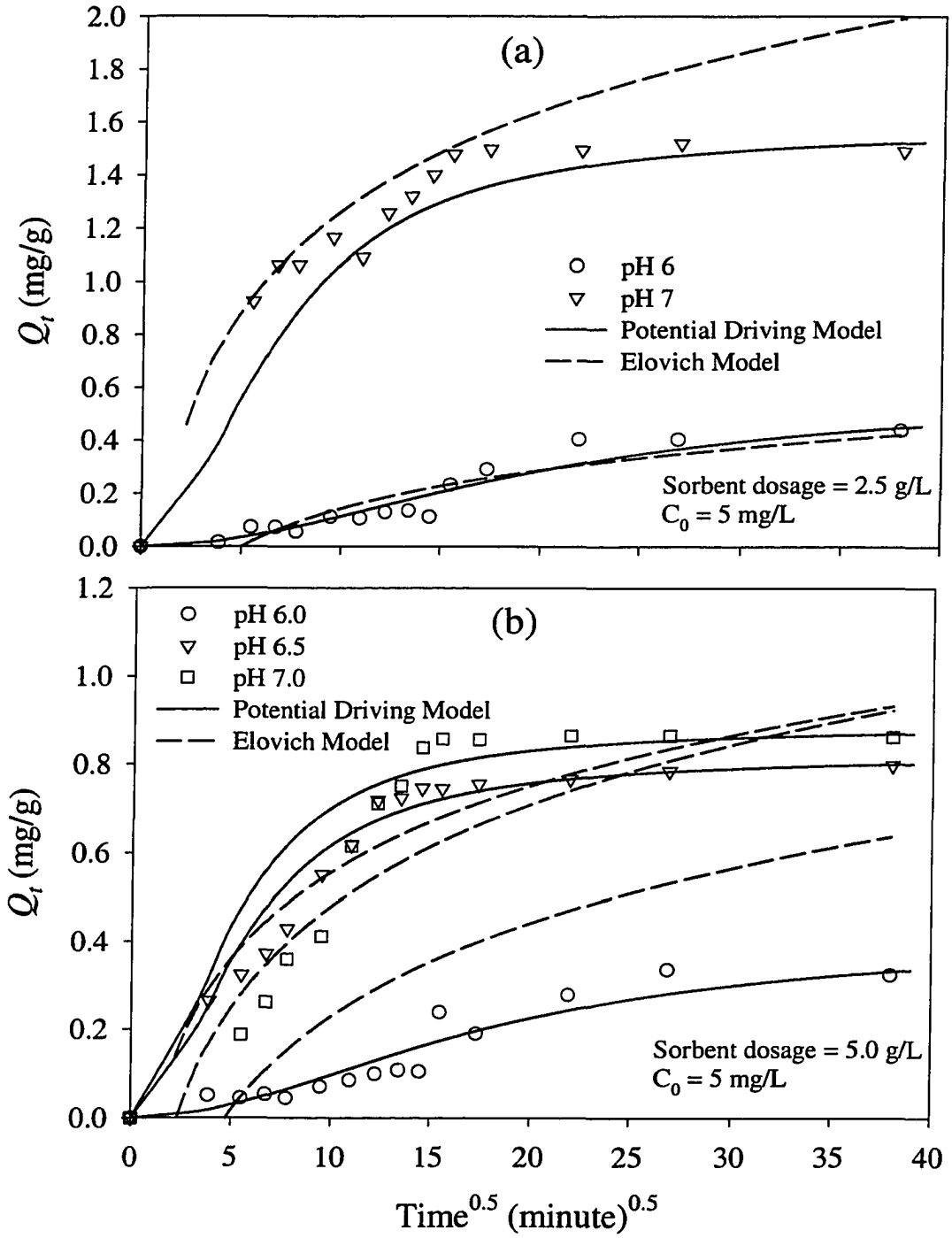


Figure 6.4 Adsorption kinetics of Pb on MOPM with model simulations.

Table 6.2 The metal ion sorption kinetic modeling constants for the potential driving model and the Elovich model for single metal systems*.

| Modeling element | pH | Sobent dosage (g/L) | Potential Driving Model | | | Elovich Model | | Psuedo-second Order Model | | Parabolic Diffusion |
|---|---|---|---|---|---|---|---|---|---|---|
| | | | #Experimental $C_e$ (mg/L) | Modeled $C_e$ (mg/L) | $k/a$ (L/mg min) | $\alpha$ (mg/g-min) | $\beta$ (g/mg) | Modeled $C_e$ (mg/L) | $k/a$ (L/mg min) | $D/r^2$ |
| Pb | 6.0 | 2.5 | 3.904 | 3.561 | 0.0016 | 0.0041 | 9.59 | 3.753 | 0.059 | 0.0038 |
| Pb | 6.0 | 5.0 | 3.375 | 2.962 | 0.0016 | 0.0034 | 13.05 | 2.645 | 0.113 | 0.0123 |
| Pb | 6.5 | 5.0 | 1.005 | 0.905 | 0.0076 | 0.0739 | 7.10 | 1.643 | 0.132 | 0.0923 |
| Pb | 7.0 | 2.5 | 1.274 | 1.075 | 0.0082 | 0.0596 | 3.01 | 1.034 | 0.418 | 0.1882 |
| Pb | 7.0 | 5.0 | 0.686 | 0.575 | 0.0088 | 0.1472 | 7.38 | 0.382 | 0.878 | 0.0091 |
| Cu | 6.0 | 2.5 | 3.916 | 3.794 | 0.0008 | 0.0275 | 15.15 | 3.794 | 0.080 | 0.1187 |
| Cu | 7.0 | 5.0 | 1.320 | 1.159 | 0.0018 | 0.0454 | 8.26 | 1.076 | 0.172 | 0.1011 |
| Cd | 7.0 | 5.0 | 2.578 | 2.328 | 0.0014 | 0.0091 | 9.56 | 3.060 | 0.069 | 0.0257 |
| Zn | 7.0 | 5.0 | 3.014 | 2.802 | 0.0016 | 0.0071 | 11.27 | 2.162 | 0.110 | 0.0285 |

Ce: equilibrium metal concentration (mg/L);
K/a: rate constants
$\alpha$ and $\beta$: constants in Elovich model;
$D/r^2$: diffusion coefficients.

*The initial heavy metal concentrations for all cases were 5 mg/L;
#The experimental equilibrium concentration is the aqueous metal concentration after 24 hours reaction time.

The Pb adsorption data with various pH and sorbent dosages are shown in Figures 6.3 and 6.4. Figure 6.3 illustrates a series of data plotted so that the constants in the Elovich model (Equation 1) and potential driving kinetic model (Equation 12) can be determineded. The calculated modeling constants and the linear correlation coefficients under different metal concentration and pH condition are shown in Tables 6.3. The potential driving model plots of $\frac{t}{C_0 - C_t}$ versus $t$ have a high linearity as shown in Figure 6.3(a) and Table 1 with the coefficients of determination above 0.98 except for the case of Pb adsorption at pH 6. By contrast, the Elovich plots of $Q_t$ versus $\ln(t)$, resulted in coefficients of determinations lower than 0.90, and indicated multiple linear segments as shown in Figure 6.3(b). Although suggesting a mechanistic conclusion from a plot of an empirical equation to experimental data should be done cautiously, some researchers have suggested that "breaks" or multiple linear segments in an Elovich plot of $Q_t$ versus $\ln(t)$ could indicate a changeover from one type of binding site to another type of site having different reaction kinetics (Atkinson 1970; Chien and Clayton 1980). In this research, a two-stage Elovich plot can be observed: the first relatively steep stage indicates a fast adsorption reaction that takes place on the outer layer and readily available sites; and second almost horizontal stage could involve the inner layer of not readily available sites, such as adsorption sites located in the micropores that appear in the SEM and BSE images of the MOPM. Figure 6.4 summarizes the experimental data along with model predictions using the potential driving model and the Elovich model. The agreement between the experimental data set

and the model fitting curves indicate high coefficients of determination for the potential driving model as summarized in Table 6.1. These results indicate that the potential driving model has good model applicability for the experimental data, and potential driving force can be utilized to explain the overall kinetics of divalent heavy metal adsorption on MOPM.

The reaction rate constants (*k/a*) are related to initial pH, and the *k/a* values increase from 0.0016-L/mg-min to 0.0088-L/mg-min as pH increase from 6 to 7 for a fixed sorbent dosage of 5.0-g/L. However, the *k/a* values did not appear to correlate to sorbent dosage for the single metal systems as shown in Table 6.3. For example *k/a* values were the same (0.0016-L/mg-min) at pH 6 and at a pH of 7 for the sorbent dosage of 2.5 and 5.0-g/L. The higher the solution pH, the higher the charge density on the MOPM surface, and thus the higher the reaction rate constants. Application of the Elovich model to Pb removal at pH 6 provides good agreement with the experiment data, while at higher pH the Elovich model has poor modeling capability. Ungarish and Aharoni (1980) have pointed out the inappropriateness of the Elovich equation at very low and very high surface coverage. The diffusion coefficients calculated from the slope of the linearized form of parabolic diffusion equation were shown in Table 6.3. Since the pore size ($r$) distribution of MOPM is considered as a constant, diffusion coefficients ($D$) is proportion to the values ($D/r^2$) list in Table 6.3 by a factor of pore size ($r^2$). Results show that the diffusion coefficients are different for Pb adsorption onto MOPM at different pH and sorbent dosages. Combining the Rankin equation and

Stokes-Einstein equation, the diffusion coefficients of the diffusion in liquid-filled pores can be calculated as following equation (Cussler 1984).

$$D = \frac{k_B T}{6\pi\mu R_0}[1 + \frac{9}{8}(\frac{2R_0}{d})\ln(\frac{2R_0}{d}) - 1.54(\frac{2R_0}{d}) + O(\frac{2R_0}{d})] \quad (13)$$

where $k_B$ is Boltzmann's constant, $\mu$ is the solvent viscosity, T is absolute temperature, $R_0$ is the solute radius and d is pore diameter. According this equation, diffusion coefficient for specific ion should not change with solution pH and sorbent dosages. Therefore, physically, diffusion alone cannot fully describe the kinetics of divalent heavy metal adsorption onto MOPM.

Figure 6.5 shows data for various divalent heavy metals plotted for the derivation of modeling constants for the Elovich (Equation 1) and potential driving kinetic model (Equation 14). The potential driving model shows excellent applicability for different divalent heavy metal and sorbent dosages as shown in Figure 6.5(a). The correlation coefficients are higher than 0.97, and all modeled equilibrium metal concentration are very close to the experimental data as summarized in Table 1. The Elovich plot of $Q_t$ versus ln($t$) illustrated in Figure 6.5(b) also shows two-stage adsorption kinetics for Cu, Zn and Cd as discussed above for Pb adsorption. Despite the different adsorption behavior for different heavy metals, the applicability of the Elovich model appears to be still related to coverage. As an indication of the applicability to coverage, the values of goodness of fit shown in Table 6.1 decrease from 5.208 for Pb at pH 7 and sorbent dosage of 5-g/L, which has the highest coverage on the media, to 0.007 for Cu at pH 6 and sorbent dosage of 2.5-g/L, the lowest coverage on the media.

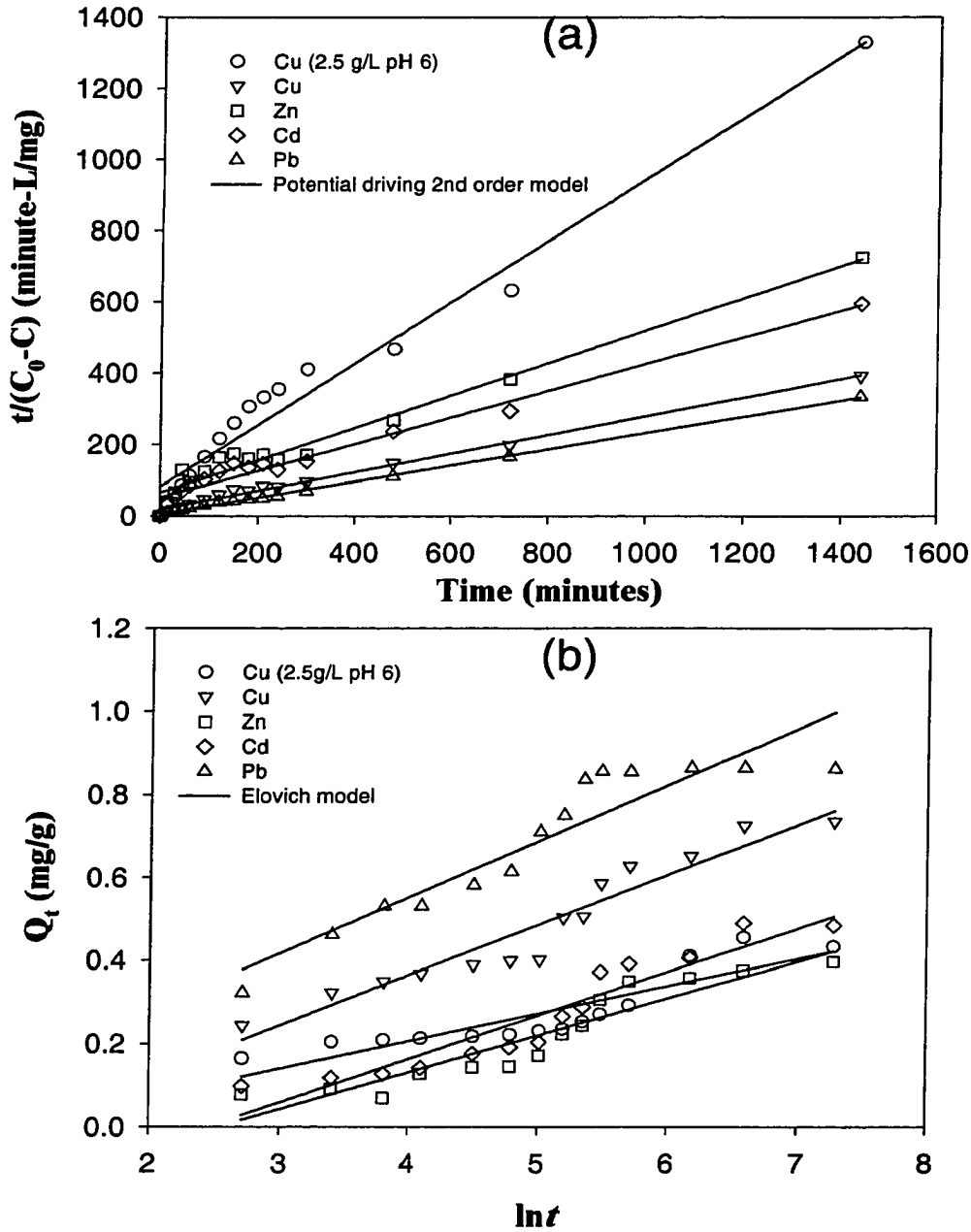


Figure 6.5 Linearized plot for potential driving model (a) and Elovich model (b). Except stated in the figure, the initial metal concentration is 5-mg/L, sorbent dosage is 5-g/L, and ionic strength is 0.01-M $NaNO_3$.

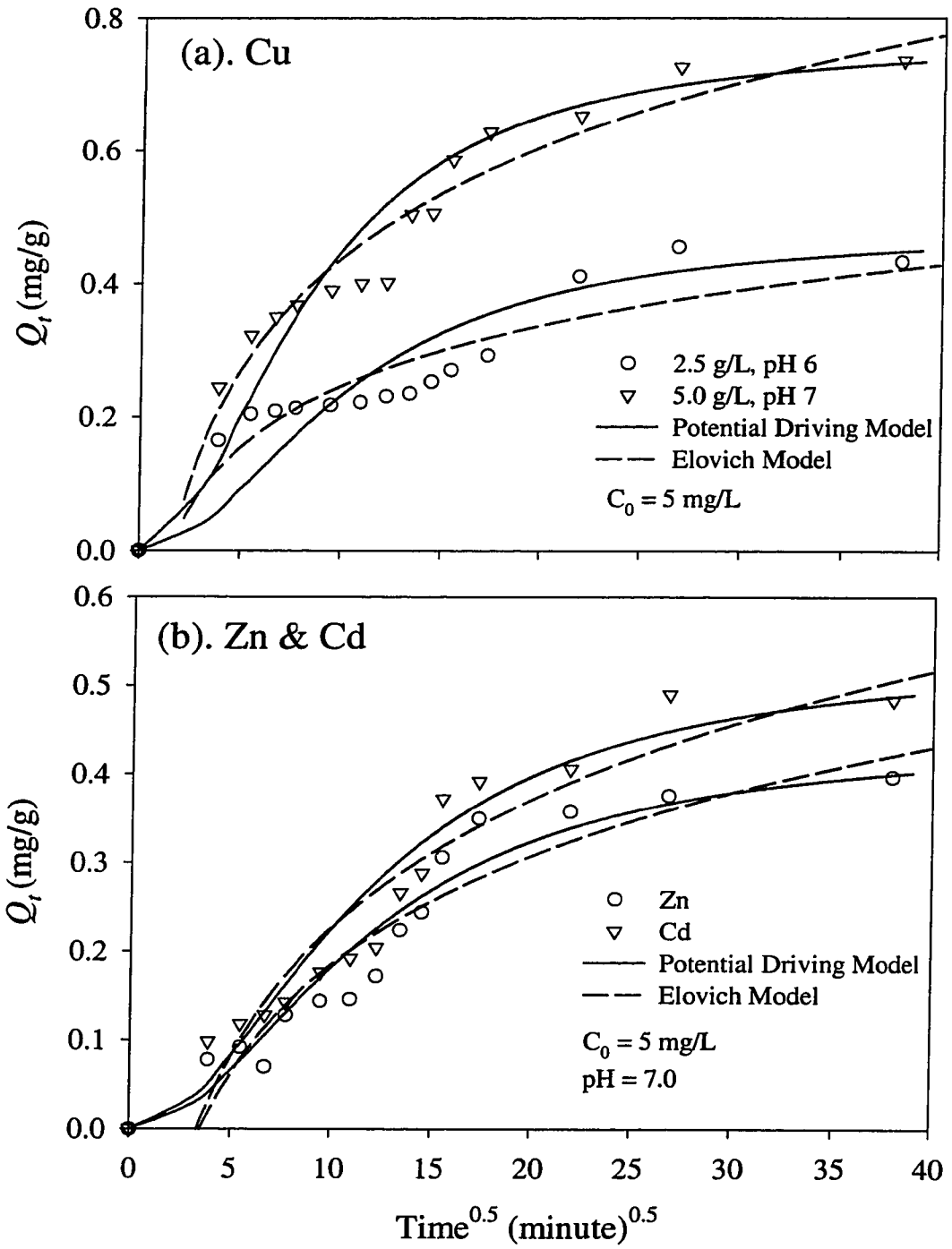


Figure 6.6 Adsorption kinetics of Cu, Cd and Zn on MOPM with model simulations.

The potential driving model fit the experimental data well for all divalent heavy metals studied as shown in Figure 6.6. The adsorption reaction rate constants (*k/a*) in Table 3 can be related to the adsorption affinity for the divalent heavy metals. For example, although the initial molar concentrations for Pb, Cd, Cu and Zn are 0.024, 0.045, 0.078 and 0.077 mM respectively, Pb, which has highest adsorptive affinity to MOPM, has the largest value of *k/a* as compare to the other heavy metals studied as shown in Table 6.3. Elovich model curves show a larger deviation from the experimental data and resulting coefficients of determination for the Elovich model are lower than those for the potential driving model. Compared the diffusion coefficients of parabolic diffusion model for Pb, Cu, Zn and Cd at pH 7 and sorbent dosage of 5g/L, the decreasing order of Cu > Zn > Cd > Pb obeys the calculated result of equation (13) since the hydrated metal ion radius ($R_0$) has the reversed order as Cu (2.07 Å) < Zn (2.17 Å) < Cd (2.28 Å) < Pb (2.74 Å) (Richens 1997; Magini 1988). Trivedi and Axi (2001) used the site activation theory to predict surface diffusivity by assuming a sinusoidal function describing the surface potential alone the oxide surface. The predicted result also indicated the same order of surface diffusivity for Cu, Zn, Cd and Pb.

### 6.5.3 Equilibrium Times

As show in Figures 4 and 6, although the equilibrium concentrations are very different as a function of initial pH and sorbent dosages, the reactions generally achieve equilibrium within 5-hours. The reported equilibrium time for divalent heavy metal adsorption onto the surface of hydrous oxide varies from several minutes (Langmuir

1997) to as long as a hundred hours (Langmuir 1997, Trivedi and Axe 2001). For divalent metal adsorption onto manganese oxide surfaces, the experiments of Morgan and Stumm (1964) demonstrated that equilibrium was achieved in less than one hour; while the experiments of Murray *et al* (1968) took several hours; and those of Laitinen and Zhou (1988) and Trivedi and Axe (2001) took several days to reach the final equilibrium. The principal reason for these differences might be the different manganese oxide structure generated by different preparation methods. The physical states of the manganese oxide is another important factor, and generally, compared to those hydrous state manganese oxides, the solid state oxide required longer time to reach equilibrium (Farley et al 1985). In this study, a fast adsorption reaction occurred within 30-minutes generally accounting for over 50% of the total removal time. Following the initial fast reaction, a slower reaction continued over time from 5 to 15-hours, as a function of different initial pH, sorbent dosages, and nature of the solutions. The experiments of Hayes and Leckie (1986) and Yasunaga and Ikeda (1986) suggest that fast reactions are most likely a chemical reaction with surface sites that are readily accessible to the divalent cation. The secondary slow reactions have been observed on many different oxides and generally three possible explanations are applied: (1) diffusion to internal sites, such the micropores shown in SEM image of Figure 1, (2) surface precipitation or (3) adsorption to sites that have a slower rate due to low affinity (Strawn et al 1998; Axe and Anderson 1997; Towle et al 1997; Scheidegger and Sparks 1996; Loehr and Webster 1996).

## 6.6 Conclusion

A manganese oxide coated polymeric medium (MOPM) utilized in an upflow sorptive buoyant media clarifier (SBMC) as a storm water Best Management Practice (BMP), was characterized using scanning electronic microscopy (SEM), and adsorption kinetics were studied using a flowthrough batch reactor. Results indicated that the general adsorption kinetics for MOPM can be described as a fast adsorption reaction occurring within 30-minutes followed by a slower reaction that continued from 5 to 15-hour, as a function of initial pH and sorbent dosages. A potential driving kinetic model was developed based on an elementary second order rate law. Experimental data were predicted using this model and a number of other kinetic models were compared using experimental data. Manganese oxide surface morphology and the ability of a parabolic diffusion model to predict the adsorption kinetics of MOPM suggest diffusion controlled adsorption for divalent heavy metals on MOPM. Based on a goodness of fit test, the potential driving model best represented the experimental data. Using the potential driving model, it was found that rate constants were increased with increasing solution pH, but were independent to the sorbent dosages. Results indicated that metal ions with the highest adsorption affinity had the highest rate constants.

# CHAPTER 7. MANGANESE OXIDE COATED CEMENTIOUS MEDIA FOR STORM WATER TREATMENT—HEAVY METAL ADSORPTION EQUILIBRIA AND KINETICS

## 7.1 Introduction

Polluted storm water runoff is a leading cause of impairment to nearly 40 percent of U.S water bodies which do not meet water quality standards (USEPA 1996). Recently promulgated National Pollutant Discharge Elimination Systems (NPDES) Phase II Stormwater Regulations (1999a), are intended to permit and control discharges to receiving waters. These discharges include overland flow, pavement sheet flow or discharges from municipal separate storm sewer system (MS4s). Storm water runoff from anthropogenic land uses or activities can harm surface water resources and, in turn, cause or contribute to an exceedance of water quality standards by changing natural hydrological patterns, accelerating stream flows, destroying aquatic habitat, and elevating pollutant concentrations and loadings. Such runoff may contain or mobilize high levels of contaminants, such as sediment, suspended solids, nutrients, heavy metals and other toxic pollutants (USEPA 1992).

A storm water best management practice (BMP) is a technique, measure or structural control that is used for a given set of conditions to manage the quantity and improve the quality of storm water runoff in the most cost-effective manner (USEPA 1999b). BMPs can be either engineered and constructed systems (structural BMPs), or institutional, education or pollution prevention practices (nonstructural BMPs). Filtration is one of the pollutant removal mechanisms in urban storm water BMPs. Media used in the filtration system of the structural storm water BMPs include soil,

sand, gravel, peat, compost, and various combinations such as peat/sand, soil/sand and sand/gravel. USEPA (1993) has evaluated structural BMPs and summarized the heavy metal removal efficiency of 50-80% for surface sand filters and other media filter. No adsorption capacity data was available for heavy metal removal by storm water media filter BMPs. Since storm water filtration systems are originally designed for particle removal, silica sand and sand/peat mix are the most common media used, and adsorption was generally considered an auxiliary removal mechanism. Considering the high percentage of dissolved heavy metals, removal of heavy metals in storm water runoff should involve adsorption as well as filtration, and a high heavy metal adsorption capacity for the media also should be considered because of longer maintenance time intervals and lower cost for regeneration. For dissolved heavy metal removal, silica sands were utilized unsuccessfully as filter media for storm water BMPs according to the current National Stormwater BMP Database (2001). In 1998 EPA conducted sampling activities at a peat/sand filter in Montgomery County, Maryland, and the results indicated a limit treatment capability for heavy metals (USEPA 1999b).

Filters using engineered sorptive media with high capacity for dissolved heavy metal and particle-bound metal removal will be utilized for in-situ or centralized storm water treatment. Examples include partial exfiltration reactors (PER) and sorptive media clarifiers (SMC). The engineered media such as the oxide coated cementitious filter media with high surface area and amphoteric surface charge can be utilized to carry out the combined unit operations of filtration and surface complexation for a range of treatment configurations and BMPs. Such treatment can be designed as a

passive and integral part of existing urban infrastructure, for example urban and transportation infrastructure, or can be designed as a centralized storm water treatment component. The quantitative heavy metal adsorption properties and behavior of the engineered media must be known for the process design, control and optimization. Therefore, experimental studies and modeling of heavy metal adsorption properties and behavior are required for a quantitative evaluation of storm water media.

### 7.2 Objectives

In the present research, manganese oxide coated cementitious media (MOCM) were evaluated through batch scale adsorption equilibrium and kinetic studies. The physical and chemical characteristics of manganese oxide coated media have been examined (Liu *et al* 2001a). However the heavy metal adsorption equilibria have not been studied, and therefore the first objective was to evaluate the adsorption capacity for divalent heavy metals typically found in urban storm water, Pb, Cu, Cd and Zn. The second objective was to examine adsorption isotherms and mechanisms to model the adsorption behavior of MOCM. The third objective was to investigate heavy metal adsorption kinetics for MOCM. The goal of this study was to evaluate the adsorptive capacity and simulate the adsorptive behavior for heavy metal removal from storm water using MOCM that would be used in BMPs such as sorptive media clarifiers (SMC).

### 7.3 Background

Cement has been frequently employed as the primary reagent for the stabilization and solidification of hazardous wastes (LaGrega et al 1994; Cartledge et al

1990). Cement-based stabilization is best suited for inorganic wastes, especially those containing heavy metals (LaGrega et al 1994; Roy et al 1992). The major constituents of Portland cement are calcium silicates which undergo hydration to produce a considerable amount of calcium hydroxide during the setting period (Taylor 1997). For example the hydration of tricalcium silicate formed about 75 parts of tobermorite gel and 49 parts of calcium hydroxide (Czernin 1980). In the resulting high pH cement matrix, heavy metals are retained in the form of insoluble hydroxide or carbonate salts within the hardened structure (LaGrega et al 1994). Studies have shown that lead, copper, zinc and cadmium are likely to bond in the cementitious matrix by chemical fixation, forming insoluble compounds (Cartledge et al. 1990; Cocke and Mollah 1993; Lin et al. 1993).

Iron oxide coated materials for heavy metal removal have been proved successful for the enhancement of treatment capacity and efficiency when compared with uncoated filter media, such as silica sand (Sansalone and Buchberger 1995; Sansalone 1999; Khaodhiar et al 2000; Joshi and Chaudhuir 1996; Benjamin et al 1996), granular activated carbon (Reed et al 2000) and polymeric media (Liu et al 2001b; 2001c). While there is a significant database for aqueous heavy metal treatment by iron oxide-coated sand for waste streams other than storm water, there is no database on the manganese oxide coating of cementitious media or its performance for treatment of urban storm water. Cementitious media can be generated from concrete rubble or recycled concrete. Concrete is one of the primary components of C&D wastes which result from the construction, renovation, and demolition of buildings, roads, bridges, and other constructed

structures. The United States Environmental Protection Agency (USEPA) recently estimated that 136,000,000 tons of building-related construction and destruction (C&D) debris were generated in the United States in 1996 (USEPA 1998). The benefits of such C&D use are availability and waste utilization of cementitious infrastructure material or recycled cementitious material. In addition, for heavy metals, cementitious media usually can create an alkaline aqueous environment since calcite ($CaCO_3$), portlandite ($Ca(OH)_2$) and calcium silicate hydrate are major components of the concrete, and all contribute alkalinity. This alkaline environment will not only improve the heavy metal removal efficiency by precipitation of dissolved metals, but also benefit the electrostatic interaction between the manganese oxide coating and dissolved cationic heavy metal, because manganese oxides have larger negative surface charge in higher pH solutions (Liu *et al* 2001a).

## 7.4 Materials and Methods

### 7.4.1 Materials for Batch Studies

Manganese oxide coated cementitious media (MOCM) were prepared using an oxidation coating method. Details of this coating process and the physical and chemical media characteristics were described in chapter 3. The manganese oxide coated cementitious media were irregular in shape with a diameter range from No. 8 mesh (2.38-mm) to No. 20 mesh (0.85-mm), with a resulting $d_{50}$ of 1.41-mm and a mean specific gravity, $\rho_s$ = 2.58. Specific surface area (SSA) of the media was 17-$m^2$/g, determined using a modified ethylene glycol monoethyl ether (EGME) measurement

method (Sansalone *et al.* 1998). All the surface characteristics of the coated media utilized in this study have been detailed in chapter 3.

Batch solutions of Pb, Cu, Cd and Zn were prepared from 1000-ppm reference standard solutions for each metal. The reference standards were concentrated solutions of $Cd(NO_3)_2$, $Cu(NO_3)_2$, $Pb(NO_3)_2$, and $Zn(NO_3)_2$. The ionic background was fixed at 0.01-M as $NaNO_3$. In storm water, ionic strength can vary from 0.0008 to 0.17-M as $NaNO_3$ (Hird and Sansalone, 2001). Adjustments for pH were carried out with trace-metal 1-N $HNO_3$ or 1-N NaOH. The pH of the metal solutions were adjusted to the initial experimental values, sealed and set overnight. On the following day the pH was readjusted to the initial experimental value before initiating batch experiments. Heavy metal analysis was by inductively coupled plasma-mass spectroscopy (ICP-MS) (Perkin-Elmer Elan 6000).

### 7.4.2 Adsorption Equilibrium Studies

The sorption equilibrium, which is usually characterized by the adsorption isotherm, is commonly measured by adding a known amount of sorbate to a known amount of sorbent in an aqueous solution and analyzing the resulting concentration of solute in solution. United States Environmental Protection Agency (US EPA) and National Bureau of Standards (NBS) recommends 2-liter bottles in a rotary tumbler for completely mixed batch reactor for batch-type procedures for estimating soil adsorption of chemicals (Roy *et al* 1992a). In spite of the apparent ease of such experiments, many source of errors are possible (Roy 1992b). With respect to the use of a rotary tumbler one problem encountered was the abrasion of the oxide coating from oxide-coated

cementitious media in the tumbling process. Such abrasion and separation led to significant experimental difficulty and representative analyses were difficult.

An important alternative technique for the classic batch experiment is the use of a re-circulating flow-through reactor for the determination of sorption parameters (Carski 1985; Miller 1989; Celorie 1989; Qualls 1992). In this form of a batch experiment, heavy metal solution is recirculated through a short column containing sorbents as a flow-through reactor. In this study, to avoid experimental difficulties associated with abrasion of the oxide surface from media, a short column (25.4-mm ID, 50.8-mm length, Teflon PFA column) packed with test media served as the flow-through reactor. The pH was not adjusted during the reaction period, and any pH drift was measured and recorded throughout the experiment. A series of metal solutions, of which sorbent to solute ratio ranged from 0.1-g/L to 10-g/L, were recirculated through the batch reactor by a peristaltic pump at a flow rate of 500-mL/min, a calculated flow rate approximately equal to the surface loading rate of a rotary tumbler operating with 2-L bottles and 29-rpm. Metal aqueous solutions were studied at initial contaminated heavy metal concentration (1 to 5-ppm), ionic strength of 0.01-M as $NaNO_3$ and pH of 5 to 7, and all reactions were kept under a nitrogen atmosphere. After a reaction period that ranged from 48 to 72-hours in the flow-through reactor, the equilibrium pH values were measured, and samples were taken from each reactor, then fractionated, acidified and analyzed. The filtered samples (using 0.45-μm membrane filter) were acidified with trace metal $HNO_3$ on a 5% v/v basis and analyzed for equilibrium aqueous phase heavy metals using ICP-MS analysis. A reactor containing no sorbent was included as control

at each pH. The solid phase heavy metal concentrations were calculated as the difference between initial and final concentrations. The relationship between aqueous and solid phase heavy metal equilibrium concentration was developed for each given set of solution conditions.

The goals for another set of isotherm experiments were to enable the extensive evaluation of the effects of pH on heavy metal adsorption. These experiments were conducted in an identical process as described above except for the following two changes. First, all samples had the same dry mass of sorbent (5-g/L), and second, the initially adjusted pH of individual samples were varied between 3 and 10. At the end of reaction period, equilibrium pH values were measured as well as the aqueous heavy metal concentrations. The amount adsorbed by the solid phase was calculated based on the difference between the initial contaminated heavy metal concentrations and the final equilibrium aqueous heavy metal concentrations.

### 7.4.3 Adsorption Kinetic Study

Adsorption kinetics were investigated in the recirculating flow-through reactor described above. Each experiment used 2-L of solution (supplied from Teflon PFA reservoirs) containing 5-mg/L heavy metal concentrations at 0.01-M ionic strength as $NaNO_3$. The pH was not adjusted during the reaction period, and any pH drift was measured and recorded every 10 minutes by a computer controlled data acquisition system. Prior to recirculating, two filtered and two unfiltered aqueous samples were taken from the reactor to verify the initial target heavy metal concentration. 5-mL sample were extracted from the solution and filtered though a 0.45-μm membrane filter

using syringe sampler with a polypropylene syringe filter at predetermined time intervals. The pH drift was measured every 10 minutes. The duration of experimental runs ranged from 48 to 72 hours. The samples were acidified in trace metal $HNO_3$ to a 5% v/v basis and analyzed for the target heavy metal concentrations by ICP-MS analysis. The solid phase heavy metal concentrations were calculated based on the difference between initial and final concentrations. The relationship between liquid and solid phase heavy metal equilibrium concentration was developed for each given set of solution conditions.

### 7.4.4 Metal Analysis

Metal analysis was conducted with an inductive coupled plasma mass spectrometer (ICP-MS) (Elan 6000, Perkin-Elmer Science) employing four-point standard calibration prior to analysis of samples. The measuring conditions were 100 ms, 50-sweeps/reading, and 3 replicates. The internal standards were Scandium (Sc 45), Germanium (Ge 74), Rhodium (Rh 103) and Lutetium (Lu 175), which were added to the samples to give a concentration of 10 μg/L respectively. The elements were measured at m/z values of 63 for copper, 64 for zinc, 114 for cadmium and 208 for lead. Analytical controls were maintained throughout including use of control and blank samples, mass balance checks, and standard solution quantity checks of every 7 samples.

## 7.5 Result and Discussion

### 7.5.1 Adsorption Equilibria

There are some practical difficulties for the investigation of divalent heavy metal adsorption behaviors of cementitious media because of the complexity of chemical compositions and high alkali surfaces which generate high pH in solution. MOCM has a relatively uniform surface coating layer, which mainly contains manganese, calcium and silica as described elsewhere (Liu et al 2001a). Divalent heavy metal adsorption by manganese oxide is very sensitive to the pH of the aqueous solution (Liu et al 2001c; Trivedi and Axe 2000; Catts and Langmuir 1986). Therefore, controlling the pH of aqueous solution may alter the surface physico-chemical characteristics for MOCM, and as a result aqueous solution pH was not changed by adding acid or base. In this study, the equilibrium pH generated by MOPM was recorded and considered as the pH where the adsorption reaction was taking place.

**Pb adsorption.**

According to the chemical stoichiometric calculation, most of the aqueous Pb will precipitate at solution pH greater than 5 under the solution conditions in this study. There are very small differences between total Pb concentration and dissolved Pb concentration (fractionated at the 0.45-μm level) in the high equilibrium pH ranges as shown in Figure 7.1. Differences are considered to be the part of Pb removed by precipitation. Thus, in the presence of MOCM, precipitation appears not to be the main removal mechanism for dissolved Pb. When the equilibrium pH is lower than 5, as in the case of initial pH of 4 and sorbent dosage of 0.1-g/L, a significant removal was

observed because of surface complexation. For the relatively high sorbent dosages, there are very similar pH drift patterns. The equilibrium pH for high sorbent dosages are close to a value of 9.9. This is the pH of the same solution condition with an infinite solid of calcite (9.89 if calculated with MINTEQA4), one of the main surface chemical compositions of MOCM determined through SEM and XRD analysis (Liu et al 2001a). These adsorption results verify the divalent heavy metal removal mechanism described in the MOCM surface characterization part (Liu et al 2001a). The combination of manganese oxide and calcite on the MOCM surface would facilitate heavy metal adsorption by generating a relatively high pH layer immediately adjacent to the media surface thus creating a high pH environment in a packed or fluidized filtration bed. Heavy metals such as Pb and Cu could be captured on the sorptive filter media through surface complexation or filtration of metal precipitates. Therefore, using MOCM as a filter medium for divalent heavy metal removal of storm water treatment can combine the unit operation of filtration and the unit process of adsorption or surface complexation. Another important benefit is the higher negative surface charge on manganese oxide obtained with the increase of the pH on the media surface layer.

**Cu adsorption.**

The adsorption profiles for Cu were similar to Pb adsorption with MOCP as shown in Figure 7.2. If no sorbent is present, aqueous Cu would start to precipitate at pH 5.5 (calculated value by MINTEQA4) for the solution conditions of this study. The small difference between total Cu concentration and dissolved Cu concentration indicate precipitation caused by the high pH was not the primary removal mechanism.

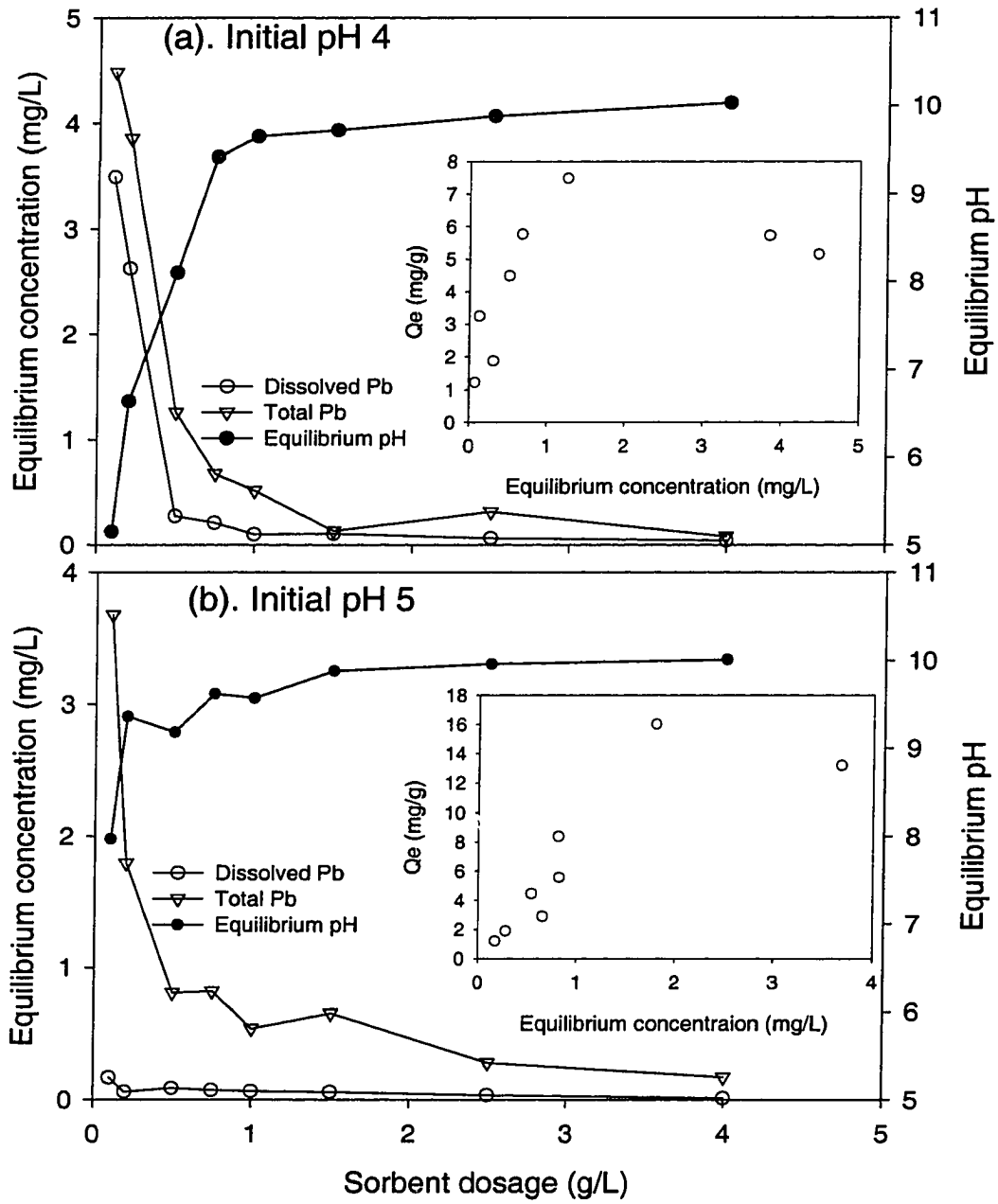


Figure 7.1 Pb adsorption and equilibrium pH as a function of sorbent dosages at initial pH of 4 (a) and initial pH of 5 (b). Ionic strength is 0.01-M $NaNO_3$ and initial Pb concentration is 5-mg/L ($2.4\times10^{-5}$ mol/L).

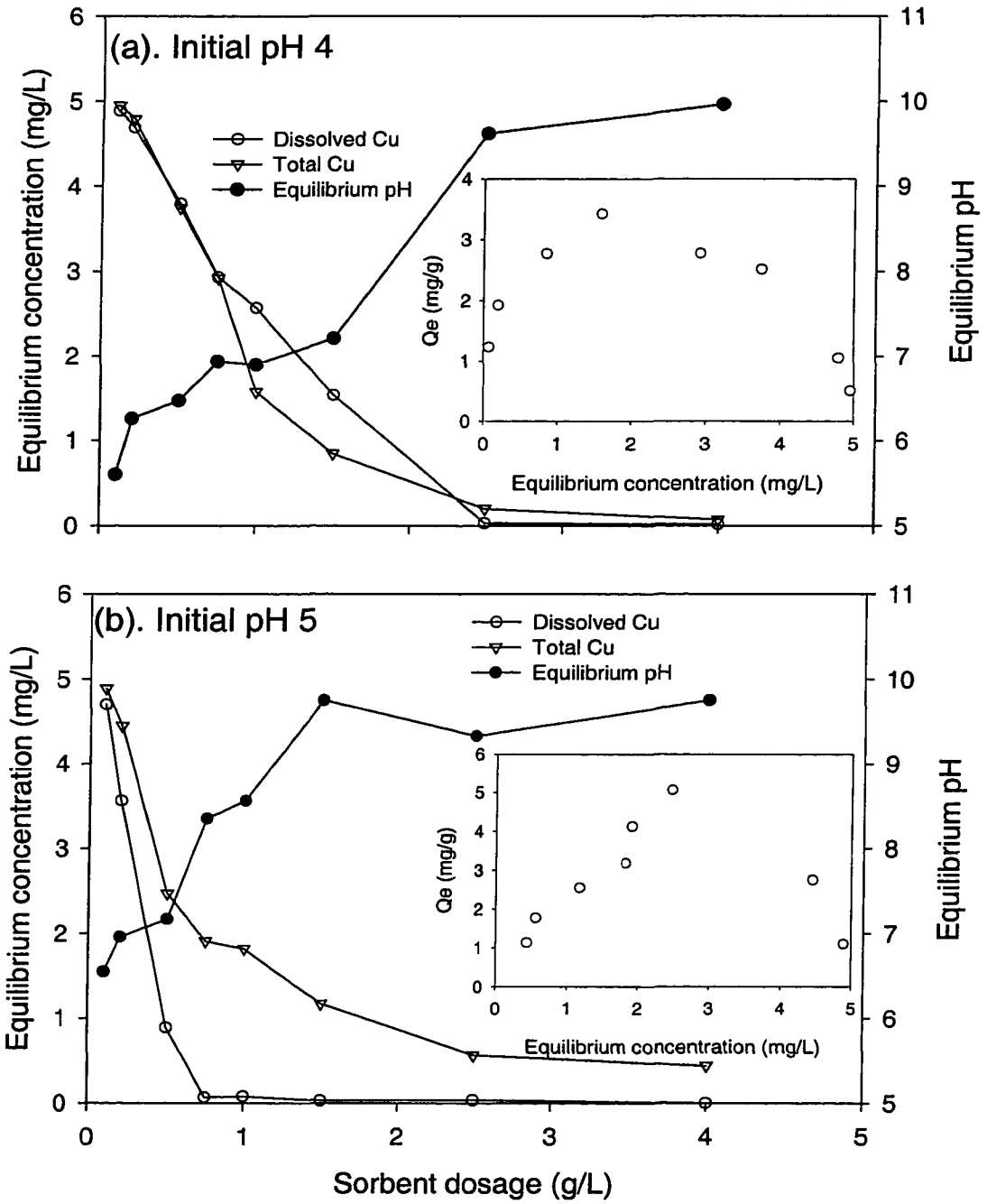


Figure 7.2 Cu adsorption and equilibrium pH as a function of sorbent dosages at initial pH of 4 (a) and initial pH of 5 (b). Ionic strength is 0.01-M $NaNO_3$ and initial Cu concentration is 5-mg/L ($7.94 \times 10^{-5}$ mol/L).

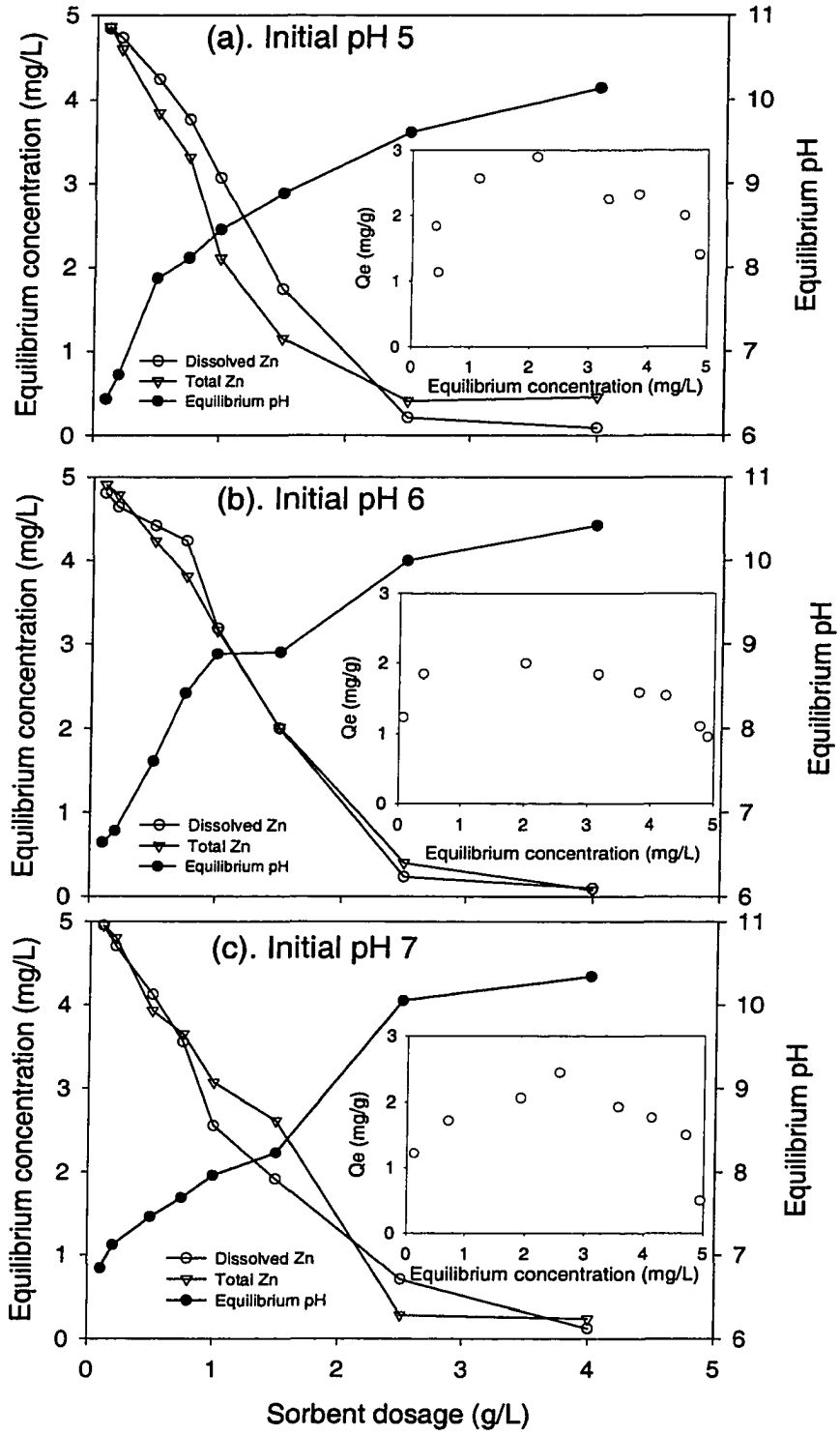


Figure 7. 3 Zn adsorption and equilibrium pH as a function of sorbent dosages at initial pH of 5 (a), 6 (b) and 7 (c). Ionic strength is 0.01-M $NaNO_3$ and initial Zn concentration is 5-mg/L ($7.81 \times 10^{-5}$ mol/L).

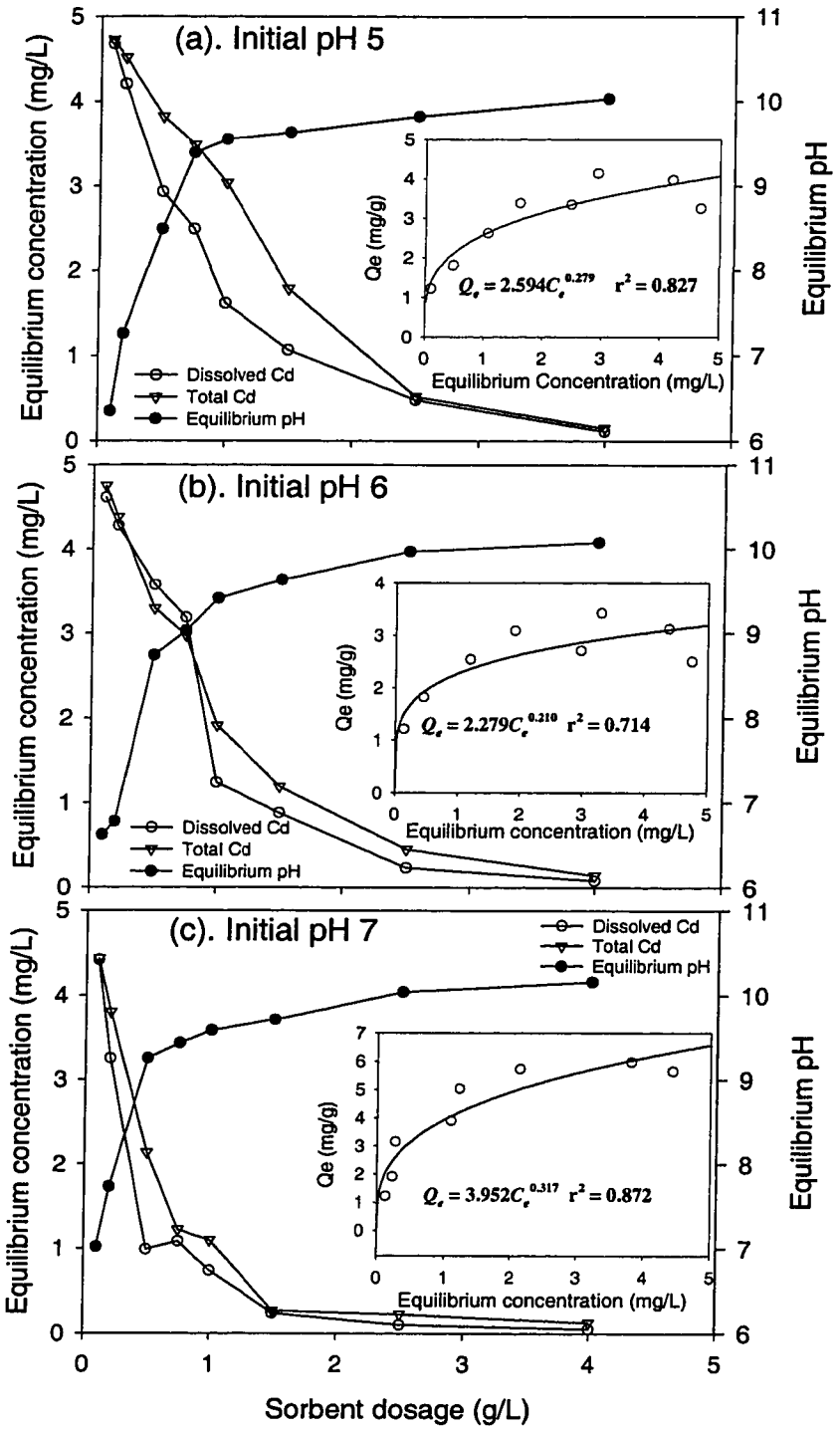


Figure 7.4 Cd adsorption and equilibrium pH as a function of sorbent dosages at initial pH of 5 (a), 6 (b) and 7 (c). Ionic strength is 0. 01-M $NaNO_3$ and initial Cd concentration is 5-mg/L ($4.39\times10^{-5}$ mol/L).

Although the equilibrium pH varied for different sorbent dosages, the equilibrium pH values for the high sorbent dosages stay around 9.9 as discussed above. The adsorption capacities for Cu adsorption by MOCM are smaller than Pb adsorption capacities. This indicated that adsorption affinities for Pb are more favorable than for Cu on MOCM, which is the same order observed for manganese oxide (Langmuir 1997) and manganese oxide coated polymeric media (Liu et al 2001c).

**Zn adsorption.**

The Zn adsorption profiles of MOCM are very similar for initial solution pH of 5, 6 and 7 as shown in Figure 7.3. The difference between initial solution pH may be eliminated by the high buffer capacity of calcite and other amphoteric oxides on the MOCM, resulting in very similar pH drift patterns among initial solution pH of 5, 6, and 7. The differences between the total aqueous Zn concentration and the dissolved Zn concentration are not statistically significant for any of the three pH levels at a confidence level of 0.95. This implies the main removal mechanism was surface complexation rather than precipitation.

**Cd adsorption.**

Comparing the Cd adsorption profiles of MOCM as shown in Figure 7.4 with these of the other divalent heavy metals shows the similar patterns and thus similar adsorption behavior by MOCM. McKenzie (1989) summarized that divalent heavy metal can be strongly adsorbed by manganese oxides and the adsorption behaviors for manganese oxide are also similar. If we assume manganese oxide is the main effective sorbent species on the MOCM surface, divalent heavy metal adsorption properties

similar to manganese oxide would be expected for MOCM. Cd is the only divalent heavy metal that still can fit into a Freundlich adsorption isotherm for MOCM. However, the correlation coefficients are lower than 0.9, resulting from the parabolic trend in the high equilibrium level as shown for the experimental data in Figure 7.4.

Table 7.1 Freundlich model coefficients for MOCM sorbent isotherms.

| $pH_i$[a] | $pH_e$[b] | Metal | $K_F$[d] | StdErr[e] | n[d] | StdErr | $r^2$ |
|---|---|---|---|---|---|---|---|
| 4 | 5.15-10.01 | Pb | 4.411 | 0.212 | 0.328 | 0.046 | 0.589 |
| 5 | 7.91-10.03 | Pb | 6.411 | 0.122 | 0.876 | 0.091 | 0.866 |
| 4 | 5.60-9.96 | Cu | 2.444 | 0.079 | 0.197 | 0.009 | 0.723 |
| 5 | 6.55-9.75 | Cu | 2.253 | 0.312 | 0.483 | 0.014 | 0.616 |
| 5 | 6.43-10.14 | Zn | 1.943 | 0.231 | 0.233 | 0.025 | 0.464 |
| 6 | 6.64-10.42 | Zn | 1.645 | 0.329 | 0.058 | 0.007 | 0.294 |
| 7 | 6.84-10.34 | Zn | 1.737 | 0.265 | 0.141 | 0.011 | 0.650 |
| 5 | 6.35-10.03 | Cd | 2.594 | 0.472 | 0.279 | 0.041 | 0.827 |
| 6 | 6.62-10.08 | Cd | 2.279 | 0.387 | 0.210 | 0.037 | 0.714 |
| 7 | 7.02-10.04 | Cd | 3.952 | 0.211 | 0.317 | 0.018 | 0.872 |

[a] Initial pH of the metal solution.
[b] pH range of samples at equilibrium (0.1-4.0g/L dose range).
[c] Ionic strength of background solution using $NaNO_3$.
[d] Based on the Freundlich model $Q_e = K_F C_e^n$ where $Q_e$ is in mg/g and $C_e$ is mg/L.
[e] Standard error for estimated parameter.

Adsorption data for each initial pH data set for Pb, Cd, Cu and Zn were fit by Freundlich isotherms, and the model correlation coefficients are generally low as illustrated in Table 7.1, which shows other parameters for Freundlich isotherms as well. The Inset isotherm plots for Figure 7.1 through 7.4 illustrate an increase of adsorption capacity at lower equilibrium divalent heavy metal concentrations where the equilibrium pH is high (ranging from 7 to 10) and a decrease at high equilibrium metal concentration level where the equilibrium pH and sorbent dosages are low. The

relationship between aqueous solution pH and surface charge density of manganese oxide may explain this parabolic type adsorption isotherm for MOCM. Low sorbent dosages result in low solution pH, and low solution pH causes a low net negative charge density for the MOCM surface. If the equilibrium pH is lower than the pH at the point of zero charge, the surface charge of MOCM can become positive. In addition, the surface charge densities for different sorbent dosages are different for the same initial pH. At high equilibrium Pb levels, which implies low sorbent dosage and low resulting solution pH, a low resulting surface charge density may cause a lower adsorption capacity than that of higher sorbent dosages. The interplay between sorbent dosage and surface charge density generates a parabolic shaped adsorption isotherm. Site heterogeneity may also contribute to this type of adsorption behavior as reported for manganese oxide by Catts and Langmuir (1986). Benjamin and Leckie (1981) found that, for most metal ions, fractional adsorption decreases with increasing total metal concentration in a system with a fixed quantity of iron oxide, even when surface complexation sites are available and in excess. These studies demonstrate energy levels were different among the adsorption sites. At low site coverage, as is the case of high sorbent dosages, the most energetic sites dominate the reaction, and adsorption isotherms may follow a Langmuir isotherm, which assumes one uniform adsorption energy sites existed for the adsorbent. When the site coverages are very high, such as the case of low sorbent dosages, the most energetic sites are filled and adsorption in lower adsorption energy level sites occurs.

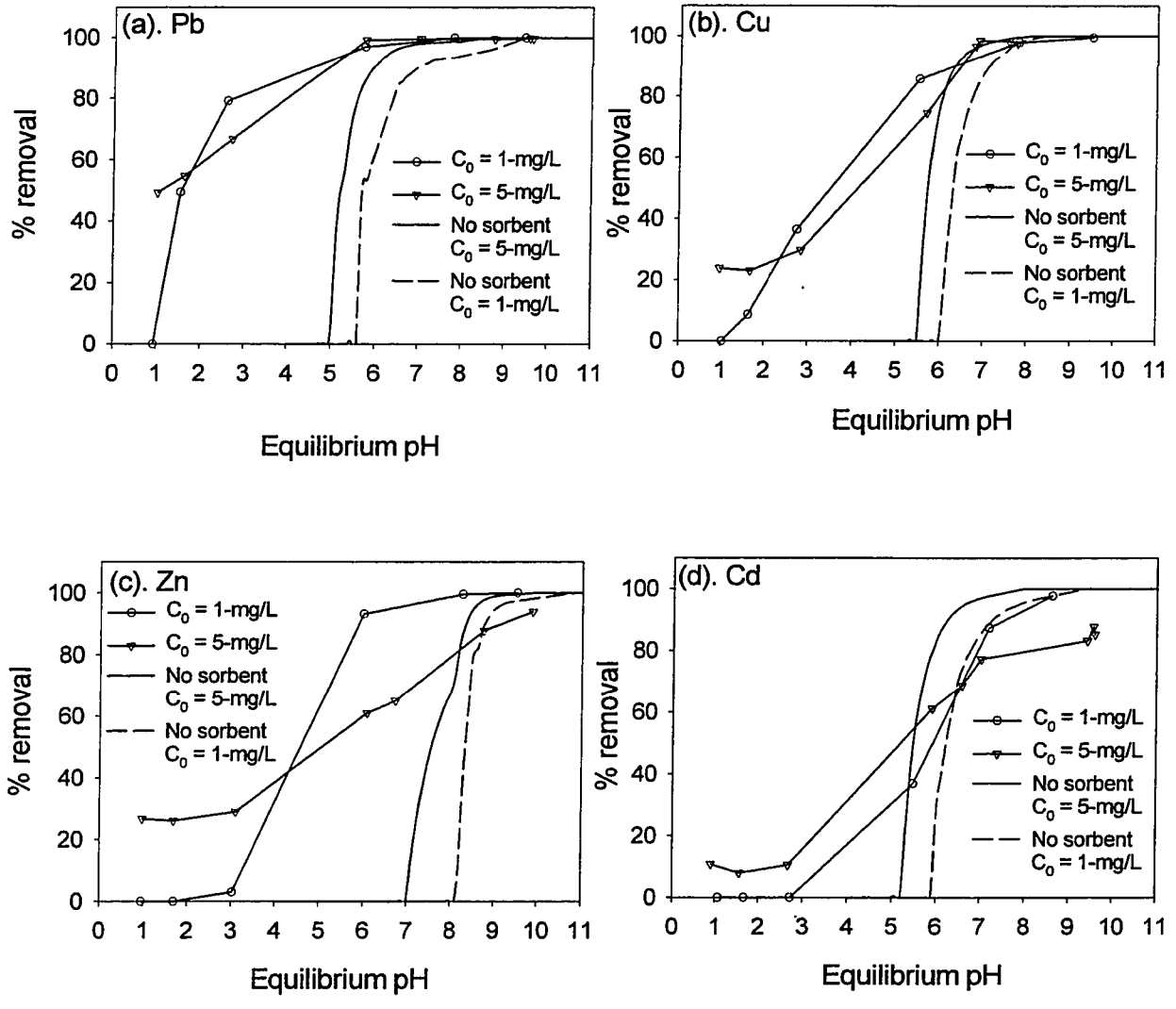


Figure 7.5 Divalent heavy metal adsorption as a function of pH for initial metal concentrations of 1-mg/L and 5-mg/L. Ionic strength is 0.01-M $NaNO_3$, and sorbent dosage is 1-g/L. The solid and dashed lines illustrate MINTEQL modeled removal percentage by precipitation as no sorbent presented in the solution and initial heavy metal concentration of 5 and 1-mg/L respectively.

**Adsorption as a function of equilibrium pH.**

As shown in Figure 7.5, the divalent heavy metal adsorption as a function of pH demonstrate "S-type" sharp adsorption edges, which have been observed for divalent heavy metal adsorption of many metal oxides (Christophi and Axe 2000; Langmuir 1997; Stumm and Morgan 1996). To distinguish adsorption from precipitation, the solutions without MOCM sorbent were modeled using MINTEQA4 to simulate divalent heavy metal removal with precipitation as the only effective mechanism. Since the MOCM surface contains calcite (Liu et al 2001), and a significant amount of calcium was detected in the aqueous solution of adsorption equilibrium studies, infinite solid of calcite was assumed in the MINTEQA4 model in order to simulate the aqueous solution condition in adsorption equilibrium studies.

Strictly speaking, sorption process, the loss of a chemical species from an aqueous solution phase to a contiguous solid phase, includes three principal mechanisms, adsorption, precipitation and absorption (Sposito 1986). The inherently macroscopic, indirect nature of the data produced by the measurements such as the chemical composition of an aqueous solution phase, limit their applicability to determine sorption mechanism (Sposito 1986). For example, the experimental observation that an ion-activity product is smaller than a corresponding solubility constant by an order of magnitude or less provides no evidence as to general mechanism of a sorption process (Sposito 1984). In this study, MINTEQA modeled percentage removal curves are the boundary of saturation for aqueous heavy metals as shown in Figure 7.5. The right hand side of the curves indicate undersaturated conditions for each

metal hydroxide or carbonate in aqueous solution, and the left hand side is the oversaturated conditions. In low pH range (pH < 5), the aqueous heavy metals are unsaturated, and the ion-activity products for these divalent heavy metals and hydroxyl or carbonate can be several orders of magnitudes less than their solubility constant. Therefore, adsorption is the dominant removal mechanism. In the neutral and high pH range, the aqueous heavy metals are oversaturated, and the ion-activity products for these divalent heavy metals and hydroxyl or carbonate can be several orders of magnitudes greater than their solubility constant. Thus, combination of precipitation and adsorption may be responsible for divalent heavy metal removal. Adsorption and precipitation are the expected working removal mechanisms for storm water treatment using MOCM, because the pH ranges of typical urban storm water are 6 to 8, and the chemical composition of the MOCM surface will create an alkaline aqueous environment in the packed or fluidized filtration bed.

Specific adsorption was observed for all divalent heavy metals studied at an initial aqueous heavy metal concentration of 5-mg/L in the low pH range. For example, 50% of the aqueous Pb was adsorbed at a solution pH as low as 1 as illustrated in Figure 7.5. Significant adsorption was also observed for Pb, Cu, and Zn when the equilibrium pH was less than 3 at initial aqueous heavy metal concentrations of 1-mg/L. Specific adsorption of weakly hydrolyzed divalent heavy metal cations, such as Cu, Co, Ni, Pb, Zn, can occur with manganese oxides below their respective pH at the point of zero charge (MaKenzie 1989). Randall et al (1998) found that manganese oxide (cryptomelane) was able to sorb up to two thirds of the available $Cd^{2+}$ from solution at

pH as low as 2.0. Using Extended X-ray Absorption Fine Structure (EXAFS) spectroscopy to investigate the adsorption location of the sorbed $Cd^{2+}$, they found $Cd^{2+}$ sorption to the inner structure of manganese oxide (tunnel sites of cryptomelane) is likely to be energetically favourable. The chemical composition of MOCM may also be responsible for this phenomenon. Although equilibrium pH in the bulk solution is very low, it is still possible to form a higher pH environment within a very thin aqueous $H_2O$ layer immediately adjacent to the MOCM surface. In this layer the pH can be greater than $pH_{PZC}$ in the measured bulk solution, and the net surface charge could remain negative for MOCM. Comparing the adsorption affinities of these four divalent heavy metals for MOCM, the order is Pb > Cu > Zn > Cd, the same adsorption affinity order for manganese oxide summarized by McKenzie (1989). This order was expected since the main chemical composition for the MOCM surface is manganese oxide as described elsewhere (Liu et al 2001a).

### 7.5.2 Adsorption Kinetics

The adsorption kinetics varied for divalent heavy metals, initial aqueous solution pH, and sorbent dosages as shown in Figures 7.6 and 7.7. The differences between divalent heavy metal kinetics are due to the difference in binding energies between the specific divalent heavy metal and MOCM. Initial aqueous solution pH would affect the resulting bulk solution pH, which is a very sensitive factor for the surface charge density and electric double layer of MOCM (Liu et al 2001a). Sorbent dosages are related to the sorbate coverage. If the sorbate coverage were low enough that the most energetic binding sites are enough to accept all the sorbed specific divalent heavy metal

cations, it is expected that the effect of sorbent dosage on adsorption kinetics would be small. For the case of high sorbate coverage with adsorption needing to involve lower energy level sites, the effect of sorbent dosage on adsorption kinetics would become significant, such as the case for Zn and Cd as shown in Figure 7.7 (a) and (b).

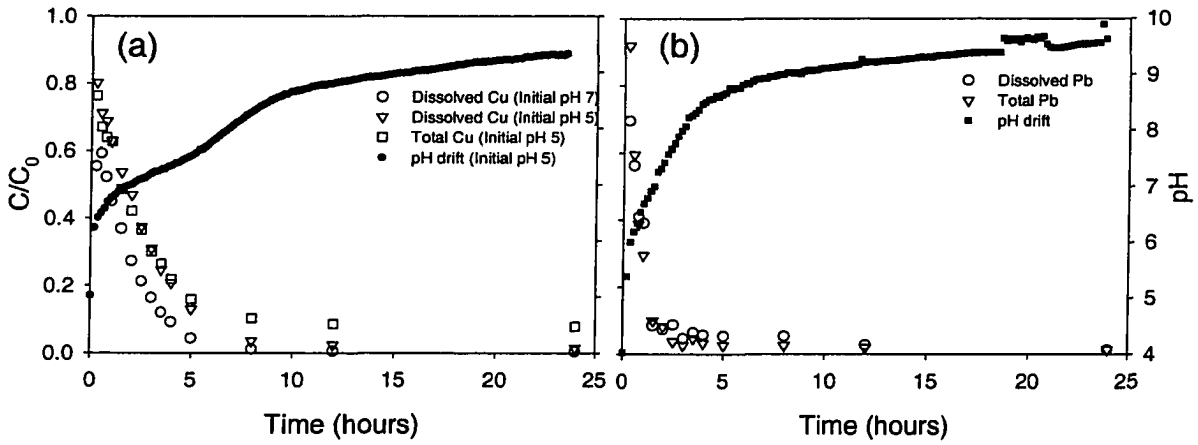


Figure 7.6 Adsorption kinetics and pH drift for divalent heavy metal adsorption of MOCM. The initial heavy metal concentration is 5-mg/L. (a) Adsorption kinetics for Pb. The initial pH is 4, and the sorbent dosage is 2.5-g/L; (b) Adsorption kinetics for Cu. the initial pH are 5 and 7, and the sorbent dosage is 2.5-g/L.

Adsorption of Pb, the most favorable divalent heavy metal species for adsorption in this study, has the shortest equilibrium time of approximately 2-hours as shown in Figure 7.6 (a). Adsorptions of Cu, Zn and Cd for MOCM have similar equilibrium times of 5 hours. These equilibrium times for MOCM are almost the same as that of manganese oxide coated polymeric media (MOPM) described elsewhere (Liu et al 2001c). The equilibrium time of adsorption of divalent heavy metal for hydrous metal oxides varies from several minutes (Langmuir 1997) to as long as hundreds of

hours (Trivedi and Axe 2000; Langmuir 1997). Equilibrium times of divalent heavy metal adsorption on manganese oxide was also reported to vary from within an hour to several days. For example, Morgan and Stumm (1964) reported an equilibrium time of less than one hour; Murray *et al* (1968) found an equilibrium time of several hours; and those of Laitinen and Zhou (1988) and Trivedi and Axe (2000) took several days to reach final equilibrium. Although a relatively uniform layer of manganese oxides was coated onto the cementitious media surface, morphology and composition analysis still demonstrate that the MOCM surface is heterogeneous (Liu et al 2001a). For the adsorption by a heterogeneous surface, in most cases, both chemical kinetics and multiple transport processes occur simultaneously, and distinguishing one from the other is extremely difficult or impossible in some cases (Sparks 1999). If the time scale for the transport step is either comparable to or much longer than that for chemical reaction, the kinetics of adsorption will reflect transport control, not reaction control (Sposito 1994). Since most of the chemical reaction times required to attain equilibrium are within an hour, transport processes are obvious by one of the main control factors for divalent heavy metal adsorption kinetics of MOCM, if the kinetics in this study is not fully transport limited. Transport processes include transport in the bulk solution phase, film diffusion or intraparticle diffusion which is the transport across a liquid film at the solid-solution interface, and pore diffusion or interparticle diffusion which include diffusion of sorbate occluded in marcopores, micropores, and along pore-wall surfaces. Since the solutions were pumped in a flow-through reactor, a 2.54-cm diameter and 5-cm long cylinder, at 500-ml/min, a turbulent flow was maintained as the

solution made contact with the packed bed of MOCM. It is unlikely that bulk solution transport and intraparticle diffusion were rate limiting beyond an hour. Therefore, limitation of the sorption reaction by interparticle diffusion, driving the sorbate toward "hidden" surface sites might be the explanation of divalent heavy metals adsorption kinetics for MOCM. Porous MOCM surfaces illustrated in previous surface characterization research (Liu et al 2001) strengthen the possibility of this theory.

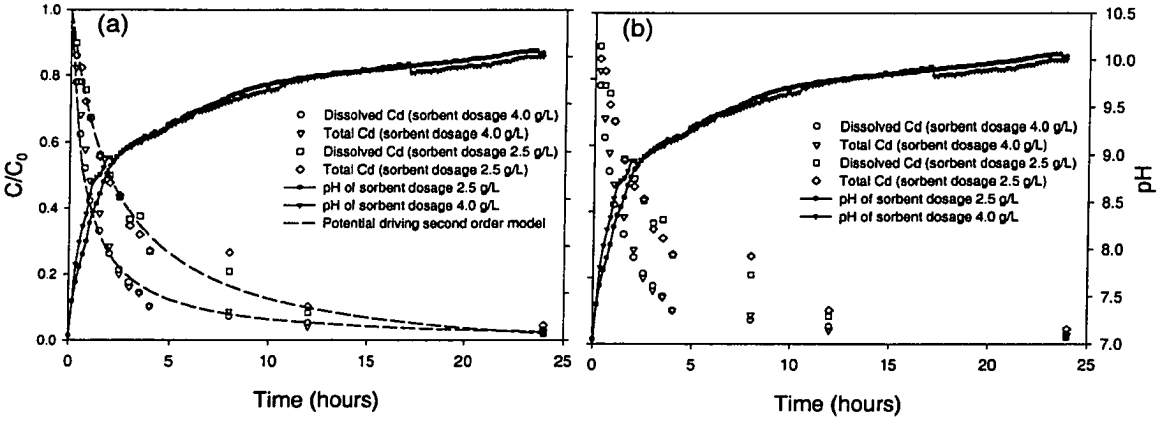


Figure 7.7 Adsorption kinetics and pH drift for divalent heavy metal adsorption of MOCM. The initial heavy metal concentration is 5-mg/$L_3$ (a) Adsorption kinetics for Zn. the initial pH are 5 and 6, and the sorbent dosages are 2.5-g/L and 4.0 g/L; (b) Adsorption kinetics for Cd. the initial pH is 7, and the sorbent dosages are 2.5-g/L and 4.0 g/L.

The pH drifts exhibited a biphasic pattern, a sharp increase in the first hours and a flatter second stage taking over 20-hours, as shown in Figures 7.6 and 7.7. The adsorption equilibria were almost achieved within the first stage. An increase in pH will increase net negative surface charge and effective (or energetically ready) surface sites of MOCM, while sorbate coverage also increases at the same time. Therefore, the

profiles of adsorption kinetics were determined by the interaction of pH drift and sorbate coverage. For example, Pb adsorption kinetics illustrated a very sharp decrease of aqueous Pb concentration within an hour as the pH of the aqueous solution increased at almost the same rate from 4 to 7. Since viable surface adsorption sites for Pb are abundant enough even in low pH conditions, the increase of pH can only accelerate the adsorption rate. In the case of Cd, adsorption kinetics for a sorbent dosage of 2.5-g/L and initial pH of 7, even at such a high pH level, the increase of viable sites still may not catch up with the step of increase of sorbent coverage, and thus a deceleration of adsorption rates was observed as shown in Figure 7.7 (b).

The pH drift profiles are significantly different for Zn adsorption between sorbent dosages 4.0-g/L and 2.5-g/L in both initial pH 5 and 6 as shown in Figure 7.7 (a). In contrast there is little difference in pH drift profiles for Cd adsorption at an initial pH of 7 as shown in Figure 7.7 (b). The initial pH values can be the important factor in this case since the dissolutions of calcite or portlandite are the pH determinant reactions. The sorbent dosages, which indicate the amount of these reactants, are more sensitive in lower initial solution pH as shown in Figure 7.7 (a) than the higher initial pH condition. Moreover, in pH 7, with the presence of calcite, most of the aqueous Cd would precipitate in bulk solution instead of being adsorbed onto the MOCM surface. In this case, solution pH may also be affected by the precipitation reaction which little connection to the sorbent dosages.

## 7.6 Summary and Conclusions

The results of divalent heavy metal adsorption equilibrium studies for MOCM indicated that adsorption rather than bulk solution precipitation is the main removal mechanism. Formation of favored pH conditions resulting in a higher net negative surface charge because of the chemical composition of the MOCM surface, a combination of calcite and manganese oxide, suggest that media such as MOCM can be utilized in BMPs that combine filtration and adsorption or surface complexation for a sorptive media clarifier (SMC). Freundlich isotherm fitting for each initial pH data of Pb, Cu and Zn was unsuccessful. Parabolic-shaped adsorption isotherms for divalent heavy metal adsorption by MOCM demonstrate that at least two or more adsorption energy levels exist for the surface sites of MOCM.

Results of percentage removal of divalent heavy metals as a function of pH demonstrate that adsorption is the dominant removal mechanism in the low pH range, and the combination of precipitation and adsorption may be responsible for divalent heavy metal removal in the neutral to high pH range. Significant adsorption occurred at initial aqueous concentration of 5-mg/L for all the divalent heavy metals studied, and initial aqueous heavy metal concentration of 1-mg/L for Pb, Cu, and Zn at equilibrium pH less than 3, suggest a specific adsorption of divalent heavy metal by MOCM. The relative divalent heavy metal adsorption affinities of MOCM are Pb > Cu > Zn > Cd, the same adsorption affinity order observed for manganese oxides, such as birnessite and cryptomelane.

The adsorption kinetics varied for divalent heavy metals, initial aqueous solution pH, and sorbent dosages. Adsorption of Pb, the most favorable divalent heavy metal specie for adsorption in this study, has the shortest equilibrium time of approximately 2 hours. Adsorptions of Cu, Zn and Cd for MOCM have similar equilibrium times of approximately 5 hours. The divalent heavy metal adsorption profiles and the porous surface morphology of MOCM suggest that limitation of the sorption reaction by interparticle diffusion, which drives the sorbate toward inner surface sites, might be the explanation of divalent heavy metal adsorption kinetics by MOCM. A biphasic pH drift pattern was observed as a sharp increase in the first hour and a flattened second stage lasting for over 20 hours. The adsorption equilibria were achieved within the first stage. The profiles of adsorption kinetics were determined by the interaction of pH drift and sorbate coverage since an increase in pH will increase the net negative surface charge and effective (or energetically ready) surface sites of MOCM, while sorbate coverage also increases at the same time.

# CHAPTER 8. MANGANESE OXIDE COATED CEMENTIOUS MEDIA FOR STORM WATER TREATMENT—SURFACE COMPLEXATION AND KINETIC MODELING

## 8.1 Introduction

Cementious materials are ubiquitous in the urban and built environments because such materials are fundamental to many cast-in place and pre-cast construction. The United States Environmental Protection Agency (USEPA) reports that concrete is one of the primary components of an estimated 136,000,000 tons of construction and destruction (C&D) wastes which result from the construction, renovation, and demolition of buildings, roads, bridges, and other man-made structures (USEPA 1998). Research into the interaction between heavy metals and cementitious materials have mostly been related to solidification/stabilization using cement binders for the disposal of hazardous wastes containing high level heavy metals (Cartledge et al 1990; Roy et al 1992). Although other mechanisms such as physical encapsulation (Roy et al 1992) have been discussed, precipitation was considered the most important immobilization mechanisms (Cartledge et al 1990; LaGrega et al 1994). The results of chemical interactions between Cr(VI) and hydrous concrete particles indicated that redox, adsorption, and precipitation are the three major reactions occurring at the concrete-water interface, and in the pH range from 4.0 to 9.0, the adsorption reaction is mainly responsible for Cr(VI) removal by forming surface complexes such as XH-$HCrO_4$ and XH-$CrO_4$ (Weng et al 1996). While little or no information is available on the behavior of selected heavy metal cations behavior on cementitious media, extensive studies have

been carried out for heavy metal adsorption onto hydrous metal oxides (Dzombak and Morel 1990; Stumm and Morgan 1996; 1992; Langmuir 1997).

Applications of a surface complexation model to the adsorption reaction at a solid-water interface have proved successful for selected natural mineral oxides (Stumm and Morgan 1996; 1992; Langmuir 1997). In addition, a database is developing for the parameters necessary to model different metal oxides, such as iron oxides (Dzombak and Morel 1990) and manganese oxides (Smith and Jenne 1991; Langmuir 1997).

Compared to these intensively studied pure hydrous oxides, heavy metal adsorption to solids with heterogeneous surfaces, such as natural environmental media and cementitious media, has been often represented by empirical approaches and in a narrow range of experimental conditions due to their variable natures and heterogeneity (Papini 1999; Cernik et al 1995; Kinniburgh 1986). Adsorption kinetics for solids with heterogeneous surfaces have been studied extensively in relation to soil physical chemistry, and chemical kinetics including the basic rate laws were applied successfully to model adsorption kinetics on heterogeneous soil surfaces (Sparks 1999; 1984; Sposito 1984). The adsorption kinetic processes be broken down into chemical kinetics and multiple transport processes, which include interparticle diffusion and intraparticle diffusion. However, in most cases, both chemical kinetics and multiple transport processes are occurring simultaneously. Thus, the determination of chemical kinetics, which can be defined as "the investigation of rates of chemical reactions and of molecular processes by which reactions occur where transport is not limiting", is extremely difficult, if not impossible, in heterogeneous systems (Sparks 1999). In some

cases, an overall rate covering all the processes was assumed to simplify the presentation of kinetics on the solids with heterogeneous surfaces. For example, average adsorption kinetics very similar to that of the complexation reactions for humic substances were applied to heterogeneous surfaces by including the hypothesis that effective or average rate constants provide a useful representation of a system that in reality exhibits a broad spectrum of surface reactivity (Sposito 1994).

**8.2 Objectives**

The goal of this study was to simulate adsorptive behavior for heavy metal removal from storm water using MOCM that would be used in treatment systems such as packed bed and fluidized bed reactors, as well as sorptive media clarifiers (SMC) and partial exfiltration reactors (PER). In part I, divalent heavy metal adsorption equilibria and kinetics of manganese oxide coated cementitious media (MOCM) were discussed. In Part II, a triple layer model (TLM) is used to simulate and predict divalent heavy metal adsorption behavior by MOCM. The intrinsic surface complexation constants for divalent heavy metals were optimized using FITEQL-TLM. Combining modeled total removal results with speciation diagrams, the contribution of precipitation in bulk solution and surface complexation was distinguished. Adsorption kinetics were modeled with the Elovich model and a potential driving second order model developed in previous studies (Liu et al 2001b; 2001d). Adherences of the models to experimental data were compared by means of goodness of fit.

## 8.3 Methods

### 8.3.1 Surface Complexation Model

A number of surface complexation models have been developed (Davis and Kent 1990; Dzombak and Morel 1990; Stumm 1992; Stumm and Morgan 1996), and research has shown promise in simulation of adsorption behavior between various sorbents and sorbates at trace levels (Westall and Hohl 1980; Dzombak and Morel 1987). According to surface complexation theories, adsorption is considered to be the result of a reaction between the ionic species and the ionized surface sites of an adsorbent. An electrical double layer, which is present immediately adjacent to the adsorption surfaces, is considered as a basic component of all these models. There are three distinct but interrelated phenomena incorporated into metal ion adsorption. These phenomena include surface ionization, complexation between ionized sites and ionic species, and the establishment of an electrical double layer in the aqueous solution immediately adjacent to the surfaces (Yiacoumi and Tien 1995).

The triple layer model (TLM) is considered the most versatile surface complexation model in that it accounts for the observation that adsorption of some species involves strong chemical bonding while others experience relatively weak electrostatic attraction to surfaces (Langmuir 1997). The triple layer model partitions the electrical double layer into two constant-capacitance layers and an outer diffuse layer. In the triple layer model, the consideration for the location of the surface complexation in the electrical double layer includes three adsorption planes, the surface plane (0-plane), the inner Helmholtz plane (β-plane), and the outer Helmholtz plane (d-

plane) (Stumm and Morgan 1996). Strongly adsorbed species, such as divalent transition metal ions (including most heavy metals), are adsorbed in the 0-plane of the sorbent surface (Davis and Kent 1990). The bonding of these strongly adsorbed species is assumed to be comparable to the bonding experienced by aqueous cations and ligands of inner-sphere solution complexes (Ligands displace one or more cationically bonded water molecule ligands and form bonds usually with partial covalent characteristics). β-plane species, separated as they are from the surface by water of hydration and by adsorbed species in the 0-plane, are surface bonded via long-range, weak coulombic forces, and such bonding is equivalent to that experienced by ions that form aqueous ion pairs or outer-sphere complexes, which involve the association of a hydrated cation and anion held by long-range electrostatic forces (Smith and Jenne 1991).

Surface protonation and deprotonation reactions are basic to the surface complexation models and may be written in the form

$$SOH_2^+ = SOH + H_s^+ \quad (1)$$

$$SOH = SO^- + H^+ \quad (2)$$

where S represents the solid sorbent surface, and $H_s^+$ represents a hydrogen ion at the surface. The activity of $H_s^+$ can be assumed to be related to the bulk $H^+$ activity through a Boltzmann factor:

$$\left(H_s^+\right) = (H^+)e^{\left(\frac{-\psi_0 F}{RT}\right)} \quad (3)$$

where $\psi_0$ is the average potential of the 0-plane as postulated by the Stern-Grahae modification of the Gouy-Chapman description of the electrical double layer, $F$ is

Faraday constant (96480 C/mol), $R$ is the ideal gas constant (8.314 J/mol K), and $T$ is the absolute temperature. The mass action and the intrinsic constants are

$$\frac{1}{K_{a1}^{\text{int}}} = \frac{(SOH_2^+)}{(SOH)(H^+)e^{\left(\frac{-\psi_0 F}{RT}\right)}} \tag{4}$$

$$\frac{1}{K_{a2}^{\text{int}}} = \frac{(SO^-)(H^+)e^{\left(\frac{-\psi_0 F}{RT}\right)}}{(SOH)} \tag{5}$$

where $K_{a1}^{\text{int}}$ and $K_{a2}^{\text{int}}$ are intrinsic constants for equation (1) and (2).

For a divalent heavy metal cation, the following surface complexation reaction and mass action expressions illustrate the determination of stoichiometric coefficient for these components.

$$SOH + M_s^{2+} = (SOM_s)^+ + H^+ \tag{6}$$

the substitution of equation (1) and together with

$$(M_s^{2+}) = (M^{2+})e^{\left(\frac{-\psi_\beta F}{RT}\right)^2} \tag{7}$$

provide the mass action expression for the intrinsic surface complexation constant as follows.

$$K_{M^{2+}}^{\text{int}} = \frac{(SOM^+)(H^+)e^{\left(\frac{-\psi_0 F}{RT}\right)}}{(SOH)(M^{2+})e^{\left(\frac{-\psi_\beta F}{RT}\right)^2}} \tag{8}$$

where $(M_s^{2+})$ is the activity of $M^{2+}$ (mol/L) on the sorbent surface, $(M^{2+})$ is the metal concentration in the solution (mol/L), and $\psi_\beta$ is the electric surface potential of the β-plane.

### 8.3.2 Kinetic Model

Various possible mechanisms are involved in the transfer of an adsorbate to the adsorption sites. These include transport to the surface by convection or molecular diffusion, attachment to the surface, surface diffusion, dehydration, and formation of a bond with the surface constituents (Stumm 1992). A number of models have been developed for simulating adsorption kinetics of metal ions adsorbed onto various sorbent surfaces. These kinetic models include first order ($ln[1-(C_t/C_\infty)]$ vs $t$), second order ($1/[1-(C_t/C_\infty)]$ vs $t$), power function ($ln(C_t)$ vs $ln(t)$), simple Elovich ($C_t$ vs $ln(t)$), and parabolic diffusion equation ($(C_t/C_\infty)$ vs $t^{-0.5}$) (Sparks, 1989), as well as a model depicted as a surface complexation reaction rate related to an outer-sphere complex formation constant ($K_{OS}$) (Stumm and Morgan, 1996). In this study, an adsorption kinetic model developed for buoyant manganese oxide coated polymeric media (MOPM) described elsewhere (Liu et al 2001b; 2001c) was applied to the experimental kinetic data for MOCM.

### 8.4 Experimental Methodology

The experimental materials, batch adsorption equilibrium, kinetic experiments, and metal analyses are described in chapter 7. In chapter 8, adsorption equilibria were modeled using a triple layer surface complexation model in FITEQL (Herbelin and Westall 1999), a computer program for determination of chemical equilibrium constants from experimental data. The adsorption kinetics were modeled using a potential driving second order model and the Elovich model.

## 8.5 Results and Discussions

### 8.5.1 Surface Complexation Modeling

As discussed in a previous study (Liu et al 2001a), X-ray dot mapping images showed high concentrations of manganese and oxygen, indicates that MOCM surfaces are mainly manganese oxides. Comparison of divalent heavy metal adsorption of MOCM with δ-manganese oxides in Part I indicated that the two have very similar behaviors such as effects of pH, and adsorption affinities for divalent heavy metals. The previous study of manganese oxide coated polymeric media (Liu et al 2001c; 2001d) also verifies this similarity between δ-manganese oxide and manganese oxide coated media. Therefore, to simplify the modeling approach, the assumption was made that manganese oxide is the only effective site on the MOCM surface. The presence of calcite and other hydrolysis products on the MOCM surface make the conventional potentiometeric titration impossible since protonation of calcite or portlandite would be the dominant reaction instead of hypothetical surface protonation and deprotonation reactions as described in equation (1) and (2). Determining intrinsic surface acidity constants through a zeta potential measurement for concrete particles as described by Weng et al (1996) may avoid this difficulty. However, a limitation of particle size for the zeta potential meter did not allow measuring diameters as large as 2-mm for MOCM, and reducing the diameter to fit the sizing requirements for zeta potential measurements may significantly alter the surface characterizations which are essential for estimation of the intrinsic surface acidity constant for MOCM. In this study, intrinsic surface acidity constants of MOCM were assumed to be the same as that of

manganese oxides summarized by Smith and Jenne (1991) and Langmuir (1997). In addition to intrinsic surface acidity constants, TLM simulations also need estimates of the surface site density, specific surface area of MOCM, and inner and outer layer constant capacitances. All the parameters needed for TLM are summarized in Table 8.1. A surface site density of 3.0-sites/nm$^2$ was estimated using surface charge data of MOCM and methodology from a previous (Liu et al. 2001a) study, at a manganese oxide coverage rate of 95% on the MOCM surface. Reported surface site density varied from 2-sites/nm$^2$ to 18-sites/nm$^2$ for hydrous manganese oxide due to differences in preparation method and solution conditions (Langmuir 1997). The surface site density used in this study is close to the one for δ-manganese oxide recommended by Davis and Kent (1990). The outer layer constant capacitance ($C_2$) was set equal to 0.2-F/m$^2$ according to convention (Langmuir 1997). Usually, inner layer constant capacitance ($C_1$) values are adjustable to optimize TLM simulations using empirical adsorption data. In the present study, an inner layer constant capacitance of 2.4-F/m$^2$ was selected as proposed for δ-manganese oxide by Catts and Langmuir (1986).

FITEQL version 4.0 (Herbelin and Westall 1999), a simulation program that includes a nonlinear least square optimization algorithm, was used to estimate intrinsic surface complexation constants for divalent heavy metals by MOCM. Surface complexation equations and divalent heavy metal hydrolysis reaction constants were required for FITEQL-TLM optimization, and the optimized intrinsic surface complexation constants are summarized in Table 8.2. All the model optimization converged, and the fitting parameter, SOS/DF, which represents the sum of the squares

of the errors (SOS) between experimental and model values divided by the degrees of freedom (DF), was generally located in or close to the general range of 0.01-20 (Herbelin and Westall 1999).

Table 8.1 Surface complexation model parameters.

| Parameter | Values | Sources |
|---|---|---|
| Specific Surface Area ($m^2/g$) | 17 | Liu et al. 2001a |
| Site density (sites/$nm^2$) | 2 | Liu et al. 2001a |
| Solid concentration (g/L) | 1 | This study |
| Inner layer capacitance $C_1$ ($F/m^2$) | 2.4 | Catts and Langmuir 1986 |
| Outer layer capacitance $C_2$ ($F/m^2$) | 0.2 | Langmuir 1997 |
| $\log K_{Na}^{int}$ | 3.5 | Smith and Jenne 1991 |
| $\log K_{a1}^{int}$ | -6.2 | Smith and Jenne 1991 |
| $\log K_{a2}^{int}$ | 1.6 | Smith and Jenne 1991 |

Compared to the divalent heavy metal intrinsic surface complexation constants for pure manganese oxides, the modeled intrinsic constants ($\log K_M^{int}$) for MOCM are significantly different. For example, TLM intrinsic constants for adsorption by δ-manganese oxide were 1.8, -0.1, -1.5 and -2.0 for $\log K_{Pb}^{int}$, $\log K_{Cu}^{int}$, $\log K_{Zn}^{int}$ and $\log K_{Cd}^{int}$, respectively (Langmuir 1997; Smith and Jenne 1991). Comparing the intrinsic surface complexation constants among the different sources, uncertainties can exist even for the same substance. Smith and Jenne (1991) have discussed the uncertainties due to several possible sources including the difference of the site density, surface loading of the adsorbate on the oxide, adsorbate/adsorbent ratio, and the assumption of dominant specific adsorption metal species (for example, the results of Hayes and Leckie (1987) indicated that the divalent metal (e.g., Cd) is the predominant adsorbing

species rather than the hydrolyzed cation calculated for the outer-sphere model). For manganese oxides, the difference of the surface complexation constants are much larger than can be accounted for by the reported site density and may result from the use of materials with different surface properties (Smith and Jenne 1991). For example, the preparation of $\delta$-$MnO_2$ with reproducible surface properties is very difficult (Stroes-Gascoyne *et al.* 1986). In addition, another two important factors also need to be addressed when comparing intrinsic surface complexation constants of manganese oxide coated media to those of hydrolyzed pure manganese oxide colloids. One differing factor is that pure hydrous manganese oxides used in those studies have SSA larger by three orders of magnitude due to their much smaller size; Another factor is the difference between flow-through and batch experimental contact between sorbent and solution. Adsorption capacities of pure manganese oxide were generally measured at a completely mixed suspension. In these mixed suspensions, manganese oxide minerals were of micron-scale size, and the suspension offerred easier capture and transport for divalent heavy metal cations from bulk solution to colloid size manganese oxide particles. The relative values of the intrinsic constants imply the adsorption affinity. The order of adsorption affinity for divalent heavy metal onto MOCM is Pb > Cu > Zn > Cd, which is the same order observed for manganese oxide coated polymeric media (Liu et al. 2001d) and manganese oxides (Langmuir 1997; MaKenzie 1989).

The adherence of TLM curves to the experimental adsorption data indicate a good applicability of TLM as shown in Figure 8.1 for Pb adsorption onto MOCM. Even at very low pH where specific adsorption takes place between a positively charged

surface and divalent heavy metals, a successful fit was observed for initial Pb concentration of 1-mg/L. However, TLM does not fit well for the initial Pb concentration of 5-mg/L in the pH region where specific adsorptions occur. As discussed in part I of this study, there are two reasons suggested for this result in such a low pH region. First, divalent heavy metal migrated in the manganese oxide structure, and second, the special chemical composition of the MOCM surface consisting of a mix of calcite and manganese oxide.

Table 8.2 Equilibrium constants for triple-layer modeling of adsorption edge

| Reaction | Log K | Sources |
|---|---|---|
| ***Surface acidity Reaction*** | | |
| $>MnOH + H^+ \Leftrightarrow >MnOH_2^+$ | -6.2 | Smith and Jenne (1991) |
| $>MnOH \Leftrightarrow >MnOH_2^+ + H^+$ | 1.6 | Smith and Jenne (1991) |
| ***Zinc*** | | |
| ***Surface reaction*** | | |
| $Zn^{2+} + >MnOH \Leftrightarrow >MnOZn^+ + H^+$ | -5.04 | This study |
| ***Hydrolysis reaction*** | | |
| $Zn^{2+} + H_2O \Leftrightarrow >ZnOH^+ + H^+$ | -9.00 | Smith and Martell (1976) |
| $Zn^{2+} + 2H_2O \Leftrightarrow >Zn(OH)_2 + 2H^+$ | -17.90 | Smith and Martell (1976) |
| $Zn^{2+} + 3H_2O \Leftrightarrow >Zn(OH)_3^- + 3H^+$ | -28.40 | Smith and Martell (1976) |
| ***Lead*** | | |
| ***Surface reaction*** | | |
| $Pb^{2+} + >MnOH \Leftrightarrow >MnOPb^+ + H^+$ | -1.84 | This Study |
| ***Hydrolysis reaction*** | | |
| $Pb^{2+} + H_2O \Leftrightarrow >PbOH^+ + H^+$ | -7.71 | Smith and Martell (1976) |
| $Pb^{2+} + 2H_2O \Leftrightarrow >Pb(OH)_2 + 2H^+$ | -17.12 | Smith and Martell (1976) |
| $Pb^{2+} + 3H_2O \Leftrightarrow >Pb(OH)_3^- + 3H^+$ | -28.06 | Smith and Martell (1976) |
| ***Copper*** | | |
| ***Surface reaction*** | | |
| $Cu^{2+} + >MnOH \Leftrightarrow >MnOCu^+ + H^+$ | -4.11 | This Study |
| ***Hydrolysis reaction*** | | |
| $Cu^{2+} + H_2O \Leftrightarrow >CuOH^+ + H^+$ | -6.30 | Smith and Martell (1976) |
| $Cu^{2+} + 2H_2O \Leftrightarrow >Cu(OH)_2 + 2H^+$ | -12.80 | Smith and Martell (1976) |
| $Cu^{2+} + 3H_2O \Leftrightarrow >Cu(OH)_3^- + 3H^+$ | -14.50 | Smith and Martell (1976) |
| $Cu^{2+} + 4H_2O \Leftrightarrow >Cu(OH)_3^{2-} + 4H^+$ | -16.40 | Smith and Martell (1976) |
| $2Cu^{2+} + 2H_2O \Leftrightarrow >Cu_2(OH)_2^{2+} + 2H^+$ | -17.70 | Smith and Martell (1976) |
| ***Cadmium*** | | |
| ***Surface reaction*** | | |
| $Cd^{2+} + >MnOH \Leftrightarrow >MnOCd^+ + H^+$ | -7.84 | This study |
| ***Hydrolysis reaction*** | | |
| $Cd^{2+} + H_2O \Leftrightarrow >CdOH^+ + H^+$ | -3.9 | Smith and Martell (1976) |
| $Cd^{2+} + 2H_2O \Leftrightarrow >Cd(OH)_2 + 2H^+$ | -7.6 | Smith and Martell (1976) |

Conceptually, the TLM may have greater capability to handle the adsorption of some species involving strong chemical bonding compared to surface complexation models which experience relatively weak electrostatic attraction to the surface (Langmuir 1997). However, the TLM only adjusts the surface concentration of the sorbates by the Boltzmann factor as shown in equation (3), and determines the surface site species concentration from the pH of the bulk solution, instead of the higher pH environment within a very thin aqueous layer immediately adjacent to the MOCM surface. The speciation diagrams for initial Pb concentration of 1-mg/L and 5-mg/L are almost identical as shown in Figure 8.1 (b) and (c). The model predicted that Pb hydroxide precipitation was modeled near zero percentage of the total concentration at the entire pH region plotted. This demonstrates that surface complexation is the dominant mechanism for Pb removal by MOCM. The adsorption edges for Cu by MOCM are illustrated in Figure 8.2 (a). The representation of Cu removal in the low pH region and initial Cu concentration of 5-mg/L demonstrated a trend similar to that of Pb. The speciation distribution for an initial aqueous Cu concentration of 1-mg/L indicated a surface complexation type removal mechanism as shown in Figure 8.2 (b). Cu hydroxide was not significant in the region plotted. A flat stage was observed in the pH region of 5 to 6 for the modeled removal curve at initial aqueous Cu concentration of 5-mg/L. According to the speciation distribution diagram as shown in Figure 8.2 (c), in this pH region, the Cu hydroxide began to compete with the surface complexation species, and at pH around 8.5, precipitation exceeded surface complexation. Since typical dissolved Cu concentrations of urban storm water runoff are much less than 1-

mg/L, in the typical pH region of 6 to 8 for storm water runoff, surface complexation would be the dominant removal mechanism for the application of MOCM for urban storm water treatment.

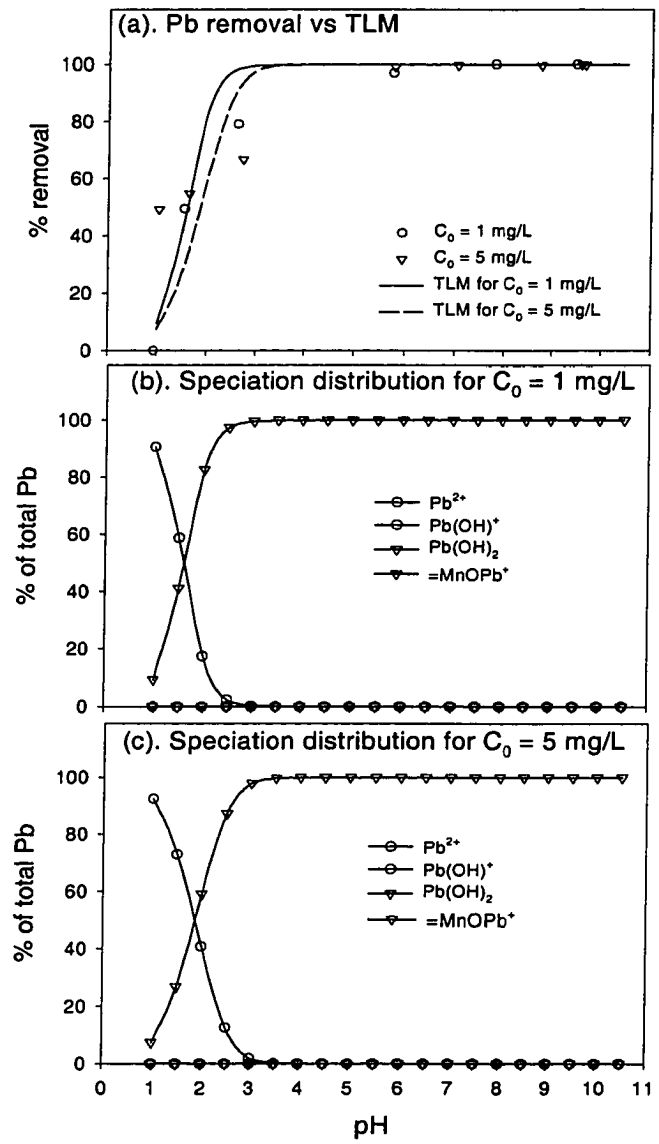


Figure 8.1 Pb adsorption and speciation as a function of pH. Ionic strength is 0.01-M $NaNO_3$, and sorbent dosage is 1-g/L. The adsorption edge is calculated with FITEQL-TLM using $\log K^{int}_{Pb^{2+}}$ of −1.84.

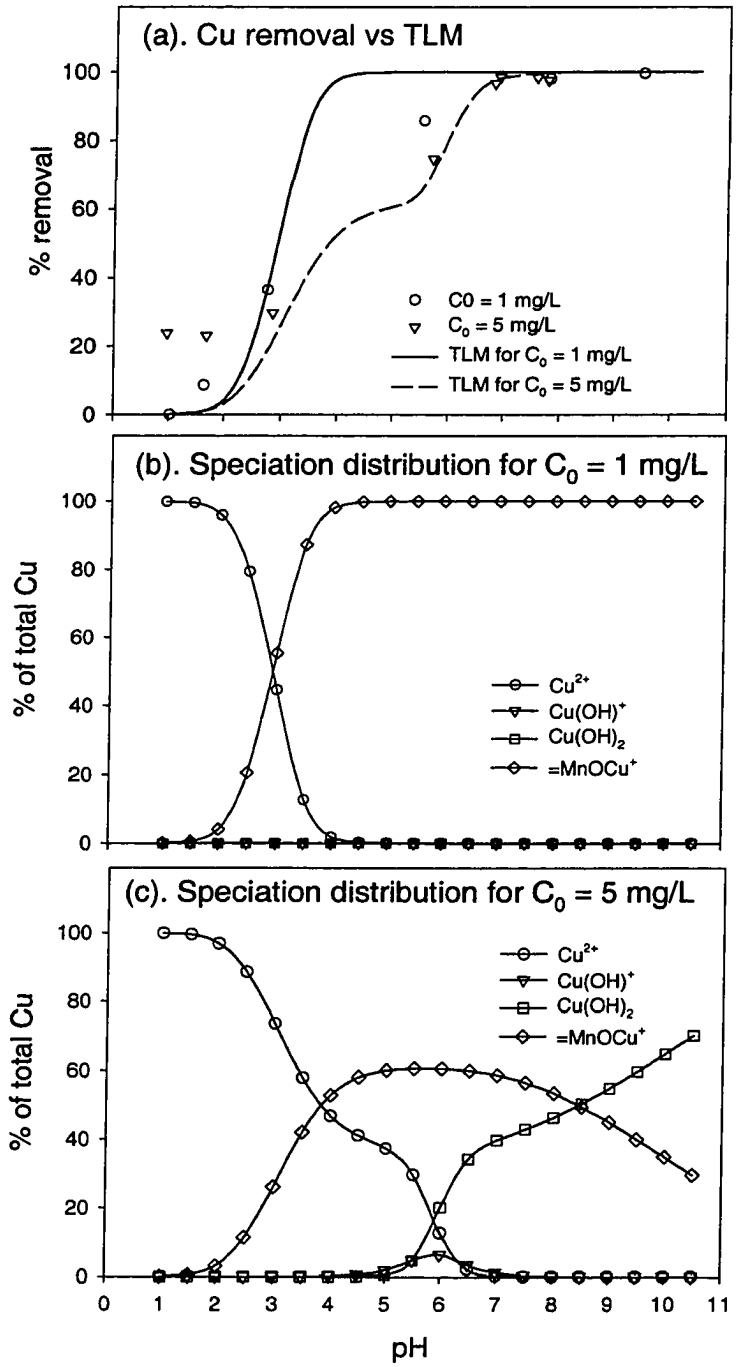


Figure 8.2 Cu adsorption and speciation as a function of pH. Ionic strength is 0.01-M $NaNO_3$, and sorbent dosage is 1-g/L. The adsorption edge is calculated with FITEQL-TLM using $\log K^{int}_{Cu^{2+}}$ of –4.11.

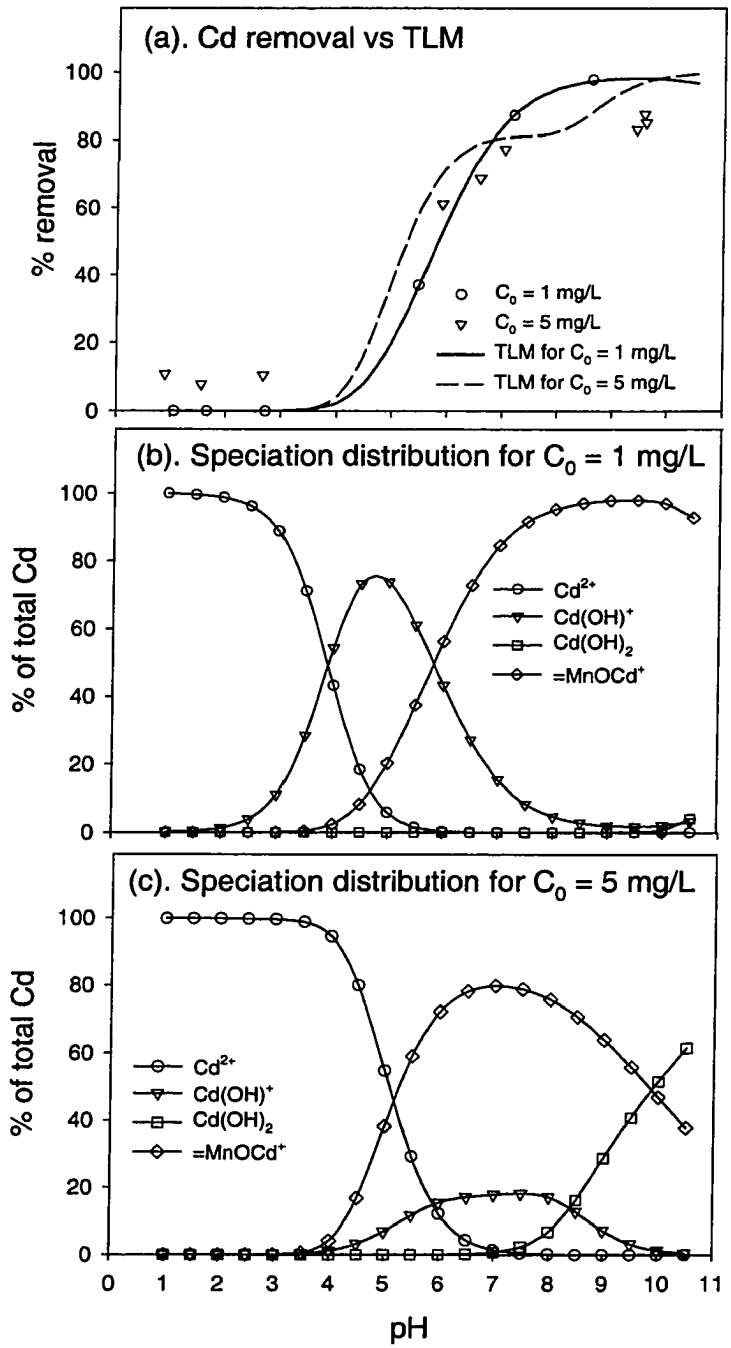


Figure 8.3 Cd adsorption and speciation as a function of pH. Ionic strength is 0.01-M $NaNO_3$, and sorbent dosage is 1-g/L. The adsorption edge is calculated with FITEQL-TLM using $\log K^{int}_{Cd^{2+}}$ of –7.84.

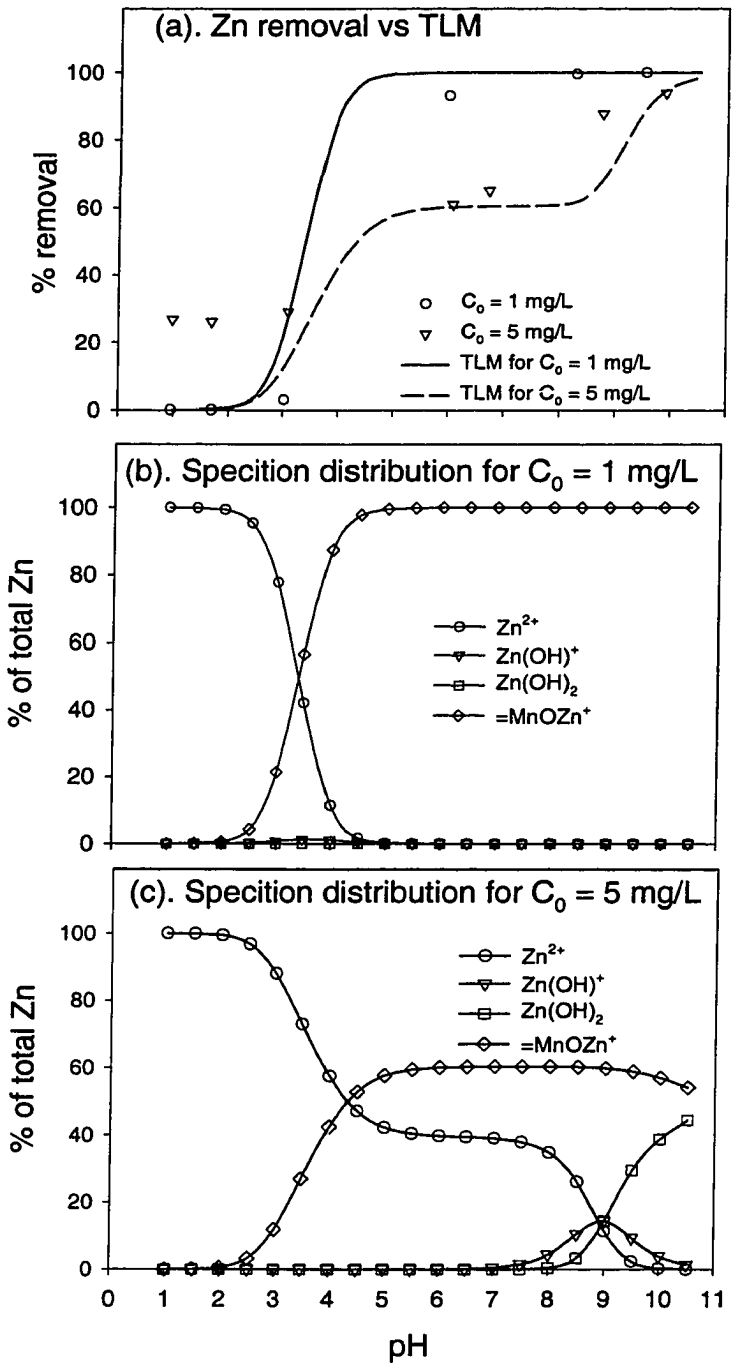


Figure 8.4 Zn adsorption and speciation as a function of pH. Ionic strength is 0.01-M $NaNO_3$, and sorbent dosage is 1-g/L. The adsorption edge is calculated with FITEQL-TLM using $\log K^{int}_{Zn^{2+}}$ of –5.04.

In contrast to Pb and Cu adsorption by MOCM, Cd removal was not significant until pH increased to 4 for initial aqueous Cd concentration of 1-mg/L as illustrated in Figure 8.3 (a). In this initial aqueous Cd concentration, $Cd(OH)_2$ does not appear until pH value greater than 10.5 as shown in Figure 8.3 (b), and this demonstrate a surface complexation type removal for such a solution condition. For initial aqueous Cd concentration of 5-mg/L, as precipitation of $Cd(OH)_2$ started at around pH 7, a flat stage was observed in the pH range of 6 to 8 for the TLM curve. This indicates that in the pH region of 4 to 7, surface complexation is dominant, while precipitation in bulk solution starts to take over after a pH of 7 and is dominant after a pH of 9.8. Figure 8.4 illustrates the adsorption edges and speciation distribution for initial aqueous Zn concentration of 1-mg/L and 5-mg/L. Surface complexation is dominant for $C_0$ = 1-mg/L, while precipitation appears at pH values greater than 7 for $C_0$ = 5-mg/L. In the typical urban storm water runoff pH region of 6 to 8 and dissolved divalent heavy metal level, generally on the order of 1-mg/L (Sansalone and Buchberger 1997), surface complexation would be the dominant removal mechanism. Therefore, for urban storm water in the pH range of 6 to 8, surface complexation of Zn is the dominant mechanism for dissolved Zn removal by MOCM by storm water treatment systems such as a PER or SMC.

### 8.5.2 Kinetic Modeling

Attempts to fit the data with a linear form of the steady-state first order reaction kinetic model were unsuccessful and not shown herein, providing evidence that the reaction kinetics data represent multiple reaction mechanisms. Figure 8.5 shows a series

Table 8.3 Kinetic modeling constants for divalent heavy metal ion sorption

| Element | Initial pH | Sobent dosage (g/L) | Potential Driving Second Order | | | | Elovich Model | | | |
|---|---|---|---|---|---|---|---|---|---|---|
| | | | $C_e$ (mg/L) | k (g/mg min) | $r^2$ | $\chi^2$ | α | β | $r^2$ | $\chi^2$ |
| Pb | 4.0 | 2.5 | 0.027 | 0.021 | 0.99 | 0.305 | 0.380 | 3.196 | 0.75 | 1.504 |
| Cu | 7.0 | 2.5 | 0.167 | 0.011 | 0.99 | 0.183 | 0.222 | 3.051 | 0.89 | 0.377 |
| Cu | 5.0 | 2.5 | 0.333 | 0.005 | 0.99 | 0.214 | 0.056 | 2.357 | 0.94 | 0.299 |
| Zn | 5.0 | 4.0 | 0.144 | 0.019 | 0.99 | 0.407 | 0.068 | 3.781 | 0.82 | 0.811 |
| Zn | 5.0 | 2.5 | 0.476 | 0.004 | 0.98 | 0.487 | 0.043 | 2.010 | 0.88 | 0.649 |
| Zn | 6.0 | 2.5 | 0.083 | 0.002 | 0.97 | 0.461 | 0.028 | 1.998 | 0.91 | 0.521 |
| Zn | 6.0 | 4.0 | 0.065 | 0.017 | 0.99 | 0.492 | 0.054 | 3.669 | 0.82 | 0.843 |
| Cd | 7.0 | 4.0 | 0.015 | 0.018 | 0.99 | 0.028 | 0.092 | 4.572 | 0.90 | 1.623 |
| Cd | 7.0 | 2.5 | 0.356 | 0.003 | 0.99 | 0.027 | 0.040 | 2.376 | 0.98 | 0.123 |

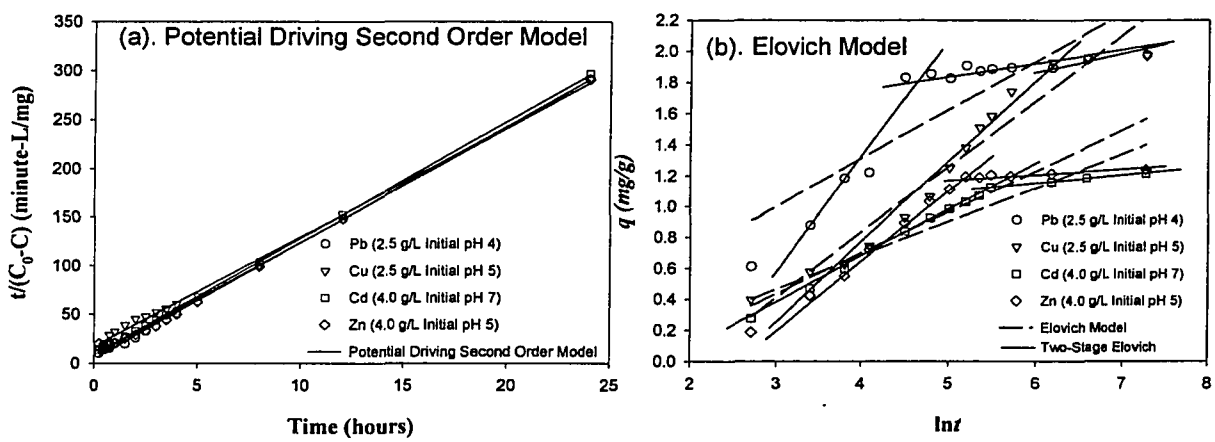


Figure 8.5 (a). Application of potential driving second order model to data; (b). Application of Elovich model to data. The initial heavy metal concentration is 5-mg/L, and the ionic strength is 0.01-M NaNO3. The initial pH and sorbent dosages are shown in the figures.

of data plotted so that the constant in the potential driving second order model (Equation 15) and the Elovich model (Equation 16) can be derived. The calculated modeling constants and the linear correlation coefficients are shown in Table 3. The potential driving second order plot for the four divalent heavy metals studied under such solution condition as shown in Figure 8.5 (a) are illustrated a very similar kinetic pattern. Model correlation coefficients of 0.97 to 0.99 for all cases also demonstrate a good consistency and applicability of the potential driving second order model for divalent heavy metal adsorption by MOCM as shown in Table 8.3. Conceptually, the driving potential in this kinetic model is the tendency to move from an unsteady state to a steady state (equilibrium). To utilize a second order rate expression, two potentials were considered. These were the potential of the sorbate in solution (tendency from divalent heavy metal concentration in time $t$ to equilibrium concentration) and the potential of adsorption sites on the sorbent surface. If the rate were transport-limited and required a long equilibration time, the interpretation in terms of driving potential would include lower potential for both sorbate in bulk surface and adsorption sites on the sorbent surface. By contrast, the Elovich plot of $Q_t$ versus ln$t$, results in correlation coefficients that are significantly lower than those of the potential driving second order model, and show two-stage linearity segements in Figure 8.5 (b). Although making a mechanistic conclusion from a plot of an empirical equation should be done cautiously, some researchers have suggested that "breaks" or multiple linear segments in an Elovich plot of $Q_t$ versus ln$t$ could indicate a changeover from one type of binding site to another having different reaction kinetics (Atkinson *et al.* 1970; Chien and Clayton

1980). In this research, a two-stage Elovich plot can be observed: the first relatively steep stage indicates a fast adsorption reaction that takes place on the outer layer at readily available sites; the second almost horizontal stage could involve the inner layer and not readily available sites, such as adsorption sites located in the micropores.

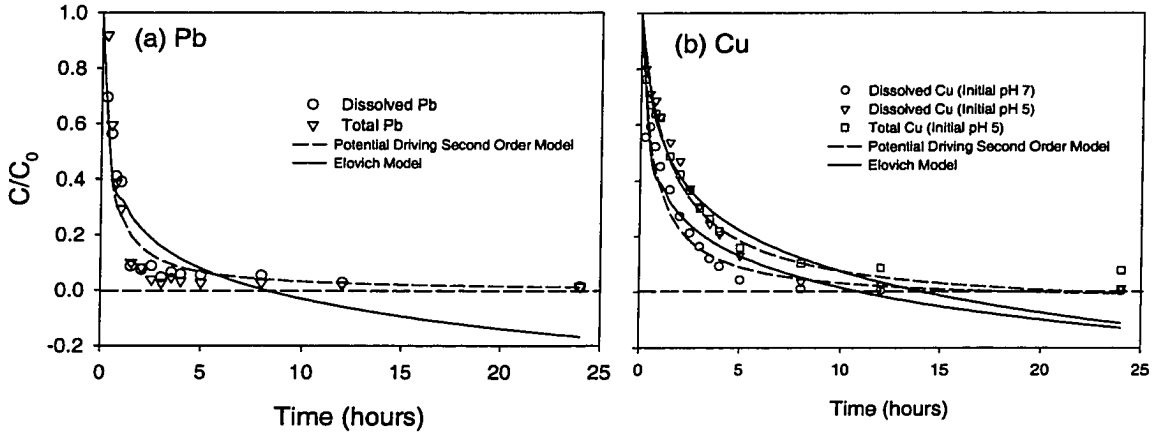


Figure 8.6 Adsorption kinetics for divalent heavy metal adsorption of MOCM. The initial heavy metal concentration is 5-mg/L, and the ionic strength is 0.01-M $NaNO_3$. (a) Adsorption kinetics for Pb. The initial pH is 4, and the sorbent dosage is 2.5-g/L; (b) Adsorption kinetics for Cu. the initial pH are 5 and 7, and the sorbent dosage is 2.5-g/L.

The results of the adsorption kinetics experiment together with simulations of potential driving second order model and the Elovich model are presented in Figure 6 and 7. The adherence between experimental data and model curves indicated that the potential driving second order model has good consistency in representing divalent heavy metal adsorption kinetics by MOCM. The representations of the kinetics have high agreement not only in the fast rate stage of the initial time region, but also in the secondary slow region and even horizontal equilibrium region since an equilibrium concentration was also obtained for the potential driving second order model. The

simulation of the Elovich model can keep a consistency in the first fast rate stage but significantly deviates in the latter slower stage. Almost all adsorption kinetics fall into the negative region, which is impossible in the experiments. This indicated the modeling limitation of the simple linear Elovich model. Some research (Ungarish and Aharoni 1981) also demonstrated that the Elovich model is not appropriate at very low and very high surface coverage of the sorbates, such as the latter stage of this study. A goodness of fit originally used for distribution fitting was adapted for examining agreement between the kinetic models and the experimental data. The values of goodness of fit for the potential driving second order model and the Elovich model under various solution conditions are shown in Table 8.3. Based on the values of goodness of fit, the potential driving second order model best represented the experimental data.

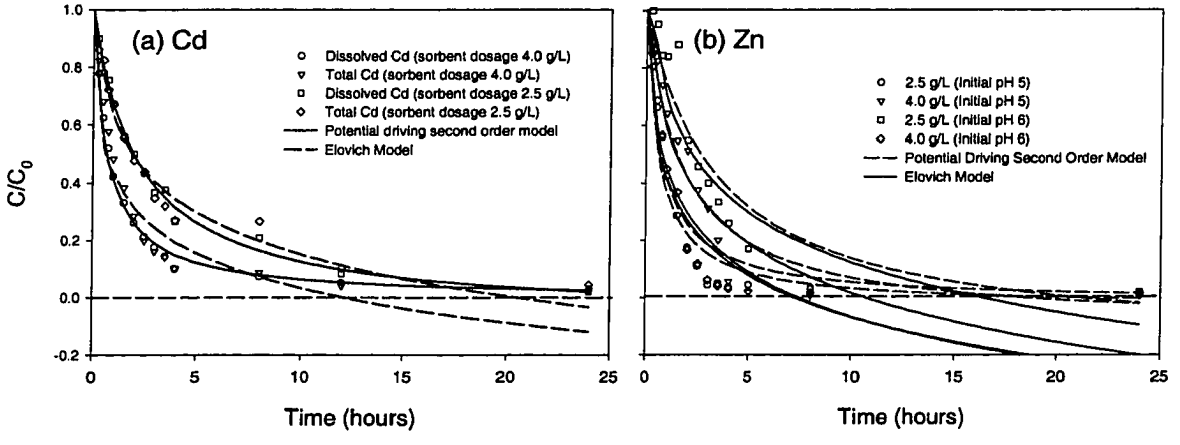


Figure 8.7 Adsorption kinetics for divalent heavy metal adsorption of MOCM. (a) Adsorption kinetics for Zn. the initial pH is 7and the sorbent dosages are 2.5-g/L and 4.0 g/L; (b) Adsorption kinetics for Cd. The initial pH are 5 and 6, and the sorbent dosages are 2.5-g/L and 4.0 g/L.

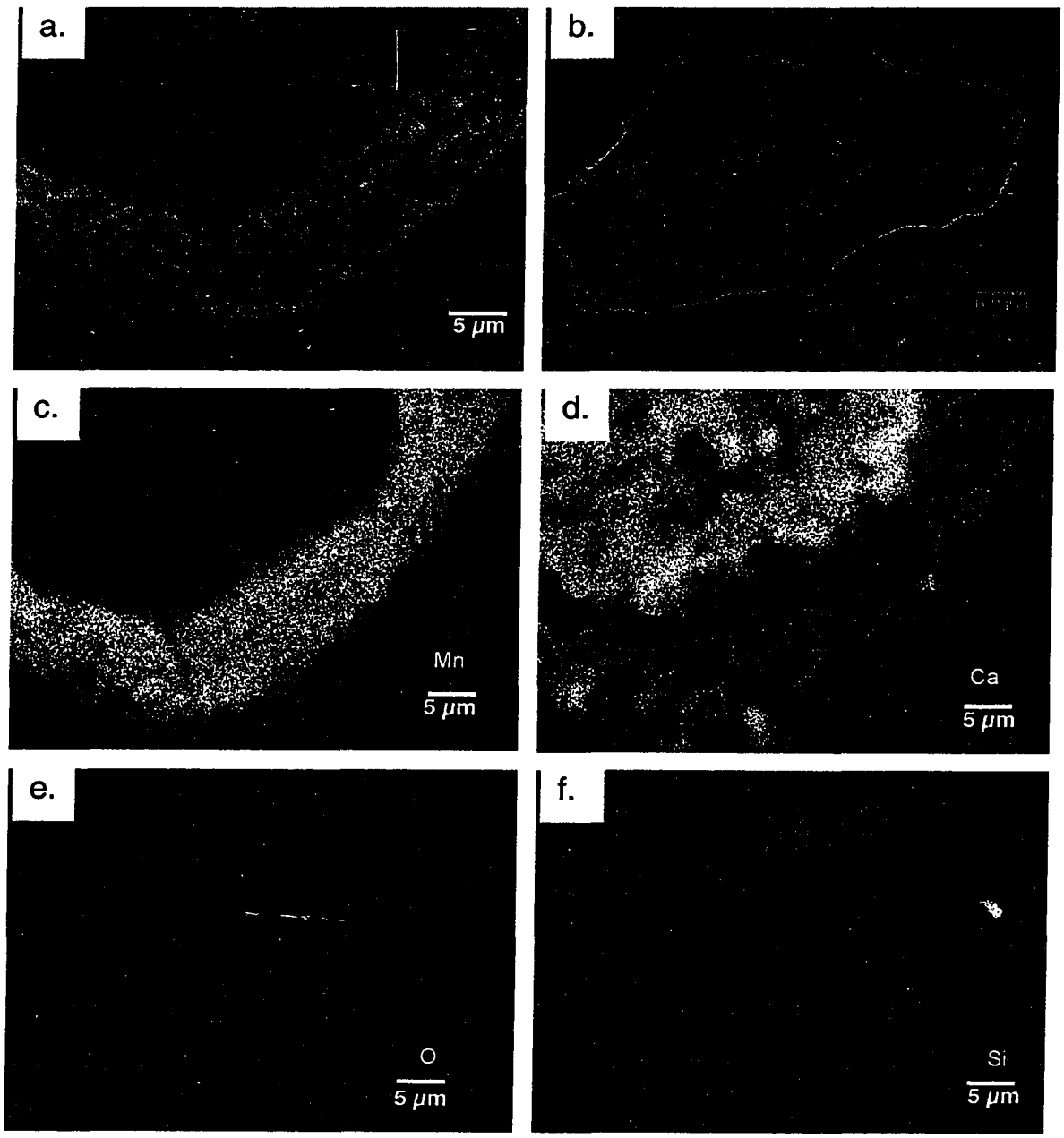


Figure 8.8 a.&b. BSE of the polished cross section of MOCM. The manganese oxide appears as bright areas. c, d, e & f. X-ray mapping of the MOCM (the same area as the BSE in (a)). The densities of the white dot stand for the abundances of the mapping element.

In this study, a fast rate in the first hour suggests that surface reactions are most likely a rate limiting process. A secondary slow stage lasting for 5 to 10-hours was observed for divalent heavy metal adsorption by MOCM, and possible rate limiting processes responsible for this secondary slow stage were interparticle diffusion, surface precipitation and energetically heterogeneous surface adsorption sites. Interparticle diffusion as a rate-limiting factor can be confirmed by the microscopy image analysis as shown in Figure 8. Surface morphology and cross section of media illustrated a porous surface for MOCM. The BSE image of Figure 8b shows that a well-defined manganese oxide coating layer encapsulated the entire cementitious matrix surface. Elementary X-ray dot mapping images (Figure 8 c, d, e & f) indicated that Mn is the most abundant element in this well-defined coating layer. The BSE images of the thin section of the coating layer also indicate a crack a cross the manganese oxide coating layer of MOCM as shown in Figure 8 (a). The SEM image of previous studies (Liu *et al.* 2001) also show that some irregular pores exist in the manganese oxide surface with dimensions varying from less than 0.1-μm to several μm. These macropores and micropores produce an intra-aggregate transport (intrapaticle diffusion) that must be considered in the kinetic model applied for the adsorption of metal ions. The surface chemical composition of MOCM, a manganese oxide and calcite mix, creates high a pH thin aqueous film immediately adjacent to the surface, and this implies a high possibility of metal hydroxide surface precipitation. The adsorption isotherm of MOCM indicated a possible interpretation of heterogeneous energetic sites as discussed in Part I. A potential driving second order model can simulate this secondary slow reaction as

shown in Figure 6 and 7. The three possible rate limiting processes can be considered the effective factor for the driving potentials of both surface sites and sorbate in bulk solution. The potential driving second order kinetic model is only concerned with the effect of observable parameters on the overall rate, such as initial solute concentration, sorbent dosage, and pH.

**8.6 Summary and Conclusions**

The intrinsic surface reaction constants for MOCM were determined through the adsorption data as a function of pH using FITEQL-TLM, and are $\log K_{Pb}^{int} = -1.84$, $\log K_{Cu}^{int} = -4.11$, $\log K_{Zn}^{int} = -5.04$, and $\log K_{Zn}^{int} = -7.84$. Surface complexation on the solid-water interface and precipitation in bulk solution were distinguished from the speciation distribution as a function of pH. At initial aqueous divalent heavy metal concentration of 1-mg/L, surface complexation was the dominant removal mechanism for all four divalent heavy metals studied over the pH range from 1 to 10. In urban storm water runoff, the typical dissolved divalent heavy metal concentrations are equal to or less than 1-mg/L, and the pH range is 6 to 8, thus, surface complexation would be the dominant mechanism for heavy metal removal in storm water treatment using MOCM as a filter medium for treatment systems such as a PER or SMC. At initial aqueous divalent heavy metal concentration of 5-mg/L, surface complexation still can be the main removal mechanism for Pb and Zn, while for Cu and Cd, precipitation was significant at higher pH, specifically, greater than 6 for Cu and greater than 7 for Cd. A potential driving second order kinetic model was applied successfully to simulate divalent heavy metal adsorption rates with correlation coefficients of 0.97 to 0.99.

Compared with the Elovich model based on the values of goodness of fit, the potential driving second order model best represented the experimental data. A fast rate in the first hour suggests that surface reactions are most likely rate limiting process. A secondary slow stage lasting for 5 to 10 hours was observed for divalent heavy metal adsorption by MOCM and possible rate limiting processes responsible for this secondary slow stage are interparticle diffusion, surface precipitation and energetically heterogeneous surface adsorption sites. In terms of potential, the three possible rate limiting processes are considered to be the main factors in the driving potentials of both surface sites and sorbate in bulk solution.

# CHAPTER 9. COMPARISON OF HEAVY METAL BREAKTHROUGH FROM SORPTIVE MEDIA FOR STORM WATER BMPs

## 9.1 Introduction

EPA promulgated the National Pollutant Discharge Elimination System (NPDES) storm water regulations for the second phase (Phase II) of storm water discharge control in 1999. Following today's rule, permit requirements for all regulated municipal separate storm sewer systems (MS4s) (both those under the Phase I program and those under Phase II) will require implementation of Control Strategies or Best Management Practices (BMPs). Similarly, EPA believes that implementation of Best Management Practices (BMPs) controls at small construction sites will also result in a significant reduction in pollutant discharges and an improvement in surface water quality (USEPA 1999b). There are a wide variety of structural BMPs in use for storm water management. Structural BMPs include engineered and constructed systems that are designed to provide for water quantity and/or water quality control of storm water runoff. Structural BMPs can be grouped into several general categories including filtration systems, detention systems, infiltration systems, retention systems, vegetated systems (biofilters) etc. A filtration system is a device that uses a media such as sand, gravel, peat or compost to separate particles or particulate-bound constituents in storm water. However most in-situ filters are designed primarily as a water quality control device designed to remove particulate pollutants. In many cases, at the upper end of an urban watershed that is impervious, heavy metals are mainly in solution (Sansalone and Buchberger 1997, Ball et al. 1991). The function of the media must include adsorption

under these conditions. Media filters are commonly used to treat runoff from small sites such as parking lots and small developments, in areas with high pollution potential such as industrial areas, or in highly urbanized areas where land availability or costs preclude the use of other BMP types.

**9.2 Objectives**

There are there major objectives for this study. Using bench scale column simulations loaded with synthetic storm water containing the Zn, Cd, Cu and Pb, the first objective of this study was to evaluate the competitive breakthrough capacity of typical filter media including silica sand and GAC compared to that of engineered oxide coated media including Fe-coated sand media (IOCS), manganese oxide coated polymeric media (MOPM), and manganese oxide coated cementitious media (MOCM). Based on these column simulations and breakthrough capacity result, the second objective was to examine sorptive media for use in storm water filter-type BMP filtration system for dissolved heavy metal removal. In addition to compare the breakthrough capacity of different media, the third objective is to study the effects of EBCT on column performance for selected media.

**9.3 Previous Work**

Treatment of storm water for water quality improvement is a relatively new practice. Until the 1990s, the majority of on-site storm water treatment focused on particle removal. Implicit with such treatment was the premise that many storm water pollutants including heavy metals were particulate-bound. These on-site treatment methods utilize basic settling basin concepts and designs to remove particles from storm

water. However, to achieve effective trapping of the finer particles, less than 40 μm, either basin surface areas were large or outflow rates were very small. In addition, such basins were not effective for dissolved and colloidal-size pollutants (Malcom 1989).

Recently, a number of researchers have investigated various aspects of passive filtration systems using natural granular materials or soils for treatment of storm water. One system, designated the Swedish Unit Superstructure, utilized porous asphalt over a graded gravel and sand subgrade resulting in concentration reductions of greater than 50 percent for total metal elements from infiltrating storm water (Niemczynowicz, 1990). Using bench scale columns to simulate storm water infiltration, Igloria et al (1997) found that in the presence of natural organic matter, heavy metals were still effectively attenuated within the soil media tested.

BMPs for heavy metals and solids are essentially garbage cans and as such they must be emptied and cleaned occasionally. The purpose of design is to provide effective capture, reasonable time between clean outs and an optimal cost between treatment alternatives. Based on this theory, for dissolved heavy metal removal, the adsorption capacity of filter media can be considered a critical factor to determine the volumes of this repository (media filter). The higher is the adsorption capacity of the filter media, the longer is the cleaning or regenerating time interval. For storm water BMPs no adsorption capacity data was available for heavy metal removal by storm water media filter BMPs. Since storm water filtration systems primarily originally designed for particle removal, silica sand and sand/peat mix are the most common media used, and adsorption is generally considered an auxiliary removal mechanism. Considering the

high percentage of dissolved heavy metals, removal of heavy metals in storm water runoff should involve both adsorption as well as filtration, and a high heavy metal adsorption capacity for the media also should be considered because of longer maintenance time intervals and lower cost for regeneration. Media engineered for BMPs such as iron oxide or manganese oxide coated media can combine the unit operation of filtration and the unit process of adsorption or surface complexation.

Many researchers have investigated the characteristics and capacity of engineered sorbent material for active process treatment of metal-bearing waters. Although GAC is widely used to remove organic compounds from wastewater, Pb-bearing wastewater also has been effectively treated using GAC columns (Reed et al., 1994). Reed at. al. (1995) demonstrated that GAC used for Pb removal could be regenerated using acid regenerant followed by a base rinse. Results indicated that the dominant removal mechanism was precipitation of Pb as $Pb(OH)_2$ instead of adsorption.

Another engineered material which functions both as a filter and sorbent for treatment of metal-bearing waste streams is Fe-coated sand. Fe-coated sand can be generated by controlled heating an aqueous solution containing iron salt, from 0.2 to 2 M, to dryness in the presence of silica sand. Process column studies have demonstrated that Fe-coated sand provided 70 to 99 percent removal efficiencies for simulated Superfund waste streams of Cd, Cu and Pb. (USEPA 1993). The Fe-coating, consisting of hydrous oxides of Fe, is amphoteric in aqueous solutions and removal of metal elements such as Pb can be maximized by control of aqueous pH levels (Theis et al. 1992). Lo et al. (1997) characterized the surface coating and adsorption properties of

Fe-coated sand and demonstrated that the coating stability was enhanced when heated to dryness at 500 °C. In addition Energy Dispersive Analysis of X-rays showed that Cu ions where chemisorbed to the Fe-coating surface.

Along with iron oxides, manganese oxides posses a pH-dependent surface charge. The point of zero charge of common forms of manganese oxides occurring in soil range from 1.5 for birnessite to 4.6 for the hollandite group (Healy et al. 1966). McKenzie (1981) measured the PZC for synthesized birnessite ranged from 1.5 to 3.0 and cryptomelane ranged from 1.5 to 2.0. Because of the low PZC, the manganese oxides have a very high negative surface charge in the range of pH values of 6 to 8 found in most of storm water runoff. Manganese oxide coated media have been prepared and characterized in the previous studies (Liu et al. 2001a; 2001b;). Batch adsorption studies were also conducted for these media (Liu et al. 2001c; 2001d; 2001f; 2001g). Studies found that manganese oxide coated polymeric media (MOPM) has a comparable or higher adsorption capacity for the divalent heavy metals compared to other commercial and research media, and the heavy metal adsorption capacity is very sensitive to the solution pH (Liu et al. 2001c; 2001d). Adsorption equilibrium and kinetic studies of manganese oxide coated cementitious media (MOCM) found that heavy metal adsorption was also pH dependent, and specific adsorption was observed at the solution pH value as low as 3.0 (Liu et al. 2001f; 2001g). The results of divalent heavy metal adsorption equilibrium studies for MOCM and speciation diagram modeled with surface complexation model indicated that adsorption, rather than bulk solution

precipitation is the main removal mechanism in the typical storm water pH range of 6 to 8.

### 9.4 Materials and Methods

#### 9.4.1 Media

Since the objective of this study is to compare and evaluated the sorptive media used or engineered for filter type storm water BMPs. Conventional filter media of silica sand and GAC were selected as well as the media engineered for combine unit operation of filtration and unit process of adsorption. The media used in this study were summarized in Table 9.1. Details regarding the physic-chemical properties of the media are described elsewhere (Liu et al. 2001a; 20001b).

Table 9.1 Media characteristics for column breakthrough experiments

| | Silica sand | IOCS | GAC | #Uncoated cementitious media | #Admixture cementitious media | #MOPM | #MOCM | #MOCS |
|---|---|---|---|---|---|---|---|---|
| Specific gravity ($\rho_s$) | 2.64 | 2.73 | 1.80 | 2.58 | 2.49 | 0.926 | 2.58 | 2.61 |
| Bulk density ($\rho_b$) ($g/cm^3$) | 1.72 | 1.72 | 0.487 | 1.26 | 1.22 | 0.58 | 1.26 | 1.72 |
| Porosity | 0.349 | 0.370 | 0.730 | 0.51 | 0.49 | 0.37 | 0.51 | 0.34 |
| *SSA ($m^2/g$) | 0.220 | 15.4 | 1021.8 | 4.08 | 10.74 | 21.17 | 17.30 | 1.51 |
| $pH_{PZC}$ | 6.8 | 8.6 | ??? | --- | 5.2 | 4.8 | 4.5 | 6.4 |
| $d_{50}$ (mm) | 0.5 | 0.5 | 0.65 | 1.41 | 1.41 | 3.44 | 1.41 | 1.19 |

*SSA was measured with EGME method.
#: Details of preparation and surface characteristics were described in Liu et al. 2001a and 2001b.
IOCS: Iron oxide coated sand
GAC: Granular activated carbon
MOPM: Manganese oxide coated polymeric media
MOCM: Manganese oxide coated cementitious media
MOCS: Manganese oxide coated sand

### 9.4.2 Experimental Matrix

Based on rainfall-runoff, snowmelt characterization and USEPA discharge criteria, Zn, Cu, Cd and Pb were chosen for the experimental column simulations. Influent metal solutions of Pb, Cu, Cd and Zn were prepared from 1000-ppm reference standard solutions of $Cd(NO_3)_2$, $Cu(NO_3)_2$, $Pb(NO_3)_2$, and $Zn(NO_3)_2$. The ionic strength for all metal solutions in DI water was fixed as 0.01-M $NaNO_3$. In storm water, ionic strength can vary from 0.0008 to 0.17-M as $NaNO_3$ (Hird and Sansalone 2001). Adjustments for pH were carried out with trace-metal 1-N $HNO_3$ or 1-N NaOH. Heavy metal analysis was carried out by inductively coupled plasma-mass spectroscopy (ICP-MS) on a Perkin-Elmer Elan 6000.

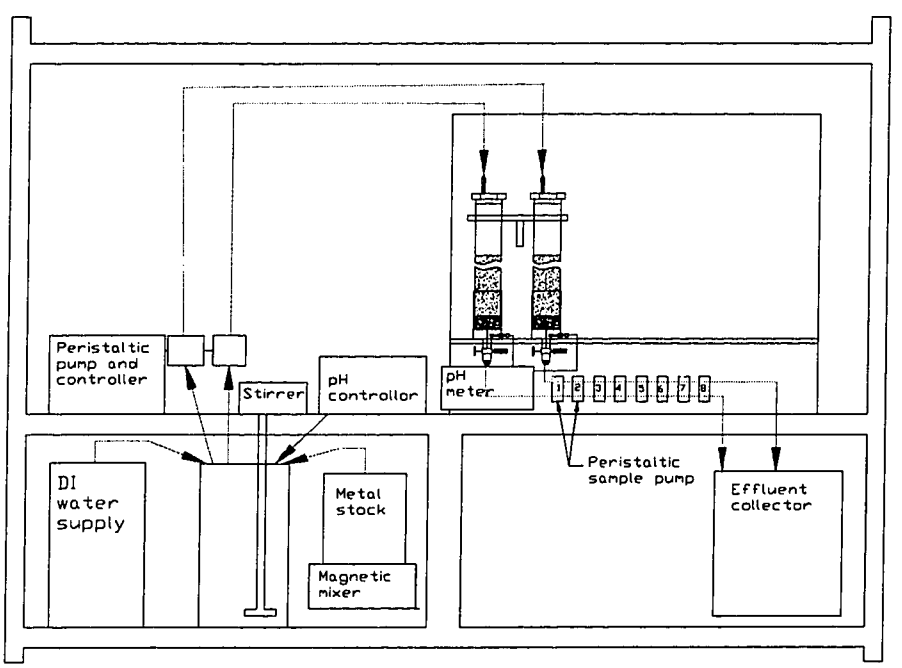


Figure 9.1 The layout of column experiment system.

Table 9.1 Influent water quality and column configurations

| | | Silica sand | IOCS | GAC | BSPET* | Uncoated cementitious media | Admixture cementitious media | MOPM | MOCM | | MOCS |
|---|---|---|---|---|---|---|---|---|---|---|---|
| **Influent pH** | | 6.5 | 6.5 | 6.5 | 6.5 | 6.0 | 6.0 | 7.0 | 6.0 | | 7.0 |
| **Ionic strength (mol/L as $NaNO_3$)** | | 0.01 | 0.01 | 0.01 | 0.01 | 0.01 | 0.01 | 0.01 | 0.01 | | 0.01 |
| **Heavy metal concentration (μg/L)** | **Zn** | 5000 | 5000 | 5000 | 5000 | 1000 | 500 | 1000 | 1000 | 500 | 1000 |
| | **Cu** | 5000 | 5000 | 5000 | 5000 | 1000 | 50 | 1000 | 1000 | 50 | 1000 |
| | **Cd** | 5000 | 5000 | 5000 | 5000 | 1000 | 50 | 1000 | 1000 | 50 | 1000 |
| | **Pb** | 5000 | 5000 | 5000 | 5000 | 1000 | 50 | 1000 | 1000 | 50 | 1000 |
| **Column ID (cm)** | | 3.81 | 3.81 | 3.81 | 3.81 | 2.54 | 2.54 | 5.08 | 2.54 | | 2.54 |
| **Bed volumes ($cm^3$)** | | 697 | 697 | 697 | 697 | 20 | 20 | 570 | 20 | | 20 |

* BSPET: Bench Scale Partial Exfiltration trench column utilized 8 cm of crushed cementitious porous pavement aggregate at the influent end with the balance of the total 61.2 cm length packed with IOCS resulting a total packed bed volume of 697 $cm^3$.

Table 9.2 Reynolds numbers and EBCT for flow rate and porous media

| | Silica sand | IOCS | GAC | BSPET | Uncoated cementitious media | Admixture cemetitious media | MOPM | MOCM | | MOCS |
|---|---|---|---|---|---|---|---|---|---|---|
| **Flow rate ($cm^3$/min)** | 50 | 50 | 50 | 50 | 10 | 10 | 40 | 20 | 10 | 20 |
| **$V_{superficial}$ (cm/min.)** | 4.39 | 4.39 | 4.39 | 4.39 | 1.97 | 1.97 | 1.97 | 3.95 | 1.97 | 3.95 |
| **$Re_d$** | 3.6 | 3.6 | 4.7 | 3.6 | 4.6 | 4.6 | 11.2 | 9.2 | 4.6 | 7.7 |
| **Flow regime** | turbulent | turbulent | turbulent | turbulent | turbulent | turbulent | turbulent | turbulent | turbulent | turbulent |
| **EBCT (min.)** | 4.4 | 4.5 | 8.1 | 4.6 | 1.1 | 1.0 | 4.6 | 0.5 | 1.1 | 0.4 |

### 9.4.3 Column Experiments

Column experiments for MOPM, MOCM and MOCS were carried out in plexiglas or Teflon PFAA columns with internal diameters of either 2.54 cm or g.08 cm. Column experiments for silica sand, IOCS and GAC were carried out in Plexiglas with a internal diameter of 3.81 cm. Packed bed lengths were dependent on media type to keep a reasonable breakthrough time. The column run configuration and the influent water quality were summarized in Table 9.2. The column diameter of 5.08 to 2.54 cm ID was based on maintaining a column diameter to media diameter ratio (D/d) greater than 12 without the introduction of significant influence on axial velocity profiles and wall skin friction in laboratory columns (Chellam and Wiesner 1993). The details of column design were shown in Figure 9.1. The main component of the experimental configuration type was a packed-bed reactor column in which each media is loaded to breakthrough capacity. The influent feed to the columns were supplied by use of a variable-flow digital driver, peristaltic pump heads and pump controller. Peristaltic pump feed lines were 4.8-mm ID flexible Viton tubing and transported influent feed from a 20-L continuously-stirred tank (CST) to the columns. Once the pumps and controller were calibrated, column runs were initiated, terminated and monitored through a computer interface to the controller. Sampling of column effluent was timed such that the breakthrough curve (BTC) can be clearly defined from a sufficient number of data points. An in-line pH measurement system was installed to measure pH drift of the effluent. Effluent pH values were recorded every 10 to 30-minutes automatically. The influents were supplied from a CST supplied by storm water, metal stock solution,

and pH and buffer solution. pH in the CST was moderated by a pH controller. The resolution of the controller was 0.1 pH units with an accuracy of ± 0.1 pH units. The controller integrates a variable-flow metering pump and proportional output programming to allow pH solution pumping to decrease proportionally until the pH set point is reached. The pH solution reservoir was a stirred 2-L glass beaker. 100 mL influent and effluent samples were collected in 125-mL wide-mouth straight-sided Teflon bottles. The effluent samples were diluted and acidified in trace metal $HNO_3$ to a 5% v/v basis and analyzed for the target heavy metal concentrations by inductive coupled plasma mass spectrometer (ICP-MS) analysis.

**9.4.4 Flow Rates and Flow Regime**

The influent flow rates were 10 to 50 mL/minute for all experimental runs. Flow was volumetrically calibrated daily and any measured variance was less than ± 2 mL/minute. Metal stock inflow to the CST was calibrated for either 2.0 or 4.0 mL/minute and influent DI water flow to the CST was calibrated to 98 or 96 mL/minute, respectively. Flow rates were calibrated twice a day and CST liquid volume was kept between 10 and 12 L. The flow regime was characterized by the Reynolds number as defined in equation (1). These numbers are tabulated in Table 9.3.

$$\mathrm{Re}_d = \frac{\rho_w V d_{50}}{\mu} \qquad (1)$$

where $\mu$ is the dynamic viscosity ($1.009\times10^{-2}$ g/(cm-sec)), V is superficial velocity (cm/sec), $d_{50}$ is the 50% diameter value located on the media diameter distribution, and

$\rho_w$ is the density of water (0.998 g/cm$^3$). The flow is located in turbulent regime as Reynolds number greater than 1.

The surface loading rate used in this study ranged from 20 to 80 L/m$^2$-min. This loading rate was chosen because it is typical of many urban storm water conditions where BMPs such as a partial exfiltration reactor (PER) are applied for in-situ treatment. For example, a peak flow of 50 L/m$^2$-min. was measured for the peak of 2-year return event at an experimental site (Sansalone and Buchberger, 1997). The decision to utilize a peak flow typical of a hydrograph from a moderately high intensity rainfall-runoff event will under-estimate PET breakthrough capacity. Other bench-scale results using columns packed with GAC and wastewater influent had improved breakthrough capacity as hydraulic loading rates were lowered. (Reed, et. al, 1996)

**9.4.5 Metal and pH Analysis**

Metal analysis was conducted with an ICP-MS (Elan 6000, Perkin-Elmer Science) employing four-point standard calibration prior to analysis of samples. The measuring conditions were 100-ms, 50 sweeps/reading, and 3 replicates. The internal standards were Scandium (Sc 45), Germanium (Ge 74), Rhodium (Rh 103) and Lutetium (Lu 175), which were added to the samples at a concentration of 10-ppb respectively. The elements were measured at m/z values of 63 for copper, 64 for zinc, 114 for cadmium and 208 for lead. Analytical controls were maintained throughout including use of control and blank samples, mass balance checks, and standard solution quantity checks of every 7 samples.

The effluent pH was measured inline using an Accumet AR50 dual channel pH/mv/conductivity meter with resolution of 0.01 pH units and an accuracy of ± 0.01 pH units.

**9.5 Results and Discussions**

**9.5.1 Silica Sand**

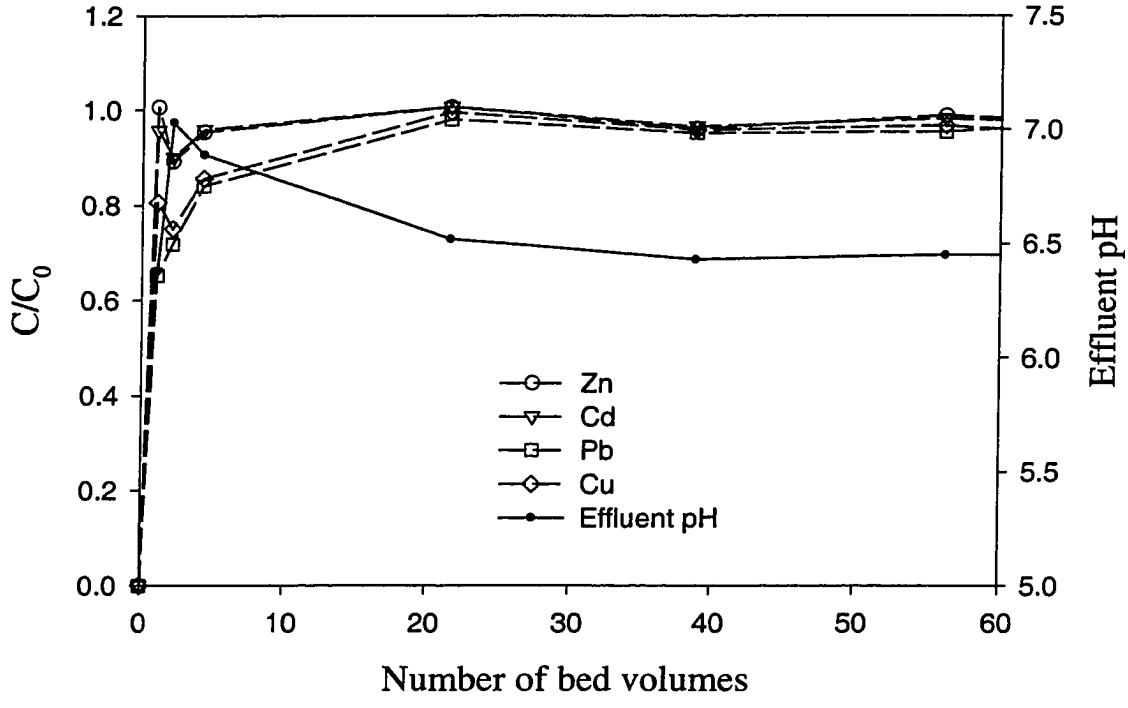


Figure 9.2 Breakthrough curve and effluent pH drift for silica sands with a influent pH of 6.5 and concentration of 5 mg/L each of Pb, Cu, Zn and Cd. EBCT = 4.4 minutes.

Sand as filter media has been applied for over a hundred years, and it is still the most widely used filter media for particle removal. For these series of experiments, silica sand used as a control media to compare breakthrough results of other media. The

ability of plain sand such as silica sand to adsorb heavy metals is generally very low. As illustrated in Figure 9.2, heavy metal breakthrough was very rapid, with a 90% breakthrough occurring within 10 bed volumes. Because of the low heavy metal capacity of plain sand, mixtures of sand and sorbent material or ion exchange material such as peat are used as a mixed filter medium. For dissolved heavy metal removal, silica sands were utilized unsuccessfully as filter media for storm water BMPs according to the current National Stormwater BMP Database (2001). In 1998 EPA conducted sampling activities at a peat/sand filter in Montgomery County, Maryland, and the results also indicated a limited treatment capability for heavy metals (USEPA 1999a). In this study, plain silica sand was served as a control for a comparison with engineered media currently in use as filter media for storm water BMPs.

### 9.5.2 Granular Activated Carbon

Normalized effluent Pb concentration ($C/C_0$) and effluent pH versus number of bed volumes (BV) treated, for 5 mg/L each of Cd, Zn, Pb and Cu, influent pH of 6.5 are presented in Figure 9.3. Breakthrough in this study was defined at $C/C_0 = 0.1$. Breakthrough was initiated at approximately 15, 45, 120, and 300 BV for Cd, Zn, Pb and Cu respectively. Although breakthrough profiles of four studied heavy metals indicated that competitive adsorption occurred for the column study, the order of breakthrough bed volumes is not necessarily represents the adsorption affinity of these four divalent heavy metals on GAC since the molar concentrations in influent solution were different. In this studied case, the influent molar concentrations of Cd, Zn, Pb and Cu were 43.8, 78.1, 24.0 and 79.4 μmol/L. Effluent pH elevated from 6.5 of the influent

solution to 8.0 at the beginning of column operation first, and then drop slowly to near influent pH level at the exhausting point. This effluent pH drifting pattern was also observed by other researchers (Reed et al. 1995; Reed and Arunachalam 1994). For example, the effluent pH for adsorption of Pb (10 mg/L, influent pH = 5.47) on virgin GAC decreased from about 7 at the beginning of the column operation to 5.4 at the end of column run (Reed and Arunachalam 1994). The mass transfer zon (MTZ) was 80 BV for Cd and Zn, and MTZ for Cu and Pb were not observed since BSPET was not exhausted for Cu and Pb at the end of column operation in this study. The mass transfer zon (MTZ) was approximated 50 BV for Cu, Zn and Cd, and 170 for Pb.

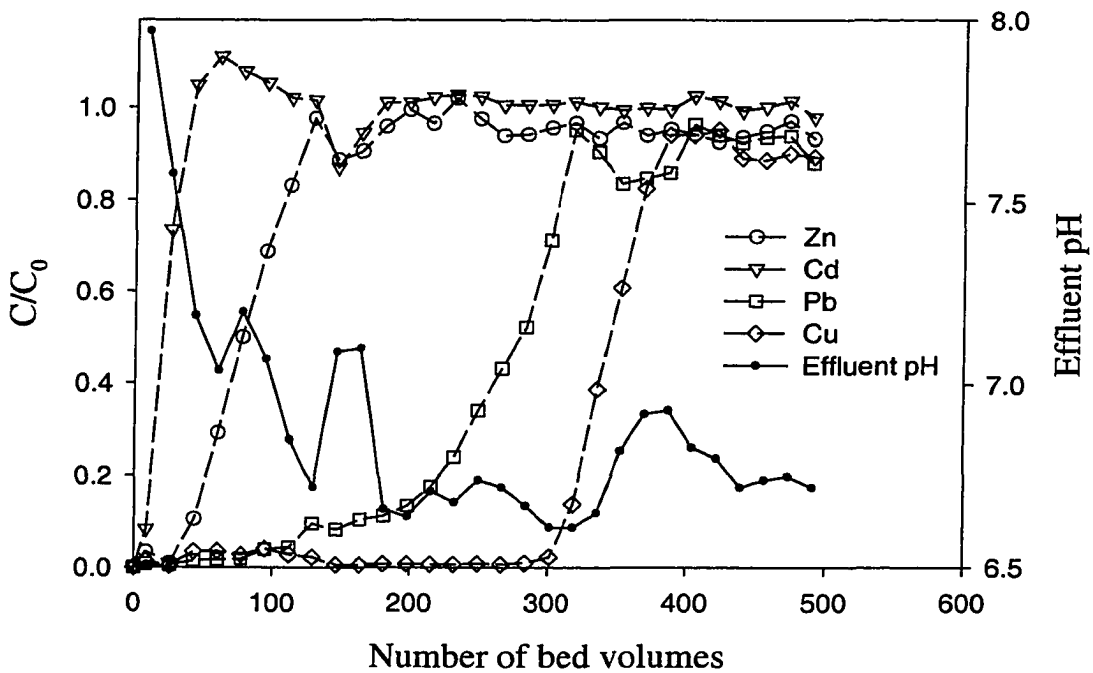


Figure 9.3 Breakthrough curve and effluent pH drift for GAC with a influent pH of 6.5 and concentration of 5 mg/L each of Pb, Cu, Zn and Cd. EBCT = 8.1 minutes.

### 9.5.3 Iron Oxide Coated Sand

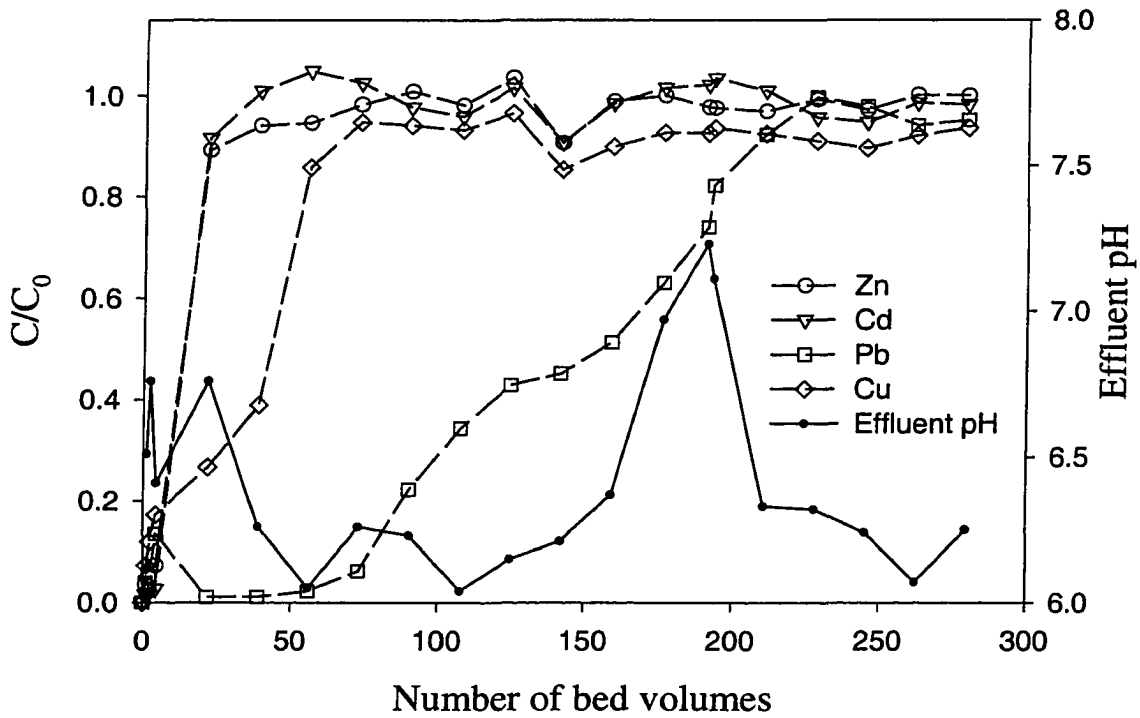


Figure 9.4 Breakthrough curve and effluent pH drift for IOCS and concentration of 5 mg/L each of Pb, Cu, Zn and Cd. EBCT = 4.5 minutes.

The column breakthrough profile of IOCS illustrates a competitive adsorption of divalent heavy metals by IOCS as shown in Figure 9.4. There is evidence that adsorption tendency of divalent transition elements by hydrous oxides often follows the Irving-Williams order, which suggests the sequence of decreasing adsorption tendency as Cu > Zn > or = Ni > Co > Fe > Mn > Ca (Stumm and Morgan 1996; Langmuir 1997). The relative percent adsorption of Pb, Cu, Zn and Cd by ferric oxyhyfroxide obeys the Irving-William order which is Pb > Cu > Cd > Zn (Langmuir 1997). In this

study, the most favorable cation, Pb, occupied almost all the adsorption sites on the IOCS in the adsorption zone of the IOCS column, thus, other less favorably adsorbed cations, such as Cd and Zn, breakthrough more rapidly. Compared to the breakthrough curves of IOCS column with silica sand column, significant improvement of Pb removal and slightly increase of adsorption capacities of Cu, Zn and Cd, was obtained through a thin iron oxide coating on the silica sand at an influent pH of 6.5. This pH was below the PZC of the IOCS, measured to be 8.5. The effluent pH drift fluctuated with the range of 6 to 7 without significant trend observed.

Figure 9.4 illustrates the breakthrough behavior of IOCS at a pH below the PZC of the IOCS. While the results in Figure 9.4 illustrate a significantly enhanced breakthrough behavior of IOCS compared to plain sand, a passive design configuration that raised the influent pH to or above the PZC of the IOCS may improve the performance of the treatment system. One such treatment system, a BSPET, was therefore examined and compared to IOCS. BSPET column utilized 8 cm of crushed cementitious porous pavement (CPP) at the influent end with the balance of the 61.2 cm length packed consisting of IOCS in a 3.81 cm inner diameter column resulting a total packed bed volume of 697 $cm^3$.

Comparing the breakthrough curves of BSPET column to the IOCS column at $C/C_0 = 0.1$, there are significant improvements for the divalent heavy metal removal as shown in Figure 9.5(a). Breakthroughs occurred at about 70, 80, 420, and greater than 600 BV for Cd, Zn, Pb and Cu respectively. This compares to the IOCS column where breakthrough occurred at less than 10 for Cu, Cd and Zn, and 80 BV for Pb. Percentage

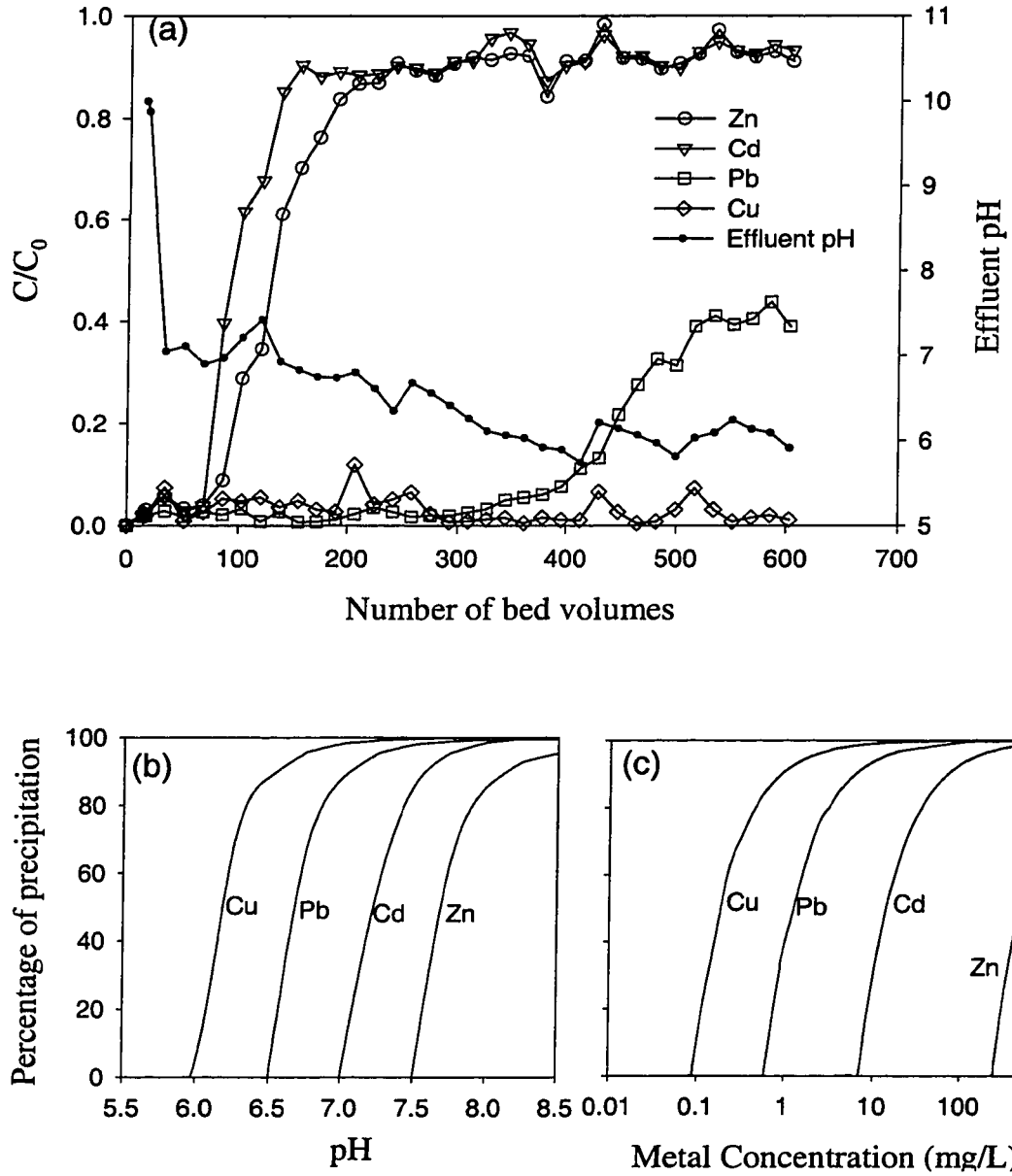


Figure 9.5. (a). Breakthrough curve and effluent pH drift for BSPET with a influent pH of 6.5 and concentration of 5 mg/L each of Pb, Cu, Zn and Cd. EBCT = 4.6 minutes. (b). percentage of precipitation metals as a function of pH. Modeled using MINTEQA with concentration of 5 mg/L each of Pb, Cu, Zn and Cd; (c). percentage of precipitation as a function of metal concentration at pH 7 using MINTEQA. Ionic strenth is 0.01 M $NaNO_3$ and constant $CO_2$ pressure is 0.00035 atm.

of particulate heavy metals as a function of pH as shown in Figure 9.5(b) was modeled using MINTEQA with influent heavy metal concentration of BSPET column, ionic

strength of 0.01 M $NaNO_3$ and constant $CO_2$ pressure of 0.00035 atm. Filtration and adsorption were both mechanisms for the removal of heavy metal from the influent feed since the influent contains both particulate (metal precipitates) and dissolved heavy metals. The CPP layer can significantly elevate the pH level in the column and will also providing alkalinity to poorly buffer storm water. For example, examining the relative fractions of dissolved and particulate fractions using MINTEQA, over 90 percent of Cu was particulate at the influent pH level of 6.5, and over 98 percent of all heavy metals examined were particulate at pH greater than 8. In the initial stage of the breakthrough curves, filtration may accounted for the majority of heavy metal removal and, in a sense, adsorption acted as a polishing process occurring in the same treatment column. Competitive adsorption cause lest adsorption favorable Zn and Cd relatively quick breakthrough after pH drop to less than 7.0, a level of which about all Zn and Cd are dissolved species. The MTZ for BSPET was 80 BV for Cd and Zn, and MTZ for Cu and Pb were not shown completely at this experimental run since BSPET was not exhausted for Cu and Pb at the end of column operation.

### 9.5.4 Manganese Oxide Coated Sand

Compare to iron oxides, manganese oxide generally have higher net negative charge and lower PZC. PZC of iron oxides were found ranging from 7 to 9 (Langmuir 1997; Dzombak and Morel 1991), while some manganese oxides such as birnssite and cryptomelane have $pH_{PZC}$ as low as 1.5 to 3.0 (McKenzie 1981). PZC results in this study were 6.4 for MOCS. Since the typical storm water pH range is from 6 to 8, manganese oxide coated sands were expected a relatively high net negative surface

charge and will facilitate the adsorption of divalent heavy metals which generally existed as cation in the storm water runoff. As shown in Figure 9.6, manganese oxide coated sand column breakthrough behavior is very similar to that of iron oxide coated sand except for a longer exhaustion time for MOCS which may due to its lower influent heavy metal concentrations. Competitive adsorption was also observed with Zn and Cd breakthrough within 10 BV, while for higher affinity cations, Cu and Pb, breakthrough

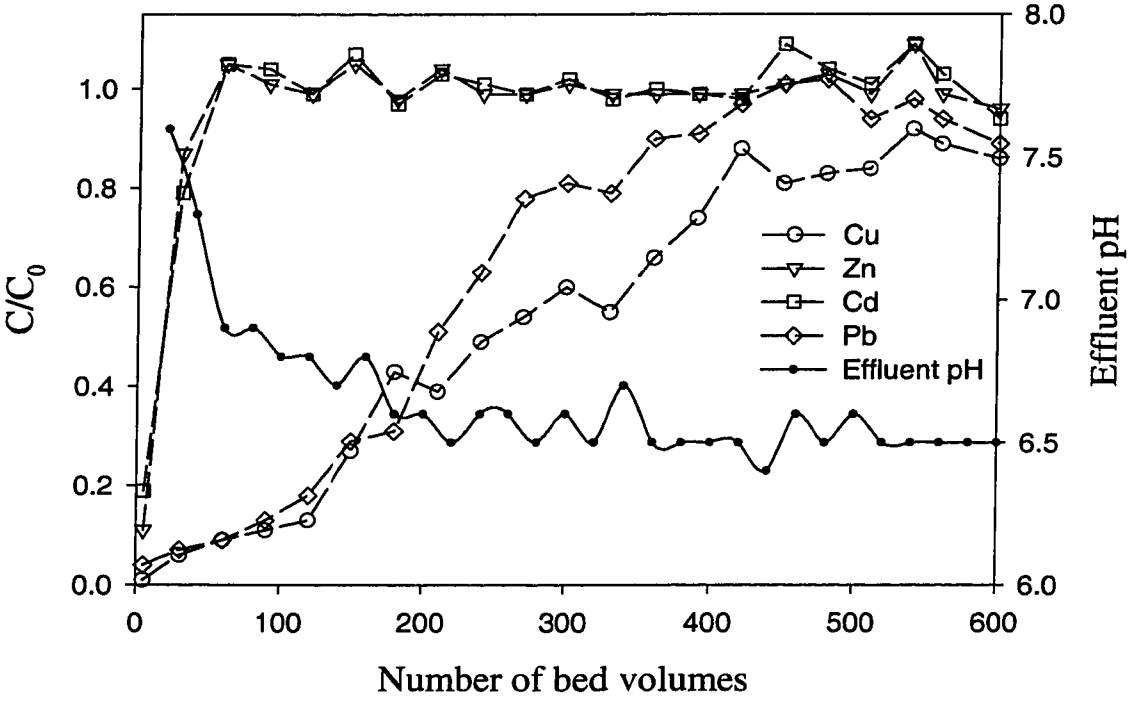


Figure 9.6. Breakthrough curve and effluent pH drift for MOCS with a influent pH of 7.0 and concentration of 1 mg/L each of Pb, Cu, Zn and Cd. EBCT = 0.4 minutes.

occurred at about 100 BV. Compare to breakthrough curve of silica sand, a manganese oxide coating layer results in a significant improvement in breakthrough capacity. Effluent pH was drop for 7.5 at the initial column operation to lower than influent pH of 7.0 rapidly and stable around 6.5 after 100 BV. This may indicate a surface complexation mechanism for divalent heavy metal removal which release protons to the solution. The MTZ for MOCS was approximately 10 BV for Cd and Zn, and 400 BV for Cu and Pb.

### 9.5.5 Manganese Oxide Coated Polymeric Media

MOPM were engineered to use its buoyant characteristics, in the BMP designs such as a sorptive buoyant media clarifier (SBMC). To compare the column adsorption behavior of MOPM and uncoated plain polymeric media, column breakthrough experiments were conducted for both media with the same influent conditions, bed volume, surface loading rate, EBCT and porosity. The uncoated polymeric media had little treatment capacity for heavy metal since breakthrough occurred within approximately 20 bed volumes as shown in Figure 9.7(b). The 0.1 C/C0 capacity for MOPM was approximately was approximately 1000, 800, 500 and 350 respectively for Pb, Cu, Zn and Cd at a surface loading rate of 80-L/m$^2$-min as shown in Figure 7(a). A relatively longer mass transfer zone (MTZ) was observed for Pb and Cu compared to MTZ of Cd and Zn since BVs from 10% breakthrough to 90% breakthrough for Cd and Zn is around 450 BVs with 1100 BVs for Pb and Cu. This compares to IOCS where the MTZ was less than 150 BV. The different removal mechanism may account for this difference since Cd and Zn are all dissolved species and surface complexation is the

main removal mechanism, while a part of Pb and Cu are particulate precipitates, and filtration and surface complexation are both working removal mechanisms.

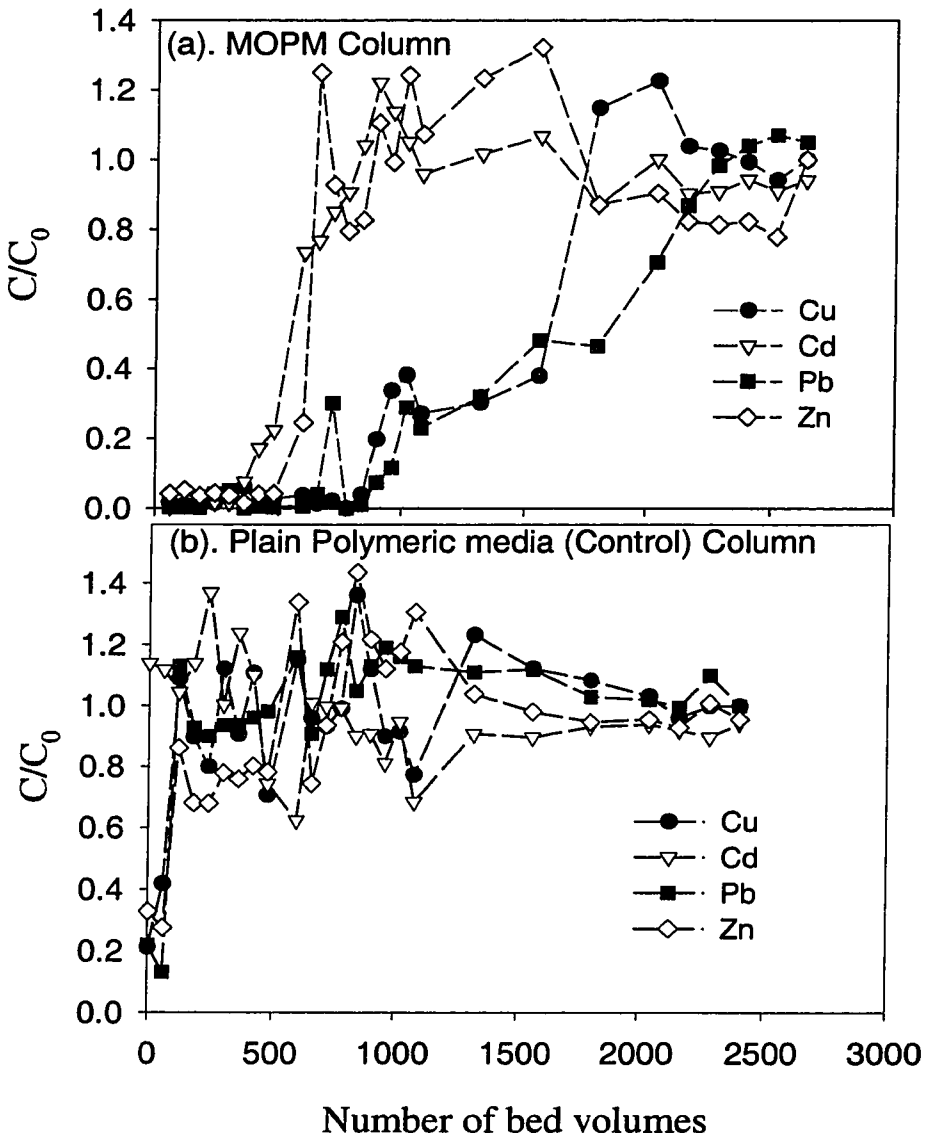


Figure 9.7.Breakthrough curve for MOPM (a) and plain polymeric media (b) with a influent pH of 7.0 and concentration of 1 mg/L each of Pb, Cu, Zn and Cd. EBCT = 4.6 minutes.

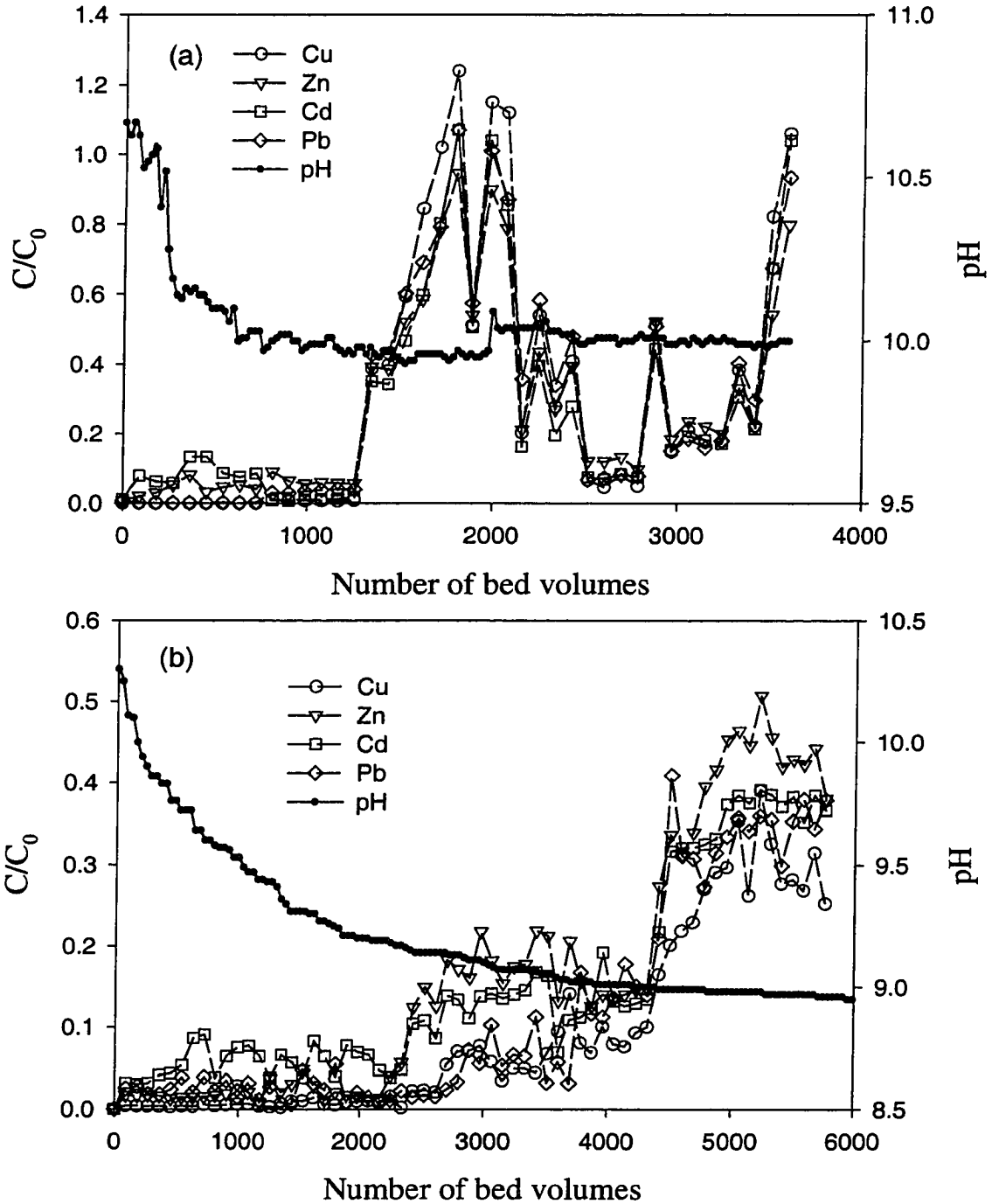


Figure 9.8. Breakthrough curve and effluent pH drift for uncoated cementitious media (a) and MOCM (b) with a influent pH of 6.0 and concentration of 1 mg/L each of Pb, Cu, Zn and Cd. EBCT = 1.1 minutes.

### 9.5.6 Manganese Oxide Coated and Uncoated Cementitious Media

The column runs of cementitious media were conducted under two separate EBCT values and influent heavy metal concentrations. Uncoated cementitious media column was run as a control for the MOCM as shown in Figure 9.8. Because of the higher surface alkalinity of the cementitous media effluent pH conditions were significantly higher than for other media. The effluent pH decreased from 10.6 at the beginning of the column operation to about 10.0 at the end of column run for uncoated cementitious media. In such a high pH condition, most of divalent heavy metals studied would be the particulate precipitates. 10% breakthrough occurred at 400 BV for Cd and 1300 BV for Zn, Cu and Pb. As an evidence of particle breakthrough for uncoated cementitious media, there were some $C/C_0$ values as high as 3.5 (not show in the Figure 9.8 (a)). Some greenish Cu precipitates could be observed in the column. Scanning electronic microscopic images also show some particulate precipitates attached on the uncoated cementitious media surfaces. Although some level of adsorption occurred in the uncoated cementitious media column, overall, filtration accounted for the majority of heavy metal removal since the breakthrough was due to particulate heavy metals passing through the column.

Three column runs were operated for manganes oxide coated cementitious media (MOCM) using the same column configuration and packing porosity. Run #1 was conducted with the same configuration used for uncoated cementitious media column which was EBCT of 1.1 minutes (surface loading rate = 40 $L/m^2$-min.), influent pH of 6.0 and concentration of 1-mg/L of Zn, Cd, Cu and Pb respectively. Run #2 was

conducted under the same conditions for run #1 except for a shorter EBCT of 0.5 minutes (surface loading rate = 80 $L/m^2$-min). Run #3 was conduct under the same conditions of run #1 except for the lower influent concentration of 0.5 mg/L for Zn and 0.05 mg/L each of Cd, Cu and Pb. The effluent pH of MOCM column run #1 decreased from 10.2 at the initial stage of the column run to about 8.9 at the end of column operation as shown in Figure 9.8(b). The breakthrough profiles of MOCM are significantly different from those of uncoated cementitious media, and the effluent heavy metal concentration remained under the 60% of the influent concentration at the end of the column operation. 10% breakthrough started at about 2500 BVs for Zn and Cd, and about 4000 BVs for Cu and Pb.

Studies of heavy metal adsorption as a function of influent pH and adsorption isotherm studies were conducted for MOCM and reported elsewhere (Liu et al. 2001e; 2001f). Using surface complexation theory, intrinsic surface complexation reaction constants were optimized from the experimental data, and the speciation results indicated that at initial aqueous divalent heavy metal concentration of 1-mg/L, surface complexation was the dominant removal mechanism for all four divalent heavy metals studied over the pH range from 1 to 10 (Liu et al. 2001f). According this theory and effluent pH condition, one can conclude the adsorption may account for the primary heavy metal removal. Small amount of greenish Cu precipitates were observed in the MOCM column after the end of run. This indicated that surface precipitation and filtration for particulate precipitates were still effective for the removal heavy metals. The "contradiction" between the explanation of surface complexation and experimental

observations can be interpret with the special chemical heterogeneity of MOCM surface which contains the mixture of calcites and manganese oxides. As postulated in the previous work (Liu et al. 2001b), the surface chemical heterogeneity between manganese oxide and calcite would facilitate heavy metal adsorption because $CaCO_3$ will create a relatively high pH solution layer around the media thus creating a high pH environment in a packed filtration bed. Heavy metals such as Pb and Cu could be easily precipitated and other heavy metals captured on the sorptive filter media through surface complexation mechanisms. To fully understand the heavy metal removal mechanisms for MOCM, such as quantitatively or even qualitatively distinguishing the removal contribution of adsorption from that of surface precipitation, are very limited by the inherently macroscopic, indirect measurements such as adsorption isotherms and reaction kinetics. However, surface spectroscopy techniques, such as extended X-ray absorption fine structure (EXAFS) spectroscopy and optical or magnetic resonance, may offer the best hope for a truly molecular level probe of the interfacial region that can discriminate among the structures that arise from diverse chemical conditions (Sposito 1986).

Figure 9.9 illustrates the column breakthrough curves and effluent pH drift for MOCM column run #2 (EBCT = 0.5 minutes). Compared to the breakthrough curves of run #1 (EBCT = 1.1 minute), this MOCM column run #2 had steeper breakthrough curves from bed volumes of breakthrough to exhaustion bed volumes, and less breakthrough bed volumes, which were about 900 for Zn and Cd and about 1200 for Pb and Cu. The effect of ECBT can be examined using a number of factors. These factors

include (1) volume of influent treated at breakthrough ($V_b$) and exhaustion ($V_{exh}$), (2) surface concentration (mg contaminant/g media) at breakthrough ($X/M_b$) and exhaustion ($X/M_{exh}$), (3) carbon usage rate (mass of media required/$V_b$), and (4) degree of column use (mass of contaminant removed at exhaustion). As EBCT is increase, $V_b$, $X/M_b$, and degree of column use increase, whereas medium usage rate decreases (Reed *et al.* 1996). As the ECBT for MOCM columns increased from 0.5 minutes (run #2) to 1.1 minutes (run #1), the values of $V_b$, $X/M_b$, and $X/M_{exh}$ increase at lest two folds as summarized in Table 4. These results indicate that the impact of EBCT for MOCM are comparable to that of GAC.

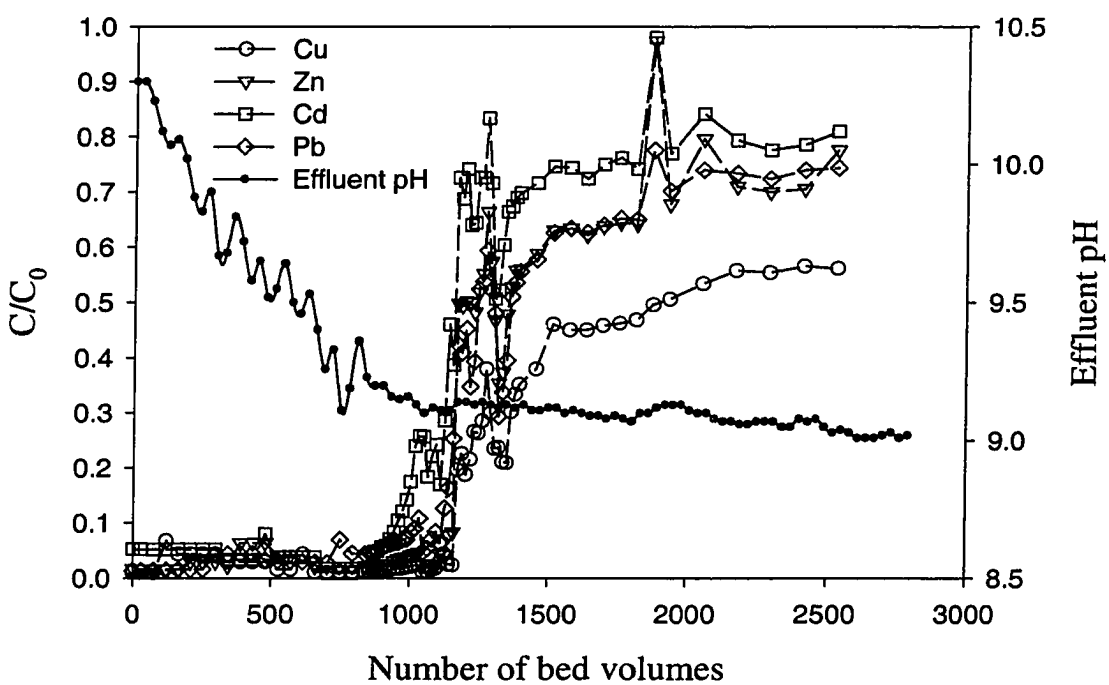


Figure 9.9. Breakthrough curve and effluent pH drift for MOCM with a influent pH of 6.0 and concentration of 1 mg/L each of Pb, Cu, Zn and Cd. EBCT = 0.5 minutes.

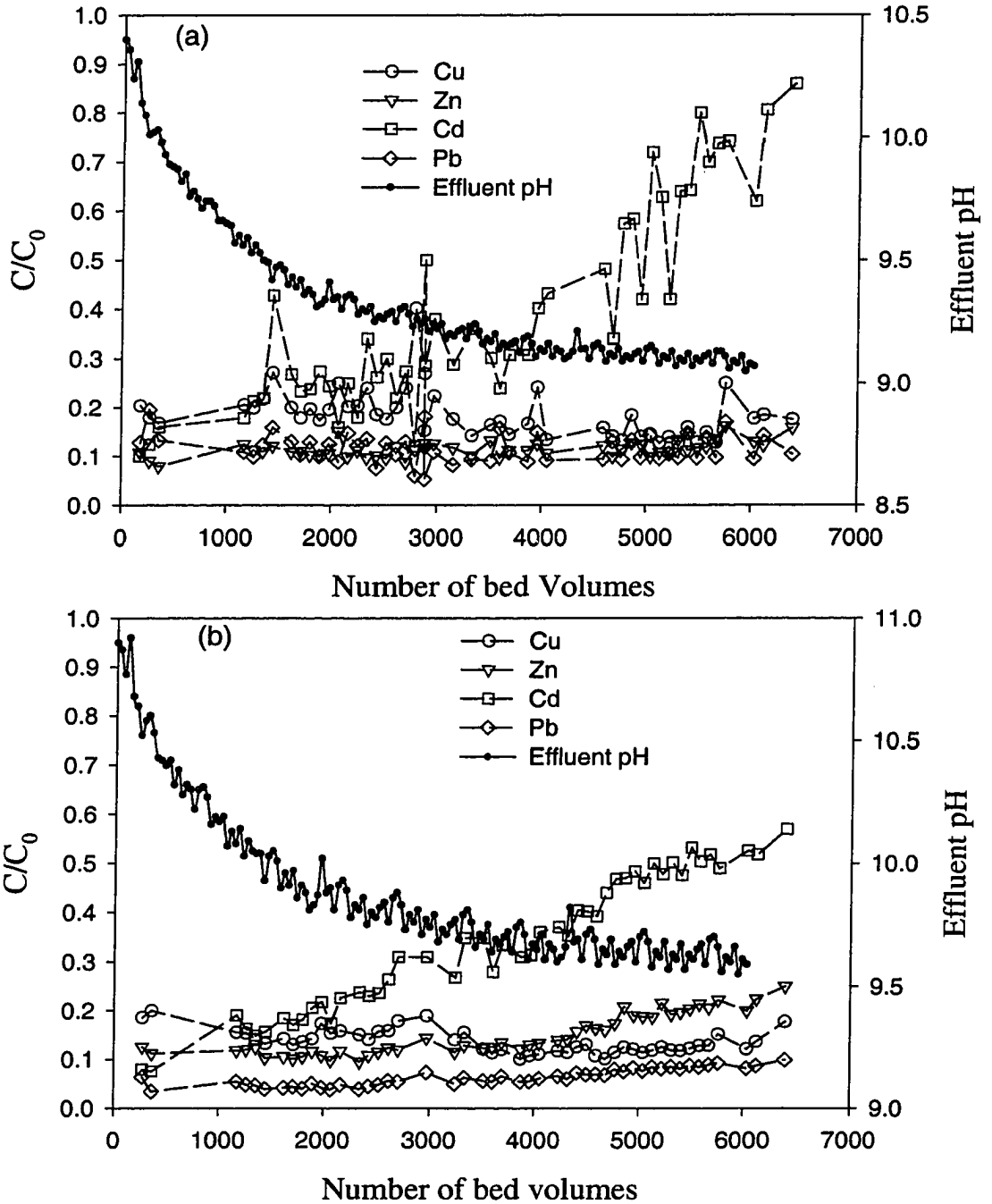


Figure 9.10.Breakthrough curve and effluent pH drift for MOCM (a) and admixture concrete (b) with an influent pH of 6.0 and concentration of 0.5 mg/L for Zn and 0.05 mg/L each of Pb, Cu, and Cd. EBCT = 1.0 minutes.

To investigate the treatment capacities for storm water runoff, an influent with pH of 6.0 and 500 μg/L for Zn and 50-μg/L each of Pb, Cd and Cu, was made as simulation of urban storm water runoff according to two years of data of event mean concentration at an urban site (Sansalone and Buchberger 1997; Sansalone et al. 1998). With the EBCT of 1.1 minutes, MOCM and admixture cementitious media (Liu et al. 2001b) have very similar breakthrough profiles as shown in Figure 9.10. Cd was the only metal cation exhausted in MOCM column run while effluent concentrations of other heavy metal cations were almost kept constantly at the range of 10 to 20 percent of influent concentration level untill the end of column operation. The adsorption may be the primary heavy metal removal mechanism, since in such a low heavy metal concentration and effluent pH level of 10.3 to 9.0 all Pb, Cd and Cu were dissolved and only approximately 57% Zn was precipitate at pH as high as 10.3 according a simulation from a MINTEQA model. The effluent pH drift is about the same as that of run #1 which has the same column operation and influent and condition except for the different heavy metal concentrations. Admixture cementitious media, which contain manganese oxide as the admixture, have the same treatment ability as that of MOCM. Cd was also the only metal exhausted in the admixture cementitious media column run. The effluent Pb concentrations were kept under 10% influent concentrations during the column operation. $C/C_0$ values of Cu and Zn were also kept constantly in the range from 0.1 to 0.2. The effluent pHs remained a 0.5 pH unit higher than that MOCM column. This indicates that filtration of admixture cementitous media column may contribute more for heavy metal removal than that of MOCM column.

Table 9.3 Media breakthrough bed volumes, breakthrough and exhaustion capacity for heavy metal adsorptions

| | | Zn | | | Cu | | | Cd | | | Pb | | |
|---|---|---|---|---|---|---|---|---|---|---|---|---|---|
| | | $X/M_b$ mg/g (mg/ml) | $X/M_{exh}$ mg/g (mg/ml) | $V_b$ (BV) | $X/M_b$ mg/g (mg/ml) | $X/M_{exh}$ mg/g (mg/ml) | $V_b$ (BV) | $X/M_b$ mg/g (mg/ml) | $X/M_{exh}$ mg/g (mg/ml) | $V_b$ (BV) | $X/M_b$ mg/g (mg/ml) | $X/M_{exh}$ mg/g (mg/ml) | $V_b$ (BV) |
| **Silica sand** | | 0 (0) | 0 (0) | 0 | 0 (0) | 0.0016 (0.003) | 0 | 0 (0) | 0 (0) | 0 | 0 (0) | 0.0015 (0.003) | 0 |
| **IOCS** | | 0.013 (0.022) | 0.019 (0.032) | > 10 | 0.006 (0.011) | 0.122 (0.210) | > 10 | 0.013 (0.022) | 0.017 (0.029) | > 10 | 0.19 (0.34) | 0.36 (0.63) | 80 |
| **BSPET** | | 0.059 (0.10) | 0.49 (0.86) | 80 | 1.64 (2.83) | 1.64 (2.83) | > 600 | 0.06 (0.10) | 0.39 (0.67) | 70 | 1.05 (1.81) | 1.53 (2.64) | 420 |
| **MOCS** | | 0 (0) | 0 (0) | > 10 | 0.028 (0.048) | 0.15 (0.25) | 100 | 0 (0) | 0 (0) | > 10 | 0.084 (0.15) | 0.11 (0.18) | 100 |
| **GAC** | | 0.40 (0.19) | 1.63 (0.80) | 45 | 3.51 (1.71) | 4.10 (2.00) | 300 | 0.02 (0.01) | 1.11 (0.54) | 15 | 1.63 (0.79) | 3.33 (1.62) | 120 |
| **MOPM** | | 0.40 (0.46) | 0.48 (0.55) | 500 | 0.56 (0.64) | 1.14 (1.30) | 800 | 0.35 (0.40) | 0.44 (0.50) | 350 | 0.84 (0.96) | 1.33 (1.51) | 1000 |
| **Uncoated cementitous media** | | 0.57 (0.66) | 0.66 (0.77) | 1300 | 0.60 (0.70) | 0.67 (0.79) | 1300 | 0.19 (0.23) | 0.66 (0.77) | 400 | 0.59 (0.69) | 0.67 (0.78) | 1300 |
| **Admixture cementitous media** | | 0 (0) | > 0.47 (> 0.52) | 0 | 0 (0) | > 0.045 (>0.05) | 0 | 0 (0) | 0.10 (0.11) | 0 | 0.20 (0.21) | > 0.20 (>0.21) | 6500 |
| **MOCM** | **Run #1** | 2.18 (2.54) | > 4.57 (> 5.33) | 2500 | 3.97 (4.64) | > 4.97 (5.80) | 4000 | 2.33 (2.72) | > 4.64 (>5.41) | 2500 | 3.69 (4.31) | > 4.83 (>5.63) | 4000 |
| | **Run #2** | 1.04 (1.21) | 1.50 (1.75) | 900 | 1.08 (1.26) | 1.78 (2.08) | 1200 | 0.88 (1.02) | 1.33 (1.55) | 900 | 1.04 (1.21) | 1.51 (1.76) | 1200 |
| | **Run #3** | 0 (0) | > 1.22 (> 1.41) | 0 | 0 (0) | > 0.24 (>0.27) | 0 | 0 (0) | > 0.16 (>0.18) | 0 | 0 (0) | > 0.27 (0.30) | 0 |

$X/M_b$ : Breakthrough capacity as $C/C_0 = 0.1$;
$X/M_{exh}$: Exhaustion capacity as $C/C_0 = 0.9$;
$V_b$: Number of bed volumes (BV) as breakthrough occurred at $C/C_0 = 0.1$;
The values in the parenthesis are the breakthrough or exhaustion capacities as the mass of contaminant per unit bed volumes.
> means breakthrough capacity are larger than the followed values (the experiment terminated before $C/C_0 = 0.9$).
Run #1: EBCT = 1.1 minutes, 1 mg/L each of Pb, Cu, Zn, and Cu, influent pH = 6.0;
Run #2: EBCT = 0.5 minutes, 1 mg/L each of Pb, Cu, Zn, and Cu, influent pH = 6.0;
Run #3: EBCT = 1.1 minutes, Zn @ 0.5 mg/L, and 0.05 mg/L each of Pb, Cu, and Cu, influent pH = 6.0.

### 9.5.7 Comparison of Column Effectiveness

10% column breakthrough bed volumes ($V_b$), breakthrough ($X/M_b$) and exhaustion capacity ($X/M_{exh}$) for heavy metal removal with sorptive media studied in this research were summarized in Table 9.4. MOCM in a run #1 configuration had the highest column breakthrough bed volumes ($V_b$), breakthrough ($X/M_b$) and exhaustion capacity ($X/M_{exh}$) of both on per mass values and per bed volume values. Even BSPET column run at higher effluent pH of 6.5 and higher heavy metal concentration 5-mg/L each of Pb, Cu, Cd and Zn, on a mass or bed volume basis, $V_b$, $X/M_b$ and $X/M_{exh}$ of MOCM in run #1 condition had twice the capacity of the BSBET, which has the second best performance of all the media studied. $V_b$, $X/M_b$ and $X/M_{exh}$ parameters for the BSBET were higher than that of IOCS or uncoated cementitious media. This indicated that mono-medium bed of IOCS or uncoated cementitious media has less effective heavy metal removal performance than the BSPET, which is dual-medium bed with the combination of IOCS and uncoated cementitious media. As discussed in previous section, IOCS was the adsorption dominant heavy metal removal in this configuration, and uncoated cementitious media was the precipitation and filtration dominant heavy metal removal. The effective combining both adsorption and precipitation filtration in one bed, such as mono-medium bed of MOCM, a dual-medium bed of IOCS and uncoated cementitious media as with the BSPET, can provide improved breakthrough as compared to media providing only one predominant removal mechanism. GAC had relatively high exhaustion capacity in this study, however, the breakthrough bed volumes were low with 15 for Cd and 45 for Zn, and its breakthrough capacity was

0.19-mg/ml for Zn and 0.01-mg/ml for Cd. This would limit GAC applicability on heavy metal removal of urban storm water treatment. Manganese oxide admixture cementitious media also provides comparable column performance for low influent heavy metal concentration. However, its $V_b$, $X/M_b$ and $X/M_{exh}$ values still lower than that of MOCM in the same operation condition. Overall, compared to other media studied, MOCM has the best column performance.

**9.6 Conclusions**

Column breakthrough experiments were conducted for different sorptive media to investigate the column performances as potential use in BMPs such as partial exfiltration trench or sorptive media clarifiers utilized for heavy metals removal from urban storm water runoff. Conventional BMP media such as silica sand exhibited almost immediate breakthrough (90% breakthrough within 10 bed volumes) served as a control media in this study against which other media were compared. Compared to breakthrough curve of silica sand, MOCS or IOCS has significant breakthrough capacities for heavy metals. A BSPET demonstrated improved breakthrough performance compared to IOCS. Precipitation, filtration and adsorption may account for the removal of heavy metal from the influent using the BSPET configuration since the influent contain both particulate and dissolved heavy metals, and the crushed cementitious porous pavement aggregate layer can significantly increase the pH level of the influent. GAC had a relatively high exhaustion capacity in this study, however, its low breakthrough bed volumes of 15 for Cd and 45 for Zn would limit GAC applicability on heavy metal removal of urban storm water treatment. MOPM was

engineered to take advantage of its buoyant characteristics, such as in a BMP design as a medium for sorptive buoyant media clarifier (SBMC). Compared to the uncoated polymeric media which almost has no treatment ability, the 10% breakthrough empty bed volumes of MOPM for Pb, Cu, Zn and Cd were significantly higher at an influent pH of 6.5, heavy metal concentration of 1-mg/L for Pb, Cu, Cd and Zn, and surface loading rate of 80-L/$m^2$-min.

Comparing the column performances of all the media used in this study, overall, MOCM has the best operation results with $V_b$, $X/M_b$ and $X/M_{exh}$ of MOCM in run #1 for conditions of surface loading rate of 40 L/m2-min, ECBT of 1.1 minute, influent Pb, Cu, Zn and Cd concentration of 1 mg/L, and influent pH of 6.0. This performance was followed by that of the BSBET configuration of dual media. As the ECBT for MOCM columns increased from 0.5 minutes (run #2) to 1.1 minutes (run #1), the values of $V_b$, $X/M_b$, and $X/M_{exh}$ increased by a factor of two. Compared to the primary removal mechanism of surface precipitation and filtration for uncoated cementitious media, the dissolved heavy metal removal mechanism for MOCM is considered as combining adsorption (or surface complexation) and filtration. This also account for MOCM's relatively high treatment ability. Manganese oxide admixture cementitious media also provides comparable column performance for simulated storm water. However, its $V_b$, $X/M_b$ and $X/M_{exh}$ values still lower than that of MOCM under the same operational conditions.

# CHAPTER 10. GLOBAL CONCLUSIONS

From various sources such as transportation activities and infrastructure, urban storm water contains significant loads of heavy metals. Promulgation of NPDES Phase II regulations has spurred development of Best Management Practices (BMPs) for in-situ control of heavy metals, and BMPs that incorporate heavy metal separation are generating more attention as the nature of storm water is better understood. In this study, the physic-chemical characteristics and adsorption behavior of amphoteric materials such as manganese oxides and iron oxides onto the substrates including silica sands, polymeric beads and cementitious particles were examined. Surface characteristics of coating media were determined by powder X-ray diffraction (XRD), infrared (IR) spectroscopy, and scanning electron microscopy (SEM) analysis. For the oxide coated polymeric buoyant media ($\rho_s < 1.0$), results indicated that oxide coatings ranged from 20 to 200-μm in depth, and surface areas were increased to above 25-$m^2$/g compared to uncoated media with a surface area less than 0.05-$m^2$/g. All manganese oxide coated media generate negative surface charge in the typical storm water pH range of 6-8. Media specific gravity remained less than 0.93 even with oxide coatings. A multiple-layer oxide coating (TCB or MOPM) provided surface characteristics that have the potential to enhance filtration and adsorption of heavy metals using coated buoyant polymeric spherical media in storm water treatment systems such as sorptive buoyant media clarifiers (SBMC).

Methods were developed to coat manganese oxides onto sand and cementitious media ($\rho_s$ > 1.0) for storm water treatment. With respect to manganese, coatings of ramsdellite produced a point of zero charge (PZC) of 5.2 while mixtures of birnessite and cryptomelane produced a PZC of 2.6. Manganese oxide increased the specific surface area (SSA) of sand and cementitious media. Manganese oxide coated sand (MOCS) produced a larger SSA (2.48-$m^2$/g) compared to birnessite-coated media (BCM) (1.51-$m^2$/g) while the two have similar surface charge (PZC = 6.4). Manganese oxide coated cementitious media (MOCM) produced a significantly larger SSA (19.49-$m^2$/g) compared to coated sand, and SEM analyses indicated the surface contained manganese oxide and calcite of thickness 10 to 30-μm. Based on the results, coated cementitious media provided surface characteristics that can significantly enhance filtration and adsorption of heavy metal in storm water, in comparison to sand.

Two manganese oxide media (MOPM and MOCP) were selected by comparing surface characterization result, and investigated for their heavy metal uptake capabilities and mechanisms through batch and column experiment.

For MOPM, Freundlich isotherms are utilized to fit the experiment data. Adsorption is pH dependent and results indicate a favorable solute pH range of > 6 for heavy metal adsorption. The relative adsorption affinity of MOPM for four divalent heavy metals typically found in storm water is Pb(II) > Cu(II) > Cd(II) > Zn(II). Adsorption rates were rapid for this flowthrough batch system with over 50% removal in the first 30-minutes and over 90% removal within 5-hours at a surface loading rate of 500 ml/$cm^2$-min. The pH drift patterns, due to surface complexation, during each

experiment, coincided with the heavy metal removal rate curve. Study results indicated the inclusion of a thin manganese coating can significantly increase media adsorption capacity. MOPM has a comparable adsorption capacity for the divalent heavy metals compared to other commercial and research media. Surface complexation modeling using FITEQL-TLM generated intrinsic surface acidity constants for the MOPM of $\log K_{a1}^{int}$ = 3.196 and $\log K_{a2}^{int}$ = -5.802. The intrinsic surface reaction constants for Pb(II), Cu(II) and Zn(II) were $\log K_{Pb}^{int}$ = –1.91, $\log K_{Cu}^{int}$ = -2.53 and $\log K_{Zn}^{int}$ = -4.45 respectively.

The results of the divalent heavy metal adsorption equilibrium study for MOCM indicated that adsorption is the dominant removal mechanism in the low pH range, and the combination of precipitation and adsorption may be responsible for divalent heavy metal removal in the neutral and high pH range. Formation of an adsorption-favored pH condition suggests that using MOCM as filter media for divalent heavy metal removal can take advantage of combining the unit operation of filtration and the unit process of adsorption or surface complexation in a BMP. Such BMPs can be a packed or fluidized filtration bed for centralized or decentralized storm water treatment systems. Parabolic adsorption isotherm results indicated that at least two or more adsorption energy levels exist for the surface sites of MOCM. Specific adsorption of divalent heavy metals by MOCM were observed at equilibrium pH less than 3. The divalent heavy metal adsorption affinities of MOCM were Pb > Cu > Zn > Cd. The adsorption kinetics varied with the nature of the divalent heavy metal, initial aqueous solution pH, and sorbent dosage. Adsorption equilibrium times of MOCM are approximately 2-hours for Pb and

5-hours for Cu, Zn and Cd. The divalent heavy metal adsorption profiles and the porous surface morphology of MOCM suggest that limitation of the sorption reaction by interparticle diffusion might be the explanation of divalent heavy metal adsorption kinetics for MOCM. The profiles of adsorption kinetics were determined by the interaction of pH drift and sorbate coverage. The intrinsic surface reaction constants for MOCM were determined through the adsorption data as a function of pH using FITEQL-TLM, and are $\log K_{Pb}^{int} = -1.84$, $\log K_{Cu}^{int} = -4.11$, $\log K_{Zn}^{int} = -5.04$, and $\log K_{Zn}^{int} = -7.84$. Surface complexation on the solid-water interface and precipitation in bulk solution were distinguished from the speciation distribution as a function of pH. At initial aqueous divalent heavy metal concentration of 1-mg/L, surface complexation was the dominant removal mechanism for all four divalent heavy metals studied over a pH range from 1 to 10. For initial aqueous divalent heavy metal concentration of 5-mg/L, surface complexation is still the main removal mechanism for Pb and Zn, while for Cu and Cd, precipitation were significant at higher pH, specifically, greater than 6 for Cu and greater than 7 for Cd. At typical solution conditions of urban storm water runoff, surface complexation would be the dominant removal mechanism for heavy metal removal in storm water treatment using MOCM as a sorptive filter medium for treatment devices designed for BMPs.

A potential driving kinetic model was developed based on an elementary second order rate law. Experimental data were predicted using this model and a number of other kinetic models were compared using experimental data. Manganese oxide surface morphology and the ability of a parabolic diffusion model to predict the adsorption

kinetics of MOPM suggest diffusion controlled adsorption for divalent heavy metals on MOPM. Based on a goodness of fit test, the potential driving model best represented the experimental data. Using the potential driving model, it was found that rate constants were increased with increasing solution pH, but were independent to the sorbent dosages. Results indicated that metal ions with the highest adsorption affinity had the highest rate constants. Potential driving second order kinetic model was also applied successfully to simulate divalent heavy metal adsorption rates with correlation coefficients of 0.97 to 0.99. Compared with the Elovich model based on the values of goodness of fit, the potential driving second order model best represented the experimental data. A fast rate in the first hour and secondary slow stage lasting for 5 to 10 hours was observed for divalent heavy metal adsorption by MOCM, and possible rate limiting processes responsible for this secondary slow stage were interparticle diffusion, surface precipitation and energetically heterogeneous surface adsorption sites.

In this study, different sorptive media column breakthrough experiments were conducted to investigate heavy metal removal capability for the possible application as sorptive media of storm water BMPs such as partial exfiltration trench or sorptive media clarifier. Compared to column breakthrough of silica sand, manganese oxide coating of MOCS or iron oxide coating of IOCS has a significant improvement of column breakthrough capacities and bed volumes. Compared the column performances of all the media utilized in this study, MOCM has the best operation results with 10% breakthrough bed volumes ($V_b$), breakthrough capacity ($X/M_b$) and exhaustion capacity ($X/M_{exh}$) two times higher than those of BSPET, the secondly best media. As the EBCT

for MOCM columns increased from 0.5 minutes to 1.1 minutes, the values of $V_b$, $X/M_b$, and $X/M_{exh}$ increase over two folds. The primary removal mechanism is surface precipitation and filtration for uncoated cementitious media, while the dissolved heavy metal removal mechanism for MOCM is considered as combining adsorption (or surface complexation) and filtration, which also account for MOCM's relatively high treatment ability.

# REFERENCES


America Water Works Association, and American Society of Civil Engineers (1998). "*Water Treatment Plant Design.*" 3rd ed., The McGraw-Hill Companies, Inc. New York.

Appelo, C. A. J., and Postma, D. (1999). "A consistent model for surface complexation on birnessite (-$MnO_2$) and its application to a column experiment." *Geochim. Cosmochim. Acta*, 63(19/20), 3039-3048.

Armstrong, L. J. (1994). "Contribution of heavy metal to storm water from automotive disc brake pad wear." *Rep. For Santa Clara Valley Nonpoint Source Pollution Control Program*, Woodward-Clyde Consultants, Oakland, Calif., 1-37.

ASTM, (1994), Standard Test Method for Specific Gravity of Soil Solids By Gas Pycnometer, Designation: D 5550 – 94

Atkinson R. J., Hingston F. J., Posner A. M., and Quirk J. P. (1970). "Elovich equation for the kinetics of isotope exchange reactions at solid-liquid interface." *Nature* (London), 226, 148-149.

Axe, L. and Anderson, P. R. (1997). "Experimental and theoretical diffusivities of Cd and Sr in hydrous ferric oxide" *J. Colloid Interface Sci.*, 185(2), 436-448.

Bajpai, S., and Chaudhuri M. (1999). "Removal of Arsenic form ground water by manganese dioxide-coated sand." *J. Envir. Engrg.*, ASCE, 125(8), 782-784.

Ball, D., Hamilton, R., and Harrison, R. (1991). "The influence of highway-related pollutants on environmental quality." R. Hamilton and R. Harrison, eds., *Highway Pollution*, Elsevier Science Publishing Company, Inc., New York, N. Y., 1-47.

Bannerman, R.T., A.D. Legg, and S. R. Greb. (1996). "*Quality of Wisconsin Stormwater, 1989-94.*" U.S. Geological Survey Open File Report 96-458. Prepared in Cooperation with the Wisconsin Department of Natural Resources. Madison, WI.

Barrettt, M. E., Malina, J. F., Charbebeau, R. J., and Ward, G. H. (1995) "Characterization of highway runoff in the Austin, Texas area." Ctr. For Res. in Water Resour., Bureau of Engrg. Res., University of Texas at Austin, Austin, Tex.

Barrettt, M. E., Zuber, R. D., Collins, E. R., Malina, J. F., Charbebeau, R. J., and Ward, G. H. (1993) "A review and evaluation of literature pertaining to the quantity and

control of pollution from highway runoff and construction." Ctr. For Res. in Water Resour., Bureau of Engrg. Res., University of Texas at Austin, Austin, Tex.

Bastian, R.K. (1997). "Potential Impacts on Receiving Waters." *Effects of Water Development and Management on Aquatic Ecosystems.* Proceedings of an Engineering Foundation Conference. L.A. Roesner, ed. American Society of Civil Engineers. New York, NY.

Benjamin, M. M., Sletten, R. S., Bailey, R. P. and Bennett, T. (1996). "Sorption and filtration of metals using iron-oxide-coated sand." Wat. Res., 30(11), 2609-2620.

Benjamin, M. M., and Leckie, J. O. (1981). "Multiple-site adsorption of Cd, Cu, Zn and Pb on amorphous iron oxide." J. Colloid Interface Sci., 79, 209-221.

Borggaard, O. K. (1983). "Effect of surface area and mineralogy of iron oxides on their surface charge and anion-adsorption properties." Clays Clay Miner., 31, 230-232.

Brunauer, S., Emmett, P. H. and Teller, E. (1938). "Adsorption of gases in multimolecular layers." J. Am. Chem. Soc., 60:309-319.

Buckland, S. T., Anderson, D. R., Burnhan, K. P. and laake, J. L. (1993). "Distance Sampling: Estimating Abundance of Biological Populations." Chapman and Hall, London.

Burns, R. G., and Burns, V. M. (1977). "Mechanism for nucleation and growth of manganese nodules." *Nature (London)*, 225, 130-131.

Burns, R. G. (1976). "The uptake of Co to onto ferromanganese nodules, soils, and synthetic manganese (IV) oxides." Geochim. Cosmochim. Acta, 40, 95-102.

Carlson K. H., and Knocke W. R. (1999). "Modeling manganese oxidation with $KMnO_4$ for drinking water treatment." *J. Envir. Engrg.*, ASCE, 125(10), 892-896.

Carski, T. H., and Sparks, D. L. (1985). "A modified miscible displacement technique fir investigation adsorption-desorption kinetics in soils." *Soil Sci. Soc. Am. J.*, 49, 1114-1116.

Carter D. L., Mortland M. M. and Kemper W. D. (1986). "*Specific Surface. In: Methods of Soil Analysis, Part 1, Physical and Mineralogical Methods.*" 2nd Ed. Arnold Klute, Eds., American Society of Agronomy, Inc, Soil Science Society of America, Inc, Madison, Wisconsin, USA.

Cartledge F. K., Butler L. G., Chalasani D., Eaton H. C., Frey F. P., Herrera E., Tittlebaum M. E. and Yang Shou-Lan (1990). "Immobilization mechanisms in solidification stabilization of Cd and Pb salts using portland-cement fixing agents." *Environ. Sci. Technol.*, 24 (6), 867-873.

Catts, J. G., Langmuir, D. (1986). "Adsorption of Cu, Pb and Zn by $\delta$-MnO2: Applicability of the side binding-surface complexation model." *Appl. Geochem.*, 1, 255-264.

Celorie, J. A., Wood, S. L., Vinson, T. S., and Istok, J. D. (1989). "A comparison of sorption equilibrium distribution coefficients using batch and centrifugation method." *J. Environ. Qual.*, 18, 307-313.

Cernik M., Borkovec M, Westall J. C. (1995). "Regularized least-squares methods for the calculation of discrete and continuous affinity distributions for heterogeneous sorbents." Environ. Sci. Technol. 29 (2), 413-425.

Chellam, S., and Wiesner M.R. (1993). "Slip flow through porous media with permeable boundaries: implications for the dimensional scaling of packed beds." Water Environmental Research, 65, 744-749.

Chen, B., Hui, C. W., and Mckay, G. (2001) "Film-pore diffusion modeling for the sorption of metal ions from aqueous effluents onto peat." *Wat. Res.*, 35(14), 3345-3356.

Chen, J. P., and Lin, M. (2001) "Equilibrium and kinetics of metal ion adsorption onto a commercial H-type granular activated carbon: experimental and modeling studies." *Wat. Res.*, 35(10), 2385-2394.

Cheung, C. W., Porter, J. F. and Mckay, G. (2001). "Sorption kinetic analysis for the removal of cadmium ions from effluents using bone char." *Wat. Res.*, 35(3), 605-612.

Chien, S. H. and Clayton, W. R. (1980). "Application of Elovich eqation to the kinetics of phosphate release and sorption in soils." *Soil Sci. Soc. Am. J.*, 44, 265-268

Christophi, C. A. and Axe, L. (2000). "Competetion of Cd, Cu, and Pb adsorption on goethite." *J. Envir. Engrg.*, ASCE, 126(1), 66-74.

Claytor, R. and T. Schueler. (1996). "*Design of Stormwater Filtering Systems.*" Prepared for the Chesapeake Research Consortium. Center for Watershed Protection. Ellicott City, MD.

Cocke, D. L., Mollah, M. Y. A. (1993). "The chemistry and leaching mechanisms of hazardous substances in cementitious solidification/stabilization systems." In Chemistry and Microstructure of Solidified Waste Forms, Spence, R. D., ed., Lewis Publishers, Boca Raton, FL, pp. 187-242.

Coffey, B. M., Gallagher, D. L., and Knocke, W. R. (1993). "Modeling soluble manganese removal by oxide-coated filter media." *J. Envir. Engrg.*, ASCE, 119(4), 679-694.

Coston J. A., Fuller, C. C. and Davis. J. A. (1995). "$Pb^{2+}$ and $Zn^{2+}$ adsorption by a nature aluminum-bearing and iron-bearing surface coating on an aquifer sand." *Geochim.Cosmochim. Acta*, 59(17), 3535-3543.

Cotton, F. A., and Wilkinson, G. (1980). "Advanced Inorganic Chemistry." 4th ed., Wiley, New York.

Crowther, D. L., Dillard, J. G., and Murray, J. W. (1983). "The mechanism of Co(II) oxidation on Synthetic birnessite." *Geochim. Cosmochim. Acta*, 47, 1399-1403.

Cussler, E. L. (1984). "Diffusion, Mass transfer in fluid systems." Cambridge University Press, New York.

Czernin, W. (1980). "Cement Chemistry and Physics for Civil Engineering." 2nd English Ed. Wiesbaden, Berlin: Bauverlag; London: Godwin; New York: Foreign Publications.

Davis, J. A. and Kent, D. B. (1990). "Surface complexation models in aqueous geochemistry." In *Mineral-water interface geochemistry*, ed Hochella, M. F., and White, A. F., Reviews in Mineralogy 23, pp. 177-260. Min. Soc. Am.

Davis, J. A., and Leckie, J. O. (1978). "Surface ionization and complexation at the oxide/water interface. II. Surface properties of amorphous iron oxyhydroxide and adsorption of metal ions." *J. Colloid Interface Sci.*, 74, 32-42.

Dong, D., Nelson, Y. M., Lion, L. W., Shuler, M. L., and Ghiorse, W. C. (2000). "Adsorption of Pb and Cd onto metal oxides and organic material in natural surface coatings as determined by selective coatings as determined by selective extractions: New evidence for the importance of Mn and Fe oxide." *Water Research*, 34(2), 427-436.

Drapper, D., Tomlinson, R., and Williams, P. (2000) "Pollutant concentrations in road runoff: southeast qeensland case study." *J. Envir. Engrg.*, ASCE, 126(4), 313-320.

Driscoll, E., Shelley, P. E., and Strecker, E. W. (1990) "Pollutant loadings and impacts from highway storm water runoff, Vols. I-IV." FHWA/RD-88-006-9, Federak Highway Administration, Washington, D.C.

Drits, V. A., Silvester, E., Dorshkov, A. I., and Manceau, A. (1997). "Structure of synthetic monoclinic Na-rich birnessite and hexagonal birnessite and selected-area electron diffraction." *Amer. Mineral.*, 82, 946-961

Dzombak, D. A., and Morel, F. M. M. (1987). "Adsorption of inorganic pollutants in aquatic in aquatic systems." *J. Hydraulic Eng.*, 113, 430-475.

Dzombak D. A. and Morel F. M. M. (1985) "Sorption of cadmium on hydrous ferric oxide at high sorbate/sorbent rations: equilibrium, kinetic and modeling." *J. Colloid Interface Sci.* 112(2), 588-598.

Dzombak, D. A. and Morel F. M. M. (1990). "Surface Complexation Modeling . Hydrous ferric oxide." Wiley-Interscience, New York.

Edward, H. S. (1996). "Uptake of heavy metals in batch systems by a recycled iron-bearing material." *Water Research*, 30(10), 2424-2434.

Elabsy, M. A., Elnaggar, I. M., Hamid, M. M. A., Aly, H. F. (1993). "Separation of uranium from thorium on cryptomelane-type hydrous manganese-dioxide." *J. Radioanal. Nucl. Chem., Articl.* 172, 145-153.

Elnaggar, I. M., Elabsy, M. A.,Abdelhamid, M. M., and Aly, H. F. (1993). "Separation behavior of uranium and thorium on cryptomelane-type hydrous manganese dioxide from aqueous solution." *Solv. Extract. Ion Ex.*, 11, 521-540.

Farley, K. J., Dzombak, D., A, and Morel, F. M. M. (1985). "A surface precipitation model for the sorption of cation on the metal-oxides." *J. Colloid Interface Sci.*, 106, 226-242.

Feng, Q., Kanoh, H., Miyai, Y., Ooi, K. (1995). "Alkali-metal ions insertion/extractions reactions with hollandite-type manganese oxide in the aqueous-phase." *Chem. Mater.*, 7, 148-153.

Fitzpatrick, E. A. (1980). "Soils. Their Formation, Classification and Distribution." Longman, London.

Fu, G., Allen, H. E., and Cowan, C. E. (1991). "Adsorption of cadmium and copper by manganese oxide." *Soil Science*, 152(2), 72-81.

Gao Y., Sengupta, A. and D. Simpson (1995). "A New Hybrid Inorganic Sorbent For Heavy Metal Removal." *Water Research*, Pergamon, 29 (9), 2195-2205.

Goldstein, J. I., Romig, A. D. Jr., Newbury, D. E., Lyman, C. E., Echlin, P., Fiori, C., Joy, D. C. and Lifshin, E. (1992). "*Scanning Electron Microscopy and X-Ray Microanalysis – A Text for Biologist, Materials Scientists, and Geologists.*" Second Ed, Plenum Press, New York and London.

Greenland, D. J., and Hayes, M. H. B. (1983). "*The Chemistry of Soil Constituents.*" Wiley, Winchester.

Hayes, K . F. and Leckie, J. O. (1986). In "*Geochmical Processes at Mineral Surfaces.*" Davis, J. A., Hayes, K. F., Eds., American Chemical Society: Washington, DC, 323, 115-141.

Hayes, K. F., Leckie, J. O. (1987). "Modeling ionic-strength effects on cation adsorption at hydrous oxide-solution interfaces." *J Colloid Interf Sci*, 115(2), 564-572.

Healey, T. W., Herring, A. P., and Fuerstenau, D. W. (1966). "The effect of crystal structure on the surface properties of a series of manganese dioxides." *J. Colloid Interface Sci.*, 21, 435-444.

Herbelin, A. L. and Westall, J. C. (1999). "FITEQL: A computer program for determination of chemical equilibrium constants from experimental data." Version 4.0, Report 99-01, Oregon State University, Corvallis, Oregon.

Herner, R. R., Skupien, J. J., Livingston, E. H. and Shaver, E. H. (1994). "Fundamentals of Urban Runoff Management: Technical and Institutional Issues. " Terrene Institute and U. S. Environmental Protection Agency, Washington DC.

Hird, J. P. and Sansalone, J. J. (2001). "Storm water runoff quality and quantity characterization from an elevated urban interstate highway." Water Environment Research, Submitted.

Ho, Y. S. and McKay, G. (1999) "The kinetics of sorption of divalent metal ions onto sphagnum moss peat." *Wat. Res.*, 34(3), 735-742

Horner, R.R., Skupien, J.J., Livingston, E. H. and Shaver, E. H. (1994). "*Fundamentals of Urban Runoff Management: Technical and Institutional Issues.*" Terrene Institute and U.S. Environmental Protection Agency. Washington DC.

Igloria R.V., Hathhorn W.E. and D. R. Yonge (1997). "NOM and Trace Metal Attenuation During Storm-Water Infiltration." *J. Hydrologic Engrg.* ASCE, 2 (3), 120-127.

Israelachvili, J. (1991) "Intermolecular & Surface Forces." 2nd ed., Academic Press INC., San Diego, California.

Joshi, A., and Chaudhuri, M. (1996). "Removal of arsenic from ground water by iron oxide-coated sand." *J. Envir. Engrg.*, ASCE, 122(8), 796-800.

Jiban, K. S., and Chaudhuri, M. (1995). "Treatment of cadmium-plating and chromium-plating wastes by iron oxide-coated sand." *Water Environmental Research*, 67(5), 788-796.

Jenne E. A. (1968). "Controls on Mn, Co, Ni, Cu and Zn concentrations in soils and water: the significant role of hydrous Mn and Fe oxides. In: *Trace Inorganics in Water.*" American Chemical Society, Washington, DC.

Khaodhiar, S., Azizian, M. F., Osathaphan, K., and Nelson P. E. (2000). "Copper, Chromium, and arsenic adsorption and equilibrium modeling in an iron-oxide-coated sand, background electrolyte system." *Water, Air, and soil Pollution*, 119, 105-120.

Kinniburgh D. G. (1986). "General purpose adsorption isotherms." Environ. Sci. Technol., 20 (9), 895-904.

Knocke, W. R., Occiano, S., and Hungate, R. (1990). "Removal of soluble manganese from water by oxide-coated filter media." *Am. Water Works Assn. Res. Found.*, Denver, Colo.

Knocke, W. R., Occiano, S. C., and Hungate, R. (1991). "Removal of soluble manganese by oxide-coated filter media: sorption rate and removal mechanism issues." *Journal American Water Works Association*, 83(8), 64-69.

Knocke W. R. and Hamon, J. R. (1988). "Soluble manganese removal on oxide-coated filter media." *J. AWWA*, 80(12), 65-70.

Krauskopf K. B. (1956). "Factors controlling the concentration of thirteen rare metals in seawater." *Geochim. Cosmochim. Acta.*, 9, 1-8.

LaGrega, M. D., Buckingham, P. L and Evans, J. C. (1994). "Hazardous Waste Management." McGraw-Hill, Inc., New York.

Lai, C. H., Lo, S. L., and Lin, C. F. (1994). "Evaluating an iron-coated sand for removing copper from water." *Water Science Technology*, 30(9), 175-182.

Laitinen, H. A., and Zhou, H. (1988). "Characteristic adsorption of Ni(II) on $MnO_2$." *J. Colloid Interface Sci.*,125(1), 45-50.

Langmuir, D. (1997). "*Aqueous Environmental Geochemistry.*" Prentice-Hall, Inc., New Jersey, USA.

Lewis, G. N., and Randall, M. (1923). Thermodynamics and the Free Energy of Chemical Substances, McGraw – Hill Book Company, Inc. New York

Li, Y., Buchberger, S. G., and Sansalone, J. J., (1999). "Variably saturated flow in storm-water partial exfiltration trench." *J. Envir. Engrg.*, ASCE, 125(6), 556-565.

Liu, D., Teng, Z., Cartledge, F. K., and Sansalone, J. J. (2001a). "Surface Characteristics of Sorptive-Filtration Storm Water Media – Part I: Low Density ($\rho_S < 1.0$) Oxide Coated Buoyant Media." *J. Envir. Engrg.*, ASCE, in press.

Liu, D., Teng, Z., Cartledge, F. K., and Sansalone, J. J. (2000b). "Surface Characteristics of Sorptive-Filtration Storm Water Media – Part II: Higher Specific Gravity ($\rho_S > 1.0$) Oxide Coated Fixed Media." *J. Envir. Engrg.*, ASCE, in press.

Liu, D., Sansalone, J. J. and Cartledge, F. K. (2001c). "Adsorption characteristics of oxide coated polymeric media ($\rho_s < 1.0$) for storm water treatment—Part I: batch equilibriums and kinetics." *J. Envir. Engrg.*, ASCE, submitted.

Liu, D., Sansalone, J. J. and Cartledge, F. K. (2001d). "Adsorption characteristics of oxide coated buoyant media ($\rho_s < 1.0$) for storm water treatment—part II equilibrium and kinetic models." *J. Envir. Engrg.*, ASCE, submitted.

Liu, D., Sansalone, J. J. and Cartledge, F. K. (2001e). "Manganese oxide coated cementious media for storm water treatment—part I: heavy metal adsorption equilibria and kinetics." *J. Envir. Engrg.*, ASCE, submitted.

Liu, D., Sansalone, J. J. and Cartledge, F. K. (2001f). "Manganese oxide coated cementious media for storm water treatment—part II surface complexation and kinetic model." *J. Envir. Engrg.*, ASCE, submitted.

Lo S., Jeng H. and C Lai (1997). "Characteristics and Adsorption Properties of Iron-Coated Sand." *Water Science and Technology*, Pergamon, 35 (7), 63-70.

Loehr, R. C. and Webster, M. T. (1996). "Behavior of fresh vs aged chemicals in soil." *J. Soil Contam.*, 5(4), 361-383.

Lygren, E., Gjessing, E., and Berglind, L. (1984). "Pollution transport from a highway." *Sci. Total Envir.*, 33, 147-159

Magini, M, Licheri, G., Piccaluga, Pinna, G. (1988) "X-ray Diffraction of Ioons in Aqueous Solutions: Hydration and Complex Formation." CRC Press Inc.

Malcom, H.R. (1989). *Elements of Urban Stormwater Design.* North Carolina State University, Engineering Extension Press.

Manceau, A., Gorshkov, A. I., Drits, V. A. (1992) *Am. Mineral.*, 77, 1144-1157.

McKenzie R. M. (1971). "The synthesis of birnessite, cryptomelane, and some other oxide and hydroxides of manganese." *Mineralogical magazine*, 38,493-502.

McKenzie R. M. (1975). "An electron microprobe study of the relationships between heavy metals and manganese and iron in soils and ocean floor nodules." *Aust. J. Soil Res.* 13, 177-188.

McKenzie R. M. (1989). "Manganese oxides and hydroxides." In: *Minerals in Soil Environments*, 2nd Ed., J. B. Dixon and S. B Weed, eds., Soil Science Society of America, Madison, Wisconsin, USA

McKenzie R. M. (1983). "The adsorption of molybdenum on oxide surfaces." *Aust. J. Soil Res.* 21, 505-513.

McKenzie R. M. (1981). "The surface charge on manganese dioxides." *Aust. J. Soil Res.* 19, 41-50.

McKenzie R. M. (1980a). "The adsorption of lead and other heavy metals on oxides of manganese and iron." *Aust. J. Soil Res.* 18, 61-73.

McKenzie R. M. (1980b). "The manganese oxides in soils." In: Geology and Geochemistry of manganese. Vol. 1. Vaarentsov, I. M.and Grasselly G. Y. (Eds.), Publ. House Hung. Acad. Sci., Budapest. 259-269.

Meng X. Letterman R. D. (1996). "Modeling cadmium and sulfate adsorption by $Fe(OH)_3/SiO_2$ mixed oxides." *Water Research*, 30(9), 2148-2154.

Merkle, P. B., Knocke, W. R., Gallagher, D. L., and Little, J. C. (1997a). "Dynamic model for soluble $Mn^{2+}$ removal by oxide-coated filter media." *J. Envir. Engrg.*, ASCE,123(7), 650-658.

Merkle, P. B., Knocke, W. R., and Gallagher, D. L. (1997b). "Method for coating filter media with synthetic manganese oxide." *J. Envir. Engrg.*, ASCE, 123(7), 642-649.

Merkle, P. B., Knocke, W. R., Gallagher, D. L., Junta-Rosso, J., and Solberg, T. N. (1996). "Characterizing filter media mineral coatings." *J. AWWA*, 88(12), 62-73.

Mihelcic J. R., Luthy R. G. (1986). "Adsorption of lead and zinc on blast-furnace iron-oxide solids." *Journal Water Pollution Control Federation*, 58(3), 242-249.

Miller, D. M., Sumner, M. E., and Miller, W. P. (1989) "A comparison of batch-generated and flow-generated anion adsorption isotherm." *Soil Sci. Soc. Am. J.*, 53, 373-380.

Morgan, J. J. and Stumm, W. (1964). "Colloid-chemical properties of manganese dioxide." *J. Colloid Sci.*, 19, 357-371.

Murray, J. W. (1975). "The interaction of metal ions at the manganese dioxide-solution interface." *Geochim. Cosmochim. Acta.*, 48, 1237-1247.

Murray, J. W. (1974). "The surface chemistry of hydrous manganese dioxide." *J. Colloid Interface Sci.*, 46, 357-371

Murray, D. J, Healy, T. W., and Ferstenau, D. W. (1968). "Adsorption from aqueous solution: Adv. Chem. Ser.," No. 79, Chap. 7, Amer. Chem. Soc., Washington, DC.

Muschack, W. (1990). "Pollution of street run-off by traffic and local conditions." *Sci. Total Envir.*, 93, 419-431

Nakanishi, H. (1967). "Kinetics of continuous removal of manganese in a $MnO_2$-coated sand bed." *Kogyo Kagaku Zasshi*, 70(4), 407.

Nebergall, W. H., Holtzclaw, H. F., and Robinson, W. R. (1980). "General Chemistry." 6th Ed., D. C. Health and Company, Lexington, Mass.

Papini M. P., Kahie Y. D., Troia B., and Majone M. (1999). "Adsorption of lead at variable pH onto a natural porous medium: Modeling of batch and column experiments." Environ. Sci. Technol., 33 (24), 4457-4464.

Parks, G. A. (1965). "The isoelectric points of solid oxides, solid hydroxides and aqueous hydroxo complex systems." Chem. Rev., 65. 177-198.

Potter, R. M., and Rossman, G. R. (1979). "The tetravalent manganese oxides: identification, hydration, and structural relationships by infrared spectroscopy." *American Mineralogist*, 64, 1199-1218.

Ran, J. N. and Gschwend, P. M. (1994). "Effect of solution chemistry on clay collide release from an iron oxide-coated aquifer sand." *Environ. Sci. Technol.* 28(9), 1717-1787.

Randall, S. R., Sherman, D. M., and Regnarsdottir, K. V. (1998). "An extended X-ray absorption fin structure spectroscopy investigation of cadmium sorption on cryptomelane ($KMn_8O_{16}$)." *Chemical Geology*, 151, 95-106.

Raven, K. P., Jain, A. and Loeppert, R. H. (1998) "Arsenite and Arsenate adsorption on ferrihydrite: Kinetics, Equilibrium, and Adsorption Envelopes." *Environ. Sci. Technol.*, , 32(3), 344-349.

Reed B.E. and S. Arunachalam (1994). "Use Of Granular Activated Carbon Columns For Lead Removal." *J. Envir. Engrg. Div.*, ASCE, 120 (2), 416-436.

Reed, B. E., Robertson, J., and Jamil, M. (1995). "Regeneration of granular activated carbon (GAC) columns used for removal of lead." *J. Envir. Engrg.*, ASCE, 121(9), 653-662.

Reed, B. E., Jamil, M., and Thomas, B. (1996). "Effect of pH, empty bed contact time and hydraulic loading rate on lead removal by granular activated carbon columns." *Water Environment Research*, 68(5), 877-882.

Revitt, D.M., Hamilton, R.S., Warren, R.S. (1990) "The Transport of Heavy Metals Within a Small Urban Catchment." *The Science of the Total Environment*, (93), 359-373.

Richens, D. A. (1997) "The chemistry of Aqua ions: Synthesis, Structure, and Reactivity. A tour through the periodic table of elements." John Wiley & Sons.

Robert Ryskin, Y. I. (1974). "The vibrations of protons in minerals: hydroxyl, water and ammonium." In: *The Infrared Spectra of Minerals*, Farmer, V. C., eds., Mineralogical Society, London.138-182.

Robert, M. and Terce, M. (1989). "Effect of gel and coatings on clay mineral chemical properties." In:, *Inorganic Contaminants in the Vadose Zone*. Eds.: B. Bar-Yosel, N. J. Barrow and J. Goldsmith. Springer, Berlin, 57-71

Roy A., Eaton H. C., Cartledge F. K., Tittlebaum M. E. (1992a) "Solidification stabilization of hazardous waste—evidence of physical encapsulation." *Environ. Sci. Technol.*, 26 (7), 1349-1353.

Roy, W. R., Krapac, I. G., Chou, A. F. J., Griffin, R. A., and Roulier, M. H. (1992a). "Technical Resource Document: *Batch-type procedures for estimating soil adsorption of chemicals.*" United States Environmental Protection Agency, Office of Solid Waste and Emergancy Response, Washington DC., EPA/530-SW-87-006-F

Roy, W. R. (1992b). "Adsorption-desorption methodologies and selected estimation techniques for transport-modeling parameters." In *Migraion and Fate of Pollutant in Soils and Subsoils.* Pretruzzelli, D., Hefferich, F. G., Eds, Springer, Berlin.

Sansalone, J. J. and Glenn, D.W. (2001). "Temporal variation in heavy metal partitioning and loading in urban highway pavement sheet flow – Implications of in-situ treatment design." *Transportation Research Record*, in press

Sansalone J. J. (1999). "Adsorptive-infiltration of metals in urban drainage – media characteristics." Sci. Total Envir., 235, 179-188

Sansalone, J. J., and Buchberger, S. G., (1997). "Partitioning and first flush of metals in urban roadway storm water." *J. Envir. Engrg.*, ASCE, 123(2), 134-143.

Sansalone, J. J., Koran, J. M., Smithson, and Buchberger, S. G. (1998). "Physical Characteristics of urban roadway solids transported during rain event." *J. Envir. Engrg.*, ASCE, 124(5), 427-440.

Sansalone, J. J., and Buchberger, S. G., (1995). "An filtration device as a best management practice for immobilizing heavy metal in urban highway runoff." *Water Sci. and Technol.*, 32(1), 119-125

Scheidegger, A. M. and Sparks, D. L. (1996). "A critical assessment of sorption-desorption mechanisms at the soil mineral/water interface." *Soil Sci.*, 161(12), 813-831.

Schwertmann U. and Cornell R. M. (1991). "Iron oxide in the laboratory-Preparation and characterization." VCH Publishers, Inc., New York.

Schwertmann, U., and Taylor, R. M. (1989). "Iron oxides." In: *Minerals in Soil Environments*, 2nd Ed., J. B. Dixon and S. B Weed, eds., Soil Science Society of America, Madison, Wisconsin, USA.

Sheindorf, C. H., Rebhun, M., and Shwintuch, M, (1981). Journal of Colloid and interface Science, 79(1), 136-142.

Skopp, J. (1986) "Analysis of time dependent chemical process in soils." J. Environ. Qual., 15, 205-213.

Smith, E. H. and Amini, A. (2000). "Lead removal in fixed bed by recycled iron material." *J. Envir. Engrg.*, ASCE, 126(1), 58-65.

Smith, E. H. (1996). "Uptake of heavy metals ion batch systems by a recycled iron-bearing material." *Water Research*, 30(10), 2424-2434.

Smith, R. W. and Jenne, E. A. (1991). "Recalculation, evaluation, and prediction of surface complexation constants for metal adsorption on iron and manganese oxides." *Environ. Sci.& Technol.*, 25(3), 525-531.

Sparks, D. L. (1999) "Kinetics and mechanisms of chemical reaction at the soilmineral/water interface," In: *Soil Physical Chemistry*, 2nd ed., Sparks D. L. eds.,CRC Press.

Sparks, D. L. (1989) "*Kinetics of Soil Chemical Processes.*" Academic Press, INC. San Diego.

Sparks, D. L. (1995). Environmental Soil Chemistry, Academic Press, San Diego.

Sposito, G. (1994) "*Chemical Equilibria and Kinetics in Soils.*" Oxford University Press, New York.

Sposito, G. (1986). ""Distinguishing adsorption from surface precipitation." In: Geochemical Processes at Mineral Surface, Eds Davis, J. A., and Hayes, K. F., American Chemical Society, Washington, D. C.

Sposito, G. (1984). "The surface chemistry of soils." Oxford Univ. Press, New York.

Stahl, R. S. and James, B. R. (1991a). "Zinc sorption by iron-oxide-coated sand as a function of pH." *Soil Sci, Soc. Am. J.*, 55, 1287-1290.

Stahl, R. S. and James, B. R. (1991b). "Zinc sorption by manganese-oxide-coated sand as a function of pH." *Soil Sci, Soc. Am. J.*, 55, 1291-1294.

Steinfeld, J. I., Francisco, J. S., and Hase, W. L., (1989). Chemical Kinetics and Dynamics, Prentic Hall, Inc., Englewood Cliffs, New Jersey.

Stenkamp, V. S. and Benjamin, M. M. (1994). "Effect of iron-oxide coating on sand filtration." *Journal American Water Works Association.* 86(8), 37-50.

Stephanie, L., Brock, N. D., Zheng, R., Giraldo, O., Zhou, H., and Suib, S. L. (1998). "A review of porous manganese oxide materials." *Chem. Matter.*, 10, 2619-2628.

Strawn, D. G., Scheidegger, A. M., and Sparks D. L., (1998). "Kinetics and mechanisms of Pb(II) sorption and desorption at the aluminum oxide-water interface." *Environ. Sci. & Technol.*, 32(17), 2596-2601.

Stroes-Gascoyne, S., Kramer J. R., Snodgrass, W. J. (1986). "A new model describing the adsorption of copper on $MnO_2$." Environ. Sci. Technol., 20(10), 1047-1050.

Stumm, W. (1992). "*Chemistry of the Solid-Water Interface, Processes at the Mineral-Water and Particle-Water Interface in Natural Systems.*" John Wiley & Sons, Inc., New York.

Stumm, W. and Morgan, J. J. (1996). "*Aquatic Chemistry: Chemical Equilibria and Rates in Natural Waters.*" 3rd Edition, John Wiley & Sons, Inc., New York.

Sverjensky, D. A. (1993). "Zero-Point-of-Charge prediction from crystal chemistry and solvation theory." Geochim. Cosmochim. Acta, 58(14), 3123-3129.

Tamura, H., Katayama, N., and Furrich, R. (1997). "The $Co^{2+}$ adsorption properties of $Al_2O_3$, $Fe_2O_3$, $Fe_3O_4$, $TiO_2$, and $MnO_2$ evaluated by modeling with the Frumkin isotherm." *J. of Colloid and Interface Sci.* 195, 192-202

Theis T. L., Iyer R., Ellis S. K. (1992). "Evaluating a new granular iron-oxide for removing lead from drinking-water." *Journal American Water Works Association*, 84(7), 101-105.

Towle, S. N., Bargar, J. R., Brown, G. E. (1997). "Surface precipitation of Co(II)(aq) on $Al_2O_3$." *J. Colloid Interface Sci.*, 187(1), 62-82.

Trivedi, P., and Axe, L. (2001) "Predicting divalent metal sorption to hydrous Al, Fe, and Mn oxides." *Environ. Sci. Technol.*, 35(9), 1779-1784.

Trivedi, P. and Axe, L. (2000). "Modeling Cd and Zn sorption to hydrous metal oxides." *Environ. Sci. & Technol.*, 34(11), 2215-2223.

Tsadilas, C. D., Dimoyiannis, D. and Samaras, V. (1998). "Boron sorption by manganese oxide-coated sand." *Commun. Soil Sci. Plant Anal.* 29 (15), 16-25.

Tsuji, M., and Abe, M. (1985). "Synthetic inorganic ion-exchange materials: XXXVIII. Acid-base properties of a cryptomelane-type hydrous manganese (IV) oxide and some chromatographic applications." *Bull. Chem. Soc.* Japan 58, 1109-1114.

Tsuji, M., Komarneni, S. (1993a). "Powder X-ray-diffraction study of a cryptomelane-type manganic acid and its alkali cation-exchanged forms." *J. Mater. Res.*, 8, 3145-3150.

Tsuji, M., Komarneni, S., (1993b). "Selective exchange of divalent transition metal ion in cryptomelane-type manganic acid with tunnel structure." *J. Mater. Res.*, 8, 611-616.

Ungarish, M. and Aharoni C. (1981). "Kinetics of chemisorption: Deducing kinetic lows from experimental data." *J. Chem. Soc. Am. Proc.*, 38, 29-35.

U. S. Army Construction Engineering Research Laboratory (1986). "Critical review of cement based stabilization/solidification techniques for the disposal of hazardous wastes." ADA-184 427, IL.

U. S. EPA. (1983). "*Results of the Nationwide Urban Runoff Program: Volume 1 - Final Report.*" Water Planning Division. Washington, DC. NTIS Publication No. 83-185552.

U. S. EPA (1992) "Environmental Impacts of Storm Water Discharges: A National Profile." EPA 841-R92-001, Office of Water, Washington, DC.

U. S. EPA (1993). "Handbook Urban Runoff Pollution Prevention and Controlling Planning." EPA-625-R-93-004, Washington, DC.

U. S. EPA (1996) "National Water Quality Inventory—1996 Reports to Congress." Environmental Protection Agency, Office of Water, Washington, DC.

U. S. EPA. (1998). "Characterization of building-related construction and demolition debris in United States." Rep. No. 530-R-98-010, Washington, D. C.

U. S. EPA (1999a) "National Pollutant Discharge Elimination System—Regulations for Revision of the Water Pollution Control Program: Addressing Strom Water Discharges; Final Rule, Report to Congress on the Phase II Storm Water Regulations." EPA 40 CFR Part 9, 122, 123, and 124

U. S. EPA (1999b). "Preliminary data summary of urban storm water best management practices." EPA-821-R-99-012, Office of Water, Washington, DC.

Van Raij, B., and M. Peech. (1972). "Electrochemical properties of some oxisols and alfisols of the tropics." *Soil Sci. Sci. Am. Proc.* 36, 587-593.

Weng C. H., Huang C. P., Allen H. E., Leavens P. B. and Sanders P. F. (1996). "Chemical interactions between Cr(VI) and hydrous concrete particles." *Environ. Sci.& Technol.*, 30(2), 371-376

Westall, J. C., and Hohl, H. (1980). "A comparison of electrostatic models for the oxide/solution interface." *Adv. Colloid Interface Sci.*, 12, 265-294.

White, J. L., and Roth, C. B. (1986). "Infrared Spectrometry." In: *Methods of Soil Analysis, Part 1, Physical and Mineralogical Methods.* 2nd Eds., Arnold Klute, eds. Soil Science Society of America, Madison, Wisconsin, USA

Yasunaga, T. and Ikeda, T. (1986). In "*Geochmical Processes at Mineral Surfaces.*" Davis, J. A., Hayes, K. F., Eds., American Chemical Society: Washington, DC, 323, 231-253.

Yiacoumi, S. and Tien, C. (1995). "*Kinetics of Metal Ion Adsorption from Aqueous solutions—Models, Algorithms, and Applications.*" Kluwer Academic Publishers, Boston.

Zasoski, R. J. and Burau, R. G. (1988). "Sorption and sorptive interaction of cadmium and zinc on hydrous manganese oxide." *Soil. Sci. Soc. Am. J.*, 52, 81-87.

# VITA

Dingfang Liu got his B. S. degree in Environmental Engineering from Nanchang Institute of Aeronautical Technology in 1993. He got his M. S. degree in Environmental Chemistry from Chinese Academy of Sciences at Beijing in 1999. In 2001, he will finish his doctoral work and obtain Doctor of Philosophy degree in Civil Engineering from Louisiana State University.

DOCTORAL EXAMINATION AND DISSERTATION REPORT

**Candidate:** Dingfang Liu

**Major Field:** Civil Engineering

**Title of Dissertation:** Investigation of Amphoteric Materials for Treatment of Heavy Metals in Storm Water

**Approved:**

Major Professor and Chairman

Dean of the Graduate School

**EXAMINING COMMITTEE:**

**Date of Examination:**

10 September 2001